mm

TP9521E

CA1
DTC800
88
D22
c.2

THE DEVELOPMENT OF BEARING CAPACITY DESIGN CHARTS FOR TRACK SYSTEMS

FINAL REPORT

Library and Information Centre /
Centre de Documentation (GSL)
RECEIVED - REÇU LE
APR 21 198
Transport Canada / Transports Canada

Prepared for

Canadian National Railways
Canadian Pacific Railways
Transportation Development Centre

by

Pamela J. Sattler
Research Engineer

and

D.G. Fredlund
Professor of Civil Engineering
University of Saskatchewan
Saskatoon, Saskatchewan
CANADA S7N 0W0

October 1988

413162

DISCLAIMER

The contents of this report reflect the current views of the research team at the University of Saskatchewan and not necessarily the official views or opinions of Canadian National Railways, Canadian Pacific Railways, or the Transportation Development Centre of Transport Canada.

Un sommaire en frangais de ce rapport est inclus avant la table des matihres.

Transport Canada   Transports Canada

PUBLICATION DATA FORM

1. **Transport Canada Publication No.**
TP 9521E

2. **Project No.**
6917

3. **Recipient's Catalogue No.**

4. **Title and Subtitle**
THE DEVELOPMENT OF BEARING CAPACITY DESIGN CHARTS FOR TRACK SYSTEMS
FINAL REPORT

5. **Publication Date**
October, 1988

6. **Performing Organization Document No.**

7. **Author(s)**
Pamela J. Sattler and D.G. Fredlund

8. **Transport Canada File No.**
D1465-438-3

9. **Performing Organization Name and Address**
University of Saskatchewan
Department of Civil Engineering
Saskatoon, Saskatchewan S7N 0W0

10. **DSS File No.**
11SD.T8200-7-7505

11. **DSS or Transport Canada Contract No.**
T8200-7-7505/01SD

12. **Sponsoring Agency Name and Address**

Transportation Development Centre
200 René-Lévesque Blvd. West
Suite 601, West Tower
Montreal, Quebec
H2Z 1X4

CN Rail
P.O. Box 8100
Montreal, Quebec
H3C 3N4

CP Rail
Windsor Station
Montreal, Quebec
H3C 3E4

13. **Type of Publication and Period Covered**
Final

14. **Project Officer**
W.G. Rowan

15. **Supplementary Notes (Funding programs, titles of related publications, etc.)**
See also **TP 9522E**, "THE DEVELOPMENT OF BEARING CAPACITY DESIGN CHARTS FOR TRACK SYSTEMS", summary report.

16. **Abstract**

The objective of this study is to present a bearing capacity type design procedure for assessing the stability of the track subgrades. A previous research program emphasized the measurement of the matric suction in the subgrade of a track structure. The current phase of the research program concentrated on the incorporation of the matric suction term into a bearing capacity design procedure. This permits the design procedure to utilize the additional strength of the soil resulting from matric suction.

Design charts have been developed for various train loads, subballast thicknesses, soil types, and design matric suction values. The design charts give a factor of safety against bearing capacity failure as a function of the above parameters.

Stresses in the subgrade are predicted utilizing the computer program **GEOTRACK** for various design train loads, subballast thicknesses, and soil parameters. The allowable stress, or bearing capacity, is determined using bearing capacity theories modified to accommodate the layered track system and also incorporate the additional strength of the soil resulting from matric suction. A comparison of predicted stresses and bearing capacity defines the factor of safety against a bearing capacity failure.

17. **Key Words**
Rail track ballast; Subballast; Subgrade; Soil mechanics; Design modelling; Load bearing capacity

18. **Distribution Statement**
Limited number of copies available on request from the Transportation Development Centre.

19. **Security Classification (of this publication)**
Unclassified

20. **Security Classification (of this page)**
Unclassified

21. **Declassification (date)**

22. **No. of Pages**
262

23. **Price**

TDC/CDT 79-005
Rev 88

Canada

Transports Canada Transport Canada

FORMULE DE DONNÉES POUR PUBLICATION

1. N° de la publication de Transports Canada
TP 9521E

2. N° de l'étude
6917

3. N° de catalogue du destinataire

4. Titre et sous-titre
THE DEVELOPMENT OF BEARING CAPACITY DESIGN CHARTS FOR TRACK SYSTEMS - RAPPORT FINAL

5. Date de la publication
octobre 1988

6. N° du document de l'organisme exécutant

7. Auteur(s)
Pamela J. Sattler and D.G. Fredlund

8. N° de dossier — Transports Canada
D1465-438-3

9. Nom et adresse de l'organisme exécutant

University of Saskatchewan
Department of Civil Engineering
Saskatoon, Saskatchewan S7N 0W0

10 N° de dossier — ASC
11SD.T8200-7-7505

11. N° de contrat — ASC ou Transports Canada
T8200-7-7505/01SD

12. Nom et adresse de l'organisme parrain

Centre de développement des transports
200 ouest, boul. René-Lévesque
Tour ouest, suite 601
Montréal (Québec)
H2Z 1X4

CN Rail
C.P. 8100
Montréal (Québec)
H3C 3N4

CP Rail
Gare Windsor
C.P. 6042 "A
Montréal(Qué
H3C 3E4

13. Genre de publication et période visée
Rapport final

14. Agent de projet
W.G. Rowan

15. Remarques additionnelles (Programmes de financement, titres de publications connexes, etc.)
Voir aussi **TP 9522E**, "THE DEVELOPMENT OF BEARING CAPACITY DESIGN CHARTS FOR TRACK SYSTEMS", Rapport Sommaire

16. Résumé

La recherche avait pour objet l'étude d'une méthode de calcul de la stabilité d'une plate-forme ferroviaire tenant compte de la portance des sols supports. Des recherches antérieures avaient débouché sur des méthodes permettant de mesurer la succion capillaire d'un sol. La présente recherche visait à élaborer une méthode de calcul de la portance qui considère ce nouvel élément qu'est la succion, de manière à pouvoir en tirer tout le parti possible.

Des courbes de calcul ont pu ainsi être développées prenant en compte des valeurs types de charges à l'essieu, d'épaisseur de la sous-couche, de classes de sols et diverses valeurs de référence de succion. On en tire un facteur de sécurité, fonction de ces paramètres, protégeant contre le risque d'un dépassement de la portance susceptible d'entraîner la ruine de la plate-forme.

Les contraintes théoriques engendrées dans la plate-forme peuvent être calculées à l'aide d'un programme informatique appelé GEOTRACK, au regard des charges à l'essieu, de l'épaisseur de la sous-couche et des caractéristiques mécaniques du sol. La contrainte admissible, ou portance, peut être déterminée en s'appuyant sur les théories reconnues, modifiées pour tenir compte de la caractéristique multicouche d'une voie ferrée et auxquelles a été ajouté l'élément de succion ainsi que l'excédent de force qu'elle autorise. En comparant la portance théorique d'un sol à la courbe de distribution des contraintes s'exerçant sur ce sol, il est possible d'obtenir un ordre de grandeur de la marge de sécurité disponible contre le dépassement de la portance du sol support.

17. Mots clés
ballast, sous-couche, plate-forme, mécanique des sols, modélisation, portance.

18. Diffusion
Le Centre de développement des transports dispose d'un nombre limité d'exemplaires.

19. Classification de sécurité (de cette publication)	20. Classification de sécurité (de cette page)	21. Déclassification (date)	22. Nombre de pages	23. Prix
Non classifié	Non classifiée		262	

ACKNOWLEDGEMENTS

The authors wish to acknowledge the financial contributions provided by Canadian National Railways, Canadian Pacific Railways, and the Transportation Development Centre of Transport Canada. Their support has made possible this research.

The authors wish to acknowledge the co-operation of Harry E. Stewart in the development of a post-processing computer package for the GEOTRACK computer program. The assistance of Leonard Lam, Clifton Associates Ltd., in the development of the GEOPLOT post-processing package and of Darrell McClarty, University of Saskatchewan, in the development of the STRESS, BEARING, and COMPARE computer programs is gratefully appreciated.

Sincere thanks are extended to Jude Loi, University of Saskatchewan, for his contributions to the design and drafting of the figures in this report. Thanks are also extended to Alex Kozlow, Gordon Putz, Greg Misfeldt and Mark Vanstone for their assistance in the laboratory. The dedication of Gladie Russell and Cathy Bohachik in the typing and publication of this report is gratefully acknowledged.

Sincere appreciation is expressed to Mr. M.J. Klassen of CP Rail, Mr. W.E. Jubien of CN Rail, and Mr. W.G. Rowan of the Transportation Development Centre for their contributions toward this study.

EXECUTIVE SUMMARY

In 1982, Professor D.G. Fredlund of the Geotechnical Group at the University of Saskatchewan, Saskatoon, Saskatchewan proposed a four-stage research program to develop a better understanding of the role played by soil suction in the behaviour and design of track system subgrades. Earlier work, now completed, was undertaken jointly with Clifton Associates Ltd., Regina, Saskatchewan and was devoted to an investigation of suitable methods for measuring soil suction in the field. Having developed suitable procedures for measuring soil suction, the objective of the present phase of research was to incorporate the soil suction term into a workable design procedure. This permits the design procedure to utilize the additional strength of the soil resulting from the suction in the subgrade.

A bearing capacity design procedure for the railway-ballast-subballast-subgrade system was developed in which the strength of the unsaturated soil is related to the stress state, material parameters, soil suction and failure geometry.

The stresses beneath the loaded track system are computed from a computer program called **GEOTRACK**, which combines the stiffness matrix of the tie-track system with a Boussinesq stress distribution in the ballast-subballast-subgrade system. Stresses are predicted for various train loads, subballast thicknesses and soil parameters.

A comparison of the subgrade system bearing capacity and the subgrade system stress distribution provides a measure of the factor of safety against a bearing capacity type failure. Design charts have been developed for typical design train loads, subballast thicknesses, soil

types, and design soil suction values. The user may choose to use the design charts or the user may choose to use the series of computer programs which were developed to compute the factor of safety against bearing capacity failure.

Present research indicates that a bearing capacity factor of safety of 2.5 to 3.0 would be reasonable for use with the design charts presented for railway systems. However, further research is required to develop confidence in the use of a particular factor of safety for the bearing capacity computation.

The bearing capacity design procedure should be used to complement existing design procedures. It is only through use that the design procedure can be assessed for approval or modification. Use of the procedure will provide feedback on an appropriate bearing capacity factor of safety for design, information on the reliability of the stress calculations, and the reliability of the soil suction parameters.

SOMMAIRE

En 1982, le professeur D.G. Fredlund du groupe géotechnique de l'Université de la Saskatchewan à Saskatoon, avait proposé le lancement d'un programme de recherche en quatre étapes ayant pour but d'approfondir l'influence de la succion capillaire sur le comportement des sols supports de voies ferrées et, partant, sur la conception de celles-ci. La phase 1 des travaux, entreprise conjointement avec Clifton Associates Ltd. de Regina (Saskatchewan), a porté exclusivement sur l'étude de méthodes permettant de mesurer la succion in situ. La recherche ayant abouti, les travaux actuels visent à intégrer l'élément que constitué la succion dans une méthode de calcul facile d'exploitation, dont l'objet est de tirer parti de l'excédent de résistance du sol conférée par cette force de succion.

C'est ainsi qu'a pu être élaborée une méthode de calcul de la portance concernant un système multicouches voie ferrée/ballast/sous-couche/plate-forme où la portance du sol support est exprimée en fonction des états de contraintes, des caractéristiques granulométriques et de la géométrie de rupture.

Les contraintes dans le sol support résultant de l'effet d'une charge en surface, en l'occurrence le système précité, peuvent être calculées grâce à un programme informatisé appelé **GEOTPACK**. Ce dernier combine la matrice de raideur du système traverse-rail à une distribution de contraintes type Boussinesq s'exerçant sur le système ballast/sous-couche/plate-forme. On obtient ainsi des courbes de contraintes en fonction des charges à l'essieu, de l'épaisseur de la sous-couche et des caractéristiques mécaniques du sol support.

En comparant la portance d'un sol à la courbe de distribution des contraintes qui s'exercent sur ce sol, il est possible de tirer un ordre de grandeur de la marge de sécurité disponible contre le dépassement de la portance du sol support. Des courbes de calcul ont été développées prenant en compte des valeurs types de charges à l'essieu, d'épaisseur de la sous-couche, de classes de sols et diverses valeurs de référence de succion. Pour calculer le facteur de sécurité, l'utilisateur a le choix entre ces courbes de calcul et une série de programmes informatiques élaborés à cette feu.

Dans l'état actuel de la recherche, un facteur de sécurité entre 2,5 et 3 semble raisonnable dans le contexte ferroviaire nous concernant. Cependant, des recherches plus poussées seront nécessaires en vie de confirmer la confiance que l'on pourrait avoir à l'égard d'un facteur de sécurité de telle ou telle valeur particulière.

Il est recommandé d'utiliser la méthode de calcul de la portance parallèlement aux méthodes courantes, de manière à mettre sa validité à l'épreuve et à déterminer si une mise au point s'avère nécessaire, avant son adoption définitive. De cette façon, on pourra déterminer le facteur de sécurité approprié en ce qui a trait à la portance, la fiabilité des calculs des contraintes et la justesse de l'appréciation des effets des paramètres de succion.

THE DEVELOPMENT OF BEARING CAPACITY DESIGN CHARTS FOR TRACK SYSTEMS

Page No.

1.0 INTRODUCTION 1

2.0 STRESS ANALYSIS 2
  2.1 The Development of a Stress Analysis Approach to Railway Design .. 2
  2.2 The Development of the GEOTRACK Model 4
  2.3 The GEOTRACK Model 11
  2.4 Use of the GEOTRACK Computer Model in a Bearing Capacity Approach to Railway Design 13

3.0 BEARING CAPACITY 24
  3.1 The Development of a Bearing Capacity Approach Railway Design 25
  3.2 Bearing Capacity Failure in a Tie-Track System 26
  3.3 The Broms Approach to Bearing Capacity 35
  3.4 The Hanna and Meyerhof Approach to Bearing Capacity 40

4.0 DESIGN PARAMETERS 43
  4.1 GEOTRACK Parameters 43
  4.2 Soil parameters: c', ϕ', ϕ^b and γ 48
  4.3 Matric Suction 67

5.0 DESIGN CHARTS 78
  5.1 Methodology 78
  5.2 Presentation of the Stress Charts 81
  5.3 Presentation of Bearing Capacity Charts 93
  5.4 Presentation of the Bearing Capacity Factor of Safety Charts 113
  5.5 Use of the Design Charts for Example Problems 123

6.0 CONCLUSIONS/RECOMMENDATIONS 134

REFERENCES 136

APPENDIX A

APPENDIX B

APPENDIX C

LIST OF TABLES

		Page No.
Table 1	Tie Parameters Used in GEOTRACK Input File	44
Table 2	Rail Parameters Used in GEOTRACK Input File	44
Table 3	GEOTRACK Parameters Varied for Any One Axle Load	47
Table 4	Literature Review Values for the Shear Strength Parameters of Clay	55
Table 5	Literature Review Values for the Shear Strength Parameters of Glacial Till	58
Table 6	Literature Review Values for the Shear Strength Parameters of Silt/Sand	59

LIST OF FIGURES

Fig. 2.1 Comparison of computer models on the basis of predicting rail deflections (adapted from Stewart and Selig (15)) 6

Fig. 2.2 Comparison of computer models on the basis of predicting rail seat load (adapted from Stewart and Selig (15)) 7

Fig. 2.3 Comparison of computer models on the basis of predicting vertical stress at the ballast surface (adapted from Stewart and Selig (15)) 8

Fig. 2.4 Comparison of computer models on the basis of predicting vertical stress at the subgrade surface (adapted from Stewart and Selig (15)) 9

Fig. 2.5 Comparison of GEOTRACK simulation data to FAST track data (adapted from Stewart and Selig (15)) 10

Fig. 2.6 Forces and elements in the GEOTRACK model (adapted from Chang, Adegoke and Selig (14)) 12

Fig. 2.7 GEOPLOT computer-generated graph showing vertical stress beneath an individual tie 14

Fig. 2.8 GEOPLOT computer-generated graph showing vertical stress beneath one tie segment for all ties 15

Fig. 2.9 Sensitivity of vertical stress output to changing axle load 18

Fig. 2.10 Sensitivity of vertical stress output to changing ballast modulus 19

Fig. 2.11 Sensitivity of vertical stress output to changing subgrade modulus 20

Fig. 2.12 Sensitivity of vertical stress output to changing ballast depth 21

Fig. 2.13 Sensitivity of vertical stress output to changing tie spacing 22

Fig. 2.14 Sensitivity of vertical stress output to changing tie EI (adapted from Stewart and Selig (15)) 23

Fig. 3.1 Three-dimensional view of the rail-tie-ballast-subballast-subgrade system 27

Fig. 3.2 Cross-sectional view of the track system showing the geometry perpendicular to the track 28

Fig. 3.3 Longitudinal view of the track system showing the geometry parallel to the track 29

Fig. 3.4 Failure geometry for the complete tie-track system for the length of the track 31

Fig. 3.5 Failure geometry for the heavily stressed outer third of the tie and the distance of a double truck loading 32

Fig. 3.6 Failure geometry for the local failure of an individual tie punching into a weak subgrade 33

Fig. 3.7 Failure geometry for a portion of the track beneath a double truck arrangement for weak subgrades 37

Fig. 3.8 Broms approach to computing bearing capacity (adapted from (2)) 36

Fig. 3.9 Components of the total cohesion term 38

Fig. 3.10 Hanna and Meyerhof approach to computing bearing capacity (adapted from (1)) 41

Fig. 4.1 Components of the shear strength of an unsaturated soil 49

Fig. 4.2 Sensitivity of ultimate bearing capacity to varying c' for constant ϕ' and ϕ^b 51

Fig. 4.3 Sensitivity of ultimate bearing capacity to varying ϕ^b for for constant c' and ϕ' 52

Fig. 4.4 Sensitivity of ultimate bearing capacity to varying ϕ' for constant c' and ϕ^b 53

Fig. 4.5 Failure envelope obtained for unsaturated glacial till with respect to changing matric suction (Gan, Fredlund and Rahardjo (66)) 62

Fig. 4.6 Results of a five stage direct shear test on a glacial lake clay 63

Fig. 4.7 Determination of the ϕ^b angle for a five stage direct shear test on a glacial lake clay 64

Fig. 4.8 Results of a three stage direct shear test on a glacial lake clay 65

Fig. 4.9 Determination of the ϕ^b angle for a three stage direct shear test on a glacial lake clay 66

Fig. 4.10 A cross-sectional diagram of the thermal conductivity sensor 68

Fig. 4.11 Typical schematic pore-water pressure profiles 70

Fig. 4.12 Actual measured pore-water pressure profile for Winnipeg glacial lake clay 71

Fig. 4.13 Typical example of suction versus time (extracted from van der Raadt (73)) 74

Fig. 4.14 Maximum and minimum recorded suction values (extracted from van der Raadt (73)) 75

Fig. 4.15 Interpreted plot of matric suction versus time of year for various depths (extracted from van der Raadt (73)) 77

Fig. 5.1 Flow chart for development of the bearing capacity design charts 79

Fig. 5.2 Option 1 "Stress Averaging Technique" 83

Fig. 5.3 Option 2 "Stress Averaging Technique" 85

Fig. 5.4 Option 3 "Stress Averaging Technique" 86

Fig. 5.5 Option 4 "Stress Averaging Technique" 87

Fig. 5.6 Stress chart for Option 1, Subgrade E = 69.0 MPa, Subballast E = 103.5 MPa 89

Fig. 5.7 Stress chart for Option 1, Subgrade E = 69.0 MPa, Subballast E = 241.5 MPa 90

Fig. 5.8 Stress chart for Option 1, Subgrade E = 6.9 MPa, Subballast E = 103.5 MPa A-1

Fig. 5.9 Stress chart for Option 1, Subgrade E = 6.9 MPa, Subballast E = 241.5 MPa A-2

Fig. 5.10 Stress chart for Option 1, Subgrade E = 41.4 MPa, Subballast E = 103.5 MPa A-3

Fig. 5.11 Stress chart for Option 1, Subgrade E = 41.4 MPa, Subballast E = 241.5 MPa A-4

Fig. 5.12 Stress chart for Option 1, Subgrade E = 69.0 MPa, Subballast E = 103.5 MPa A-5

Fig. 5.13 Stress chart for Option 1, Subgrade E = 69.0 MPa, Subballast E = 241.5 MPa A-6

Fig. 5.14 Stress chart for Option 1, Subgrade E = 103.5 MPa, Subballast E = 103.5 MPa A-7

Fig. 5.15 Stress chart for Option 1, Subgrade E = 103.5 MPa, Subballast E = 241.5 MPa A-8

Fig. 5.16 Stress chart for Option 2, Subgrade E = 6.9 MPa, Subballast E = 103.5 MPa A-9

Fig. 5.17 Stress chart for Option 2, Subgrade E = 6.9 MPa, Subballast E = 241.5 MPa A-10

Fig. 5.18 Stress chart for Option 2, Subgrade E = 41.4 MPa, Subballast E = 103.5 MPa A-11

Fig. 5.19 Stress chart for Option 2, Subgrade E = 41.4 MPa, Subballast E = 241.5 MPa A-12

Fig. 5.20 Stress chart for Option 2, Subgrade E = 69.0 MPa, Subballast E = 103.5 MPa A-13

Fig. 5.21 Stress chart for Option 2, Subgrade E = 69.0 MPa, Subballast E = 241.5 MPa A-14

Fig. 5.22 Stress chart for Option 2, Subgrade E = 103.5 MPa, Subballast E = 103.5 MPa A-15

Fig. 5.23 Stress chart for Option 2, Subgrade E = 103.5 MPa, Subballast E = 241.5 MPa A-16

Fig. 5.24 Stress chart for Option 2, Subgrade E = 6.9 MPa, Subballast E = 103.5 MPa A-17

Fig. 5.25 Stress chart for Option 2, Subgrade E = 6.9 MPa, Subballast E = 241.5 MPa A-18

Fig. 5.26 Stress chart for Option 2, Subgrade E = 41.4 MPa, Subballast E = 103.5 MPa A-19

Fig. 5.27 Stress chart for Option 2, Subgrade E = 41.4 MPa, Subballast E = 241.5 MPa A-20

Fig. 5.28 Stress chart for Option 2, Subgrade E = 69.0 MPa, Subballast E = 103.5 MPa A-21

Fig. 5.29 Stress chart for Option 2, Subgrade E = 69.0 MPa, Subballast E = 241.5 MPa A-22

Fig. 5.30 Stress chart for Option 2, Subgrade E = 103.5 MPa, Subballast E = 103.5 MPa A-23

Fig. 5.31 Stress chart for Option 2, Subgrade E = 103.5 MPa, Subballast E = 241.5 MPa A-24

Fig. 5.32 Stress chart for Option 3 comparison to Hanna and Meyerhof approach 92

Fig. 5.33 Option 1 "Bearing Capacity Configuration" 94

Fig. 5.34 Option 2 "Bearing Capacity Configuration" 95

Fig. 5.35 Option 3 "Bearing Capacity Configuration" 96

Fig. 5.36 Option 4 "Bearing Capacity Configuration" 97

Fig. 5.37 Bearing capacity by Option 1 for typical clay subgrades 99

Fig. 5.38 Bearing capacity by Option 1 for typical glacial till subgrades 100

Fig. 5.39 Bearing capacity by Option 1 for typical silt/sand subgrades 101

Fig. 5.40 Bearing capacity by Option 2 for typical clay subgrades 103

Fig. 5.41 Bearing capacity by Option 2 for typical glacial till subgrades 104

Fig. 5.42 Bearing capacity by Option 2 for typical silt/sand subgrades 105

Fig. 5.43 Bearing capacity by Option 3 for a weak clay subgrade and the absence of subballast 106

Fig. 5.44 Bearing capacity by Option 4 for typical clay subgrades 107

Fig. 5.45 Bearing capacity by Option 4 for typical glacial till subgrades 108

Fig. 5.46 Bearing capacity by Option 4 for typical silt/sand subgrades 109

Fig. 5.47 Total cohesion versus matric suction for typical clay parameters 110

Fig. 5.48 Total cohesion versus matric suction for typical glacial till parameters 111

Fig. 5.49 Total cohesion versus matric suction for typical silt/sand parameters 112

Fig. 5.50 Factor of safety for Option 1, Subgrade E = 69.0 MPa, Subballast E = 103.5 MPa 114

Fig. 5.51 Factor of safety for Option 1, Subgrade E = 69.0 MPa, Subballast E = 241.5 MPa 115

Fig. 5.52 Factor of safety for Option 1, Clay Subgrade E = 6.9 MPa, Subballast E = 103.5 MPa B-1

Fig. 5.53 Factor of safety for Option 1, Clay Subgrade E = 6.9 MPa, Subballast E = 241.5 MPa B-2

Fig. 5.54 Factor of safety for Option 1, Clay Subgrade E = 41.4 MPa, Subballast E = 103.5 MPa B-3

Fig. 5.55 Factor of safety for Option 1, Clay Subgrade E = 41.4 MPa, Subballast E = 241.5 MPa B-4

Fig. 5.56 Factor of safety for Option 1, Clay Subgrade E = 69.0 MPa, Subballast E = 103.5 MPa B-5

Fig. 5.57 Factor of safety for Option 1, Clay Subgrade E = 69.0 MPa, Subballast E = 241.5 MPa B-6

Fig. 5.58 Factor of safety for Option 1, Clay Subgrade E = 103.5 MPa, Subballast E = 103.5 MPa B-7

Fig. 5.59 Factor of safety for Option 1, Clay Subgrade E = 103.5 MPa, Subballast E = 241.5 MPa B-8

Fig. 5.60 Factor of safety for Option 1, Glacial Till Subgrade E = 6.9 MPa, Subballast E = 103.5 MPa B-9

Fig. 5.61 Factor of safety for Option 1, Glacial Till Subgrade E = 6.9 MPa, Subballast E = 241.5 MPa B-10

Fig. 5.62 Factor of safety for Option 1, Glacial Till Subgrade E = 41.4 MPa, Subballast E = 103.5 MPa B-11

Fig. 5.63 Factor of safety for Option 1, Glacial Till Subgrade E = 41.4 MPa, Subballast E = 241.5 MPa B-12

Fig. 5.64 Factor of safety for Option 1, Glacial Till Subgrade E = 69.0 MPa, Subballast E = 103.5 MPa B-13

Fig. 5.65 Factor of safety for Option 1, Glacial Till Subgrade E = 69.0 MPa, Subballast E = 241.5 MPa B-14

Fig. 5.66 Factor of safety for Option 1, Glacial Till Subgrade E = 103.5 MPa, Subballast E = 103.5 MPa B-15

Fig. 5.67 Factor of safety for Option 1, Glacial Till Subgrade E = 103.5 MPa, Subballast E = 241.5 MPa B-16

Fig. 5.68 Factor of safety for Option 1, Silt/Sand Subgrade E = 6.9 MPa, Subballast E = 103.5 MPa B-17

Fig. 5.69 Factor of safety for Option 1, Silt/Sand Subgrade E = 6.9 MPa, Subballast E = 241.5 MPa B-18

Fig. 5.70 Factor of safety for Option 1, Silt/Sand Subgrade E = 41.4 MPa, Subballast E = 103.5 MPa B-19

Fig. 5.71 Factor of safety for Option 1, Silt/Sand Subgrade E = 41.4 MPa, Subballast E = 241.5 MPa B-20

Fig. 5.72 Factor of safety for Option 1, Silt/Sand Subgrade E = 69.0 MPa, Subballast E = 103.5 MPa B-21

Fig. 5.73 Factor of safety for Option 1, Silt/Sand Subgrade E = 69.0 MPa, Subballast E = 241.5 MPa B-22

Fig. 5.74 Factor of safety for Option 1, Silt/Sand Subgrade E = 103.5 MPa, Subballast E = 103.5 MPa B-23

Fig. 5.75 Factor of safety for Option 1, Silt/Sand Subgrade E = 103.5 MPa, Subballast E = 241.5 MPa B-24

Fig. 5.76 Factor of safety for Option 2, Clay Subgrade E = 6.9 MPa, Subballast E = 103.5 MPa B-25

Fig. 5.77 Factor of safety for Option 2, Clay Subgrade E = 6.9 MPa, Subballast E = 241.5 MPa B-26

Fig. 5.78 Factor of safety for Option 2, Clay Subgrade E = 41.4 MPa, Subballast E = 103.5 MPa B-27

Fig. 5.79 Factor of safety for Option 2, Clay Subgrade E = 41.4 MPa, Subballast E = 241.5 MPa B-28

Fig. 5.80 Factor of safety for Option 2, Clay Subgrade E = 69.0 MPa, Subballast E = 103.5 MPa B-29

Fig. 5.81 Factor of safety for Option 2, Clay Subgrade E = 69.0 MPa, Subballast E = 241.5 MPa B-30

Fig. 5.82 Factor of safety for Option 2, Clay Subgrade E = 103.5 MPa, Subballast E = 103.5 MPa B-31

Fig. 5.83 Factor of safety for Option 2, Clay Subgrade E = 103.5 MPa, Subballast E = 241.5 MPa B-32

Fig. 5.84 Factor of safety for Option 2, Glacial Till Subgrade E = 6.9 MPa, Subballast E = 103.5 MPa B-33

Fig. 5.85 Factor of safety for Option 2, Glacial Till Subgrade E = 6.9 MPa, Subballast E = 241.5 MPa B-34

Fig. 5.86 Factor of safety for Option 2, Glacial Till Subgrade E = 41.4 MPa, Subballast E = 103.5 MPa B-35

Fig. 5.87 Factor of safety for Option 2, Glacial Till Subgrade E = 41.4 MPa, Subballast E = 241.5 MPa B-36

Fig. 5.88 Factor of safety for Option 2, Glacial Till Subgrade E = 69.0 MPa, Subballast E = 103.5 MPa B-37

Fig. 5.89 Factor of safety for Option 2, Glacial Till Subgrade E = 69.0 MPa, Subballast E = 241.5 MPa B-38

Fig. 5.90 Factor of safety for Option 2, Glacial Till Subgrade E = 103.5 MPa, Subballast E = 103.5 MPa B-39

Fig. 5.91 Factor of safety for Option 2, Glacial Till Subgrade E = 103.5 MPa, Subballast E = 241.5 MPa B-40

Fig. 5.92 Factor of safety for Option 2, Silt/Sand Subgrade E = 6.9 MPa, Subballast E = 103.5 MPa B-41

Fig. 5.93 Factor of safety for Option 2, Silt/Sand Subgrade E = 6.9 MPa, Subballast E = 241.5 MPa B-42

Fig. 5.94 Factor of safety for Option 2, Silt/Sand Subgrade E = 41.4 MPa, Subballast E = 103.5 MPa B-43

Fig. 5.95 Factor of safety for Option 2, Silt/Sand Subgrade E = 41.4 MPa, Subballast E = 241.5 MPa B-44

Fig. 5.96 Factor of safety for Option 2, Silt/Sand Subgrade E = 69.0 MPa, Subballast E = 103.5 MPa B-45

Fig. 5.97 Factor of safety for Option 2, Silt/Sand Subgrade E = 69.0 MPa, Subballast E = 241.5 MPa B-46

Fig. 5.98 Factor of safety for Option 2, Silt/Sand Subgrade E = 103.5 MPa, Subballast E = 103.5 MPa B-47

Fig. 5.99 Factor of safety for Option 2, Silt/Sand Subgrade E = 103.5 MPa, Subballast E = 241.5 MPa B-48

Fig. 5.100 Factor of safety for Option 2, Clay Subgrade E = 6.9 MPa, Subballast E = 103.5 MPa B-49

Fig. 5.101 Factor of safety for Option 2, Clay Subgrade E = 6.9 MPa, Subballast E = 241.5 MPa B-50

Fig. 5.102 Factor of safety for Option 2, Clay Subgrade E = 41.4 MPa, Subballast E = 103.5 MPa B-51

Fig. 5.103 Factor of safety for Option 2, Clay Subgrade E = 41.4 MPa, Subballast E = 241.5 MPa B-52

Fig. 5.104 Factor of safety for Option 2, Clay Subgrade E = 69.0 MPa, Subballast E = 103.5 MPa B-53

Fig. 5.105 Factor of safety for Option 2, Clay Subgrade E = 69.0 MPa, Subballast E = 241.5 MPa B-54

Fig. 5.106 Factor of safety for Option 2, Clay Subgrade E = 103.5 MPa, Subballast E = 103.5 MPa B-55

Fig. 5.107 Factor of safety for Option 2, Clay Subgrade E = 103.5 MPa, Subballast E = 241.5 MPa B-56

Fig. 5.108 Factor of safety for Option 2, Glacial Till Subgrade E = 6.9 MPa, Subballast E = 103.5 MPa B-57

Fig. 5.109 Factor of safety for Option 2, Glacial Till Subgrade E = 6.9 MPa, Subballast E = 241.5 MPa B-58

Fig. 5.110 Factor of safety for Option 2, Glacial Till Subgrade E = 41.4 MPa, Subballast E = 103.5 MPa B-59

Fig. 5.111 Factor of safety for Option 2, Glacial Till Subgrade E = 41.4 MPa, Subballast E = 241.5 MPa B-60

Fig. 5.112 Factor of safety for Option 2, Glacial Till Subgrade E = 69.0 MPa, Subballast E = 103.5 MPa B-61

Fig. 5.113 Factor of safety for Option 2, Glacial Till Subgrade E = 69.0 MPa, Subballast E = 241.5 MPa B-62

Fig. 5.114 Factor of safety for Option 2, Glacial Till Subgrade E = 103.5 MPa, Subballast E = 103.5 MPa B-63

Fig. 5.115 Factor of safety for Option 2, Glacial Till Subgrade E = 103.5 MPa, Subballast E = 241.5 MPa B-64

Fig. 5.116 Factor of safety for Option 2, Silt/Sand Subgrade E = 6.9 MPa, Subballast E = 103.5 MPa B-65

Fig. 5.117 Factor of safety for Option 2, Silt/Sand Subgrade E = 6.9 MPa, Subballast E = 241.5 MPa B-66

Fig. 5.118 Factor of safety for Option 2, Silt/Sand Subgrade E = 41.4 MPa, Subballast E = 103.5 MPa B-67

Fig. 5.119 Factor of safety for Option 2, Silt/Sand Subgrade E = 41.4 MPa, Subballast E = 241.5 MPa B-68

Fig. 5.120 Factor of safety for Option 2, Silt/Sand Subgrade E = 69.0 MPa, Subballast E = 103.5 MPa B-69

Fig. 5.121 Factor of safety for Option 2, Silt/Sand Subgrade E = 69.0 MPa, Subballast E = 241.5 MPa B-70

Fig. 5.122 Factor of safety for Option 2, Silt/Sand Subgrade E = 103.5 MPa, Subballast E = 103.5 MPa B-71

Fig. 5.123 Factor of safety for Option 2, Silt/Sand Subgrade E = 103.5 MPa, Subballast E = 241.5 MPa B-72

Fig. 5.124 Factor of safety for Option 3, Weak Clay by Hanna and Meyerhof Approach 120

Fig. 5.125 Factor of safety for Option 3, Weak Clay by Hanna and Meyerhof Approach 121

Fig. 5.126 Factor of safety for Option 3, Weak Clay by Hanna and Meyerhof Approach 122

1.0 INTRODUCTION

In 1982, Professor D.G. Fredlund of the Geotechnical Group at the University of Saskatchewan, Saskatoon, Saskatchewan, proposed a four-stage research program to develop a better understanding of the role played by soil suction in the behaviour and design of track system subgrades. Earlier work, now completed, was undertaken jointly with Clifton Associates Ltd., Regina, Saskatchewan, and was devoted to an investigation of suitable methods for measuring soil suction in the field. The soil suction data was collected on a continuing basis from five field sites in western Canada. A proposal for the second stage of the project was approved in October 1987 and work commenced on this project in November 1987. This report details the work performed for the second stage of the project.

Having studied techniques and procedures for measuring soil suction in the first stage of the program, the next stage of research concentrates on the incorporation of the soil suction term into a workable design procedure. The objective of the most recent research was to develop a bearing capacity design procedure for the railway-ballast-subballast-subgrade system, incorporating soil suction into the design procedure. An understanding of the role of soil suction permits the design procedure to utilize the additional strength of the soil resulting from soil suction.

The design procedure which has been developed uses a bearing capacity approach where the strength of the unsaturated soil is related to the stress state, material parameters, soil suction and failure geometry. Two methods are proposed for the estimation of the bearing capacity beneath a loaded tie-track system. The Meyerhof and Hanna approach (1) applies only to weak clay subgrades, whereas the Broms approach (2) is applicable to stronger clay, glacial till, silt and sand subgrades. The soil suction term is incorporated into both procedures.

The stresses beneath the loaded track system are calculated from a computer program called GEOTRACK, which combines the stiffness matrix of the tie-track system with a Boussinesq stress distribution in the ballast-subballast-subgrade system. The estimated bearing capacity of the subgrade system and the stress distribution beneath the loaded track structure are compared in order to develop bearing capacity factor of safety design charts for various combinations of axle load, loading configuration, soil parameters and soil suction.

2.0 STRESS ANALYSIS

One aspect of this project was to perform a stress analysis on the railway subgrade for typical loading configurations and axle loads. This section provides a brief overview to the development of a stress analysis approach to railway design. The development of computer models for stress analysis, and in particular, the GEOTRACK model is reviewed. The utilization of the GEOTRACK model for the stress analysis part of the bearing capacity approach to railway design is presented in some detail in this section and in full detail in the GEOTRACK user's manual.

2.1 The Development of a Stress Analysis Approach to Railway Design

The most notable contributions to a stress analysis approach to railway design are those of Talbot (3). Talbot first identified the rails as flexible beams which rest upon flexible supports (ties), noting that the ballast and subgrade are also flexible and yielding. Due to the stiffness of the rail and the yielding of its supports, the load from a wheel will be distributed over a number of ties. In addition, the spacing of the wheels on the railway cars longitudinally along the track influences the division of load. This complexity of interactions among the various elements of the tie-track system led to the simplification of the problem for analysis purposes. It was assumed that the rail-tie system acted as a beam continuously supported on a homogeneous, elastic medium. This became known as the beam-on-elastic-foundation approach.

At the same time that railway design approaches were being developed, procedures were evolving for computing stress distributions beneath a loaded structure. In 1885, Boussinesq, a French mathematician derived a formula to compute the vertical stress at any depth and any horizontal distance from a point load in a homogeneous, elastic, isotropic body (4). A comparison of the stress distribution computed by Talbot to the stress distribution computed by Boussinesq indicates that the results are similar (5). The results of Boussinesq have been extended to accommodate load distributions for line loads and plate loads in addition to point loads. The computations were made by superimposing the influence of the load at various points and publishing the influence coefficients in the well-known Newmark charts (6).

The first contribution to the development of theories of stress distribution beneath a layered system were presented by Burmister in his analyses of airport runways (7). Burmister solved the three-dimensional problem for general two- and three-layer systems in a form which permitted the solution throughout the depths of all layers, and for all relative strengths of the layers. The results of Burmister's solutions have been published in chart form by Poulos and Davis (8).

The computer age of the 1970's and 1980's has advanced the use of mathematical models to predict the stresses beneath the complex tie-track structure. Numerous two- and three-dimensional models have been proposed to represent the tie-track system.

2.2 The Development of the GEOTRACK Model

Four often-referenced computer models are the ARTS, PSA, ILLITRACK, and MULTA models (9). The Analysis of Rail Track Structures (ARTS) model is a three-dimensional finite element model which has been partially successful in correlation with full scale model data and readily involves exhorbitant computing costs (10). The ILLITRACK model is a psuedo-three-dimensional model incorporating two plane strain finite element models which analyze the structure in perpendicular directions in the horizontal plane (11). The ILLITRACK model was developed in response to the need to simplify the analyses and reduce computer costs. The reduction in computing costs has been at the expense of accuracy. The Prismatic Solid Analysis (PSA model) is really a system of multiple three-dimensional finite element models used to predict the stresses and strains in the various track components (12). As a result, computational costs are exhorbitant and considerable time and labour is required to create the data input.

The MULTA model was developed as a combination of two models developed by the Association of American Railroads (13). The three-dimensional finite element model called LAC is used for the superstructure analysis whereas the Burmister multi-layer elastic substructure model is used for analysis of the layered ballast-subgrade system. The MULTA model allows unrealistic tensions to develop between the tie and the ballast. Furthermore, the nonlinear and stress-dependent characteristics of the substructure cannot be modelled. However, the MULTA model does provide satisfactory comparisons with the dynamic data available from the Facility for Accelerated Service Testing in Pueblo, Colorado.

The GEOTRACK model was developed by Chang, Adegoke and Selig in 1978 as a modification of MULTA for studying the behaviour of the substructure (14). GEOTRACK uses an iterative procedure to vary the resilient modulus for the stress state in each layer. Stresses and moduli are varied until a converged solution is obtained. The model provides improved characterization of the trackbed materials by including stress-dependent nonlinear behaviour.

Figures 2.1 through 2.4 illustrate a comparison of the GEOTRACK model with some of the other computer models discussed in this section. A comparison of predicted rail deflections is shown in Figure 2.1. Figure 2.2 compares the models on the basis of predicting rail seat load. Figures 2.3 and 2.4 present comparisons between the GEOTRACK model and other models on the basis of predicted vertical stress at the ballast surface and at the subgrade surface, respectively. A comparison of predicted outputs between the GEOTRACK model and the MULTA model reveals that the GEOTRACK model is comparable to the MULTA model in prediction accuracy.

Figure 2.5 illustrates a comparison of the GEOTRACK model to data available from the FAST track, Pueblo, Colorado for the subgrade stress as a function of various wheel loads. The analytical predictions compare well with the dynamic data available from the FAST track. Stewart and

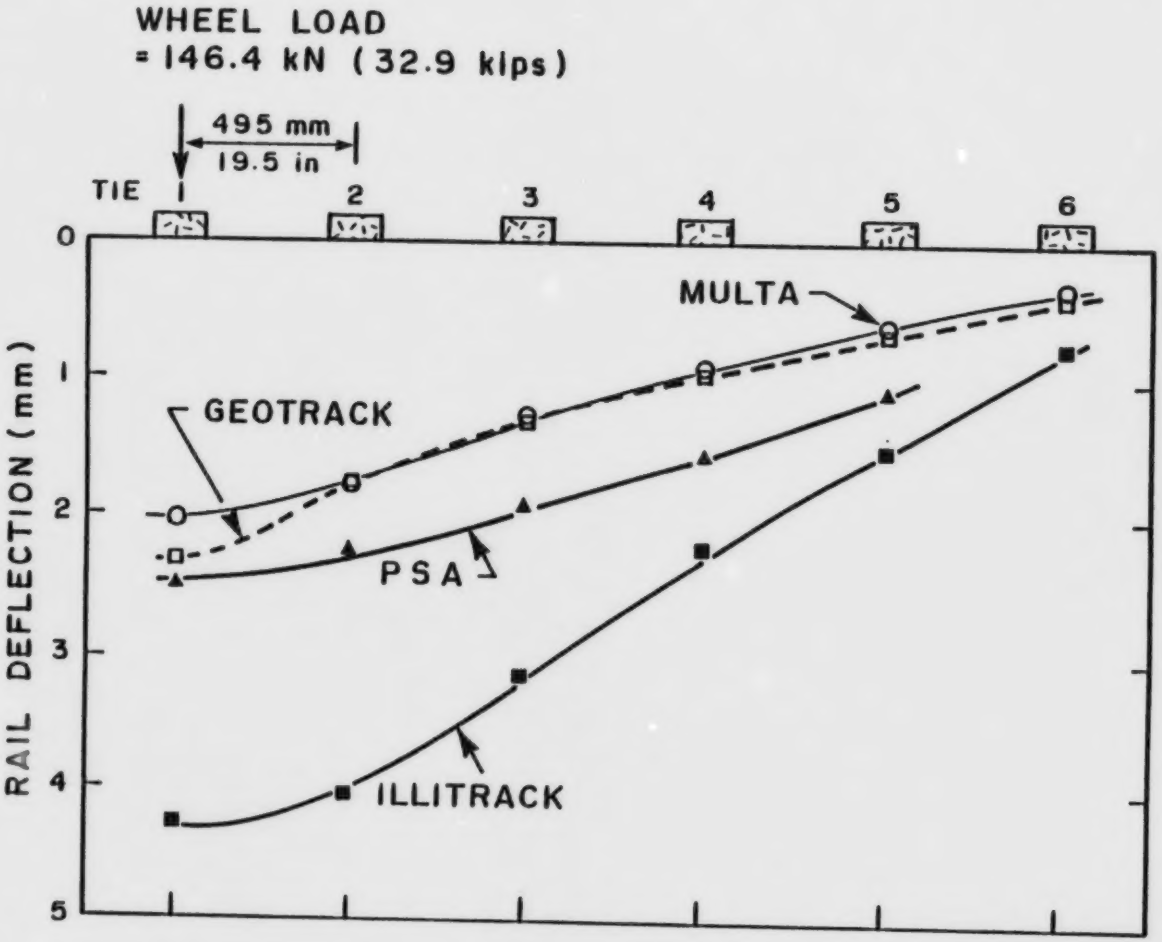

Fig. 2.1 Comparison of computer models on the basis of predicting rail deflections (adapted from Stewart and Selig (15))

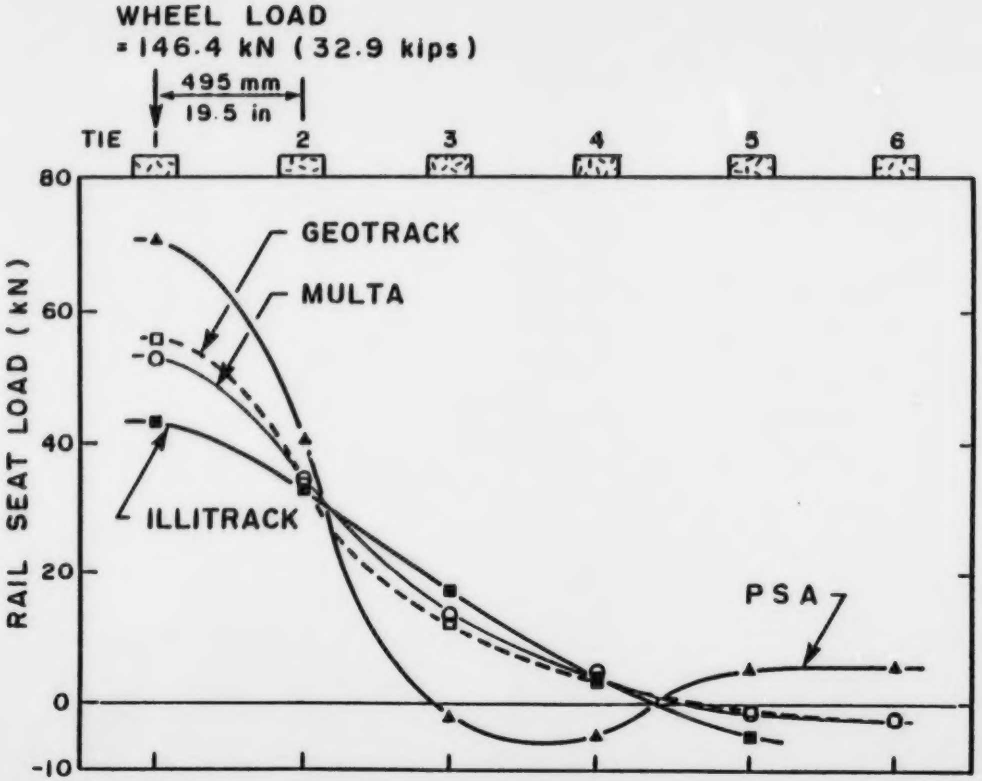

Fig. 2.2 Comparison of computer models on the basis of predicting rail seat load (adapted from Stewart and Selig (15))

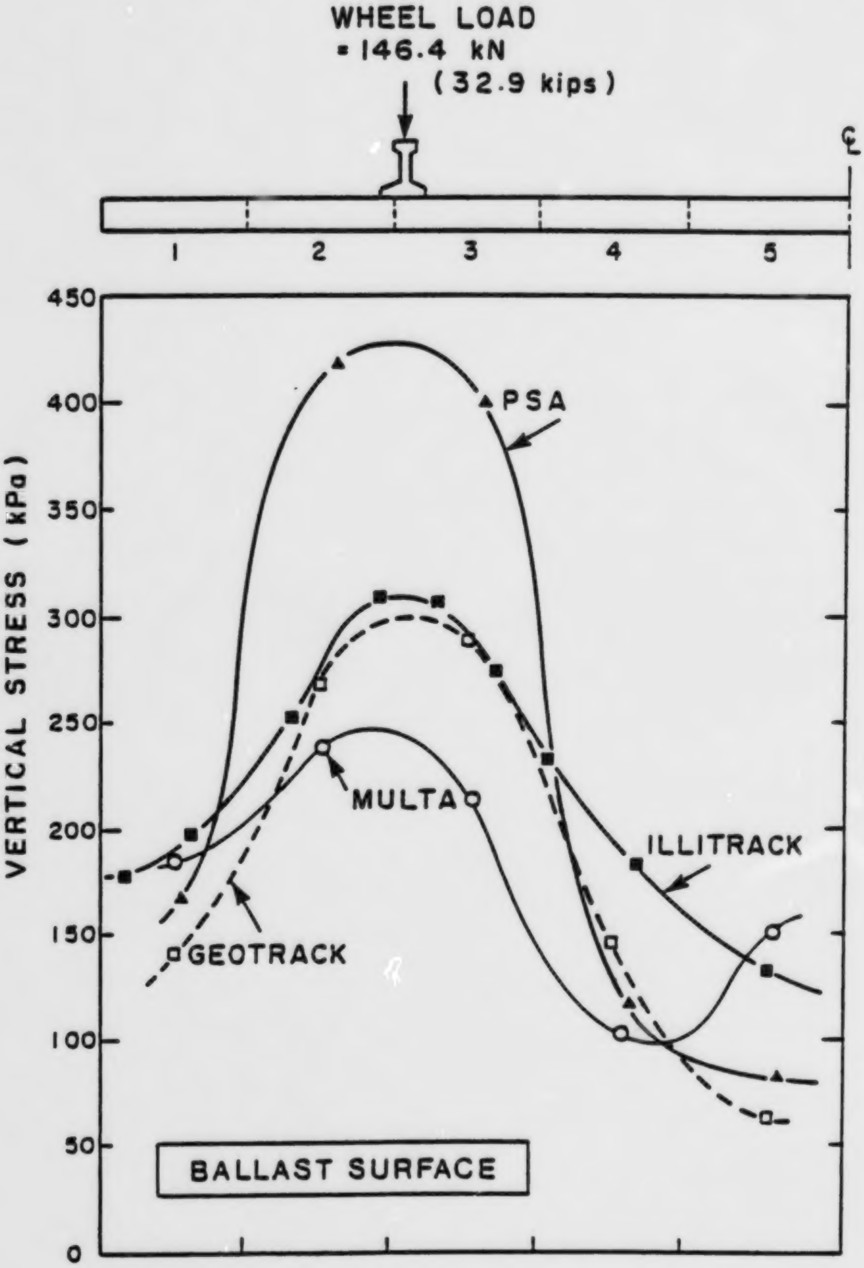

Fig. 2.3 Comparison of computer models on the basis of predicting vertical stress at the ballast surface (adapted from Stewart and Selig (15))

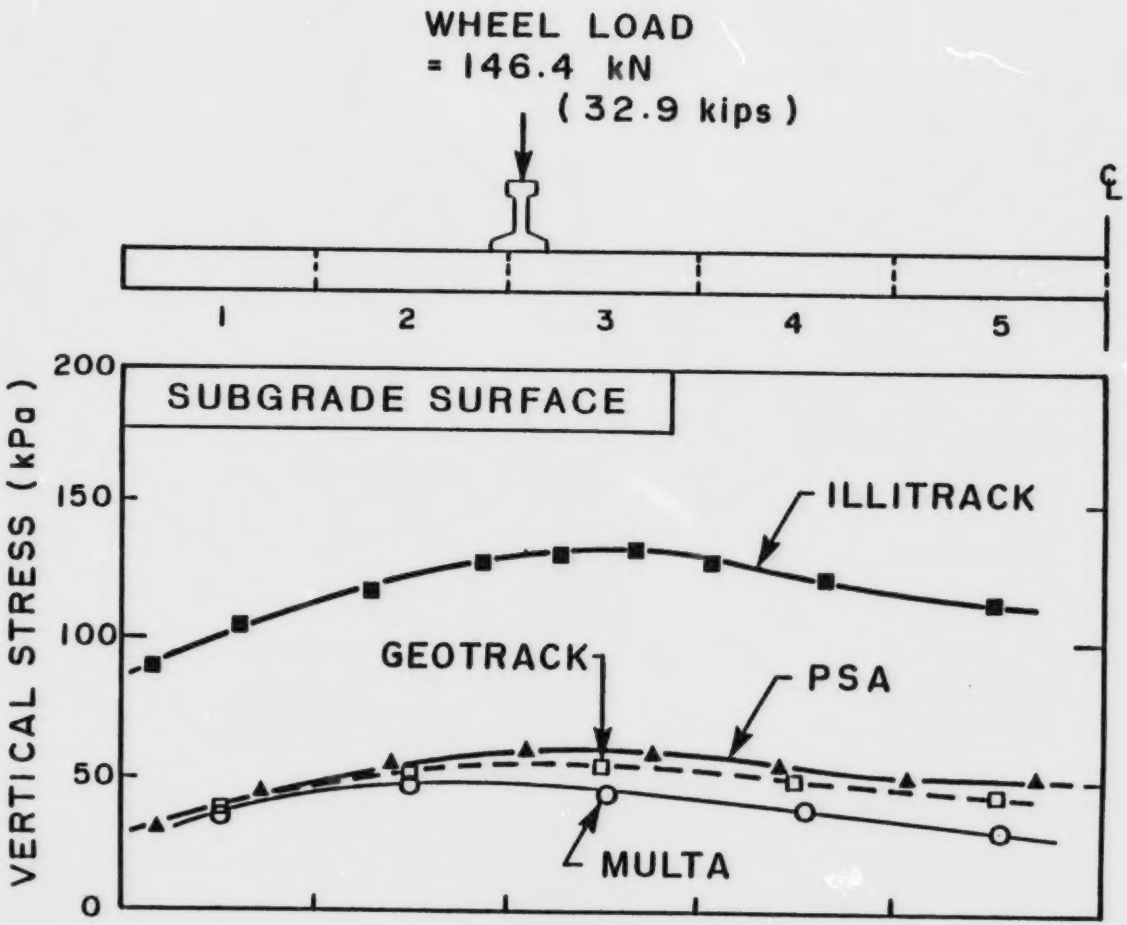

Fig. 2.4 Comparison of computer models on the basis of predicting vertical stress at the subgrade surface (adapted from Stewart and Selig (15))

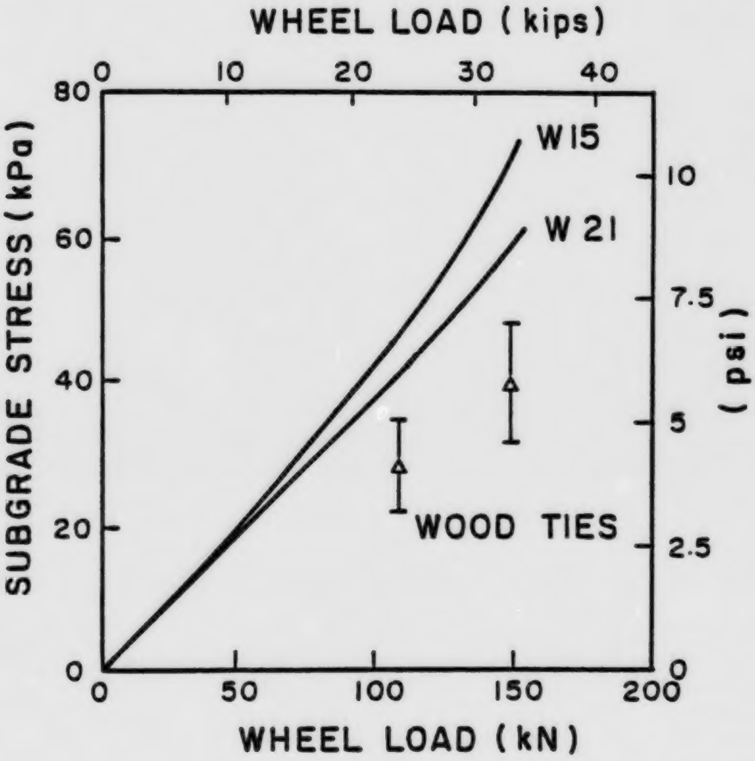

Fig. 2.5 Comparison of GEOTRACK simulation data to FAST track data (adapted from Stewart and Selig (15))

Selig (15) suggest that reasonable comparisons between the GEOTRACK model and the FAST track data occur consistently.

2.3 The GEOTRACK Model

GEOTRACK is a three-dimensional, multi-layer model for railroad track elastic response considering stress dependent material properties and the separation of the tie and ballast. The GEOTRACK model emphasizes the geotechnical aspects of track behaviour providing a complete three-dimensional stress state at any specified location within the track bed.

The rails and ties are represented by linear elastic beams with a specified modulus of elasticity, cross-sectional area, and moment of inertia. Stress is distributed from the rail to the tie and from the tie to the ballast in the form of concentrated reactions. Figure 2.6 provides a pictorial representation of how the model functions.

The ballast, subballast, and subgrade soil are represented as linear elastic layers each specified by a separate modulus of elasticity and Poisson's ratio. All layers are infinite in the horizontal plane and are situated on a half space, which is infinite in the vertical and horizontal directions.

The multi-layer system is used to develop stress and displacement influence coefficients. Compatibility of displacements and equilibrium of forces between the bottom of the rail-tie structure and the top of the foundation are then imposed to effect an overall solution to the system. The flexibility matrix for the foundation is combined with the flexibility matrix of the rail-tie system to produce a set of simultaneous equations which are solved for the stresses and

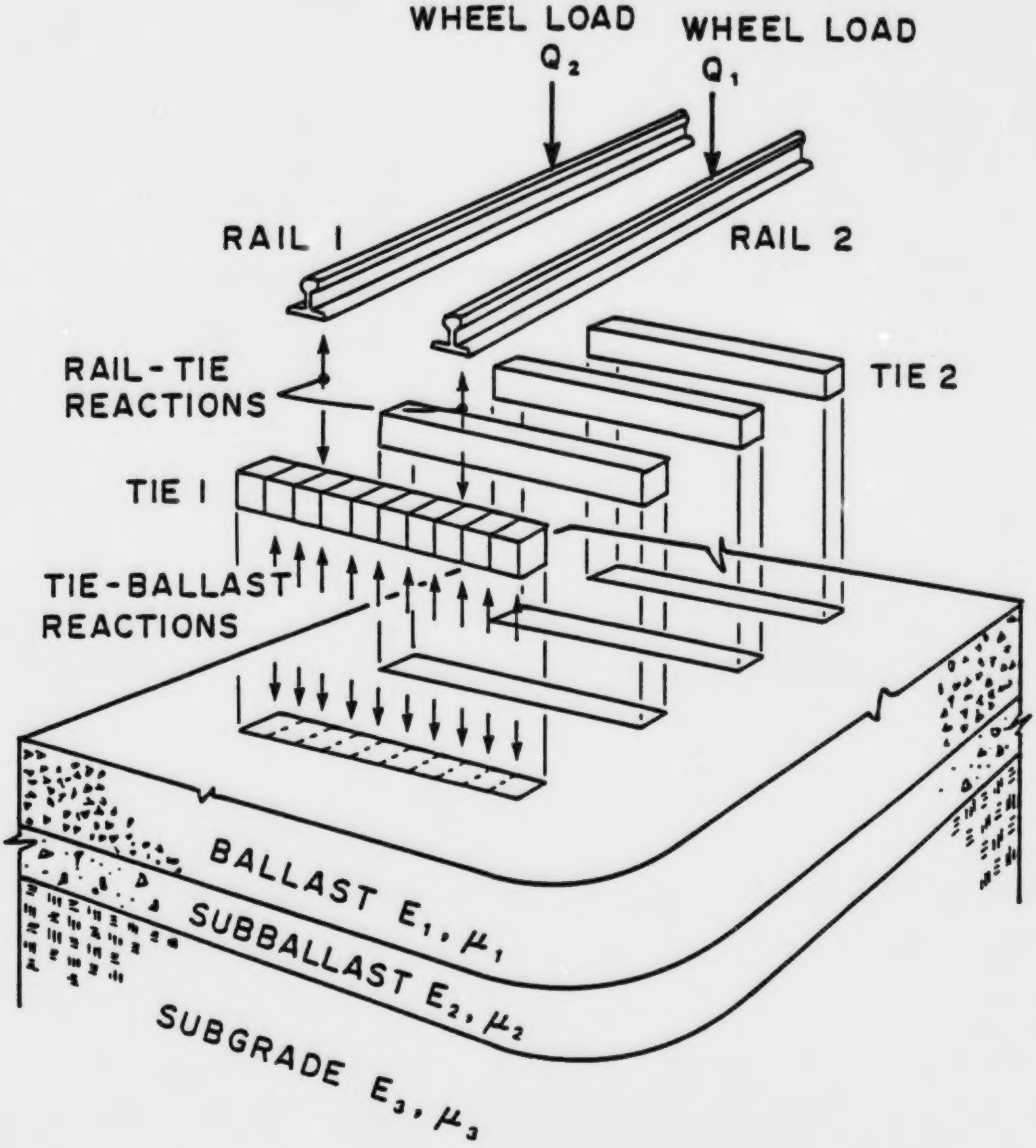
WHEEL LOAD
Q_2
WHEEL LOAD
Q_1
RAIL 1
RAIL 2
RAIL-TIE
REACTIONS
TIE 2
TIE 1
TIE-BALLAST
REACTIONS
BALLAST E_1, μ_1
SUBBALLAST E_2, μ_2
SUBGRADE E_3, μ_3

Fig. 2.6 Forces and elements in the GEOTRACK model (adapted from Chang, Adegoke and Selig (14))

displacements at the contact points between the superstructure and the substructure and the stresses and displacements at the desired locations within the layered soil system.

The GEOTRACK model was chosen to predict stresses in the subgrade for the purpose of the bearing capacity analysis. The use of the model is discussed in the next section.

2.4 Use of the GEOTRACK Computer Model in a Bearing Capacity Approach to Railway Design

In addition to computing rail-tie reactions, tie-ballast reactions, tie and rail deflections, and tie and rail bending moments, the GEOTRACK model is capable of computing the deflection and complete three-dimensional stress state at any location in the road bed. Output from the GEOTRACK computer model includes the principal stresses, the equivalent triaxial stresses, and the vertical, horizontal and shear stresses. Solutions are available for single axle and truck loading. Up to five different soil layers can be accommodated with a choice of eight unique stress dependent moduli relationships.

A post-processing graphics package was developed through this project. The computer program GEOPLOT graphs the output from the GEOTRACK model. The details on all computer programs are presented in the user's manuals included in a separate document. Figures 2.7 and 2.8 show typical vertical stress output produced by the GEOTRACK model and graphed by the post-processing package GEOPLOT. Figure 2.7 illustrates the vertical stresses beneath an individual tie for a view perpendicular to the track structure. Figure 2.8 illustrates the vertical stresses beneath one section of the track for a view parallel to the track

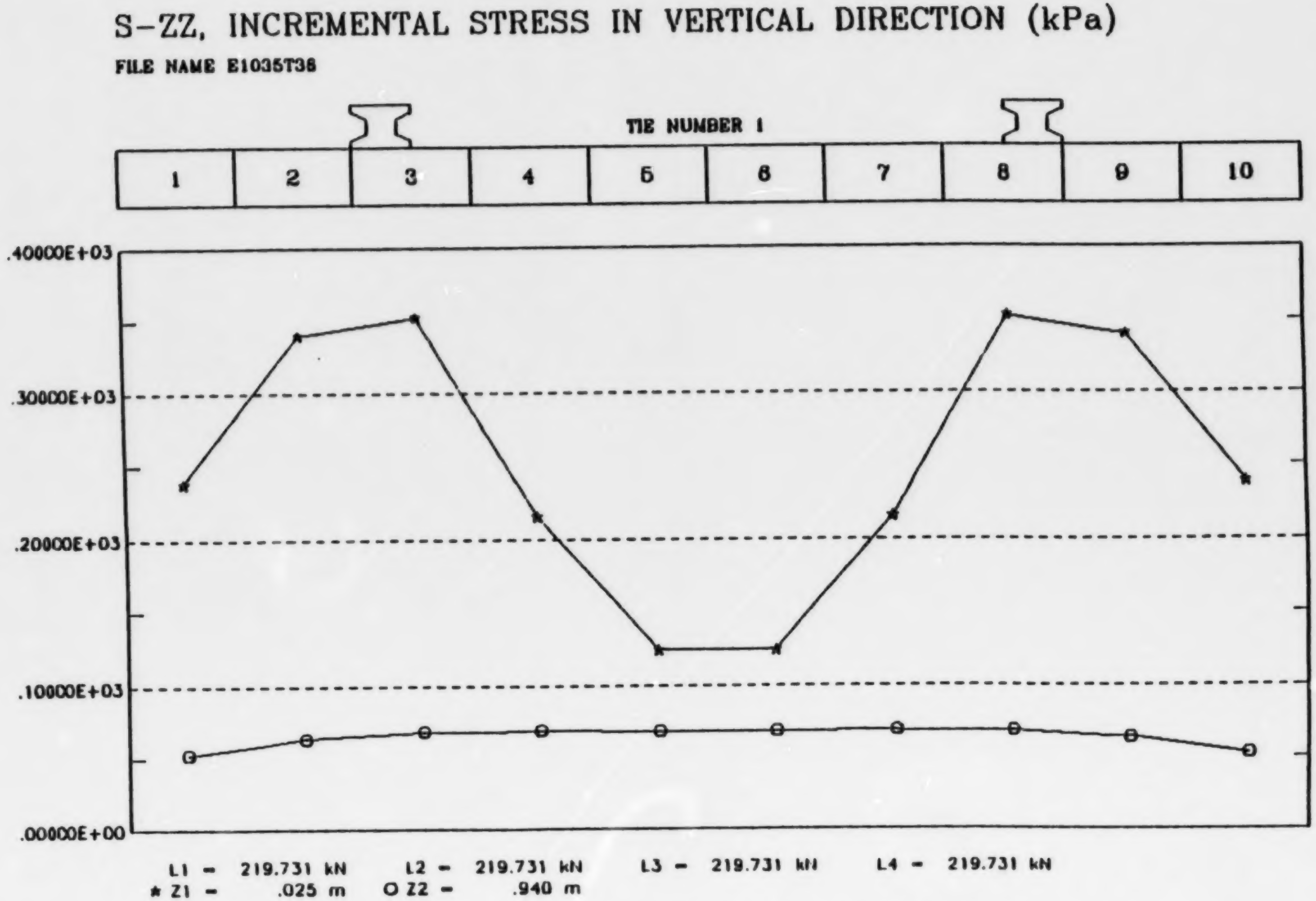

Fig. 2.7 GEOPLOT computer-generated graph showing vertical stress beneath an individual tie

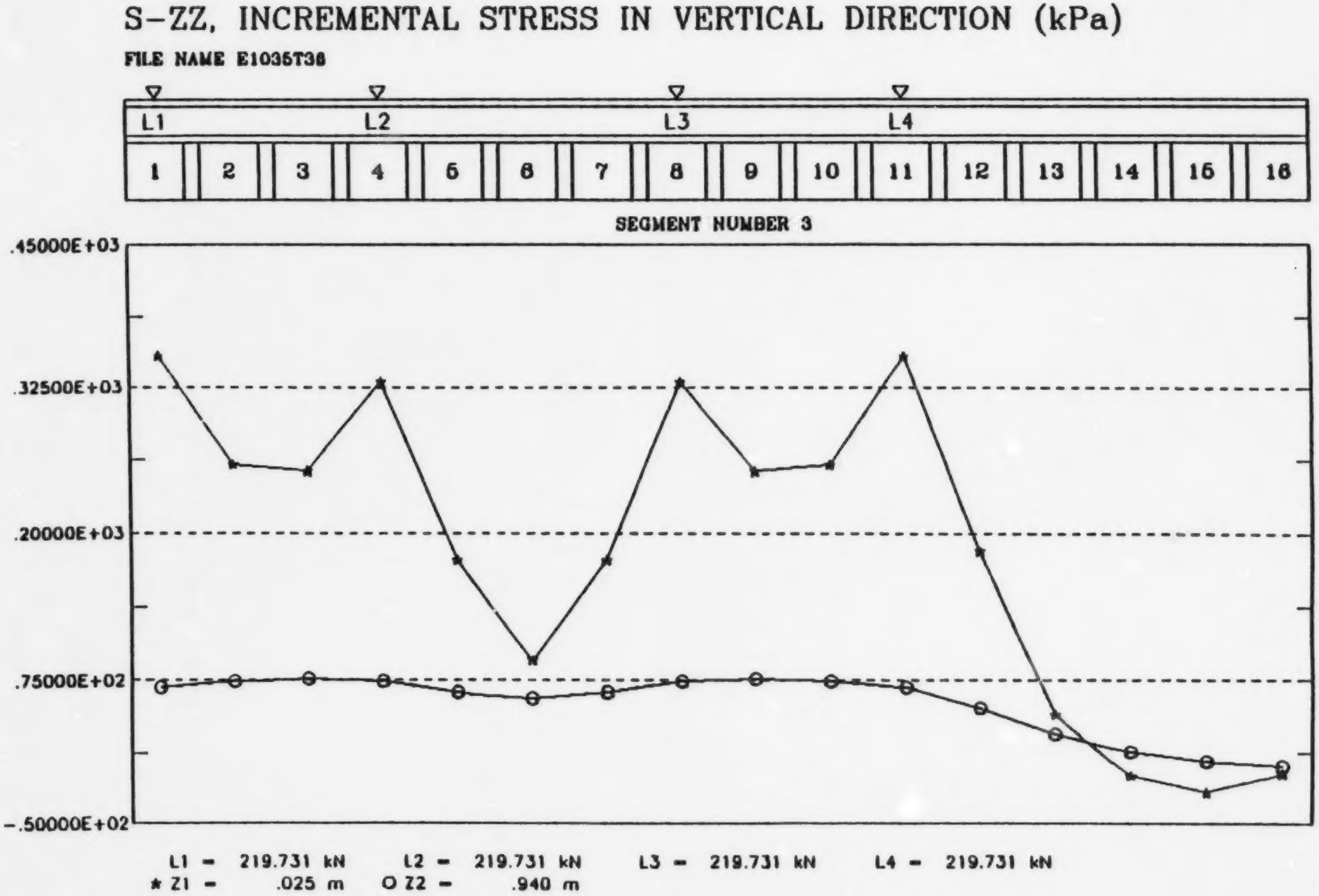

Fig. 2.8 GEOPLOT computer-generated graph showing vertical stress beneath one tie segment for all ties

structure. Additional representative graphic output is presented in the GEOPLOT user's manual.

The vertical stress at the ballast surface and the vertical stress at the subgrade surface, illustrated in Figures 2.7 and 2.8, are important to the bearing capacity design approach developed in this project. The GEOTRACK model was used to predict the vertical stress at each of the ballast and subgrade surfaces. This was accomplished using the GEOTRACK model for the maximum five soil layers (i.e., one ballast, two subballast and two subgrade layers) and two additional depth points (i.e., the ballast surface and the subgrade surface, actually 25 millimeters (1 inch) below each of the ballast and subgrade surfaces because the GEOTRACK model cannot accommodate specifications at the contact point between soil layers).

It was important that the ballast and subgrade surface depths were chosen as additional depth points. This allowed the soil parameters to be input as an average at the center of the layers depicted, thus allowing for greater accuracy in the predicted stresses. The significance of using additional depth points to represent the ballast and subgrade surfaces will become evident from the GEOTRACK user's manual and as the user becomes familiar with using the GEOTRACK computer program.

For the purposes of the bearing capacity design approach which has been developed, the GEOTRACK program was used without allowing the soil moduli to converge within the soil layers. If the moduli had been allowed to converge, the design charts presented in Sections 5.2 and 5.4 could not have been developed for specific moduli values. The design charts which have been developed may be used for the normal working range of soil moduli. Track systems placed upon weak soils, which exhibit low moduli values, should be designed using the GEOTRACK computer program for a complete stress analysis with moduli convergence.

A sensitivity analysis was performed using the GEOTRACK computer model to determine which parameters were of most significance to the output generated. Figures 2.9 through 2.14 present results of the sensitivity analysis which was performed for this project. Stewart and Selig (15) describe a more complete sensitivity analysis which was performed using the GEOTRACK model. The research undertaken as a part of this project confirms the findings of Stewart and Selig.

Figure 2.9 illustrates the sensitivity of the vertical stress to changing the axle load. As might be expected, an increase in the axle load increases both the ballast stress and the subgrade stress. Doubling the axle load essentially doubles the ballast surface stress and almost doubles the subgrade surface stress.

Figure 2.10 illustrates the sensitivity of the GEOTRACK output to changing the ballast modulus. The analysis was performed eliminating the subballast layers to reduce the number of variables. The diagram shows that increasing the ballast modulus increases the ballast stress while decreasing the stress at the subgrade surface. This suggests that as stronger ballast material is utilized, more of the stress is distributed through the ballast material.

Sensitivity of the vertical stresses to changing the subgrade modulus is shown in Figure 2.11. Increasing the subgrade moduli increases the stress which is distributed to the subgrade. At the same time, however, it should be noted that the subgrade bearing capacity would also increase. The stress at the ballast surface changes a small amount as

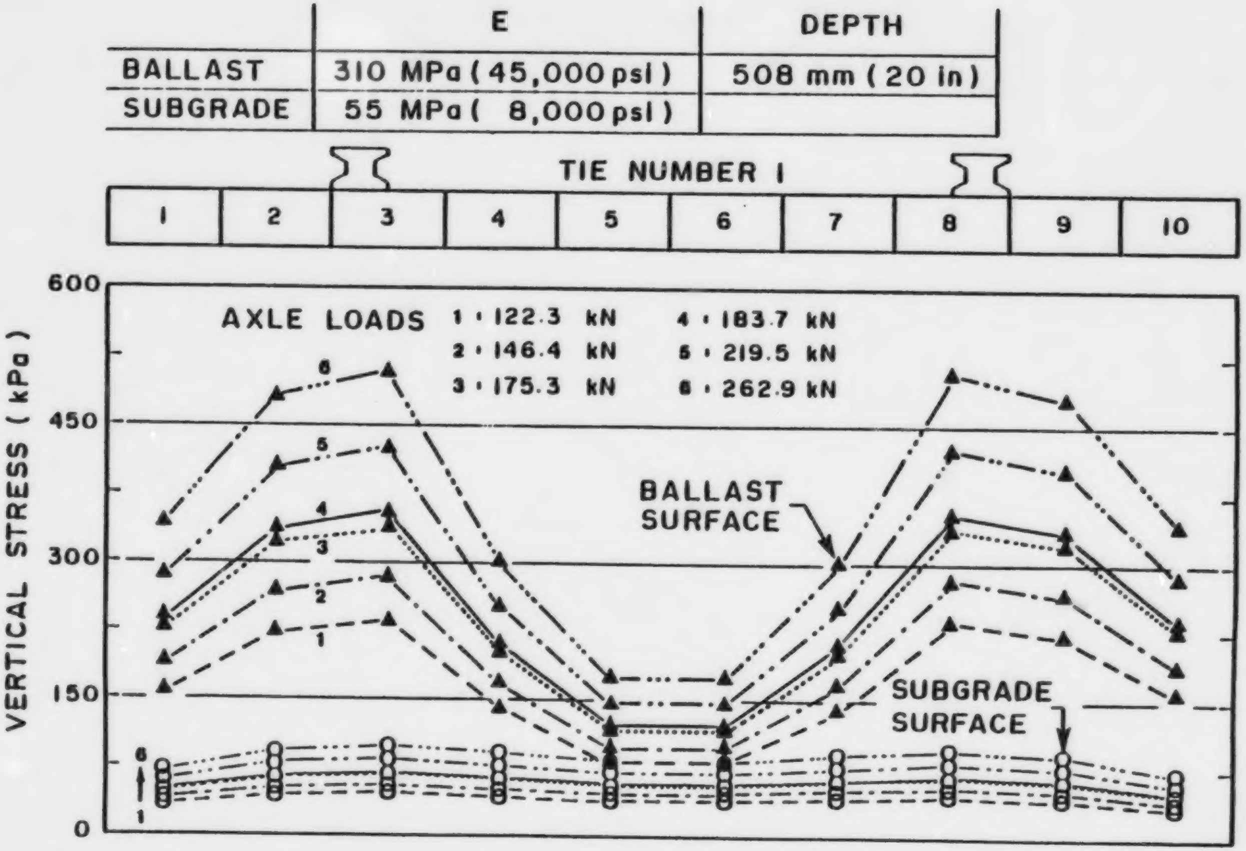

Fig. 2.9 Sensitivity of vertical stress output to changing axle load

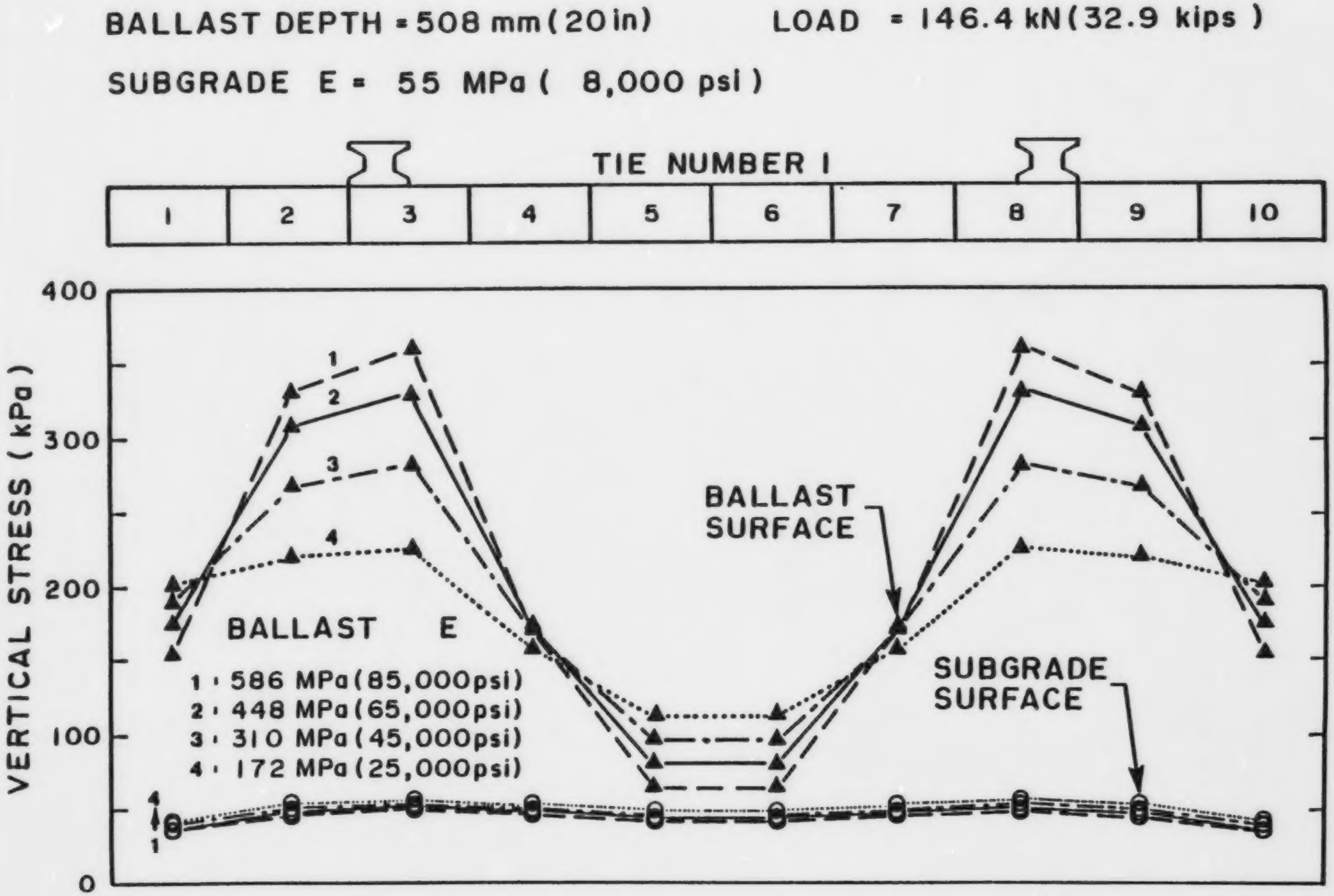

Fig. 2.10 Sensitivity of vertical stress output to changing ballast modulus

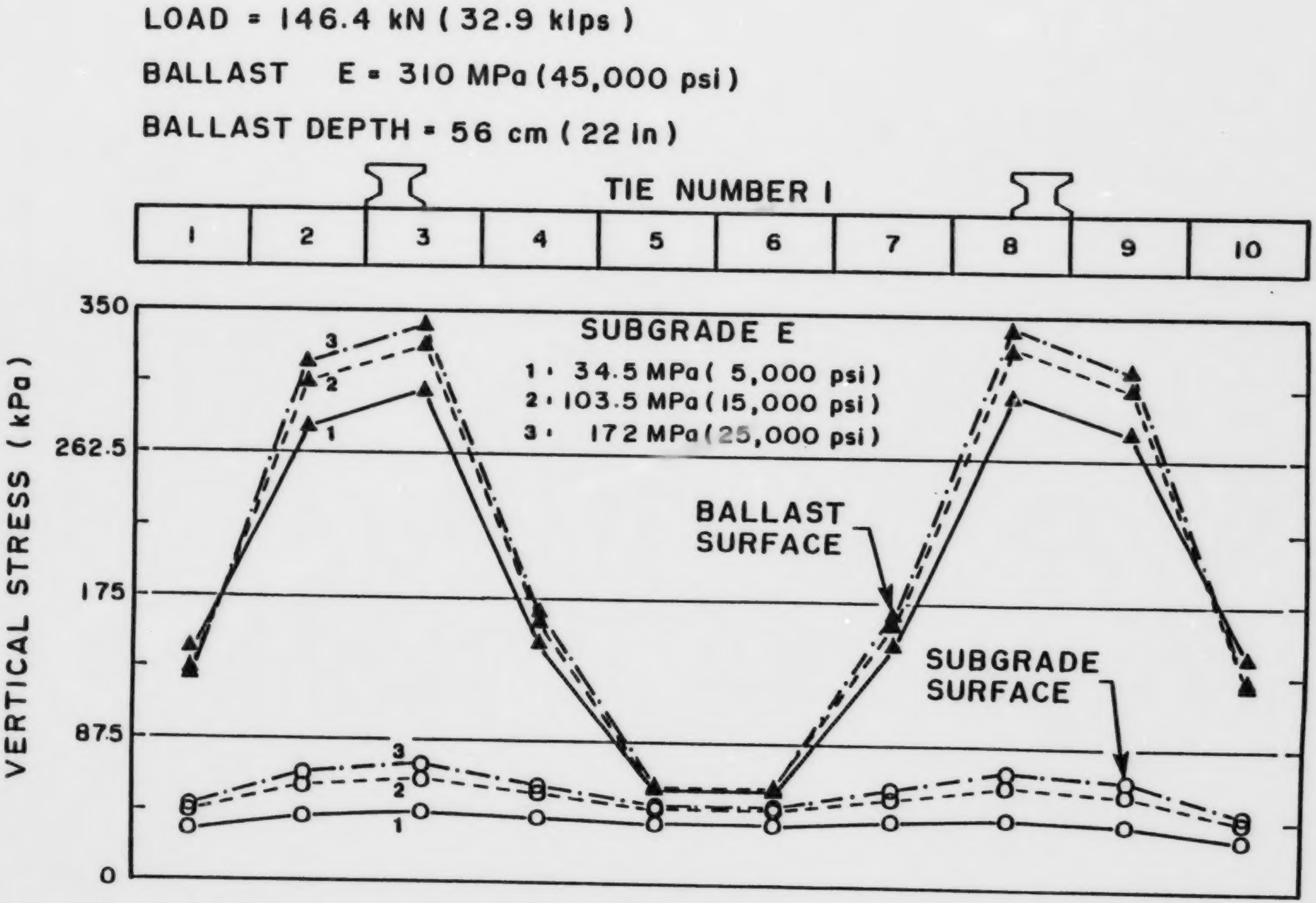

Fig. 2.11 Sensitivity of vertical stress output to changing subgrade modulus

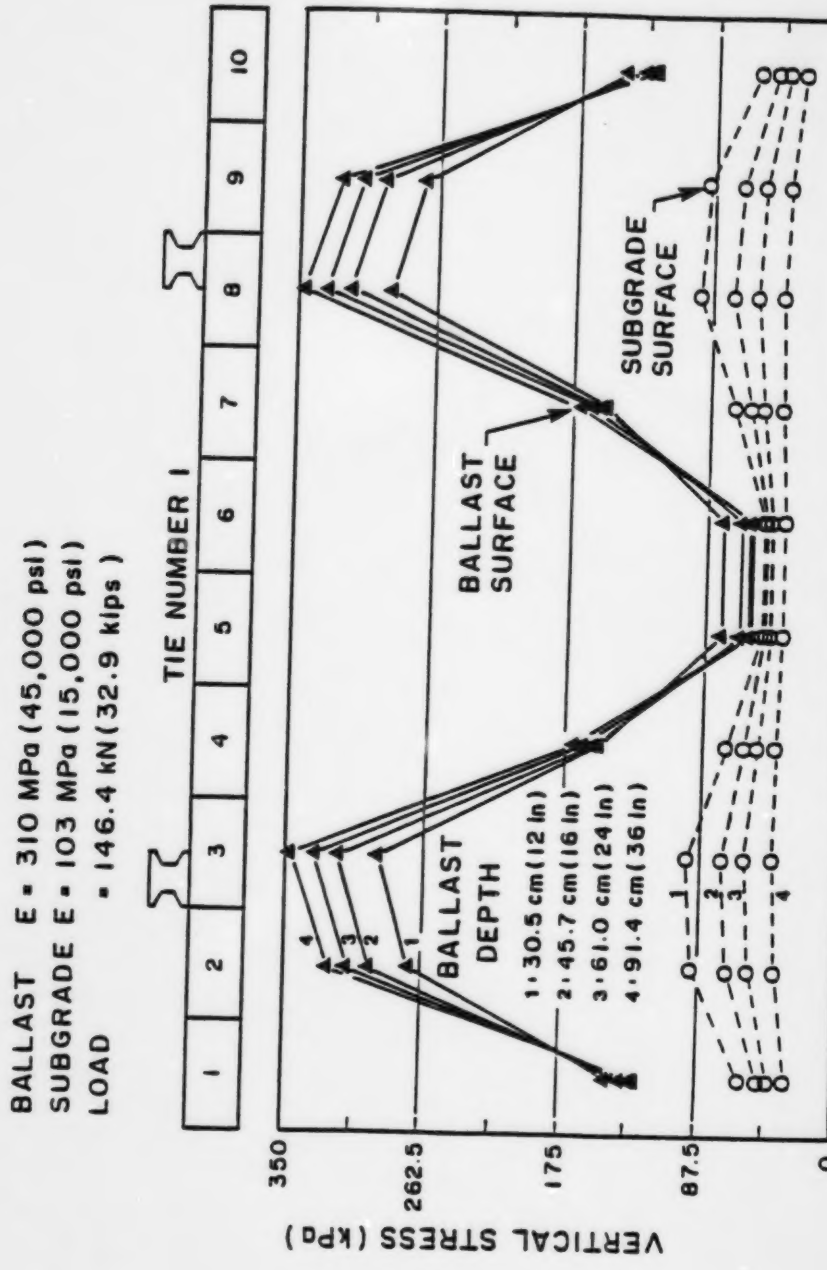

Fig. 2.12 Sensitivity of vertical stress output to changing ballast depth

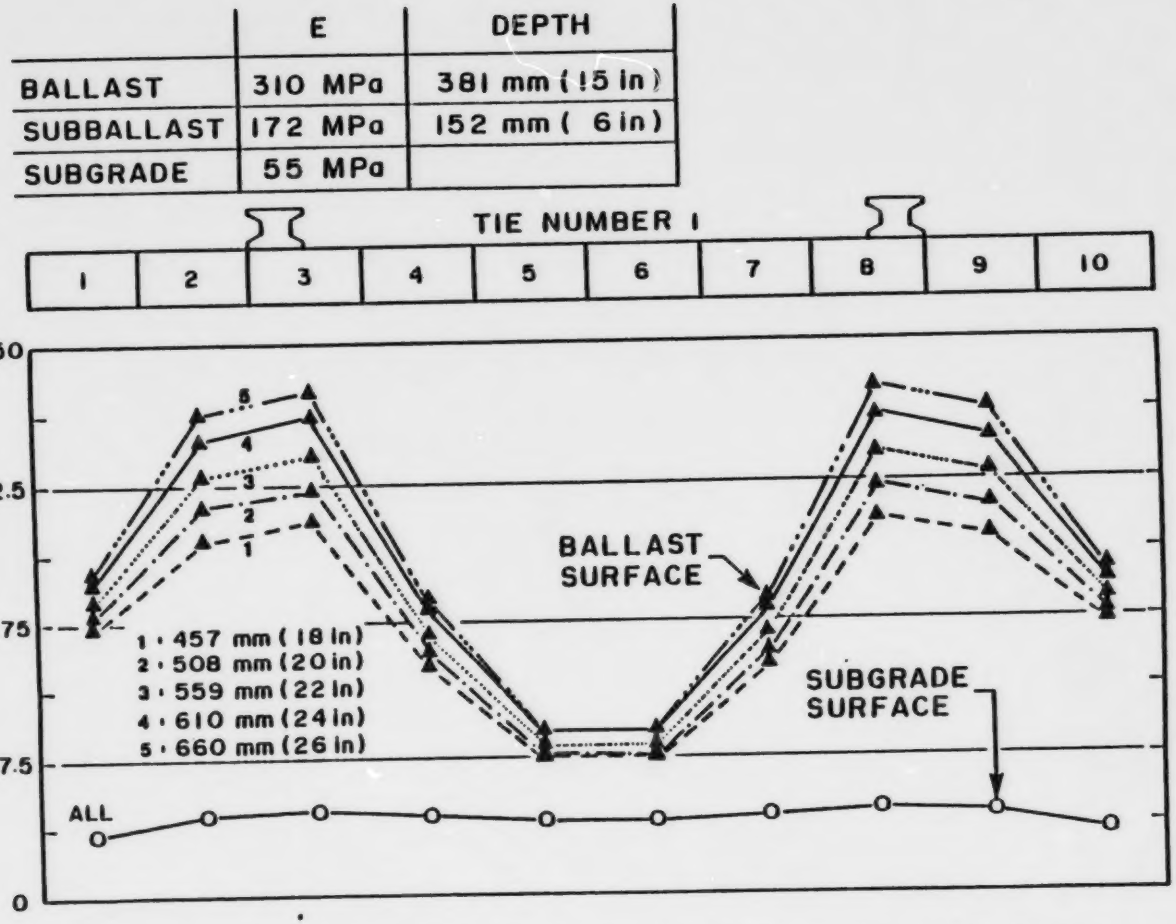

	E	DEPTH
BALLAST	310 MPa	381 mm (15 in)
SUBBALLAST	172 MPa	152 mm (6 in)
SUBGRADE	55 MPa	

Fig. 2.13 Sensitivity of vertical stress output to changing tie spacing

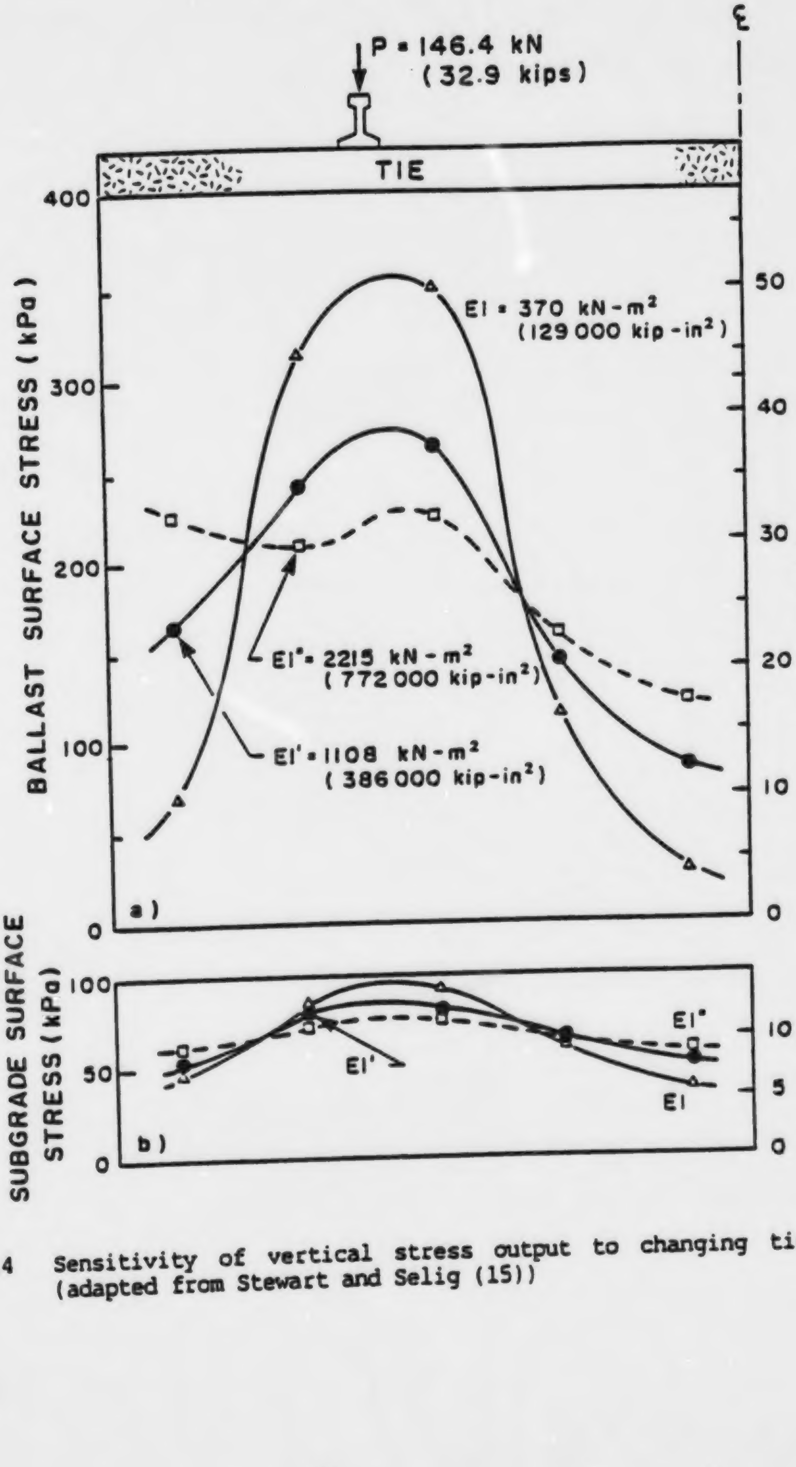

Fig. 2.14 Sensitivity of vertical stress output to changing tie EI (adapted from Stewart and Selig (15))

the subgrade moduli is varied.

Figure 2.12 shows what happens when the ballast depth is increased. As might be expected, increasing the depth of ballast reduces the stresses at the subgrade surface. Reducing the stress at the subgrade surface represents one of the primary functions of the ballast, so it is important for the model to properly represent this feature.

Changing the tie spacing has no significant effect on the subgrade surface stress as illustrated in Figure 2.13. However, the ballast surface stress increases considerably as the tie spacing is increased. Figure 2.14 illustrates the sensitivity of the ballast and subgrade stresses to the tie EI (i.e., repeated loading modulus multiplied by the tie moment of inertia) values. Again the ballast surface stress is sensitive to changing the tie parameters whereas the subgrade surface stress is not significantly sensitive to changing the tie EI values.

An outcome of the sensitivity analysis on the GEOTRACK model was the decision to vary the axle load, the subgrade E modulus, the subballast E modulus, and both the ballast depth and the subballast depth. The ballast E modulus was kept constant since ballast material is generally of consistent quality. The tie spacing and tie parameters were kept constant for the stress analysis portion of this project. However, the reader may wish to adjust the final stress analysis results to reflect the tie parameters that suit the needs at hand.

The values of the various parameters utilized in the stress analysis are discussed in Section 4.1 GEOTRACK Parameters.

3.0 BEARING CAPACITY

This section describes the development of a bearing capacity approach to railway design, the Broms' approach (2) to bearing capacity and the Meyerhof and Hanna approach (1) to bearing capacity. In addition, technical detail is provided on the geometries of various bearing capacity failures observed in the field.

3.1 The Development of a Bearing Capacity Approach to Railway Design

Characterization of soil strength beneath a loaded structure has long been expressed as a bearing capacity (Terzaghi, (16)). The ultimate bearing capacity is defined as the maximum load that the ground beneath a footing can sustain (i.e., general shear failure). Where the load settlement curve does not exhibit a peak load, the ultimate bearing capacity is taken as the load at which the curve passes into a steep and fairly straight tangent (i.e., local shear failure) (16). The first equations for bearing capacity by Terzaghi were later extended by Meyerhof to include the effects of foundation shape, eccentric loading, base roughness and varying groundwater conditions (17, 18, and 19).

The extension of bearing capacity theories to multi-layered systems was attempted by Broms in 1965 for applications to highway systems (2). The load was assumed to be transferred to the subgrade through the granular material in a 2:1 ratio of width to depth. More recently, Hanna and Meyerhof have extended the conventional bearing capacity equation to layered soils using a punching shear coefficient, thus treating the upper granular material as a continuation of the footing which punches into the weaker subgrade material, in many ways like a driven pile (1).

The extension of conventional soil mechanics to unsaturated soil mechanics has opened the way for determining the bearing capacity of railway subgrades in a less empirical manner. The soil suction term can be incorporated into the bearing capacity equation similar to shear strength extensions of unsaturated soil mechanics. The result is that the ultimate bearing capacity can now be reasonably estimated from measurements of the subgrade shear strength parameters and the subgrade soil suction.

3.2 Bearing Capacity Failure in a Tie-Track System

The determination of a unique value to represent the subgrade bearing capacity requires the choice of a possible mode of failure so that the width and length of the bearing area can be established. This is particularly true for the tie-track system in which the bearing area is an estimated portion of the entire tie-track system.

Figure 3.1 depicts a schematic of the rail-tie-ballast-subballast-subgrade system. A bearing capacity computation is a two-dimensional representation of a three-dimensional failure. The reduction of the three-dimensional problem into two dimensions introduces empiricism into the bearing capacity calculation. Further assumptions must be entertained with respect to the tie-track system to view any one failure geometry on the continuous tie-track system as a two-dimensional problem. However, observations of certain failure mechanisms in the field enable the tie-track system to be simplified into a limited number of failure configurations.

Two overall configurations must be considered for the bearing capacity analysis: 1) the geometry perpendicular to the track and 2) the geometry parallel to the track. Figure 3.2 illustrates a sectional view perpendicular to the track whereas Figure 3.3 illustrates a sectional view parallel to the track. Field observations reveal two failure

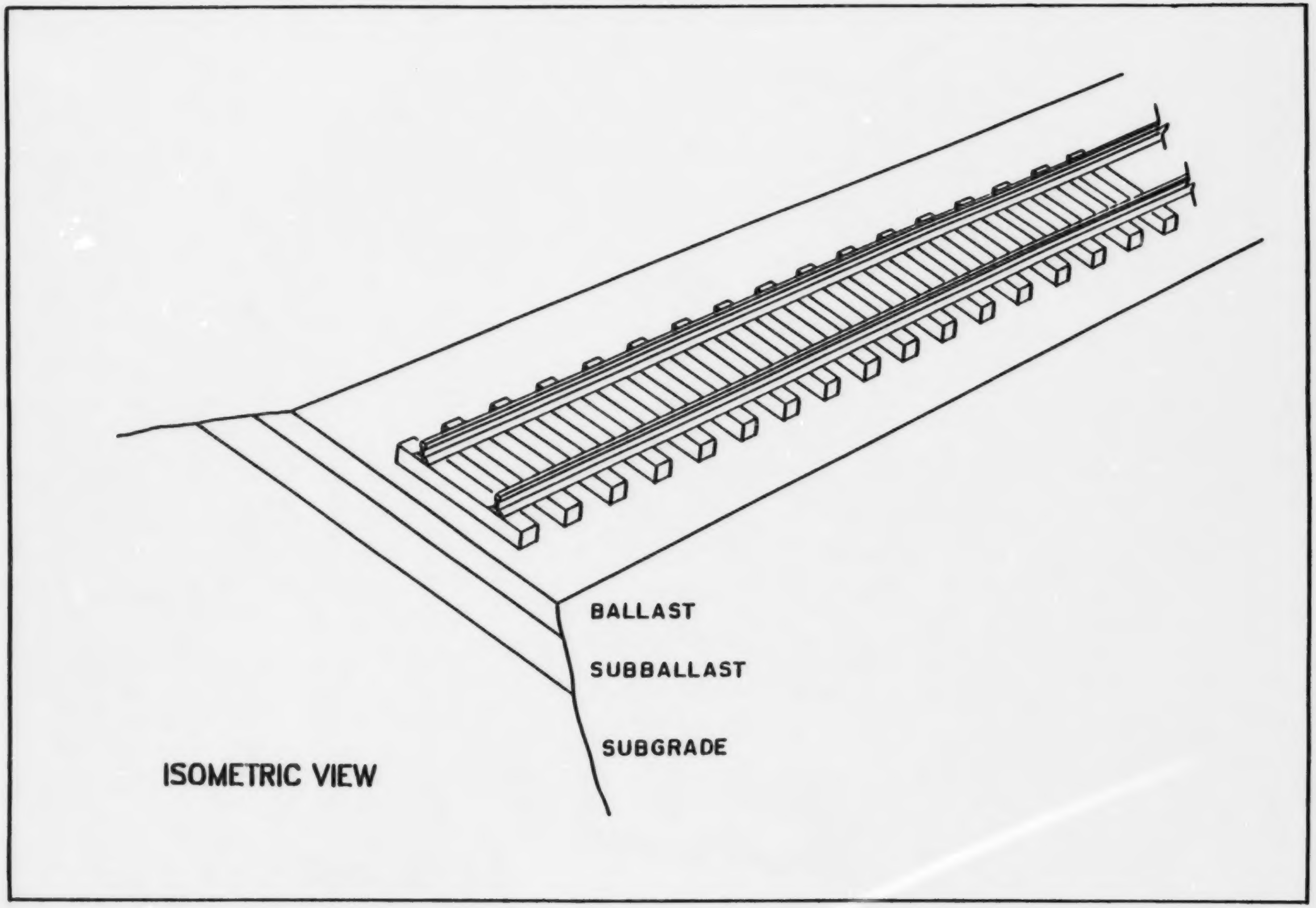
BALLAST
SUBBALLAST
SUBGRADE
ISOMETRIC VIEW

Fig. 3.1 Three-dimensional view of the rail-tie-ballast-subballast -subgrade system

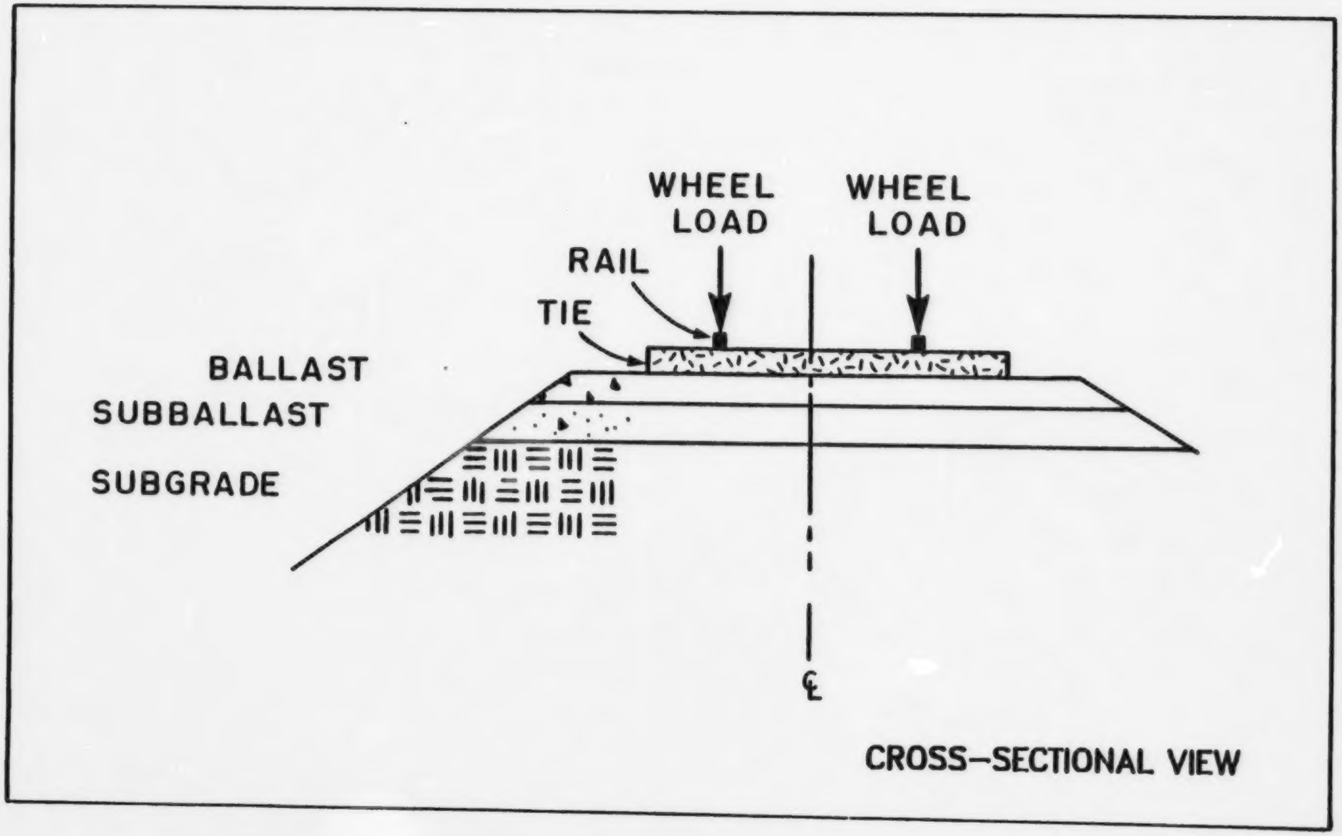
WHEEL
LOAD
WHEEL
LOAD
RAIL
TIE
BALLAST
SUBBALLAST
SUBGRADE
℄
CROSS-SECTIONAL VIEW

Fig. 3.2 Cross-sectional view of the track system showing the geometry perpendicular to the track

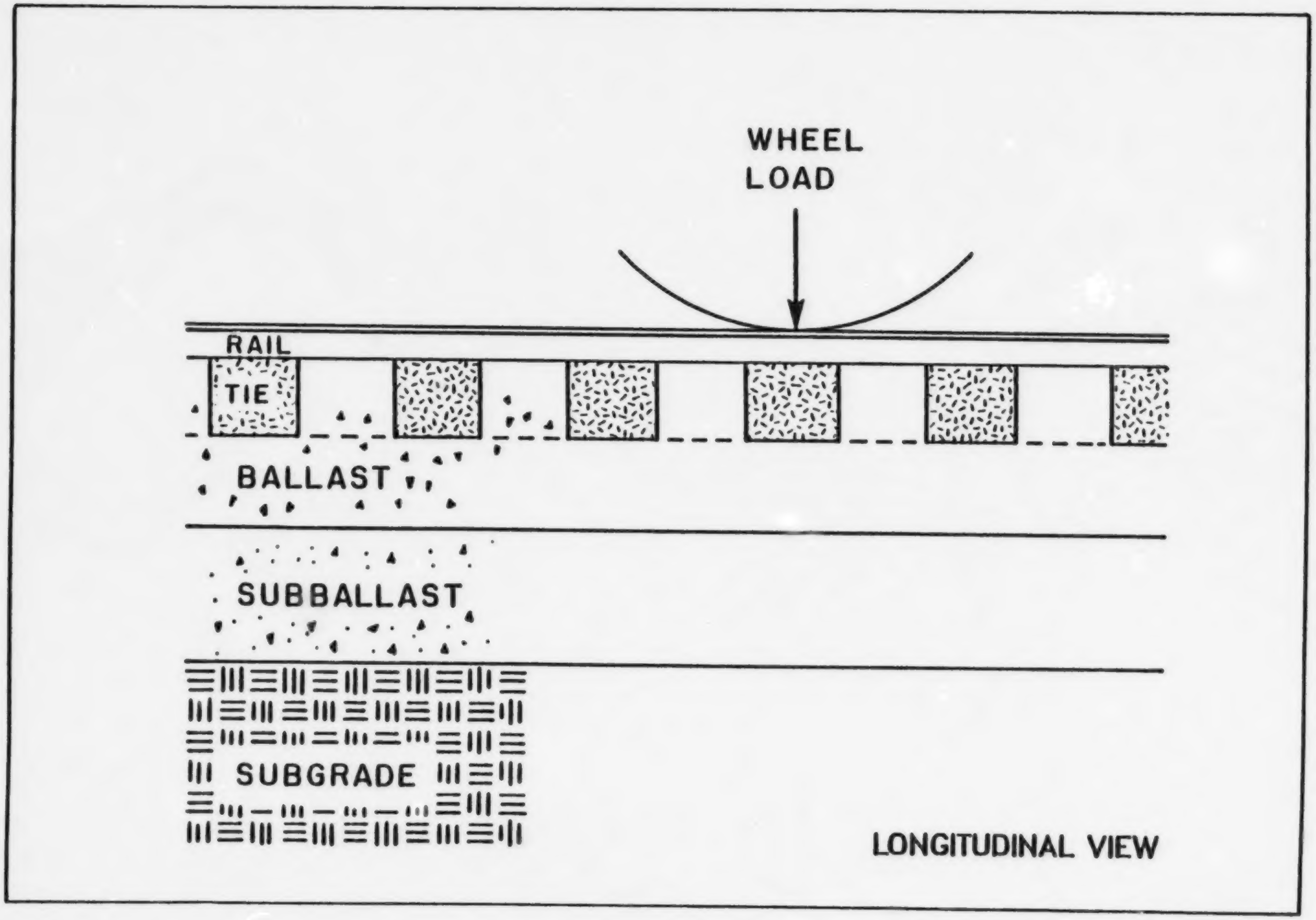
WHEEL
LOAD
RAIL
TIE
BALLAST
SUBBALLAST
SUBGRADE
LONGITUDINAL VIEW

Fig. 3.3 Longitudinal view of the track system showing the geometry parallel to the track

configurations within each of the two overall configurations, giving a total of four failure geometries which must be considered.

A sectional view of the geometry perpendicular to the track can be used to represent the two most critical failure conditions: 1) the failure of the complete tie-track system for the length of the track as shown in Figure 3.4, and 2) the failure of a portion of the track beneath the heavily stressed outer third of the tie and the distance of a double truck loading as shown in Figure 3.5. The failure conditions represented by Figure 3.5 are often recognized in the field where bearing capacity failures occur. The failure geometry depicted in Figure 3.4 is usually of lesser significance and is better analyzed using slope stability methods of analysis.

A sectional view of the geometry parallel to the track can be used to represent two failure conditions: 1) the local failure of an individual tie punching into the subgrade as shown in Figure 3.6, and 2) the failure of a portion of the track corresponding to the loading which occurs beneath a double truck arrangement between two cars as depicted in Figure 3.7. Field experience suggests that the failures represented by Figures 3.6 and 3.7 occur in the absence of subballast for extremely weak clay subgrades. Generally, the direction of the shear plane depicted in Figure 3.7 requires additional braking forces such as those which occur on corners. These two failure mechanisms are presented, but emphasis is placed upon the more critical failure geometries.

The failure geometry depicted in Figure 3.6 is analyzed by the Hanna and Meyerhof approach (1) to bearing capacity whereas the geometries illustrated in Figures 3.4, 3.5, and 3.7 are all analyzed by the Broms approach (2) to bearing capacity.

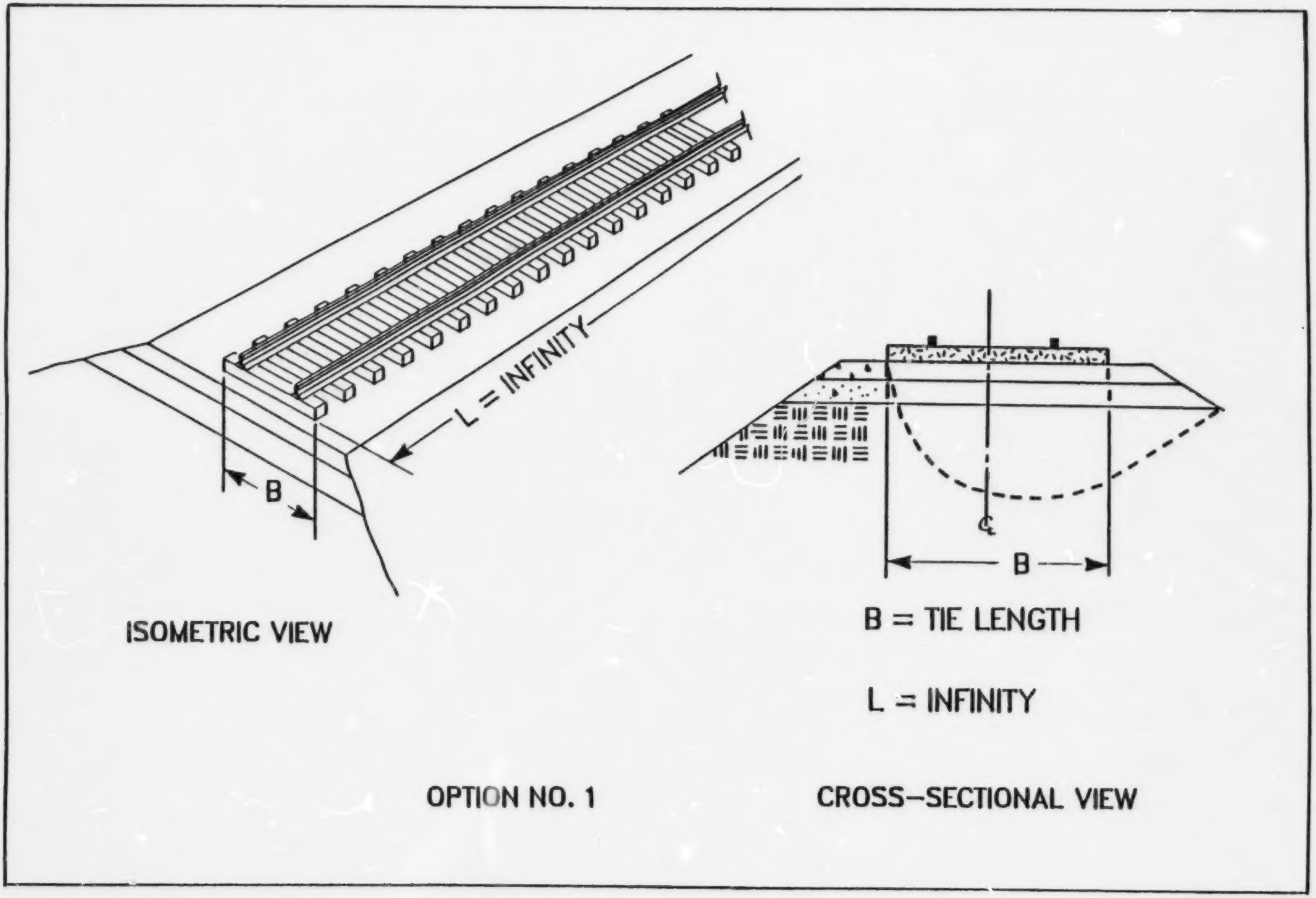
L = INFINITY
B
ISOMETRIC VIEW
B
B = TIE LENGTH
L = INFINITY
OPTION NO. 1
CROSS-SECTIONAL VIEW

Fig. 3.4 Failure geometry for the complete tie-track system for the length of the track

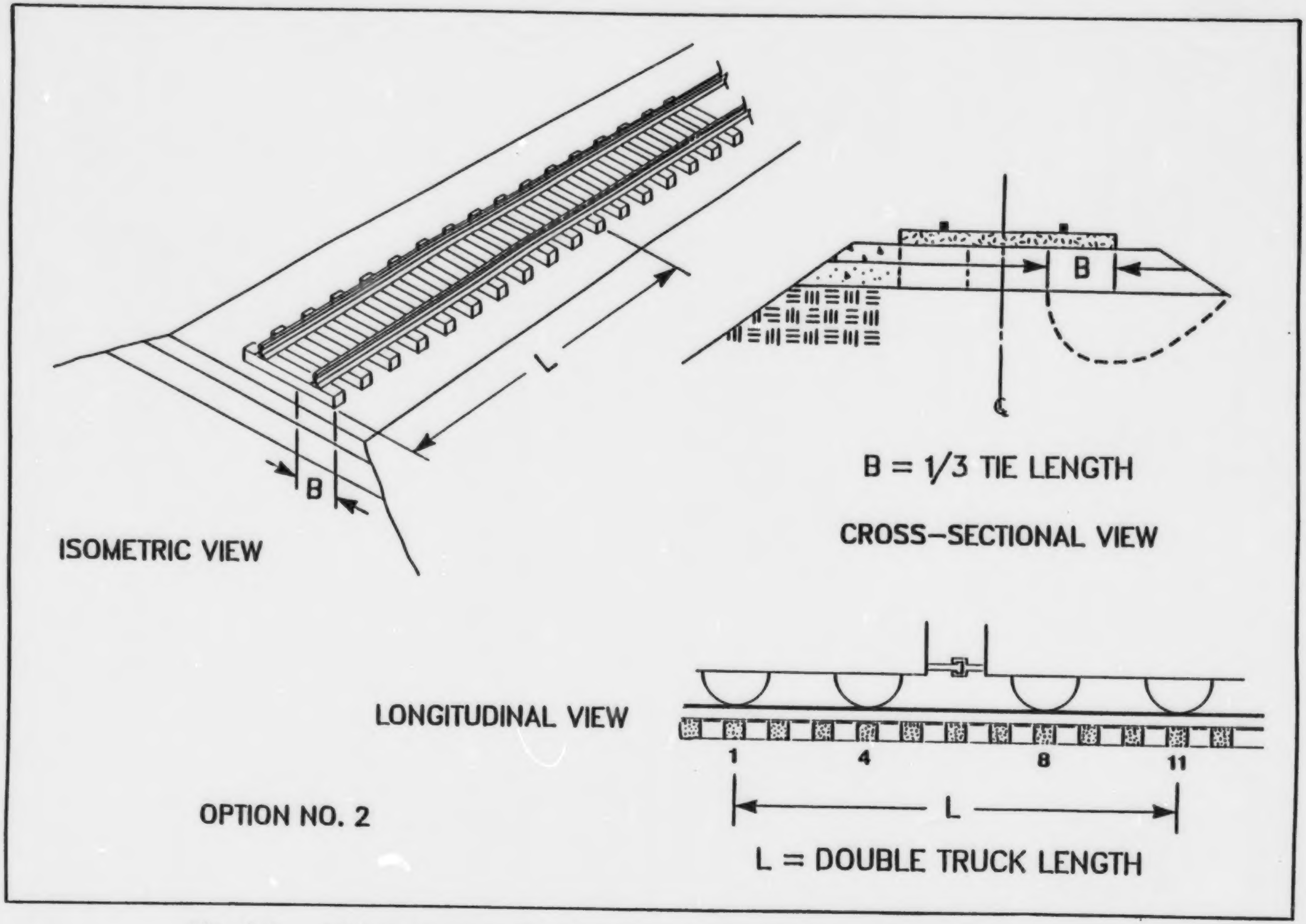
L
B
ISOMETRIC VIEW
B
℄
B = 1/3 TIE LENGTH
CROSS-SECTIONAL VIEW
LONGITUDINAL VIEW
1
4
8
11
L
L = DOUBLE TRUCK LENGTH
OPTION NO. 2

Fig. 3.5 Failure geometry for the heavily stressed outer third of the tie and the distance of a double truck loading

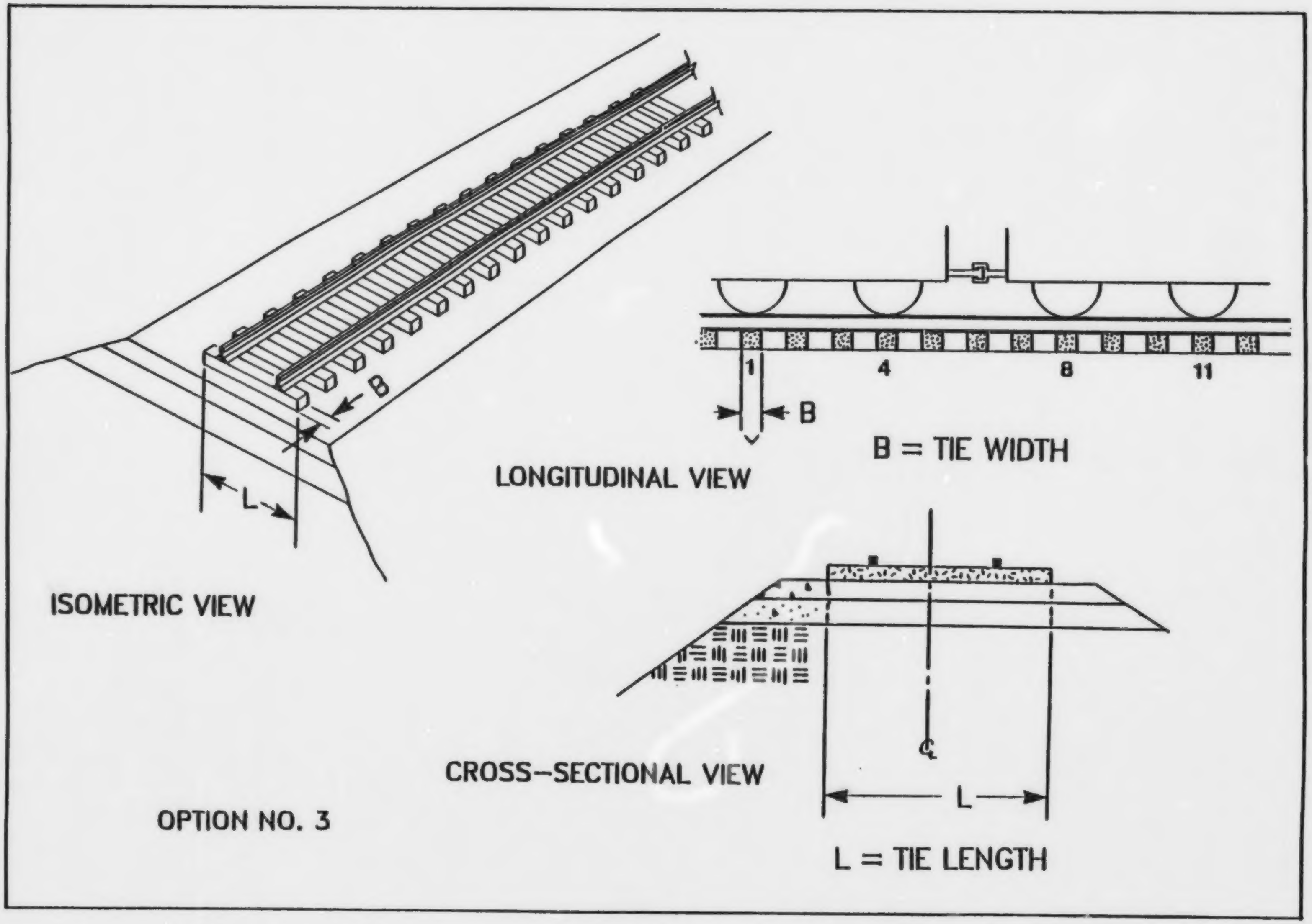

B
L
ISOMETRIC VIEW
1
4
8
11
B
B = TIE WIDTH
LONGITUDINAL VIEW
℄
L
L = TIE LENGTH
CROSS–SECTIONAL VIEW
OPTION NO. 3

Fig. 3.6 Failure geometry for the local failure of an individual tie punching into a weak subgrade

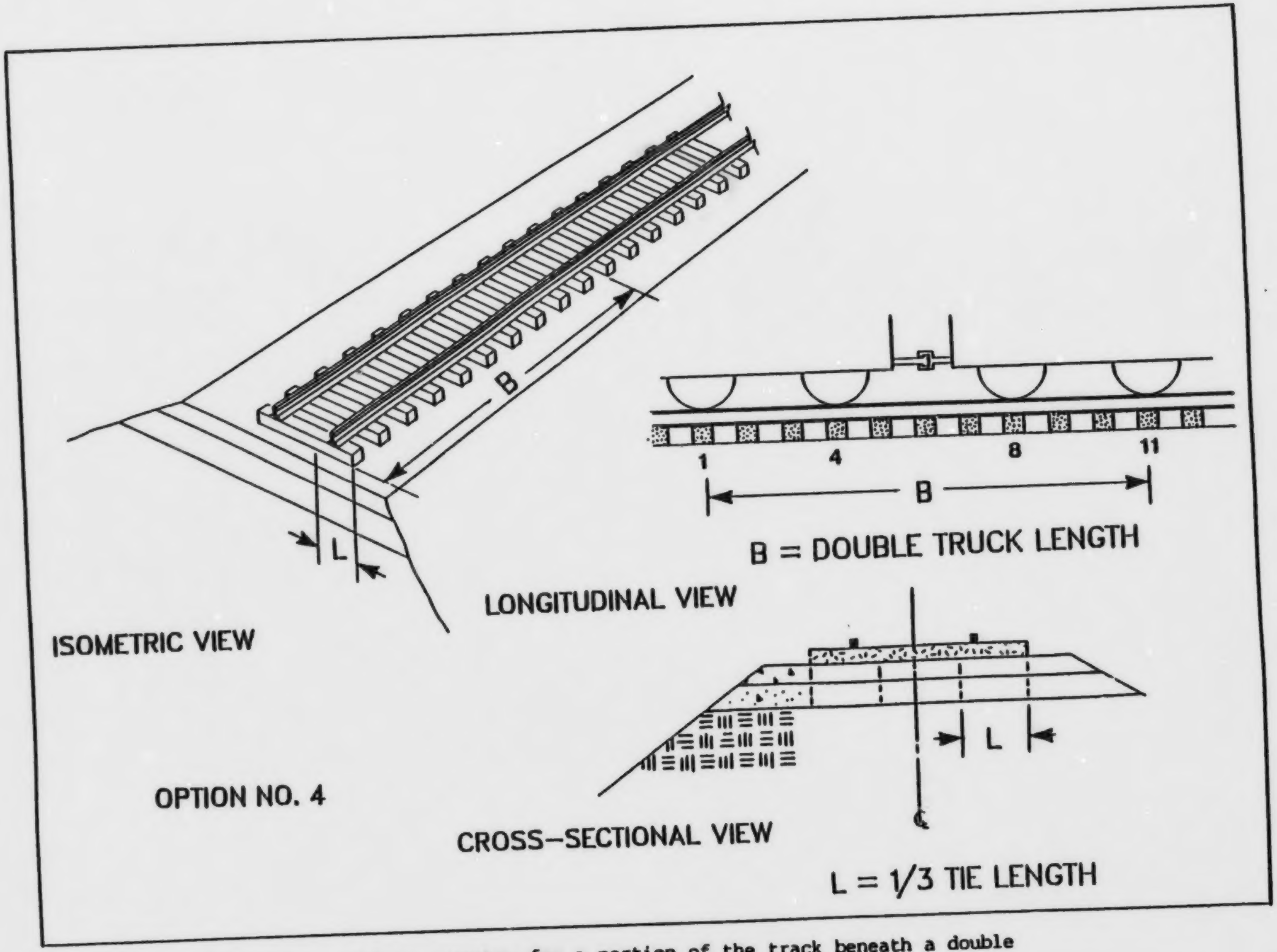
B
L
ISOMETRIC VIEW
OPTION NO. 4
1
4
8
11
B
B = DOUBLE TRUCK LENGTH
LONGITUDINAL VIEW
L
℄
CROSS-SECTIONAL VIEW
L = 1/3 TIE LENGTH

Fig. 3.7 Failure geometry for a portion of the track beneath a double truck arrangement for weak subgrades

3.3 The Broms Approach to Bearing Capacity

The Broms approach (2) to computing bearing capacity was developed for highway systems, particularly aircraft runways. Nonetheless, the analytical extension leading to the use of a highway pavement as a shallow footing can also apply to a tie-track system.

The Broms approach (2) to computing bearing capacity is illustrated in Figure 3.8. The granular material distributes the applied load to an enlarged area such that the stress at the subgrade surface is smaller in magnitude than the stress immediately beneath the footing. The conventional bearing capacity equation may be used to represent the subgrade bearing capacity, taking into consideration the decreased stress at the subgrade surface (i.e., caused by the distribution of the applied stress through the granular layers).

The approach adopted in this report uses the conventional bearing capacity equations with the actual dimensions of the footing (or tie-track system). The bearing capacity computed in this manner is then compared to the stress which reaches the subgrade surface through the granular material from the applied load (i.e., the subgrade surface stress modelled by the computer program GEOTRACK).

Broms (2) took a slightly different approach to computing the subgrade bearing capacity. Since there was no reliable method available to compute the stress at the subgrade surface, Broms used the applied load over an enlarged area of the subgrade to represent the decreased stresses which reach the subgrade surface through the granular material.

When the rail-tie system is considered as a contiguous unit placed upon the ballast and subgrade, the Broms approach provides a reasonable estimate of the general bearing capacity failures which occur under field

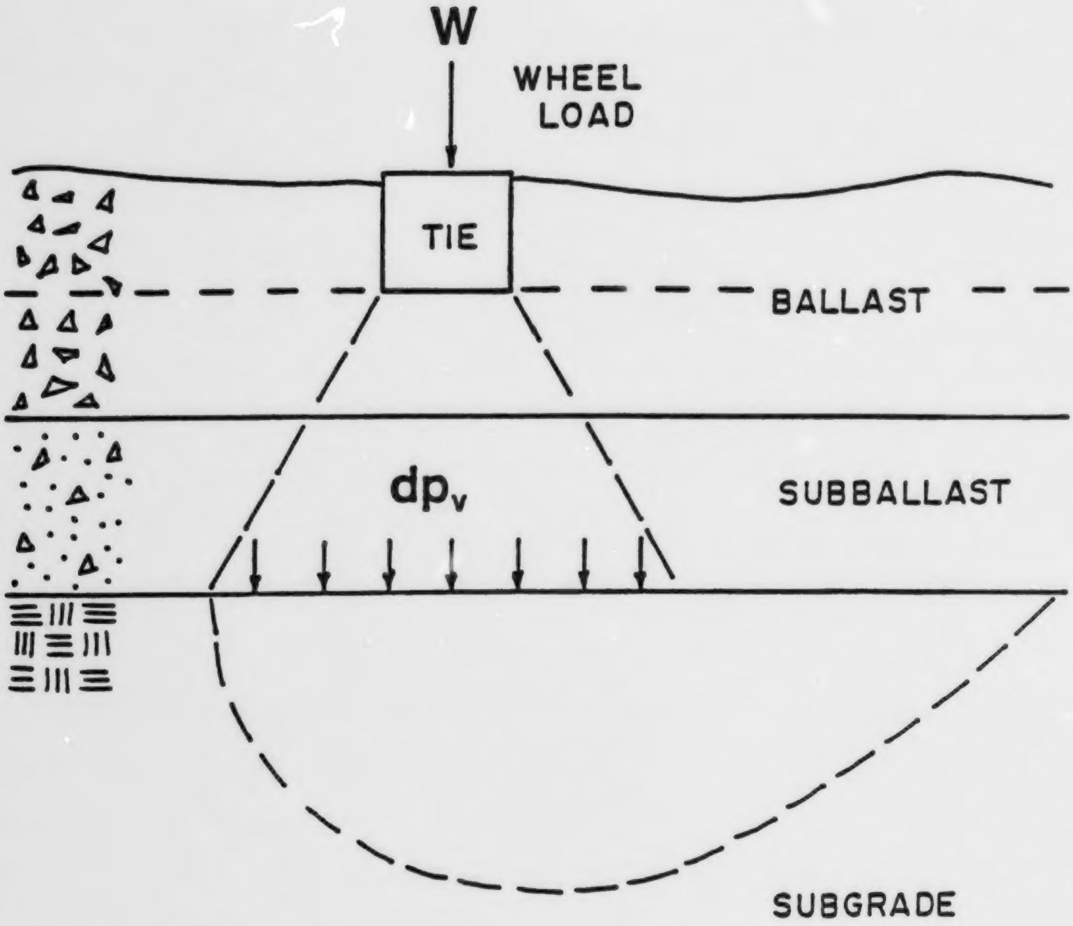
W
WHEEL LOAD
TIE
BALLAST
dp_v
SUBBALLAST
SUBGRADE

Fig. 3.8 Broms approach to computing bearing capacity (adapted from (2))

conditions. The equation for bearing capacity bears the same form as the conventional bearing capacity equation:

$$q_u = cN_c + \frac{1}{2}\gamma BN_\gamma + q_oN_q \qquad [1]$$

where:

N_c, N_γ, N_q = bearing capacity factors

c = total cohesion or undrained shear strength

γ = unit weight of the overlying ballast and subballast material

B = width of the footing (or bearing area depending upon the geometry considered)

q_o = surcharge loading

The soil suction term is incorporated into the Broms approach by replacing the undrained shear strength of the clay with the more rigorous c' and ϕ^b terms as illustrated below:

$$c = c' + (u_a - u_w)\tan \phi^b \qquad [2]$$

where:

c' = the cohesion of the subgrade

$(u_a - u_w)$ = design suction value for the subgrade

ϕ^b = rate of change of shear strength with respect to soil suction

A diagrammed representation of Equation [2] is presented in Figure 3.9.

The bearing capacity factors were computed from the following

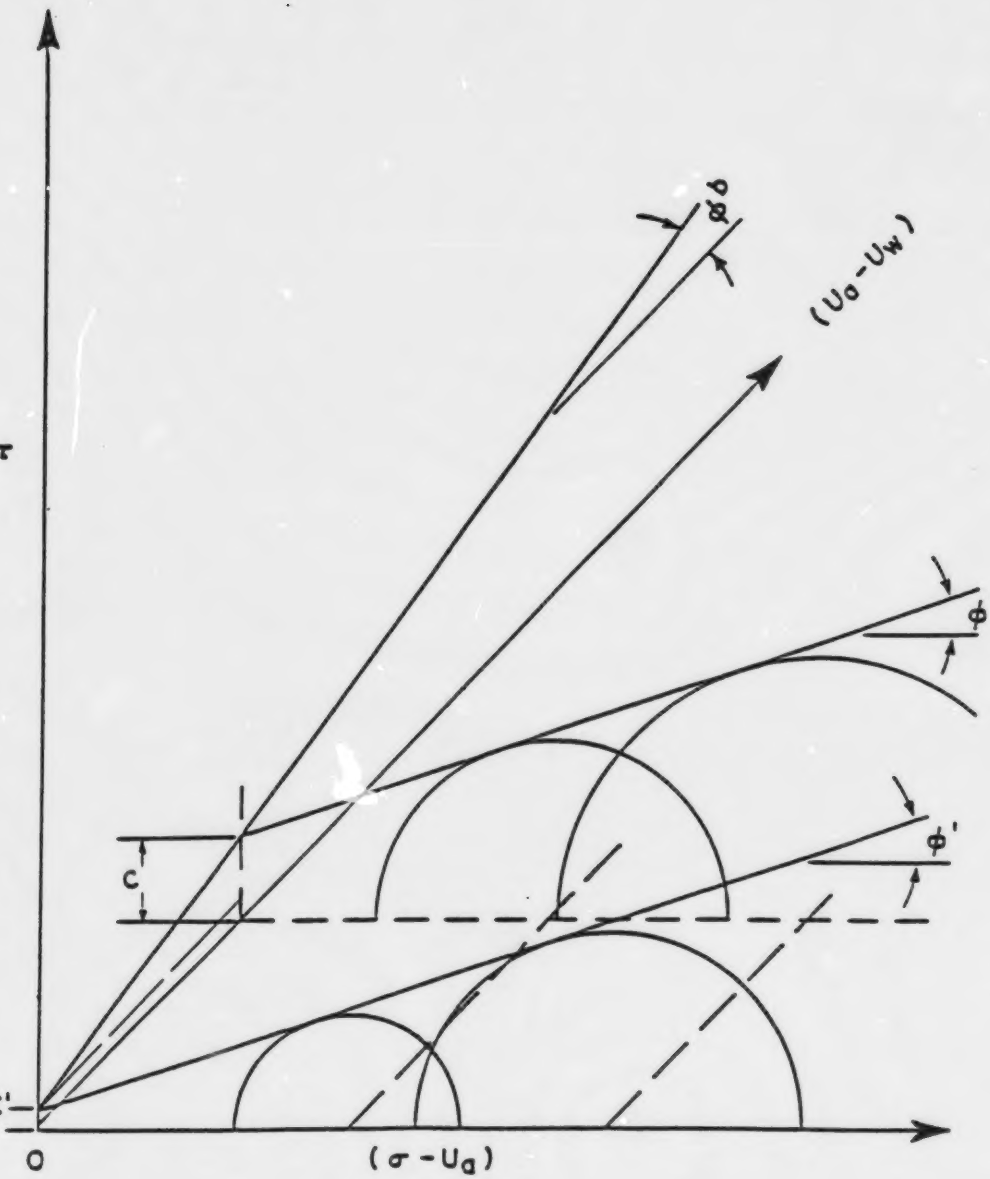
τ
φb
(Ua-Uw)
φ'
φ'
C
C'
O
(σ-Ua)

Fig. 3.9 Components of the total cohesion term

equations:

$$N_q = e^{(\pi \tan \phi')} \frac{1 + \sin \phi'}{1 - \sin \phi'} \qquad [3]$$

$$N_c = (N_q - 1)\cot \phi' \qquad [4]$$

and $$N_\gamma = 1.5(N_q - 1)\tan \phi' \qquad [5]$$

where:

ϕ' = the friction angle of the subgrade material

The equations were derived by Brinch-Hansen (20) and Vesic (21). Other published equations for the bearing capacity factors could have been used.

The Broms approach (2) to bearing capacity can be utilized for all the geometries shown in Figures 3.4 through 3.7. However, the Hanna and Meyerhof approach (1) is recommended for the configuration illustrated in Figure 3.6. When the bearing area for the Broms' approach (2) is not assumed to be infinite in length, as in Figures 3.5 and 3.7, a correction must be applied to the bearing capacity. The correction is applied in the form of shape factors which take the form shown below:

$$s_\gamma = 1 - 0.4(B/L) \qquad [6]$$

and $$s_c = s_q = 1 + (B/L)(N_q/N_c) \qquad [7]$$

where:

B = the width of the bearing area considered

L = the length of the bearing area considered

The shape factors are applied to each individual term in the same manner that the bearing capacity factors are applied to each individual term (22). Loading eccentricity factors (18) could also be applied to each individual term, but have been disregarded for simplicity in the design procedure developed.

The groundwater conditions are accommodated through the use of Equation [2] and the unsaturated soil parameters. For a high water table, the soil suction will be reduced, therefore reducing the shear strength and ultimately the bearing capacity of the soil. A discussion of appropriate design values for the soil suction referenced to the water table is located in Section 4.3.

3.4 The Hanna and Meyerhof Approach to Bearing Capacity

Figure 3.10 illustrates the derivation of the bearing capacity equation for the Hanna and Meyerhof approach. The failure mechanism assumes that a soil mass of the upper sand layer of approximately pyramidal shape is pushed into the lower clay layer. At the point of limiting equilibrium, the sum of forces in the vertical direction yields an equation for the ultimate bearing capacity of the layered system. Laboratory data collected by Hanna and Meyerhof reveal an appropriate equation for the passive earth resistance based on an assumed coefficient of punching shear (1). The resulting bearing capacity equation is:

$$q_u = cN_c + \gamma_1 H^2(1 + 2D/H)K_s \tan \phi'/B - \gamma_1 H \qquad [8]$$

where:

c = undrained shear strength of the soft clay subgrade

N_c = bearing capacity factor

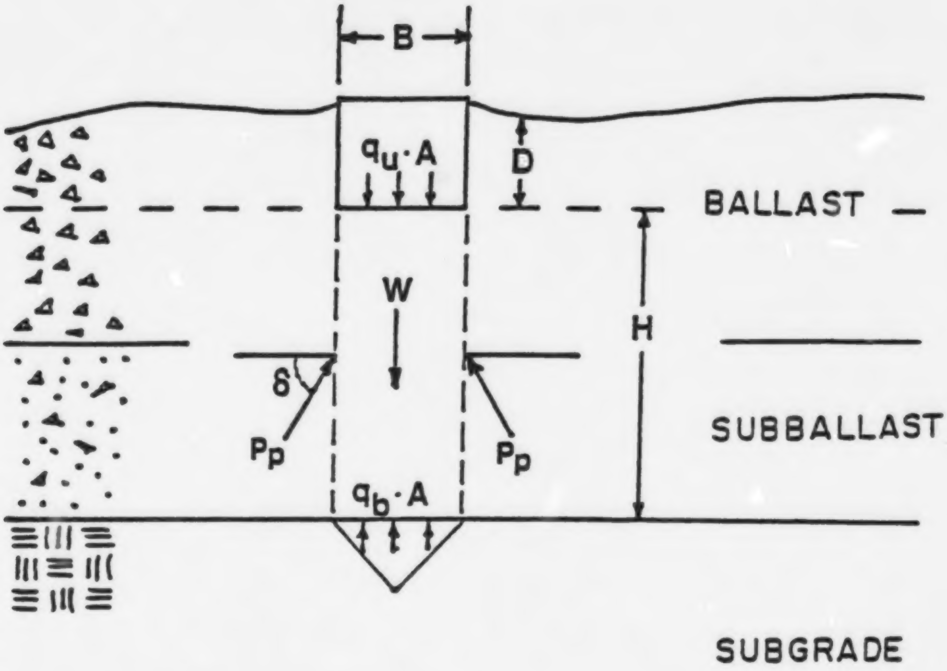
B
$q_u \cdot A$
D
BALLAST
W
H
δ
P_p
P_p
SUBBALLAST
$q_b \cdot A$
SUBGRADE

$$\Sigma F_v = 0$$

$$q_u = q_b + (2/B)(P_p \sin\delta) - \gamma H \leq q_t$$

The passive earth force is:

$$P_p = 1/2\,\gamma H^2 (1 + 2D/H) K_p / \cos\delta$$

Assume a coefficient of punching shear resistance on the vertical plane through the footing edge such that:

$$K_s \tan \text{Ø}' = K_p \tan\delta$$

$$\therefore \quad q_u = cN_c + \gamma H^2 (1+2D/H) K_s \tan \text{Ø}'/B - \gamma H$$

Fig. 3.10 Hanna and Meyerhof approach to computing bearing capacity (adapted from (1))

γ_1 = unit weight of overlying dense sand (or ballast)

H = thickness of dense sand below the bottom of the footing (or railway tie)

D = depth of embedment of the footing (or railway tie)

K_s = coefficient of punching shear resistance (determined from published charts)

ϕ' = friction angle of the upper dense sand (or ballast)

B = width of footing (or bearing area)

Again the soil suction term is incorporated into the equation as a replacement for the undrained shear strength parameter. Equation [2] and Figure 3.9 illustrate the components of the total cohesion term, c.

Kraft and Helfrich (23) suggest that the Hanna and Meyerhof approach to computing the bearing capacity is reasonably accurate for shallow footings. If an individual tie can be assumed to behave in the same manner as a shallow footing, then the results should also apply to the failure geometry illustrated in Figure 3.6. The replacement of the undrained shear strength term with unsaturated soil parameters renders the computations more rigorous since more reliable testing procedures are available for measuring these parameters. Kraft and Helfrich (23) suggested that the Hanna and Meyerhof approach cannot be extended to stronger deposits while still maintaining reliable predictions. Therefore, the Hanna and Meyerhof approach has been recommended for application to the failure depicted in Figure 3.6 for weak clay subgrades.

4.0 DESIGN PARAMETERS

This section discusses the soil and loading parameters which were used as input to the GEOTRACK program and the soil parameters: c', ϕ', ϕ^b and γ used for the bearing capacity approaches, which were previously described. The measurement and choice of a design suction value is also discussed in this section.

4.1 GEOTRACK Parameters

The input data file for the GEOTRACK program contained some values which were fixed for each computer run and some values which were varied. The parameters which were varied included: 1) axle load, 2) ballast depth, 3) subballast depth, 4) subgrade modulus, and 5) subballast modulus. The fixed parameters included: 1) tie length, 2) tie spacing, 3) tie width, 4) tie cross-sectional area, 5) tie Young's modulus, 6) tie moment of inertia, 7) tie weight, 8) rail spacing, 9) rail cross-sectional area, 10) rail Young's modulus, 11) rail moment of inertia, 12) rail weight, and 13) fastener stiffness. The choice as to which parameters to fix and which parameters to vary was facilitated by the sensitivity analysis discussed in Section 2.3.

It was assumed that wooden ties were to provide the basis for the charts. Therefore, the values computed were based on typical values for wooden ties. The values provided by the railway companies for Primary Main Line and Secondary Main Line standards were used. A summary of the tie design values used is presented in Table 1.0. A summary of the rail design values used is presented in Table 2.0. All of these values were fixed within the input file to GEOTRACK for the purposes of stress analysis.

Table 1

Tie Parameters Used in GEOTRACK Input File

Length	2.59 m	(8′ 6")
Width	229 mm	(9")
Cross-sectional area	407 cm^2	(63 in^2)
Young's modulus	1.65 x 10^7 kPa	(2.4 x 10^6 psi)
Moment of inertia	1.071 x 10^8 mm^4	(257.3 in^4)
Tie spacing	0.508 m	(20")
Tie weight	113.4 kg	(250 lbs.)

Table 2

Rail Parameters Used in GEOTRACK Input File

Rail spacing (between inside edges)	1.422 m	(4′ 8 1/2")
Cross-sectional area	86.13 cm^2	(13.35 in^2)
Young's modulus	2.07 X 10^8 kPa	(3.0 X 10^7 psi)
Moment of inertia	3.95 X 10^7 mm^4	(94.9 in^4)
Rail weight	52.16 kg	(115 lbs.)

One additional value which was fixed for the superstructure was the stiffness of the fastener. For spike and plate fastening, a stiffness of 1.25×10^6 kg/cm (7,000,000 lb./in.) is commonly used. This value was selected to represent the stiffness of the fastener in the GEOTRACK input file.

The only substructure parameter which was fixed was the ballast repeated loading modulus. This value was fixed at 241,500 kPa (35,000 psi). A typical range for the ballast modulus is 209 MPa to 310 MPa. The chosen value represents a mid to lower end ballast repeated loading modulus.

Three axle loads were used in the development of the design charts. These corresponded to: 1) a 100,000 kg (220,000 lb.) car, 2) a 119,000 kg (263,000 lb.) car, and 3) a 143,000 kg (315,000 lb.) car. Both static and dynamic loading were considered. For dynamic loading conditions, the axle load was increased by 50%.

The resultant axle loads were: 1) 245 kN static and (367 kN) dynamic for the 100,000 kg car, 2) 290 kN static and (440 kN) dynamic for the 119,000 kg car, and 3) 350 kN static and (525 kN) dynamic for the 143,000 kg car. In section 5.1 and 5.3, the design charts present the axle load as "245 kN static" and "245 kN dynamic". It is to be understood that the caption "245 kN dynamic" represents a 100,000 kg car with a static axle load of 245 kN and a dynamic axle load of 1.5 times 245 kN or 367 kN. This leaves the 50% increase for dynamic loading internal to the charts and thus avoids confusion.

For each of the axle loads analyzed, two ballast depths of 203 mm (8") and 305 mm (12") were chosen to develop the design charts. For each of the two ballast depths, four subballast depths were input to the GEOTRACK program: 1) 203 mm (8"), 2) 406 mm (16"), 3) 610 mm (24"), and 4) 813 mm (32"). Therefore, for the 203 mm (8") ballast depth, a total of four granular thicknesses were analyzed corresponding to: 1) 406 mm (16"), 2) 610 mm (24"), 3) 813 mm (32"), and 4) 1016 mm (40"). Similarly, for the 305 mm (12") ballast depth, a total of four granular thicknesses were analyzed corresponding to: 1) 508 mm (20"), 2) 711 mm (28"), 3) 914 mm (36"), and 4) 1118 mm (44"). A table of the design values used for any one axle load and a ballast depth of 203 mm is presented in Table 3.0 which summarizes the design values which were varied.

To show all the combinations of the variables would require repeating Table 3.0 for each of the three axle loads, for each of the static and dynamic loading conditions, and for each of the two ballast depths. Therefore, to show all the combinations would require the presentation of Table 3.0 a total of 3 X 2 X 2 = 12 times.

For each axle load, ballast depth, and subballast depth, the subgrade modulus and the subballast modulus were modified. Two subballast moduli were used to reflect typical values: 1) 103.5 MPa (15,000 psi) and 2) 241.5 MPa (35,000 psi). Four subgrade moduli were used to cover the enormous range of possible values. The four subgrade moduli incorporated into the chart development were: 1) 6.9 MPa (1,000 psi very soft clay), 2) 41.4 MPa (6,000 psi medium clay), 3) 69.0 MPa (10,000 psi), and 4) 103.5 MPa (15,000 psi). The summary of all variables is presented in Table 3.0.

The data file names were encoded to assist in the development of the design charts. A letter designation from A to F represented the

Table 3

GEOTRACK Parameters Varied for Any One Axle Load

File Name	Ballast Depth (mm)	Subgrade E (MPa)	Subballast E (MPa)	Subballast Depth (mm)
A115T16	203	6.9	103.5	203
A115T24	203	6.9	103.5	406
A115T32	203	6.9	103.5	610
A115T40	203	6.9	103.5	813
A135T16	203	6.9	241.5	203
A135T24	203	6.9	241.5	406
A135T32	203	6.9	241.5	610
A135T40	203	6.9	241.5	813
A615T16	203	41.4	103.5	203
A615T24	203	41.4	103.5	406
A615T32	203	41.4	103.5	610
A615T40	203	41.4	103.5	813
A635T16	203	41.4	241.5	203
A635T24	203	41.4	241.5	406
A635T32	203	41.4	241.5	610
A635T40	203	41.4	241.5	813
A1015T16	203	69.0	103.5	203
A1015T24	203	69.0	103.5	406
A1015T32	203	69.0	103.5	610
A1015T40	203	69.0	103.5	813
A1035T16	203	69.0	241.5	203
A1035T24	203	69.0	241.5	406
A1035T32	203	69.0	241.5	610
A1035T40	203	69.0	241.5	813
A1515T16	203	103.5	103.5	203
A1515T24	203	103.5	103.5	406
A1515T32	203	103.5	103.5	610
A1515T40	203	103.5	103.5	813
A1535T16	203	103.5	241.5	203
A1535T24	203	103.5	241.5	406
A1535T32	203	103.5	241.5	610
A1535T40	203	103.5	241.5	813

static or dynamic axle loads. The numbers 115, 135, 615, 635, 1015, 1035, 1515, and 1535 represented both the subgrade and subballast E modulus in ksi (i.e., in A115T16, 115 represents a subgrade E modulus of 1 ksi and a subballast E modulus of 15 ksi. The 'T' stands for total granular thickness and the last pair of numbers designate the total granular thickness in inches (i.e., in A115T16 the total granular thickness was 16 inches)).

4.2 Soil parameters: c', ϕ', ϕ^b and γ

The shear strength parameters required for a bearing capacity analysis are: c', ϕ', and ϕ^b. The shear strength of a material is comprised of three components, namely, 1) the effective cohesion component, 2) the frictional component, and 3) the soil suction component. Figure 4.1 illustrates how the individual components combine to represent the shear strength of a compacted, unsaturated material.

The c' parameter represents the effective cohesion component of the shear strength, whereas the ϕ^b parameter represents the soil suction component of the shear strength. Often, these two terms are grouped together and called the total cohesion (i.e., c) as presented in Sections 3.3 and 3.4.

Whereas the total cohesion term is directly incorporated into a bearing capacity approach, the frictional component indirectly influences the bearing capacity. The frictional term is incorporated into the bearing capacity equation through its relationship to the bearing capacity factors as presented in Sections 3.3 and 3.4.

In addition to the shear strength parameters, the unit weight of the material is also required in a bearing capacity approach. A typical unit

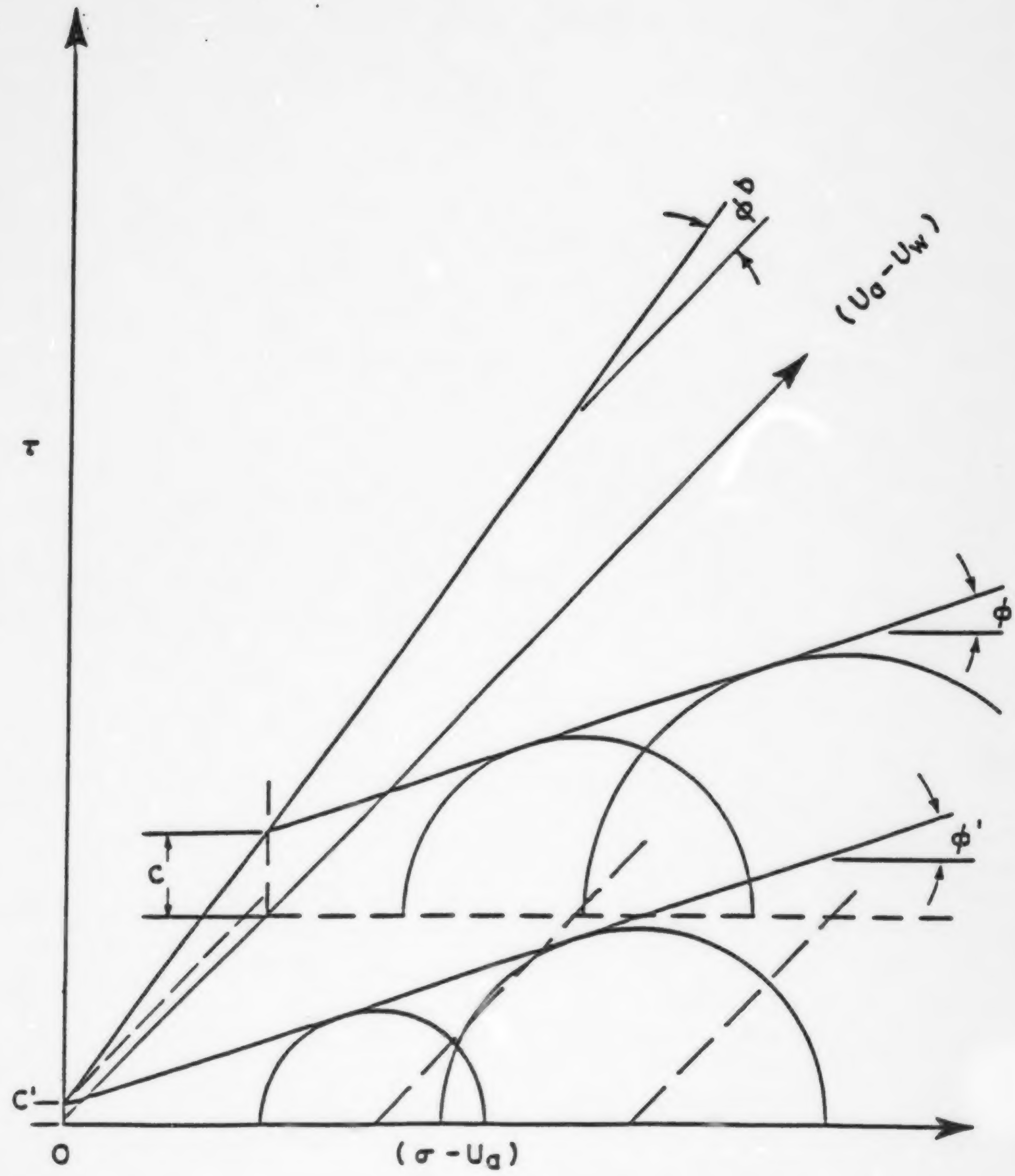

φb
(Ua-Uw)
τ
φ'
φ'
C
C'
O
(σ -Ua)

Fig. 4.1 Components of the shear strength of an unsaturated soil

weight of 18 kN/m3 was chosen to represent the subgrade and granular materials for the bearing capacity approaches presented in this report. This value was fixed for the purposes of this presentation whereas the values chosen for c', ϕ' and ϕ^b were varied.

A sensitivity analysis was performed for the Broms bearing capacity approach (i.e., as presented in Section 3.3) to determine the relationship between the ultimate bearing capacity and the various shear strength parameters.

Figure 4.2 illustrates the effect on the ultimate bearing capacity of changing the c' term. The frictional (ϕ') term and the matric suction (ϕ^b) term are held constant while the c' term is increased from 2.5 kPa to 72.5 kPa. Increasing the c' term increases the bearing capacity by a factor of N_c multiplied by c, where c is comprised of the c' term and the soil suction term. As long as ϕ' is held constant, the bearing capacity factor N_c is constant and therefore, the slope of the relationship between bearing capacity and soil suction remains constant.

If the c' term and the ϕ' term are held constant while the ϕ^b term is varied, the result is a graph like the one presented in Figure 4.3. The intercept on the bearing capacity axis remains the same for all values of the soil suction, but the slope of the relationship changes for various values of the ϕ^b term. The graph shows that for larger values of soil suction, it is important to more precisely define a value for the ϕ^b term. In other words, the error in assuming an incorrect value for ϕ^b is greater for larger design suction values.

Changing the ϕ' term while holding c' and ϕ^b constant has the effect of changing both the y-axis intercept and the slope. This relationship is presented in Figure 4.4. The error in assuming an inappropriate ϕ'

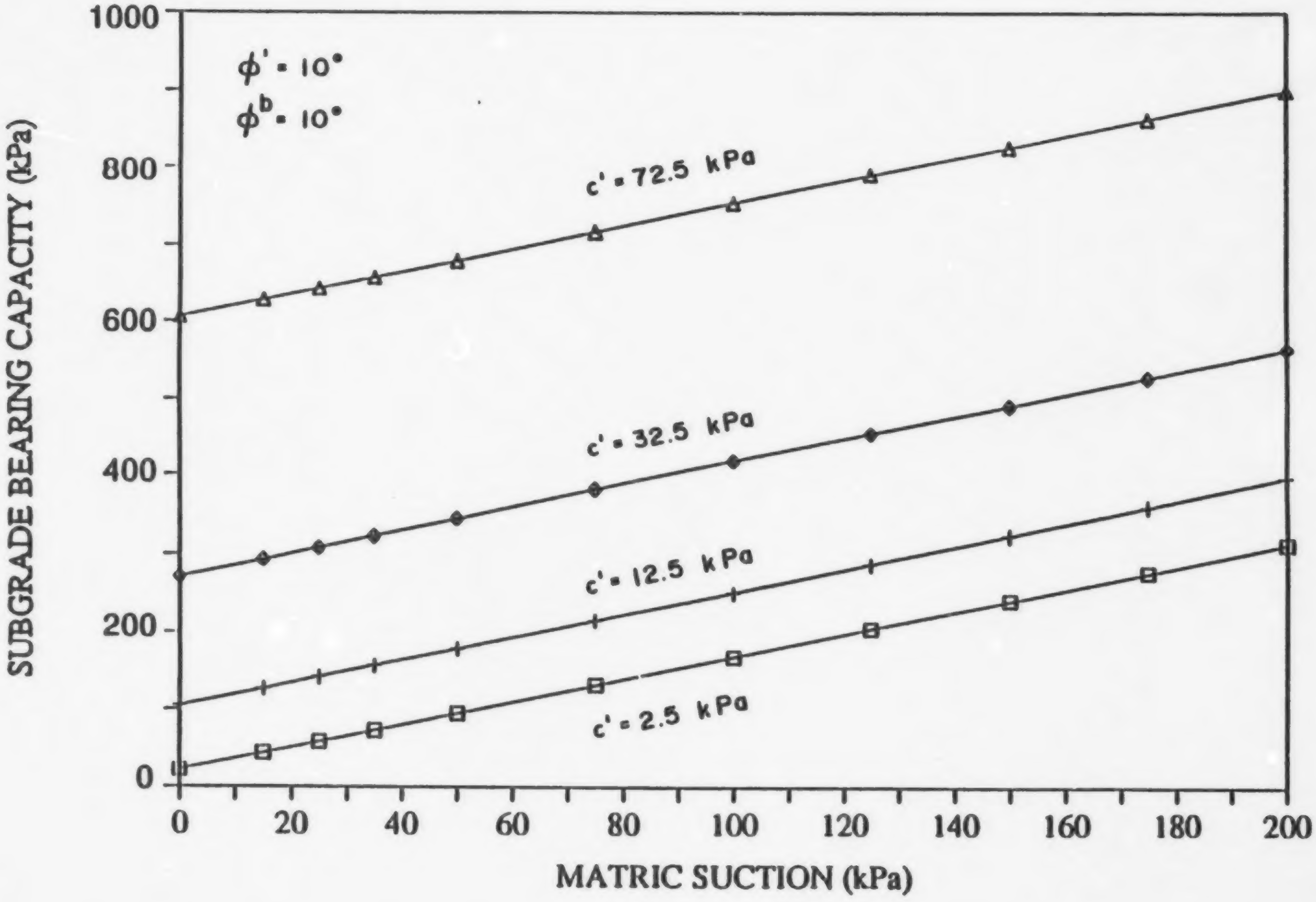

Fig. 4.2 Sensitivity of ultimate bearing capacity to varying c' for constant ϕ' and ϕ^b

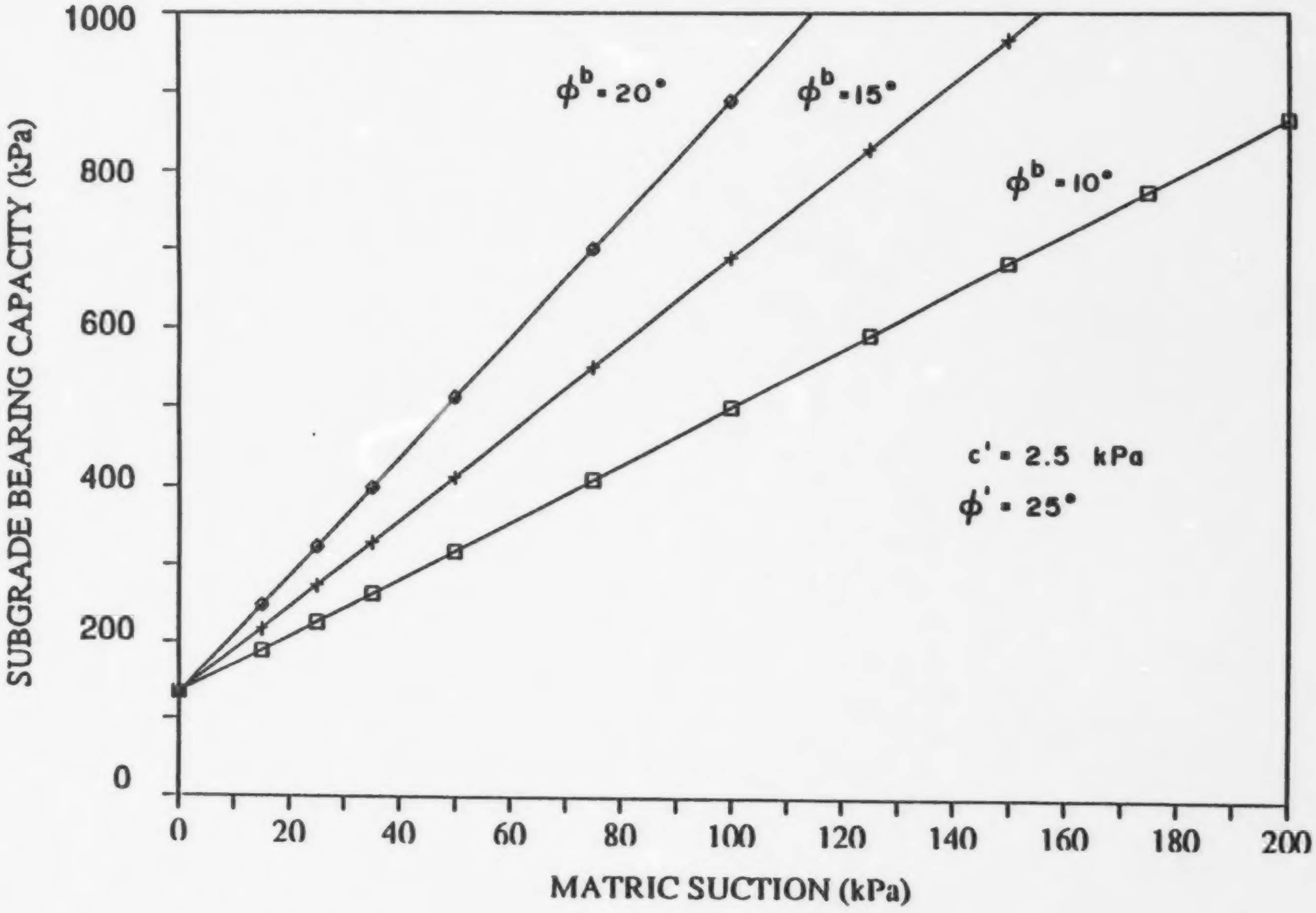

Fig. 4.3 Sensitivity of ultimate bearing capacity to varying ϕ^b for for constant c′ and ϕ'

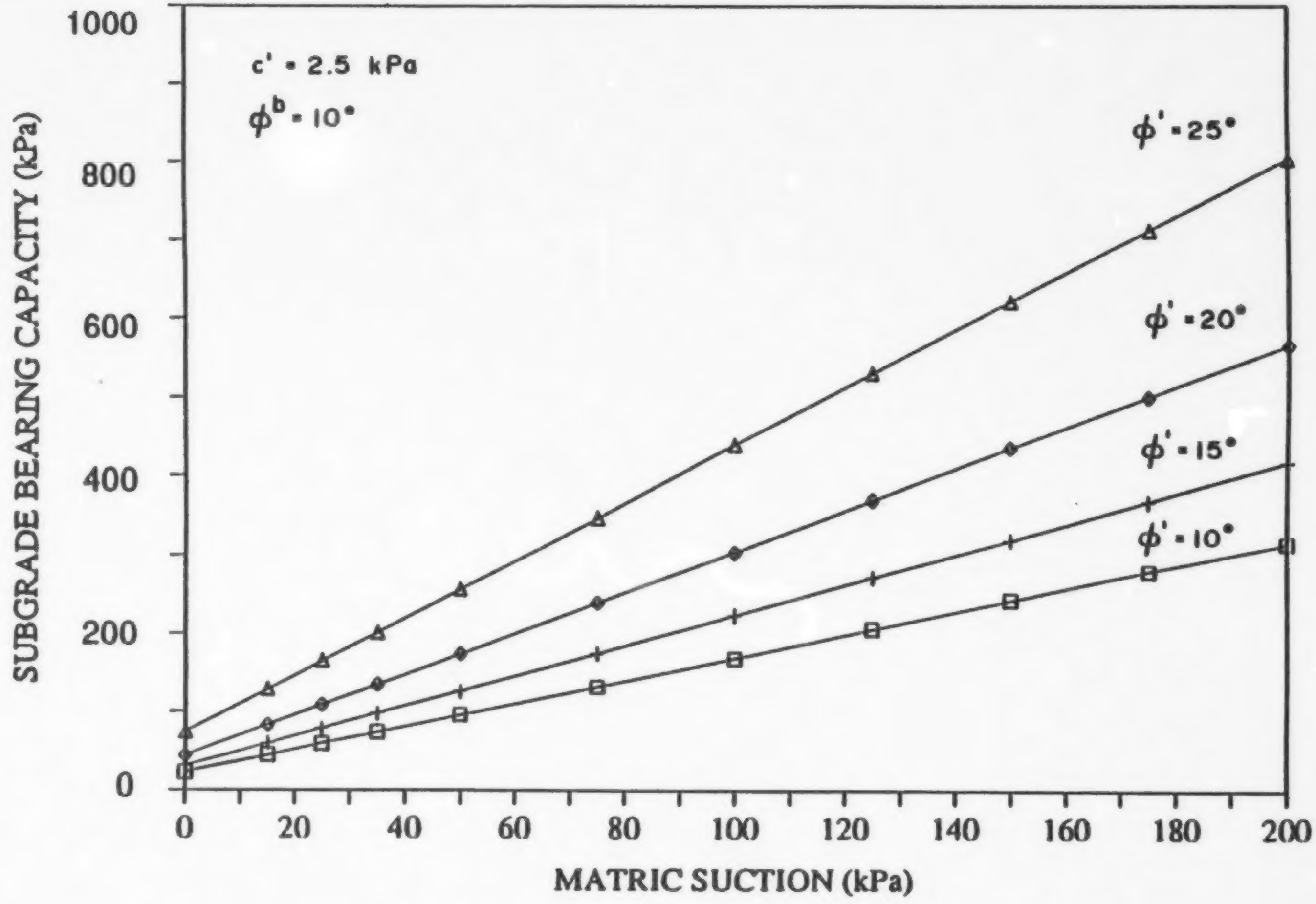

Fig. 4.4 Sensitivity of ultimate bearing capacity to varying ϕ' for constant c' and ϕ^b

value is greater for larger values of soil suction.

To simplify the bearing capacity charts, which are presented in Section 5.2, the c′, ϕ^b and soil suction were combined into a total cohesion component for plotting ultimate bearing capacity.

One aspect of this contract required the compilation of typical values for the c′, ϕ' and ϕ^b material parameters. The compilation is divided into three categories, one for each broad category of soil type, namely: 1) clay, 2) glacial till, and 3) silt and sand. Table 4.0 presents the results of a literature review on the shear strength parameters for clay. Table 5.0 presents the results of a literature review on the shear strength parameters for glacial till, and Table 6.0 summarizes the results of a literature review for silt and sand. Reference numbers are provided for the data extracted for the literature review.

TABLE 4.0 Literature Review Values for the Shear Strength Parameters of Clay

CLAY Site	c' (kPa)	f' (deg)	c'^{r} (kPa)	f'^{r} (deg)	Determined By	Ref.
WINNIPEG GLACIAL LAKE CLAY						
Transcona Elevator	28.9	12.7			CU Triaxial	(24)
Landslides Near Winnipeg					Triaxial	(25)
	6	31.7			(< 60kPa)	
	33	13			(= 60 - 240kPa)	
	3	23			(> 240kPa)	
			0	10	Direct Shear	(25)
			0	8 - 13	Back Analysis	(25)
	45	12			Back Analysis	(25)
	57	9			Back Analysis	(25)
Winnipeg Area			0 - 8	7 - 10	Direct Shear	(26)
Emerson Subdivision			1.5	7.2	Direct Shear	(27)
			.	10	Analyses	(28)
Test Trench, Floodway	59	9			CU Triaxial	(29)
Red River Floodway	44.8	12			CU Triaxial	(30)
	31.0	16.5			CD Triaxial	(30)
Brown Clay	42.0	19.1			Analyses	(31)
			0	8.4	Analyses	(31)
Grey Clay	10.7	21.9			Analyses	(31)
			0.4	7	Analyses	(31)
Plastic Clay	6.2	18.3			Analyses	(31)
			0	11	Analyses	(31)
REGINA GLACIAL LAKE CLAY						
Embankment at Belle Plaine	37	20.4			CU Triaxial	(32)
	0	13	(Large Strains)		CU Triaxial	(32)
	14	7.5	(Large Strains)		CU Triaxial	(32)
			5	7.7	Direct Shear	(32)
	6.9	15.5			CU Triaxial	(33)
			0	13	Direct Shear	(33)
			14	7.5	Direct Shear	(33)
Regina Beach	22.5	12.2			Direct Shear	(34)
			0	5 - 7	Analyses	(34)
CLAY SHALE						
Maymont, SK			0	8 - 28	Direct Shear	(35)
	15	38			Direct Shear	(35)
			0	8.2	Analyses	(34)

Nipawin			0	8 - 15	Direct Shear	(36)
Bridge, SK			0	10	Analyses	(34)
Maidstone			0	8.5 - 15	Direct Shear	(36)
Bridge, SK			0	10	Analyses	(34)
	13.8	26.5			CU Triaxial	(36)
Little Smoky			0	14 - 17.5	Direct Shear	(37)
Landslide,			13	14 - 19.5	Direct Shear	(37)
Peace River, AB						
	0	32			CU Triaxial	(37)
Little Smoky			0	7.5	Direct Shear	(36)
Bridge, AB			0	7.5	Analyses	(34)
Borden			10	7.8	Direct Shear	(34)
Bridge, SK			3.5 - 5.0	6.5 - 10.5	Analyses	(34)
Lumsden, SK			0	9	Analyses	(35)
Gardiner Dam, SK			0	7.0 - 10.5	Analyses	(35)
CM Beaver Creek, SK			0	6.6 - 10.6	Direct Shear	(38)
			0	6 - 8	Back Analyses	(38)
Denholm, SK	64	0			Back Analyses	(39)
	0	9.9			Back Analyses	(39)
Spinney Hill, SK						
	0	8.7			Back Analyses	(40)
	28	0			Back Analyses	(40)
Edmonton, AB						
	57.5	14	0	12	Direct Shear	(41)
	55 - 57.5	14 - 24				(42)
			0	12 - 17		(42)
Edgerton, AB						
Brown - silty			0	10	Direct Shear	(43)
	70	23			CU Triaxial	(43)
			0	23	Analyses	(43)
Grey - silty			0	19	Direct Shear	(43)
	160	41			CU Triaxial	(43)
			0	41	Analyses	(43)
Grey - bentonitic			0	8	Direct Shear	(43)
			0	8	Analyses	(43)
Brown			0	10	Direct Shear	(43)
	70	23			CU Triaxial	(43)
			0	10	Analyses	(43)

Gronlid, SK	3.5	7.5			Direct Shear	(44)
OTHER CLAYS						
Glacial Lake Clay						
McBride, BC			0	12 - 16	Direct Shear	(45)
	22.5	13			CU Triaxial	(45)
	19.8	20			Direct Shear	(45)
Champlain Clay, Quebec	10	33			CU Triaxial	(46)
	3	27			Back Analysis	(46)
North Ridge Dam, AB	24.8	21.8				(47)
Shellmouth Dam	12.4	25.8				(47)
Seven Sisters Dike, MB	13.8	14.5				(47)
Red River Dike, MB	10.3	24				(47)
La Salle Dam, MB	22.1	15				(47)
Stiff Clay	15	20.5				(48)
	12.7	19.7				(48)
Edmonton Plastic Clay	28	27			CU Triaxial	(42)
	20	24			CU Triaxial	(41)
Lake St. John, Quebec	47.5	33			Triaxial	(49)
			4.5	33	Direct Shear	(50)
Ottawa, ON	8.8	36.8			Triaxial	(51)
Toronto, ON	20	24	0	16	CD Triaxial	(52)
Gronlid, SK	0	13			Direct Shear	(44)

TABLE 5.0 Literature Review Values for the Shear Strength Parameters of Glacial Till

GLACIAL TILL Site	c' (kPa)	ϕ' (deg)	c'^r (kPa)	ϕ'^r (deg)	Determined By	Ref.
Beaver Creek, SK			0	15	Direct Shear	(53)
	0	25			Triaxial	(53)
Rogers Pass, BC	0 - 25	30 - 40			Back Analysis	(54)
Welland Canal						
	0 - 10	19 - 25			CD Triaxial	(55)
	0 - 10	17 - 23			CD Triaxial	(55)
	10	25			CD Triaxial	(55)
	7.5	23			CD Triaxial	(55)
Battleford Formation, SK						
	24 - 35	29.5 - 31.5			CU Triaxial	(56)
	27.6	31.5			CU Triaxial	(57)
Floral Formation, SK						
	24 - 35	27 - 29			CU Triaxial	(56)
	34.5	29.3			CU Triaxial	(57)
Sutherland Formation, SK						
	31 - 41	22.5			CU Triaxial	(56)
	44.5	23			CU Triaxial	(57)
Gronlid, SK	34.5	29			CU Triaxial	(44)
Typical Till	5	24				(41)
Wesleyville Till, Toronto. ON	50	35			Triaxial	(58)
Edmonton, AB	28	27			CU Triaxial	(42)
Warman, SK	0	27			Back Analyses	(59)
	37.2	0			Back Analyses	(59)
	7	22.5			Triaxial	(59)
	32 - 42	22.5			Triaxial	(59)

TABLE 6.0 Literature Review Values for the Shear Strength Parameters of Silt/Sand

SILT/ SAND	Site	c′ (kPa)	ϕ' (deg)	Determined By	Ref.
LOOSE SILT/SAND					
	Silty Sand	0	27 - 33		(60)
	Sandy Gravel	0	35		(60)
	Inorganic Silt	0	27 - 30		(60)
MEDIUM DENSE SILT/SAND					
	Nonplastic silt	0	28 - 32		(61)
	Uniform Fine to Medium Sand	0	30 - 34		(61)
	Well Graded Sand	0	34 - 40		(61)
	Sand and Gravel	0	36 - 42		(61)
DENSE SILT/SAND					
	Silty Sand	0	30 - 34		(60)
	Well Graded Sand to Sandy Gravel	0	45 - 50		(60)
	Inorganic Silt	0	30 - 35		(60)
	Nonplastic silt	0	30 - 34		(61)
	Uniform Fine to Medium Sand	0	32 - 36		(61)
	Well Graded Sand	0	38 - 40		(61)
	Sand and Gravel	0	40 - 48		(61)
NATURAL					
	Drynoch Slide, BC				
	Volcanic Ash	0	21.3	Direct Shear	(62)
	Aeolian Sand	0	15.0	Direct Shear	(62)
		0	17.2	Back Analyses	(62)
	Toronto, ON	0	29	CD Triaxial	(52)
	Silt	0	19	CD Residual	(52)
	Lake Sand	0	35		(41)
	SK Sand	0	40		(41)
	Welland Canal, ON Silt	0 - 10	30	CD Triaxial	(55)
	Winnipeg, MB				
	Silt	11.7	31.5	Working Stress	(31)
		0	23	Residual	(31)
		8.3	25.3	Along Layers	(31)

For Winnipeg glacial lake clay, typical values of c′ range from 3 kPa to 59 kPa, whereas typical values of ϕ' range from 9 degrees to 31 degrees. Residual values for ϕ' range from 7 to 13 degrees for Winnipeg clay with a cohesion intercept close to zero. The literature review reveals that Winnipeg clay is variable in nature.

Typical values for Regina glacial lake clay range from 0 to 37 kPa for c′ and from 7.5 degrees to 20.5 degrees for ϕ'. Residual values of ϕ' for Regina clay range from 5 to 13 degrees. Table 4.0 also presents the results for various clay shales and other clays.

Glacial till, by its nature is a variable material. The values in Table 5.0 reflect this variability. Values for c′ vary from 0 kPa to 50 kPa, whereas values for ϕ' vary from 17 degrees to 35 degrees. Silt and sand, on the other hand, are usually quite uniform. This is reflected in the values presented in Table 6.0. Typical values for the ϕ' term vary from 27 to 39 with a cohesion intercept (i.e., c′) of zero.

Within the last few years, techniques have been developed at the University of Saskatchewan to measure the ϕ^b angle for an unsaturated soil (i.e., the rate of increase in shear strength with respect to soil suction). Complete details on the apparatus and equipment design for measuring ϕ^b are published in Gan and Fredlund (63) and Gan (64). Testing proceeds as a multi-stage direct shear test for pre-selected values of soil suction. Prior to 1987, values had been determined for some samples of silt and some samples of glacial till. No testing had been performed on clay. As a part of the present research project, some testing was performed on a glacial lake clay. Further research is required to broaden the data base.

Published values of the ϕ^b value for silt lie in the range of 12 to

16 degrees for a low density material and 16 to 22 degrees for a high density material (Ho and Fredlund, 1982 (65)). Unpublished measurements of the ϕ^b value for Cranbrook show it to be about 15 degrees.

A value of 15 degrees for ϕ^b has often been chosen for analysis purposes. However, the value chosen for analysis should not be greater than the ϕ' angle. Recent research has suggested that the ϕ^b angle is equal to the ϕ' angle at saturation (Fredlund, Rahardjo and Gan (66)). At larger suctions, the ϕ^b angle is less than the ϕ' angle and reaches a constant residual value (66). Therefore, for design purposes, the ϕ^b angle should be assumed to be less than or equal to the ϕ' angle (66). This phenomenon is illustrated in Figure 4.5 for a glacial till material.

Laboratory testing for the ϕ^b parameter for glacial till was conducted as a thesis project and published in 1986 by Gan (64). Typical values lie between 7 degrees and the upper limit for this material of 25 degrees. Laboratory testing from the thesis indicated that a reasonable design value for ϕ^b would be close to 15 degrees.

Figures 4.6 through 4.9 present a summary of the laboratory results conducted on a glacial lake clay as a part of this research project. Figure 4.6 shows the shear stress versus horizontal displacement for each of the five stages performed on the first sample of clay. The five stages correspond to five matric suction values, namely: 1) 50 kPa, 2) 75 kPa, 3) 100 kPa, 4) 200 kPa, and 5) 300 kPa. The peak shear stresses from Figure 4.6 are plotted against the soil suction values to determine the ϕ^b angle in Figure 4.7. A ϕ^b angle of 25.8 degrees was determined for the first sample of the glacial lake clay.

A second sample was prepared for measuring the ϕ^b angle. Three stages corresponding to suctions of 75 kPa, 200 kPa and 300 kPa were

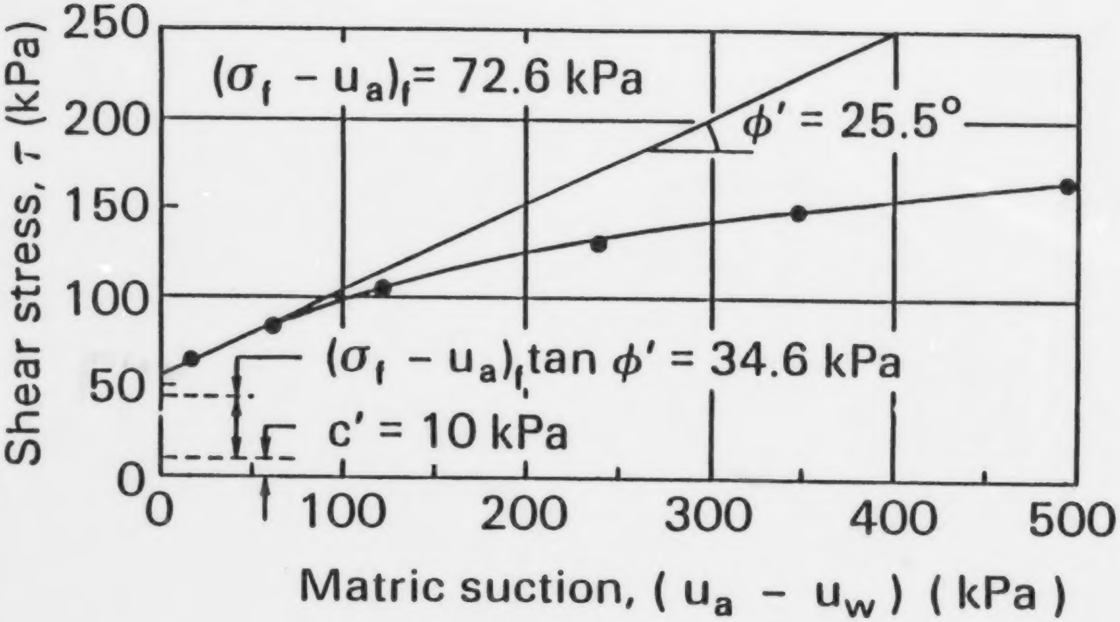

Fig. 4.5 Failure envelope obtained for unsaturated glacial till with respect to changing matric suction (Gan, Fredlund and Rahardjo (66))

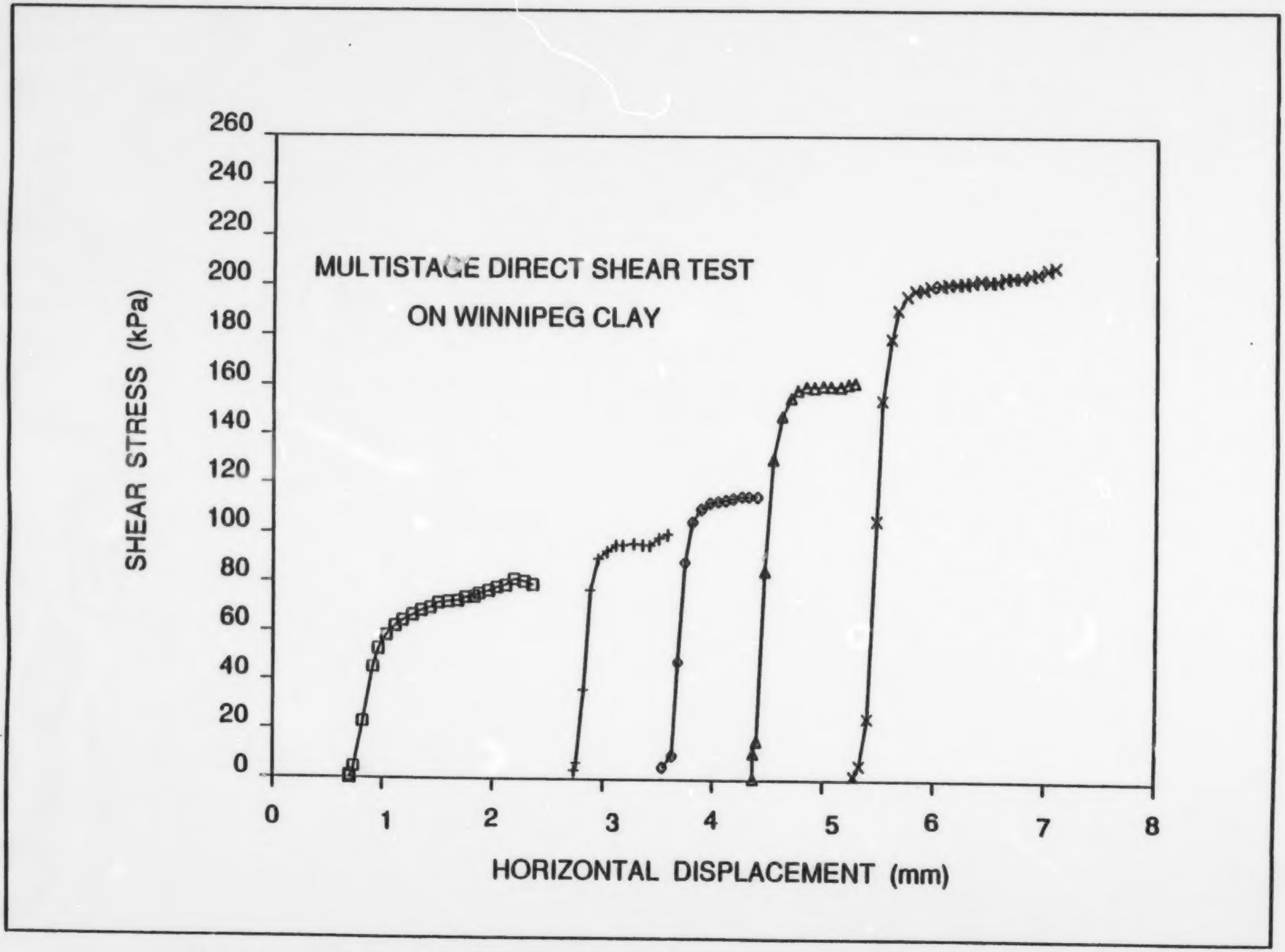

Fig. 4.6 Results of a five stage direct shear test on a glacial lake clay

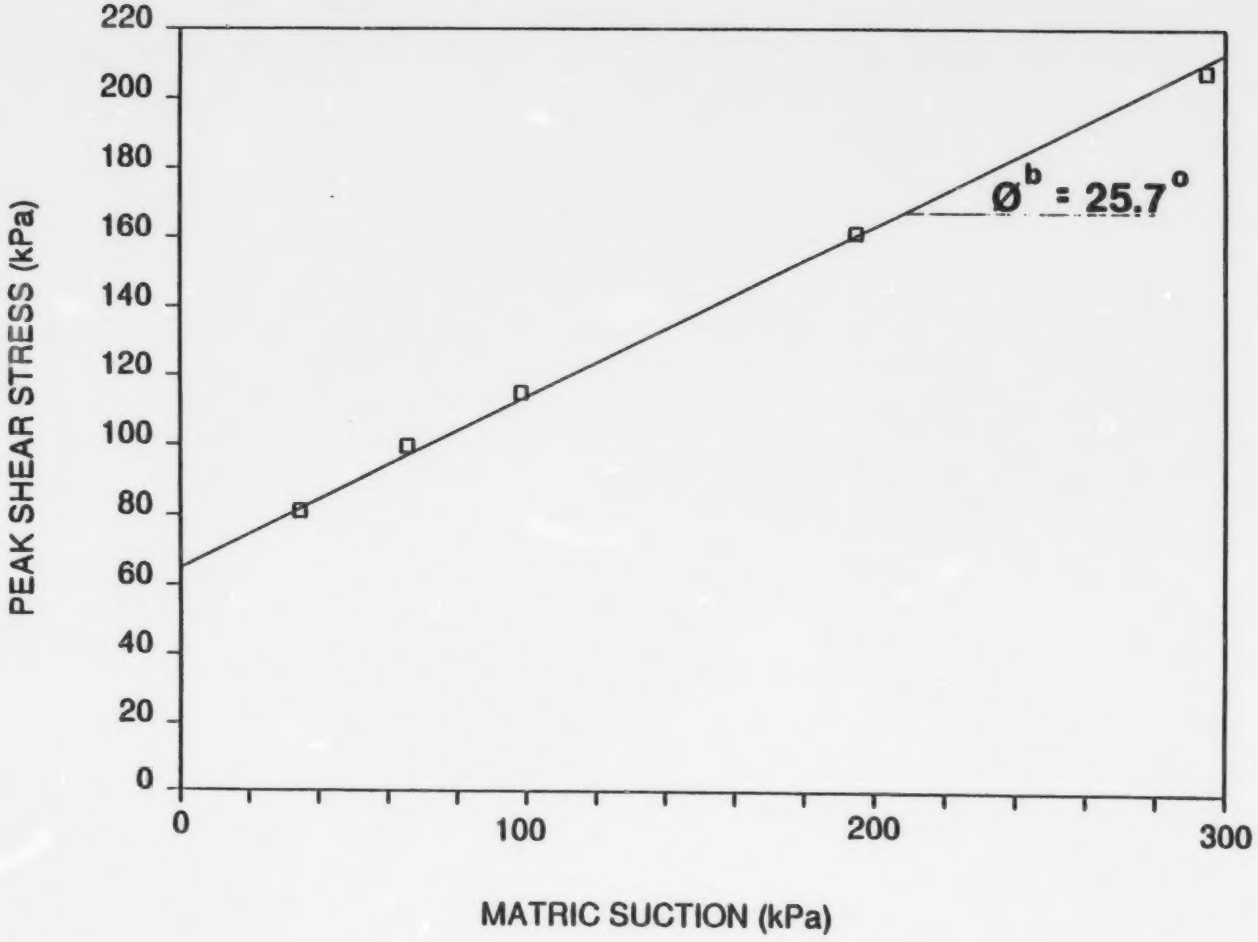

Fig. 4.7 Determination of the ϕ^b angle for a five stage direct shear test on a glacial lake clay

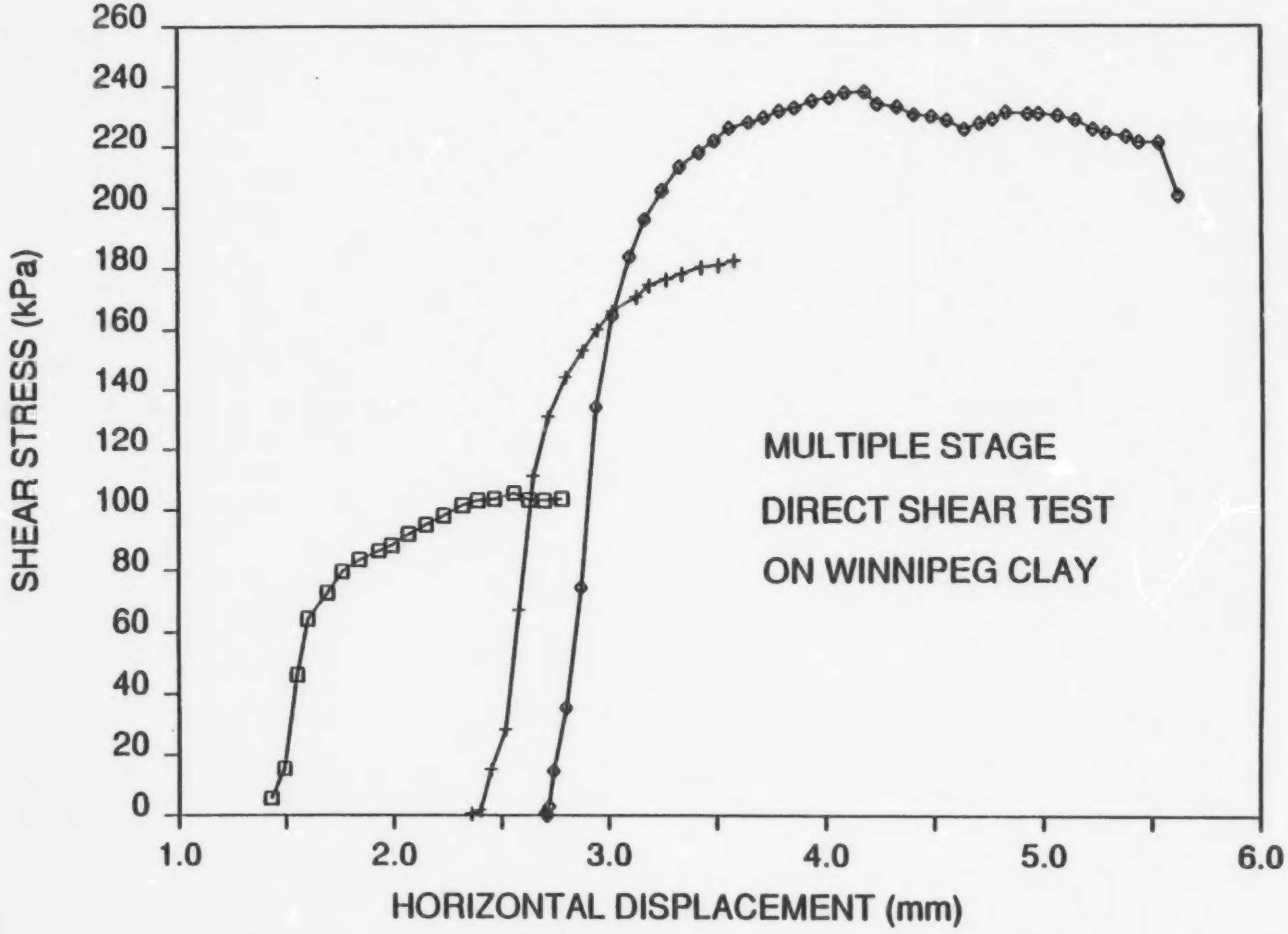

Fig. 4.8 Results of a three stage direct shear test on a glacial lake clay

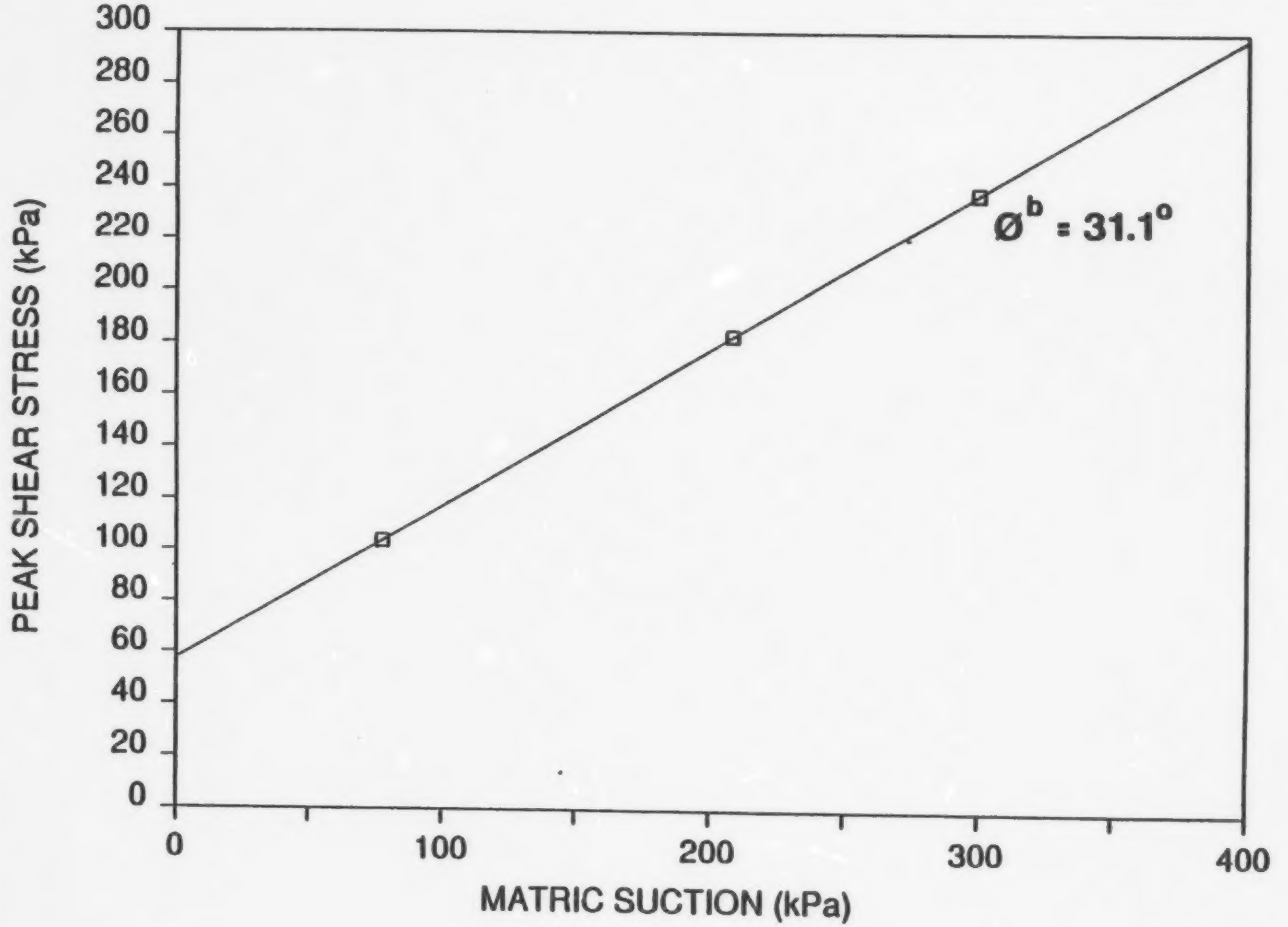

Fig. 4.9 Determination of the ϕ^b angle for a three stage direct shear test on a glacial lake clay

performed on the second sample. A summary of the shear stress versus horizontal displacement for the second sample is illustrated in Figure 4.8. The peak shear stress from each stage for the second sample are plotted in Figure 4.9. An angle ϕ^b even higher than 25 degrees was measured. These results do not appear to be completely consistent with results for other materials which suggest that a ϕ^b angle of 15 degrees is an appropriate design value. Further research should be conducted to broaden the data base for the ϕ^b angle. However, it may be that when highly plastic clays are near 100% saturation, the ϕ^b angle may approach ϕ'.

4.3 Matric Suction

The last design parameter to be discussed is the soil suction or matric suction term. Continuing research at the University of Saskatchewan is devoted to the use of the thermal conductivity sensor to measure soil suction insitu or in the laboratory (67, 68, and 69).

The AGWA-II sensor consists of a thermister and a 20 ohm heater embedded in a porous ceramic block. Figure 4.10 shows a cross-sectional diagram of the thermal conductivity sensor. The amount of water in the block affects the heat dissipation characteristics of the block. Measurements are made by inserting the sensor into the soil and allowing the water content of the block to come to equilibrium with the water content of the soil. Therefore, the water content in the block, and ultimately the water content and soil suction in the surrounding soil, can be calibrated against the heat dissipation characteristics for the block.

A schematic representation of a soil suction profile beneath a

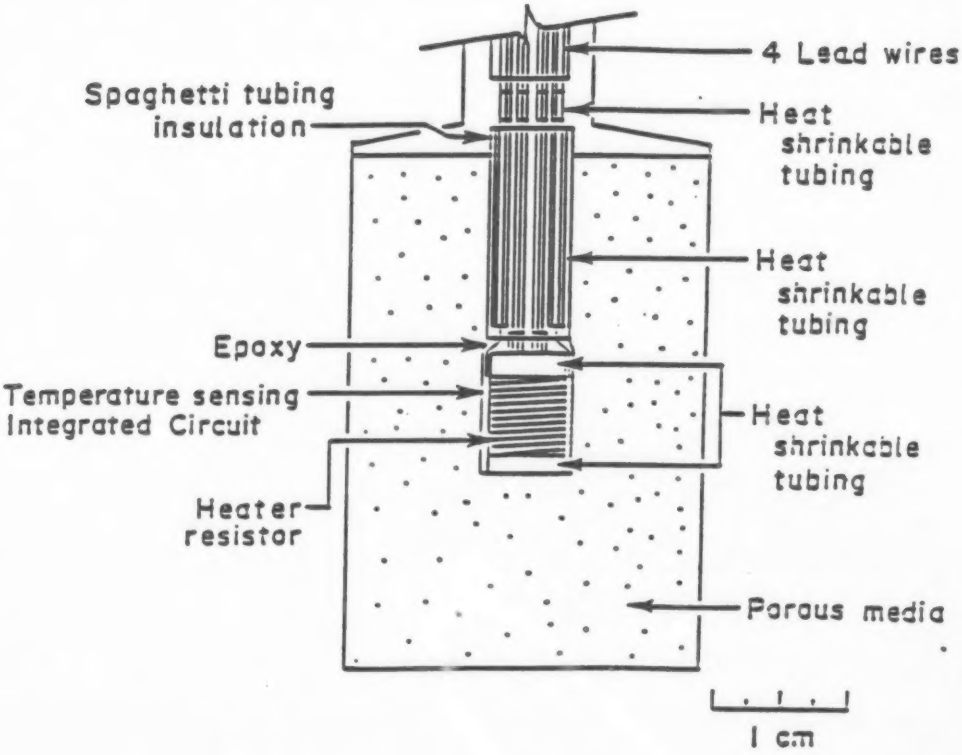
4 Lead wires
Spaghetti tubing insulation
Heat shrinkable tubing
Heat shrinkable tubing
Epoxy
Temperature sensing Integrated Circuit
Heat shrinkable tubing
Heater resistor
Porous media
1 cm

Fig. 4.10 A cross-sectional diagram of the thermal conductivity sensor

tie-track system is presented in Figure 4.11. The diagram shows three scenarios: 1) a typical schematic suction profile for equilibrium with the ground-water table, 2) a typical schematic suction profile for excessive flooding at the surface, and 3) a typical schematic suction profile for excessive dessication at the soil surface. Due to the continuous cycle of wetting and drying which occurs at the ground surface, an actual soil suction profile may take any form between the schematic representations in Figure 4.11.

Figure 4.12 shows an actual pore-water pressure profile determined for the subgrade beneath a railway track in Winnipeg, Manitoba. The soil suction measurements were performed in the laboratory on Shelby tube samples derived from various test-holes beneath the site (31 and 32). The overburden pressure was subtracted from each of the soil suction measurements to compensate for the expansion of the Shelby tube sample upon removal from the tube. This calculation assumes that the pore-pressure parameter relating total stress change to a change in pore-water pressure is 1.0. The complete details regarding the use of thermal conductivity sensors to measure soil suction on Shelby tube samples in the laboratory is presented by Sattler, 1988 (70).

Despite the variability in suction measurements, Figure 4.12 reveals a trend in which the average pore-water pressure is slightly less than the equilibrium hydrostatic line (i.e., the average suction is therefore slightly greater than if the soil were in equilibrium with the water table). The water table is clearly evident from the suction measurements and a decrease in suction (i.e., increase in pore-water pressure) is evident immediately above the water table.

Suppose the water table at the Winnipeg, Manitoba site had been

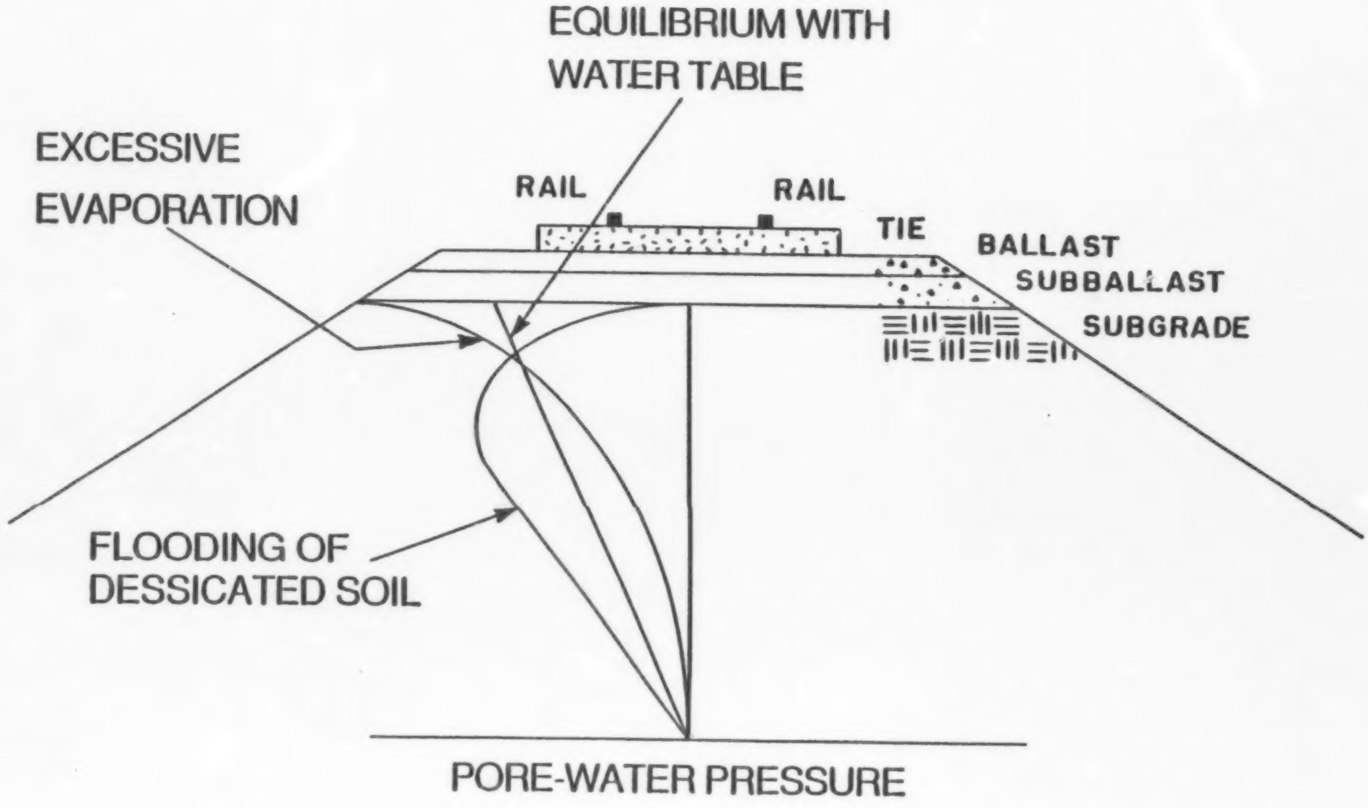
EQUILIBRIUM WITH
WATER TABLE
EXCESSIVE
EVAPORATION
RAIL
RAIL
TIE
BALLAST
SUBBALLAST
SUBGRADE
FLOODING OF
DESSICATED SOIL
PORE-WATER PRESSURE

Fig. 4.11 Typical schematic pore-water pressure profiles

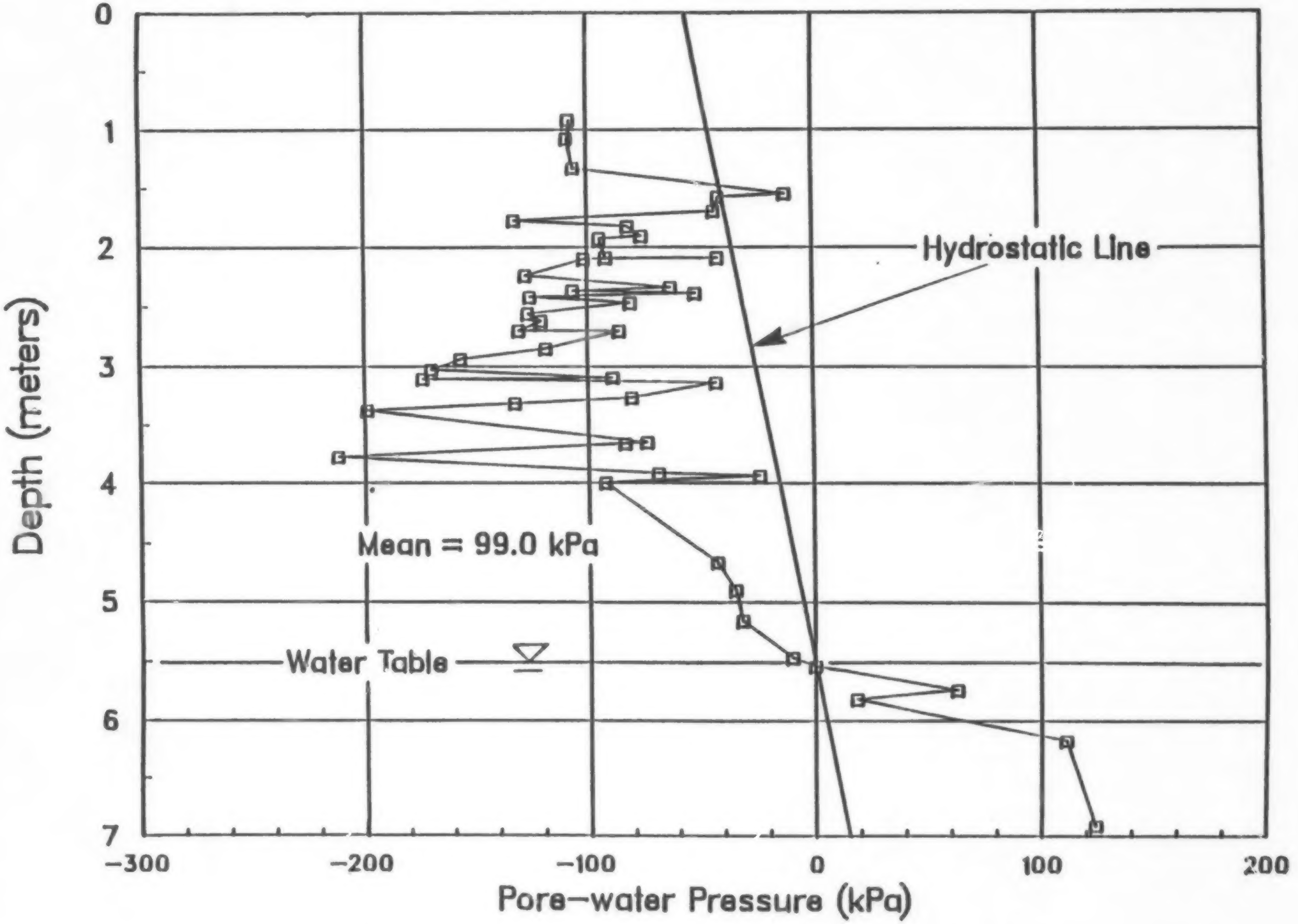

Fig. 4.12 Actual measured pore-water pressure profile for Winnipeg glacial lake clay

deeper. Then, the soil suction measurements at the surface would theoretically have been greater than those which were actually measured. The choice of a design suction value would also have been greater. Conversely, if the water table were located at a shallower depth, the chosen soil suction design value would be smaller.

Measurements of soil suction greatly in excess of those falling on the equilibrium hydrostatic line with the ground-water table should be regarded with caution. It is recommended that the design suction value be compared to the equilibrium hydrostatic line in all design situations. A design suction which greatly exceeds the suction values on the equilibrium hydrostatic line should not be used. Experience with the use of soil suction design values will determine the degree to which the design suction value may be greater than the equilibrium hydrostatic suction values.

The large amount of scatter in the data presented in Figure 4 12 made the selection of a soil suction value for design somewhat difficult. For the particular case described (28), a design suction value was chosen as the mean of the measurements minus one standard deviation for the upper 4 m. The suction was then assumed to decrease linearly to the water table. In many cases, there may be insufficient data to use this type of a statistical approach and reliance must be placed upon engineering judgement. It should be noted that when dealing with an assessment of volume change related to expansive soils, a design analysis may need to be based on the mean and possibly the mean plus one standard deviation (70).

The data presented in Figure 4.12 represented a variation in matric suction from 0 kPa to 280 kPa (28). When the soil suction values were adjusted for overburden pressure, the soil suction varied from 0 kPa to 210 kPa (28). Neglecting the linear increase in soil suction above the water table, the average soil suction was 99.7 kPa and the mean minus one standard deviation was 54.8 kPa (28). The design value represented a statistical analysis performed on the data for one point in time (i.e., in early spring of 1988). It would be desirable to complement the data with suction values for different seasons and under varying rainfall conditions.

In addition to the determination of soil suction using laboratory measurements, considerable data has already been accumulated insitu from several sites in Western Canada (71, 72 and 73). For a site located near Belle Plaine, Saskatchewan soil suction measurements varied from 75 to 250 kPa for a stiff, highly plastic clay (71). Measured suctions for Bechard, Saskatchewan varied from 130 kPa to 225 kPa for a similar material (71). A highly plastic clay near Regina, Saskatchewan showed matric suction measurements between 60 and 275 kPa whereas a glacial till material located near McLean, Saskatchewan yielded suction measurements between 60 and 160 kPa (71). A silty fill near Fort Saskatchewan, Alberta produced matric suctions between 0 and 200 kPa (71).

A thesis produced by van der Raadt in 1988 presents the complete results of the matric suction measurements (73).

Figure 4.13 shows a typical plot of suction versus elapsed time for a sensor located at Belle Plaine, Saskatchewan (73). The measured soil suction varies with the season, but not nearly as much as might be expected. For the purposes of computing bearing capacity, it is desirable to choose an average (or lower) design value for suction.

Figure 4.14 shows the extremes in minimum recorded and maximum

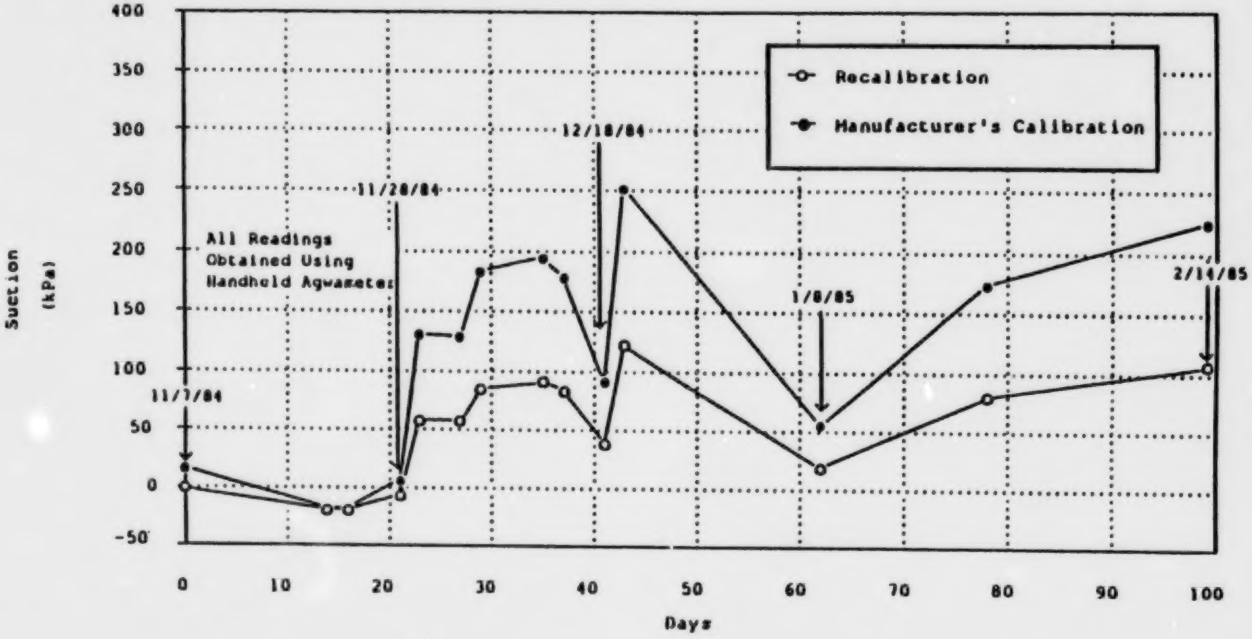

Fig. 4.13 Typical example of suction versus time (extracted from van der Raadt (73))

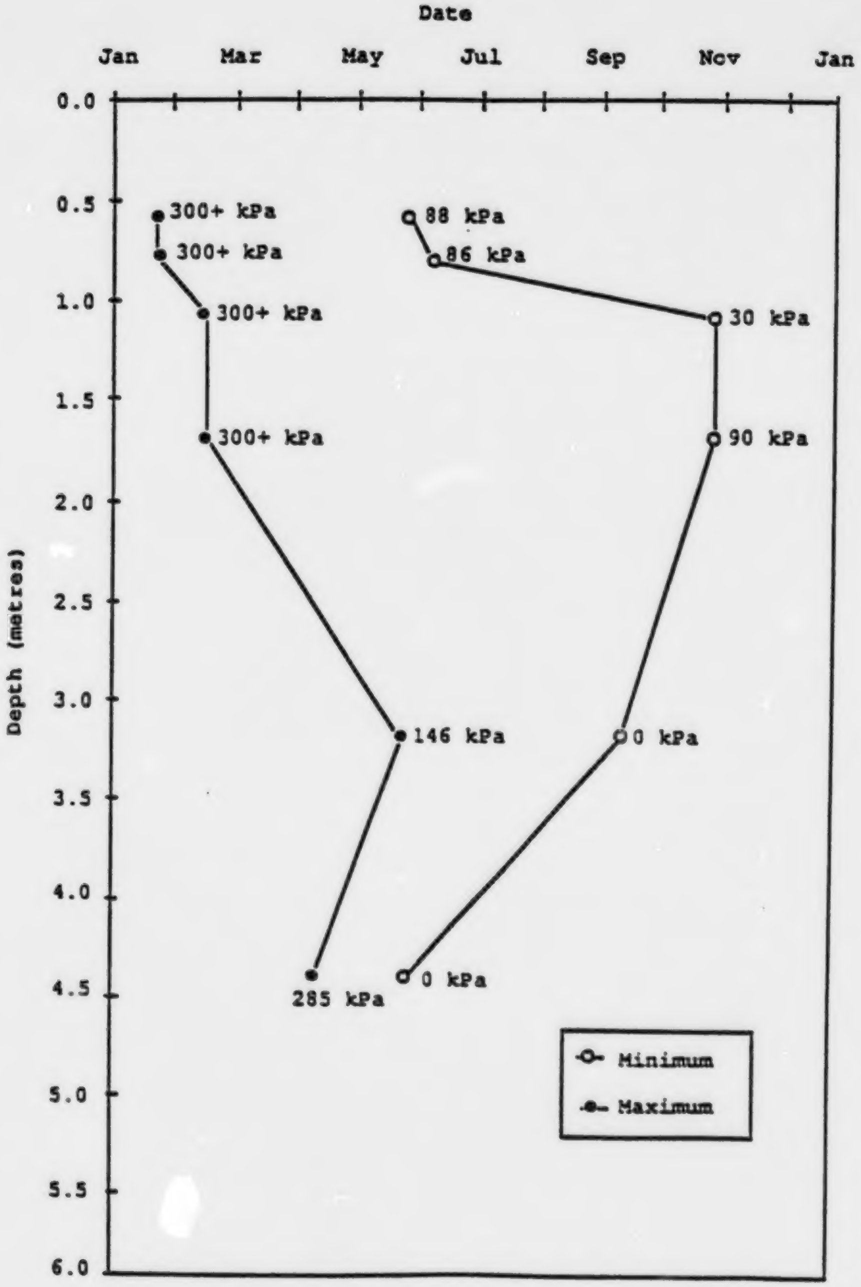

Fig. 4.14 Maximum and minimum recorded suction values (extracted from van der Raadt (73))

recorded suctions measured by van der Raadt (73). The maximum recorded suctions are quite similar and possibly represent the inadequacy of the measuring device for larger values of soil suction. The minimum recorded values vary from 0 kPa to 90 kPa.

Figure 4.15 shows an interpreted plot of soil suction data versus time for various seasons of the year and various depths for Regina, Saskatchewan (73). The greatest extremes in suction measurement are from near the surface. At depth, the soil suction remains essentially constant. The plot also reflects the lag time for various depths between the surface and the depth at which soil suction no longer changes. Further data collection and use will contribute to the data base upon which this plot was based, making future approximations of design values more precise.

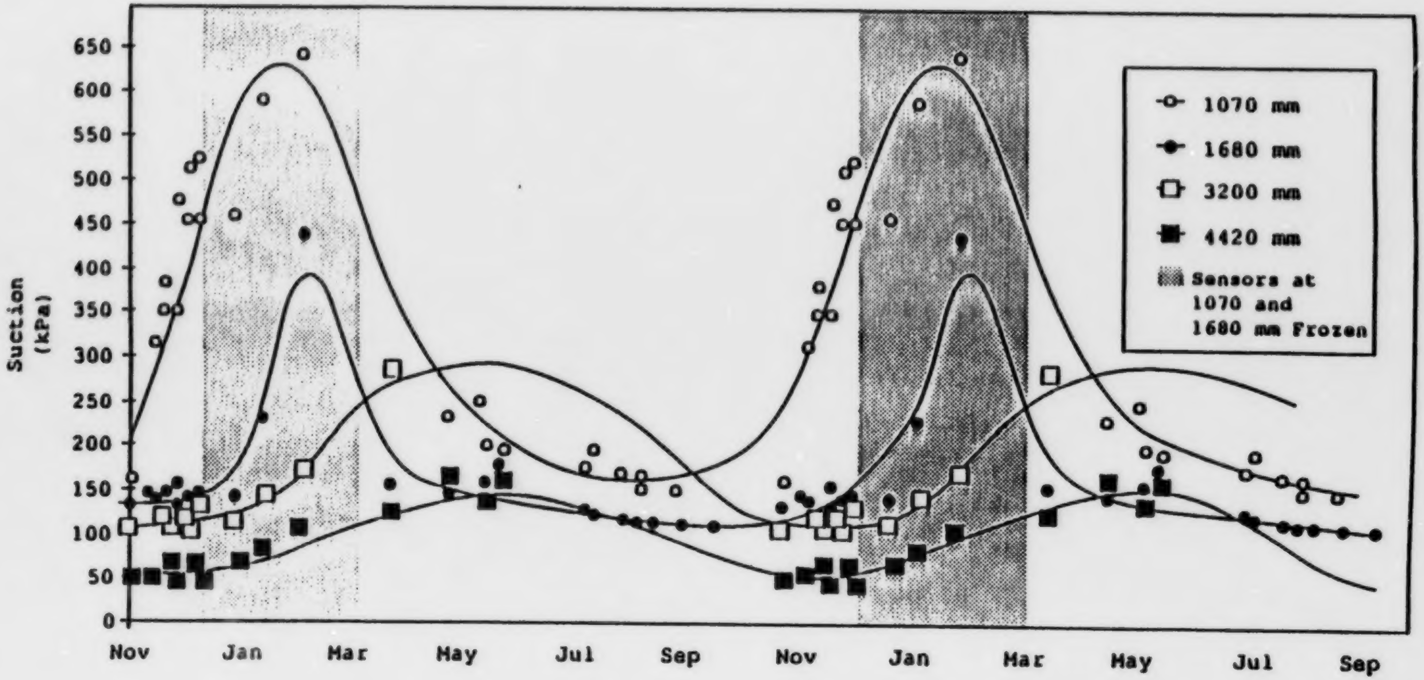

Fig. 4.15 Interpreted plot of matric suction versus time of year for various depths (extracted from van der Raadt (73))

5.0 DESIGN CHARTS

This section presents the methodology used to develop the design charts. The charts are 1) the stress charts derived from the stress analysis, 2) the bearing capacity charts derived from utilization of the bearing capacity approaches, and 3) the bearing capacity factor of safety charts which represent a comparison of the stress analysis results to the bearing capacity results. Example problems showing how to use the design charts are presented in Section 5.5.

5.1 Methodology

A flow chart showing the methodology behind the production of the design charts is presented in Figure 5.1. An introduction to the stress analysis portion of the flow chart has been presented in Section 2.0 while an introduction to the bearing capacity approaches to design have been presented in Section 3.0. Section 4.0 discussed the values of the parameters used in the two sides of the flow chart. More details as to how the two sides of the flow chart combine to produce the bearing capacity factor of safety charts are discussed next.

The GEOTRACK computer program was used for the stress analysis portion of the flow chart. Input to the GEOTRACK computer program included the soil parameters and loading configurations which have already been presented in Sections 2.0 and 4.1, respectively. Output from the GEOTRACK computer program was briefly discussed in Section 2.3. The GEOPLOT post-processing program was used to provide graphical output from the GEOTRACK program. For the purposes of averaging the output stress distributions, the post-processing computer package STRESS was developed.

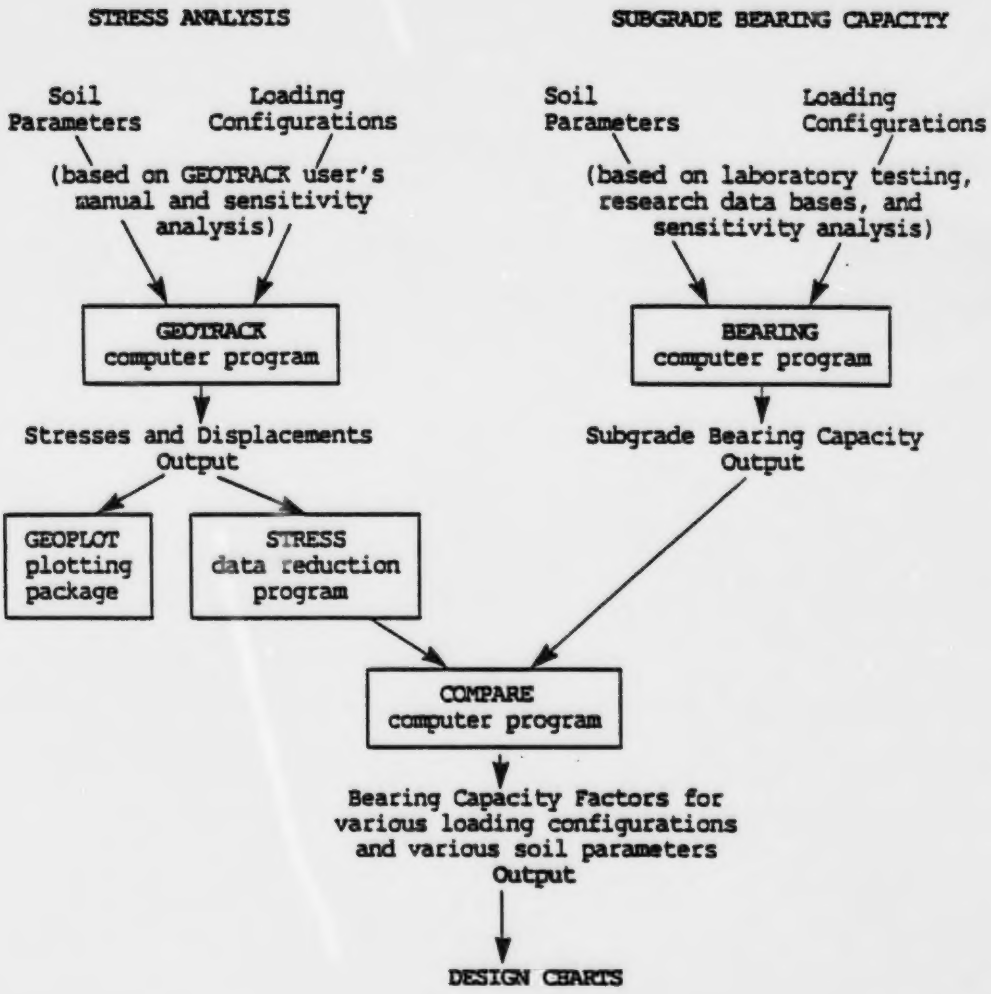
STRESS ANALYSIS
SUBGRADE BEARING CAPACITY
Soil Parameters
Loading Configurations
(based on GEOTRACK user's manual and sensitivity analysis)
Soil Parameters
Loading Configurations
(based on laboratory testing, research data bases, and sensitivity analysis)
GEOTRACK computer program
BEARING computer program
Stresses and Displacements Output
Subgrade Bearing Capacity Output
GEOPLOT plotting package
STRESS data reduction program
COMPARE computer program
Bearing Capacity Factors for various loading configurations and various soil parameters Output
DESIGN CHARTS

Fig. 5.1 Flow chart for development of the bearing capacity design charts

The role of the GEOPLOT post-processing package was to provide a graphical representation of the stress output. The graphical output was necessary to facilitate the development of the averaging techniques used in the post-processing program STRESS and to present the output information within this report. However, the plotting files created by the program GEOPLOT were not used directly for the stress analysis. The data reduction program STRESS performed the stress distribution averaging directly on the GEOTRACK output file. Therefore, both the GEOPLOT and the STRESS post-processing packages are used in parallel on the output from the GEOTRACK computer program.

The output from the STRESS computer program was used directly in the development of the bearing capacity design charts. Therefore, the STRESS post-processing package is described in more detail in Section 5.2 whereas the GEOPLOT post-processing package is described in full detail in a separate document.

On the other side of the flow chart is the bearing capacity analysis. A computer program BEARING was developed to compute the bearing capacity for the various soil parameters and loading configurations. The input soil parameters to the program BEARING have been described in Section 4.2 and 4.3. The loading configurations for different geometries of bearing capacity failures have been described in Section 3.0. Details and output from the computer program BEARING are presented in Section 5.3.

The bearing capacity factor of safety charts were developed by comparison of the averaged stress distributions from the computer program STRESS to the bearing capacity computed from the program BEARING. A computer program COMPARE was designed to combine the STRESS output and the BEARING output files, check for loading configuration compatibility, and compute the factor of safety against a bearing capacity failure. The computer program COMPARE is described in Section 5.4. The resulting bearing capacity factor of safety charts and their use is presented in Section 5.4.

User's manuals and complete documentation for the computer programs, GEOTRACK, GEOPLOT, STRESS, BEARING, and COMPARE are organized into a separate document.

5.2 Presentation of the Stress Charts

The necessity to create a program which averages the stress distribution comes from the fact that a bearing capacity analysis produces a unique value to represent the strength of the soil whereas a stress analysis program, like the computer program GEOTRACK, creates a stress distribution (i.e., several values of stress beneath several different locations of the railway track structure). Since comparison of one value for the bearing capacity to several values representing the stress distribution would result in confusion, it was decided to average the stress distribution for comparison to the bearing capacity.

Four different loading configurations (i.e., Figures 3.4 through 3.7) are considered for a bearing capacity analysis and, therefore, four different averaging techniques must be utilized to average the stress distribution for comparison to each of the four different bearing capacity options. This averaging task is performed by the STRESS post-processing package on the output from the GEOTRACK computer program.

STRESS is an interactive computer program which prompts the user for the file on which the stress averaging is to be performed. The computer program STRESS only averages the vertical stresses at the ballast surface and at the subgrade surface since these are the output stresses required for comparison to the bearing capacity analysis. If two additional depth points are not specified in the GEOTRACK output file for the ballast surface and for the subgrade surface, then the post-processing package STRESS does not have the appropriate data upon which to average the stress distribution for comparison to the bearing capacity analysis.

The STRESS program must also be informed as to which bearing capacity loading configuration the user will wish to compare to the averaged stress distribution. If the user errs, the computer program COMPARE will report the error and the STRESS program can be rerun for the correct loading configuration. A complete user's manual for the program STRESS is included in a separate document.

The averaging techniques performed for each of the four bearing capacity options are presented in Figures 5.2 through 5.5. Each option corresponding to an averaging technique also corresponds to a bearing capacity loading configuration. In other words, the Option 1 "Averaging Technique" presented in Figure 5.2 must be compared to the Option 1 "Bearing Capacity Loading Configuration" presented in Figure 3.4 of Section 3.2, and again in Figure 5.33 in the next section.

Figure 5.2 illustrates the averaging technique for Option 1. For bearing capacity computations, Option 1 corresponds to a width, B, equal to the tie length, and a length, L, equal to infinity. Therefore, the stress distribution is averaged beneath the length of each tie for all the tie data in the GEOTRACK output file. The difference between using "L = infinity" and "L = the length for all ties" is considered insignificant by comparison to the "B" term. An overall average subgrade surface stress is the result. This value is then compared to a Broms

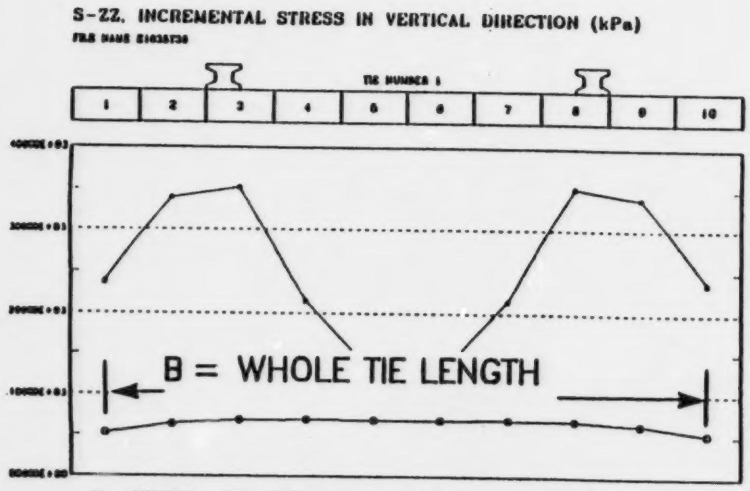

CROSS-SECTIONAL VIEW

OPTION 1

AVERAGE OF SUBGRADE SURFACE STRESSES
FOR WHOLE TIE LENGTH

FOR EACH TIE ANALYZED
ALONG LENGTH OF TRACK

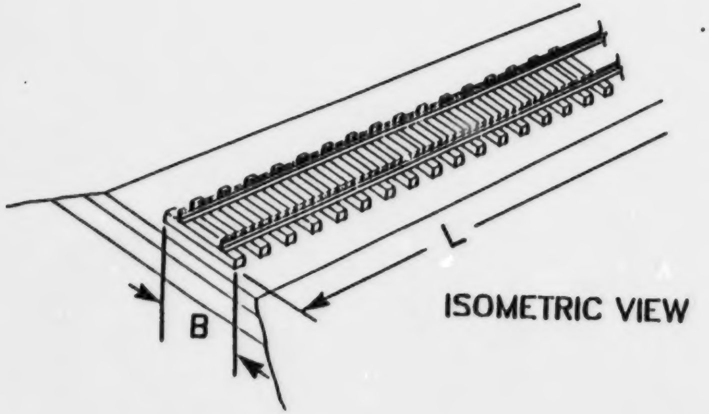

ISOMETRIC VIEW

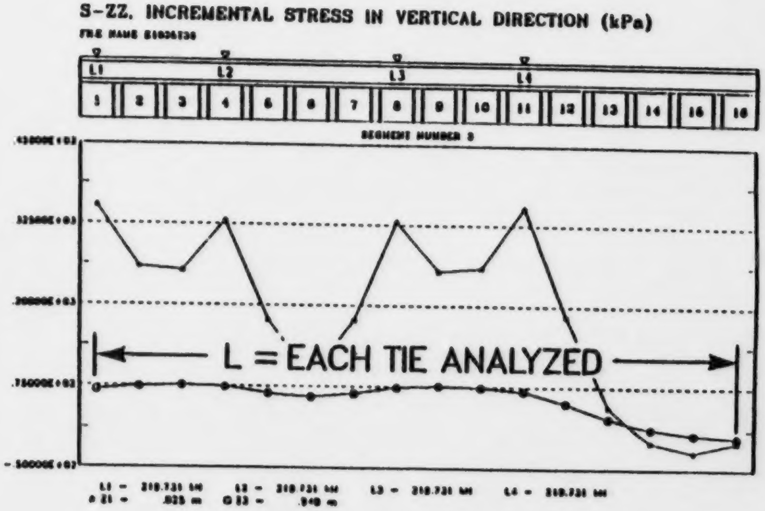

LONGITUDINAL VIEW

Fig. 5.2 Option 1 "Stress Averaging Technique"

approach (2) bearing capacity analysis for the corresponding width, B and length, L illustrated in Figure 5.33.

Figure 5.3 shows the averaging technique for Option 2. The stress distribution beneath the most heavily loaded outer 1/3 of the tie is averaged for a distance beneath the track equal to the length of two closest trucks. For bearing capacity computations, the width, B is equal to 1/3 of the tie length and the length, L is equal to the length of a double truck loading. The bearing capacity option corresponding to Option 2 of the "Stress Averaging Technique" is a Broms approach and is presented in Figure 5.34.

Figure 5.4 presents the only averaging option which can be compared to the Hanna and Meyerhof (1) bearing capacity approach. Although it is preferable to use the Hanna and Meyerhof bearing capacity approach (1) for Option 3, a Broms type approach (2) could also be used. The stress distribution is averaged beneath any one tie to result in an average stress beneath the tie. The bearing capacity approach assumes that the width for analysis, B, equals the tie width and the length, L, is infinity. The corresponding Hanna and Meyerhof approach is presented in Figure 5.35.

Option 4 presented in Figure 5.5 corresponds to a Broms bearing capacity analysis in which the width, B, is equal to the double truck length, and the length, L, is equal to 1/3 of the tie length. The Broms bearing capacity approach to which this averaging technique is compared is presented in Figure 5.36.

Typical stress charts are presented for each of the options in the next figures. However, emphasis has been placed on presenting the stress results for Option 2 because this type of bearing capacity failure is

OPTION 2

AVERAGE OF SUBGRADE SURFACE STRESSES
FOR 1/3 TIE LENGTH

FOR EACH TIE
WITHIN LENGTH OF DOUBLE TRUCK

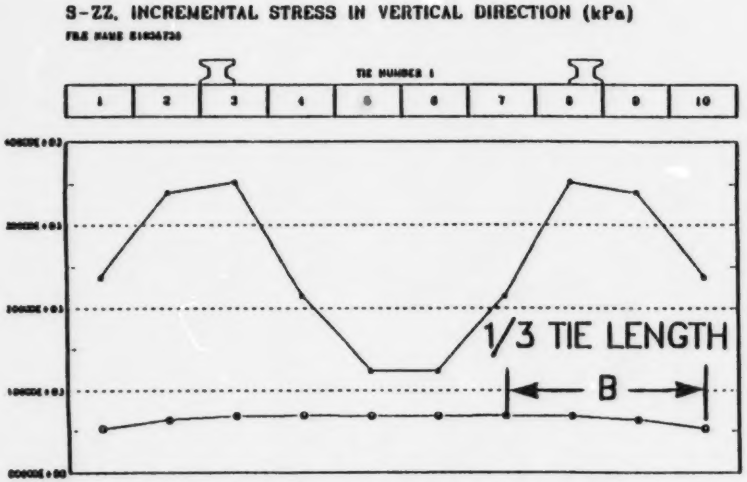

CROSS-SECTIONAL VIEW

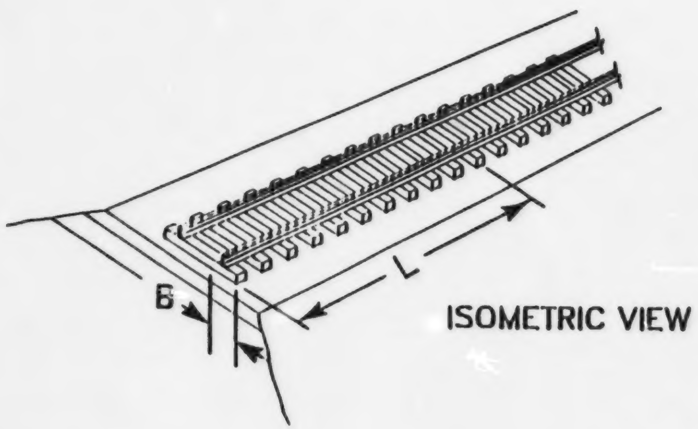

ISOMETRIC VIEW

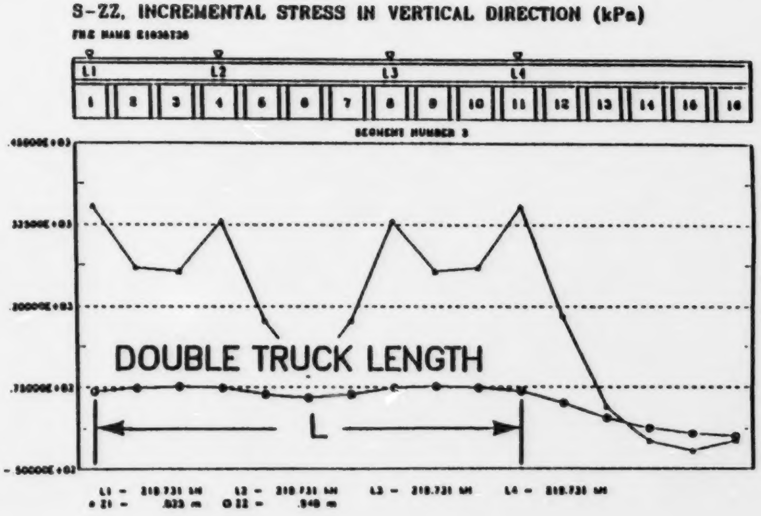

LONGITUDINAL VIEW

Fig. 5.3 Option 2 "Stress Averaging Technique"

OPTION 3

AVERAGE OF BALLAST SURFACE STRESSES

FOR WIDTH OF ONE TIE

AND LENGTH OF ONE TIE

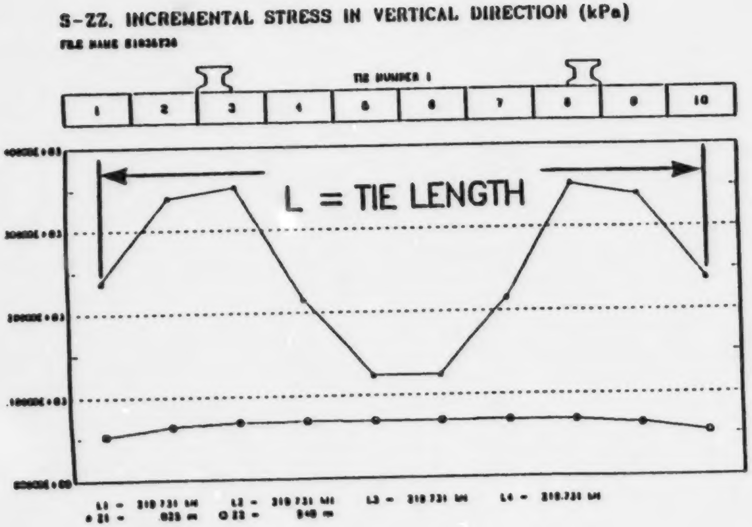

CROSS-SECTIONAL VIEW

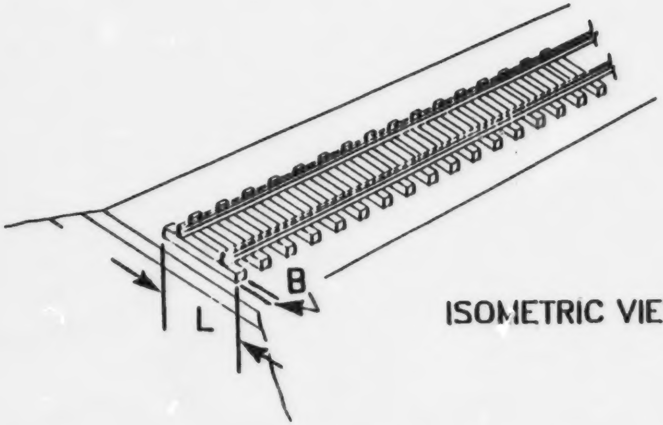

ISOMETRIC VIEW

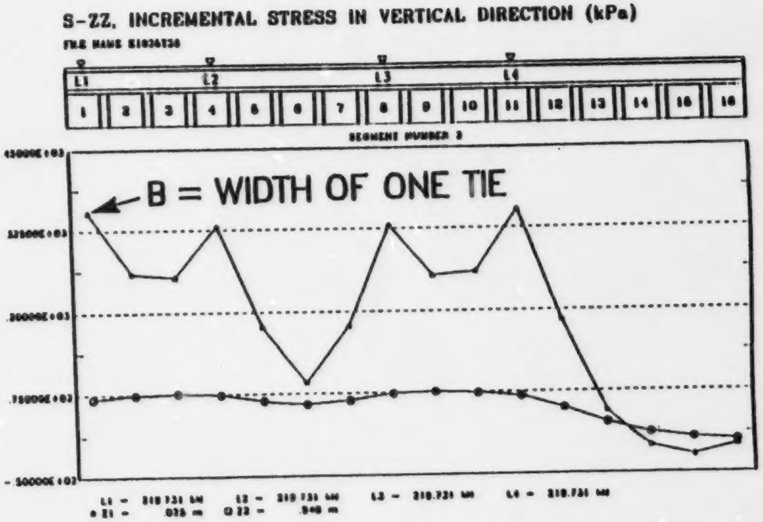

LONGITUDINAL VIEW

Fig. 5.4 Option 3 "Stress Averaging Technique"

OPTION 4

AVERAGE OF SUBGRADE SURFACE STRESSES
FOR WIDTH OF DOUBLE TRUCK

AND LENGTH OF 1/3 TIE

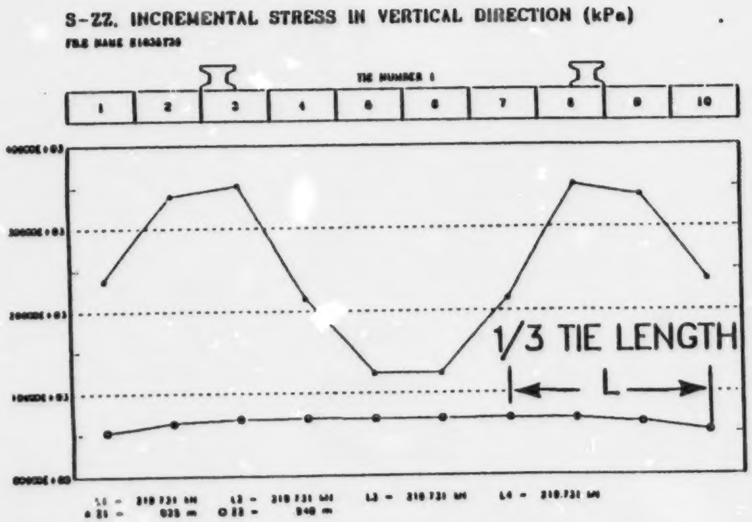

CROSS-SECTIONAL VIEW

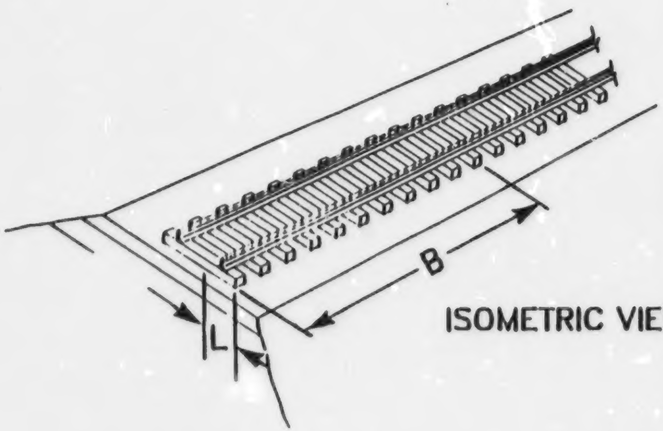

ISOMETRIC VIEW

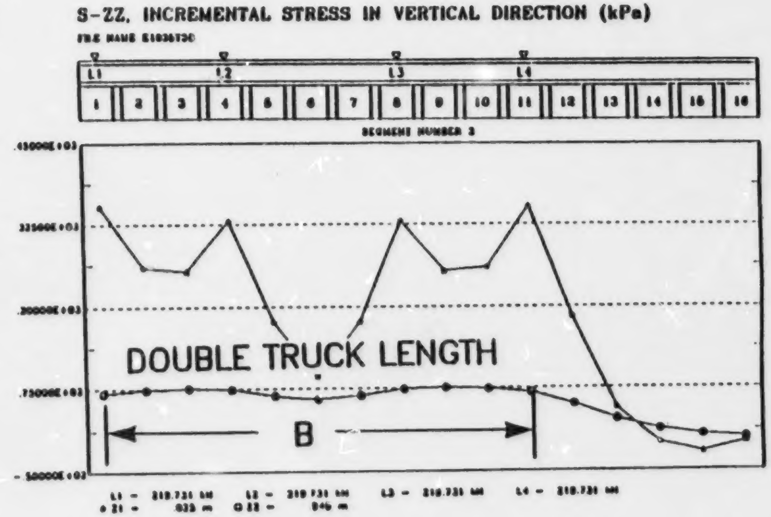

LONGITUDINAL VIEW

Fig. 5.5 Option 4 "Stress Averaging Technique"

most commonly observed in the field.

Figure 5.6 presents a summary of 12 individual GEOTRACK runs and therefore, 12 averages of each of the 12 stress distributions. All the average stresses plotted in Figure 5.6 were averaged according to the Option 1 "Stress Averaging Technique". The subgrade surface stress is presented as a function of the total granular thickness below the tie. Of the total granular thickness below the tie, 203 mm (8") of the granular material was modelled as a ballast with a 241.5 MPa E modulus. The remaining granular material was a subballast with an E modulus equal to 103.5 MPa. The subgrade E modulus was 69.0 MPa. Three dynamic axle loads were modelled corresponding to each of the three lines on the plot.

Figure 5.7 utilized all but one of the parameters described for Figure 5.6. The subballast E modulus for Figure 5.7 is equal to the ballast E modulus of 241.5 MPa, whereas in Figure 5.6 the subballast E modulus was equal to 103.5 MPa. A comparison of Figures 5.6 and 5.7 reveals that for the smaller granular thicknesses below the tie, the advantage in using a subballast with a higher E modulus is negligible. However, for greater granular thicknesses below the tie, there is some advantage in using a subballast with a higher E modulus.

Figures 5.8 through 5.15 illustrate the results for the Option 1 "Stress Averaging Technique" for a ballast thickness of 305 mm (12 in.)

Figures 5.16 through 5.23 illustrate the results for the Option 2 "Stress Averaging Technique" for a ballast thickness of 203 mm (8"). Figures 5.24 through 5.31 illustrate the results for the Option 2 "Stress Averaging Technique" for a ballast thickness of 305 mm (12"). Again the subballast depths are varied and the subgrade surface stress is plotted against the total granular thickness of the material. As described in

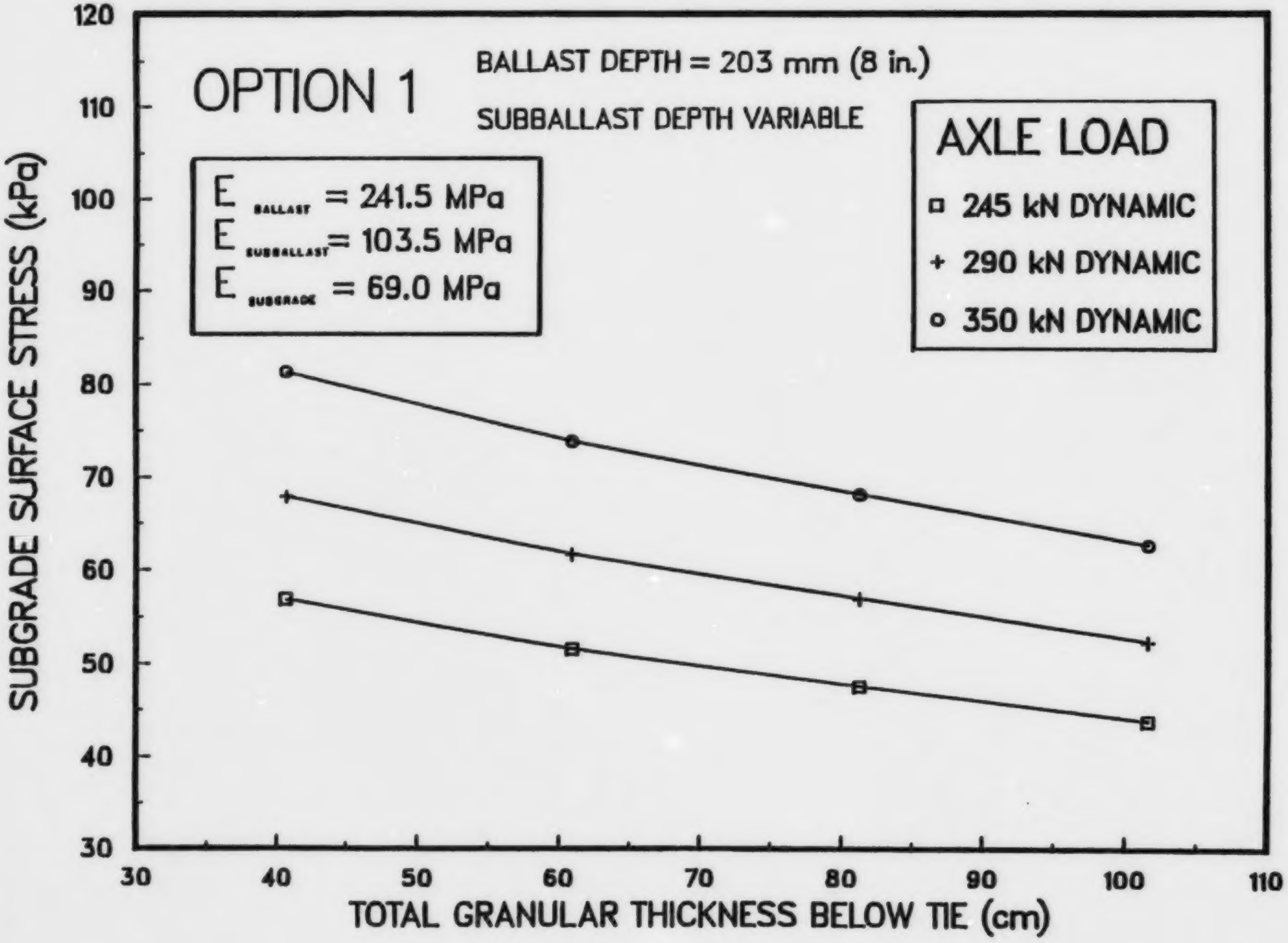

Fig. 5.6 Stress chart for Option 1, Subgrade E = 69.0 MPa, Subballast E = 103.5 MPa

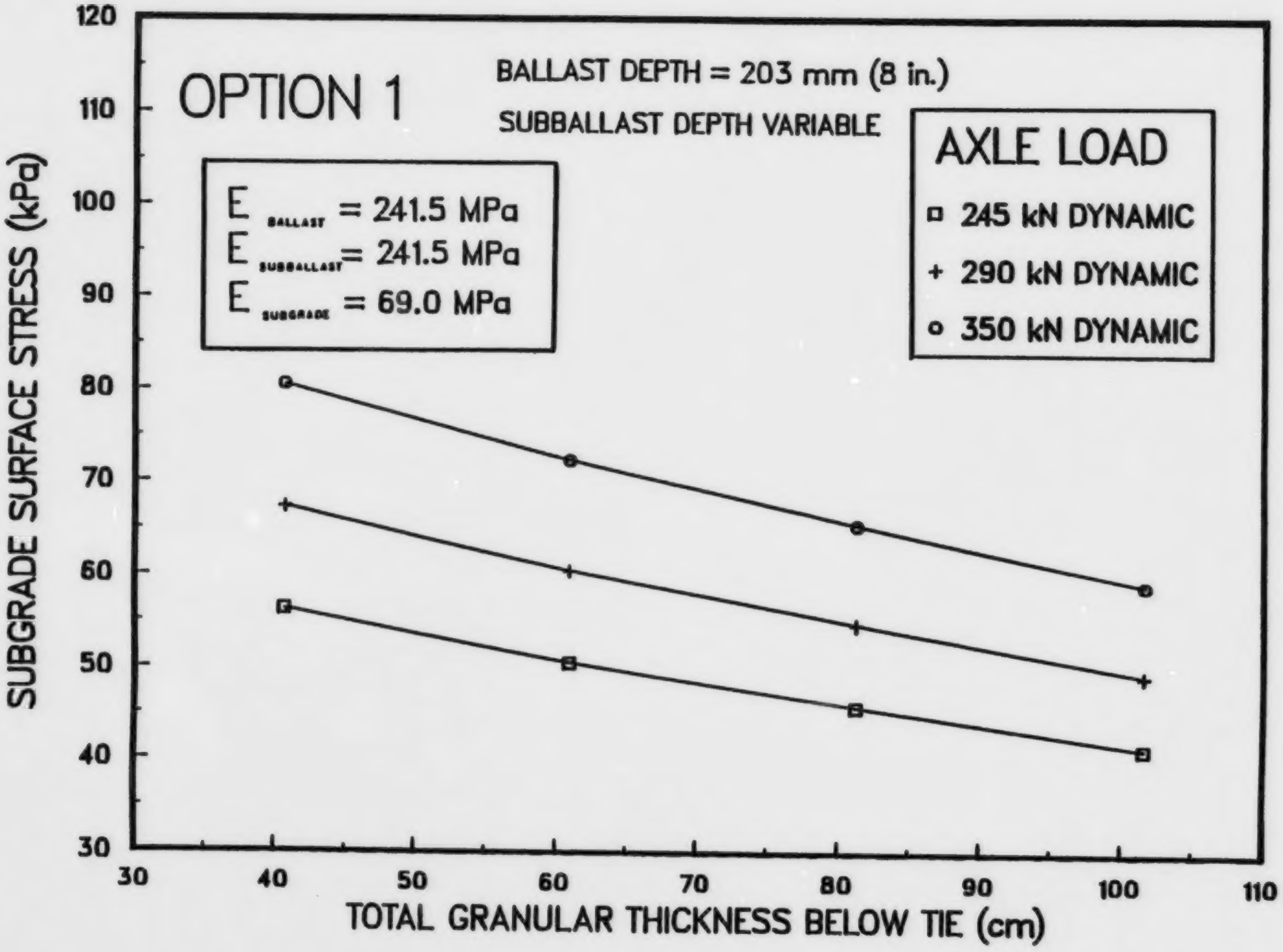

Fig. 5.7 Stress chart for Option 1, Subgrade E = 69.0 MPa, Subballast E = 241.5 MPa

Section 4.1, in addition to varying the subballast E modulus, the subgrade E moduli have also been varied and are portrayed on the stress charts. The charts present results only for the three dynamic axle loads described in the legend on each chart.

Figure 5.16 suggests significant nonlinearity in the subgrade surface stress versus total granular thickness relationship for an extremely soft subgrade. Nonlinearity in the relationship is also evident in Figures 5.24 and 5.25. Although these charts have been included for the sake of completeness, it is suggested that for extremely weak subgrades, it would be better to perform a stress analysis with the GEOTRACK computer program rather than relying on the interpolation of results within the charts.

One trend evident in the stress charts is the decrease in subgrade surface stress for the increase in subballast E modulus. Examine Figures 5.18 and 5.19 as a pair of stress charts in which only the subballast E modulus has been varied. For each pair of charts in which the subgrade modulus is kept constant and only the subballast modulus is changed, this trend is evident. This trend suggests that at larger required granular thicknesses below the tie, it is advantageous to use a better quality subballast.

A comparison between the two sets of Option 2 charts (i.e., comparing Figure 5.18 to Figure 5.26) suggests negligible reduction in subgrade surface stress for increasing the ballast depth from 203 mm (8") to 305 mm (12"). If Figure 5.18 were overlain on Figure 5.26 (being careful to match the x-axis total granular thicknesses and the y-axis subgrade surface stresses), the lines on each Figure would essentially match. The same is true for Figures 5.19 and 5.27 as a pair, Figures 5.20 and 5.28, Figures 5.21 and 5.29, Figures 5.22 and 5.30, and Figures 5.23 and 5.31.

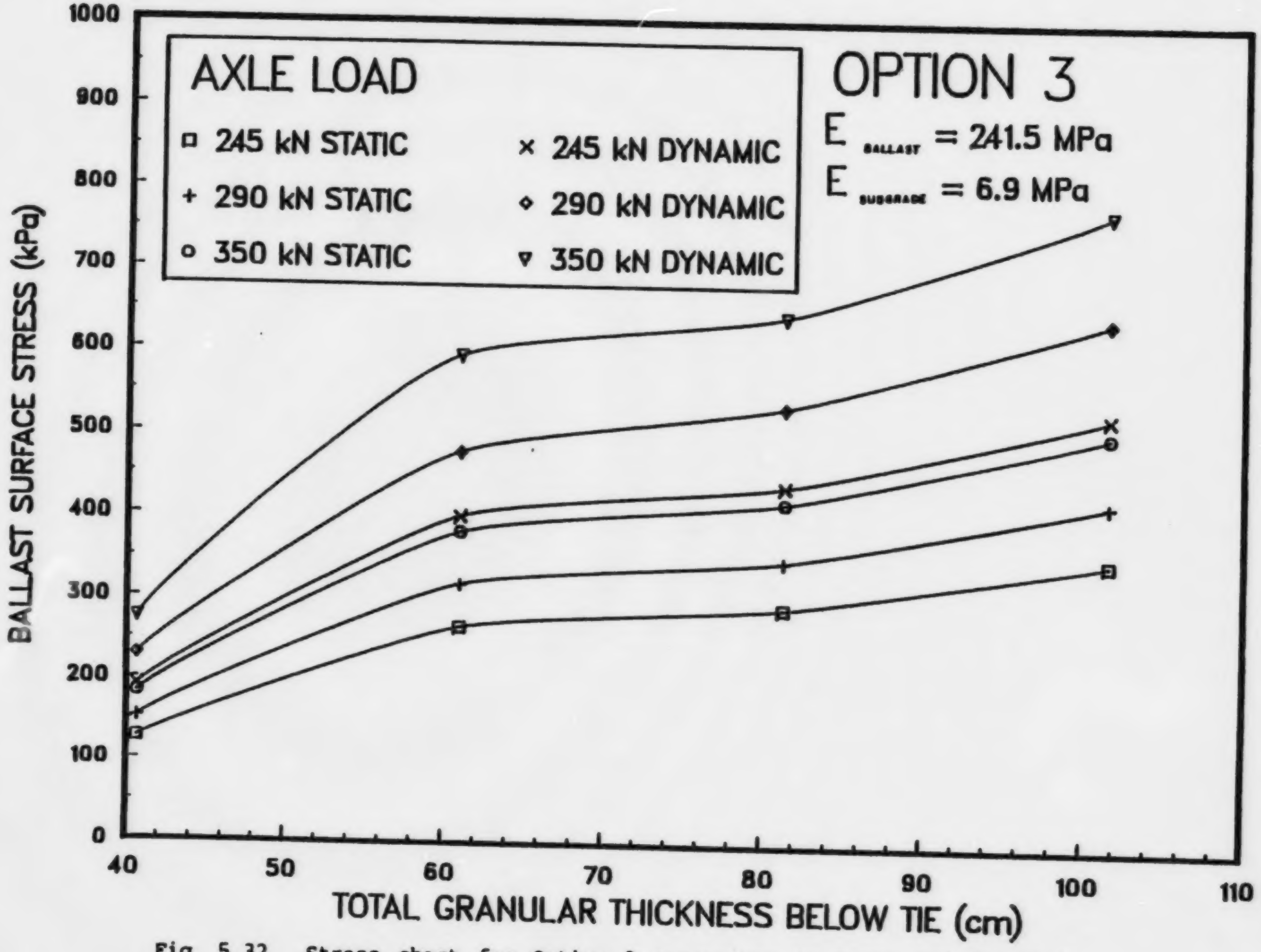

Fig. 5.32 Stress chart for Option 3 comparison to Hanna and Meyerhof approach

Figure 5.32 presents a typical stress chart for the ballast surface stress which can be compared to the Hanna and Meyerhof bearing capacity. The chart was derived using a subgrade E modulus of 6.90 MPa and a ballast E modulus of 241.5 MPa. A subballast layer was assumed to be absent. The chart shows both the static and dynamic axle load plots.

Stress charts have not been included for any Option 4 "Stress Averaging Techniques". A closer inspection of the definition of the averaging technique for each of Options 2 and 4 will reveal that the "Stress Averaging Techniques" described produce identical results. However, the resulting bearing capacities are quite different. Since the Stress Averaging Options 2 and 4 produce the same results, the charts for Option 4 were omitted for the sake of brevity.

5.3 Presentation of Bearing Capacity Charts

Bearing capacity is computed from either the Broms approach (2) or the Hanna and Meyerhof approach (1). Four different loading configurations are used for the bearing capacity computations. These configurations are described in Section 3.2 and are used for comparison to the four "Stress Averaging Techniques" presented in Figures 5.2 through 5.5. The four bearing capacity options are presented in Figures 5.33 through 5.36.

Option 1 (i.e., Figure 5.33) corresponds to a width, B, equal to the tie length and a length, L, equal to infinity. Option 2 (i.e., Figure 5.34) corresponds to a width, B, equal to 1/3 of the tie length, and a length, L, equal to the length of a double truck loading. Option 3 (i.e., Figure 5.35) corresponds to a width, B, equal to the tie width, and a length, L, equal to infinity. Option 4 (i.e., Figure 5.36)

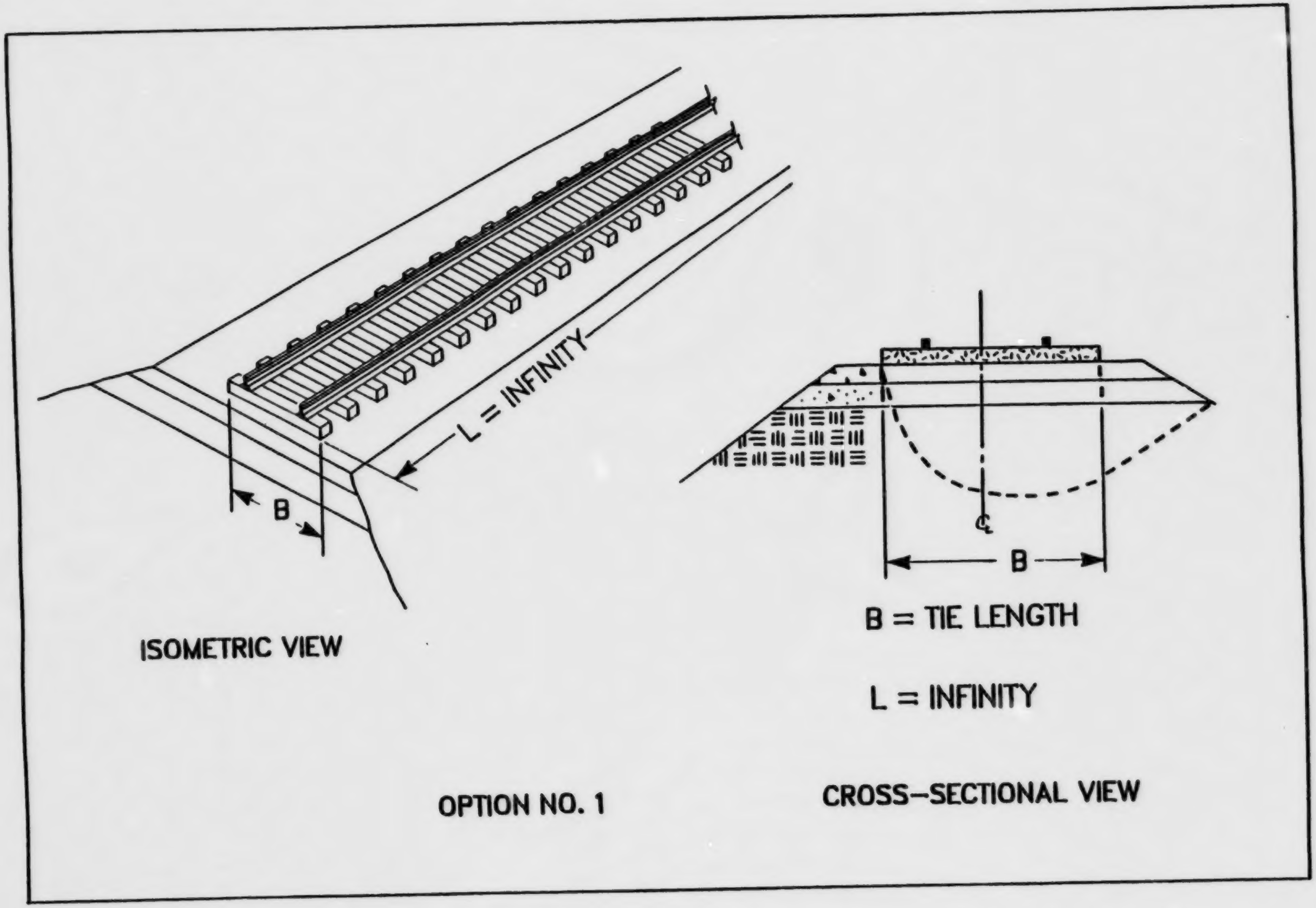
L = INFINITY
B
ISOMETRIC VIEW
℄
B
B = TIE LENGTH
L = INFINITY
OPTION NO. 1
CROSS-SECTIONAL VIEW

Fig. 5.33 Option 1 "Bearing Capacity Configuration"

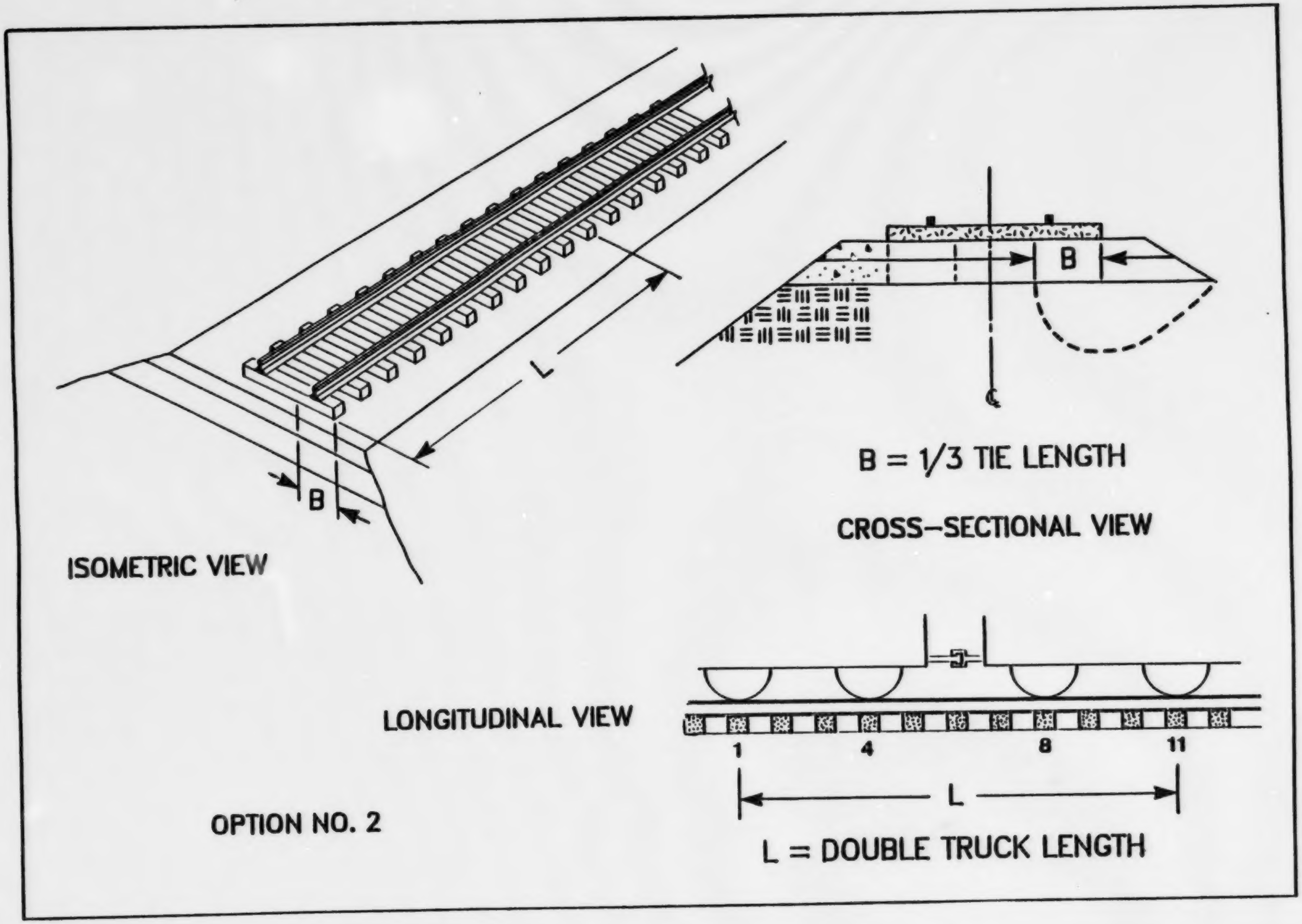
L
B
ISOMETRIC VIEW
B
℄
B = 1/3 TIE LENGTH
CROSS-SECTIONAL VIEW
LONGITUDINAL VIEW
1
4
8
11
L
L = DOUBLE TRUCK LENGTH
OPTION NO. 2

Fig. 5.34 Option 2 "Bearing Capacity Configuration"

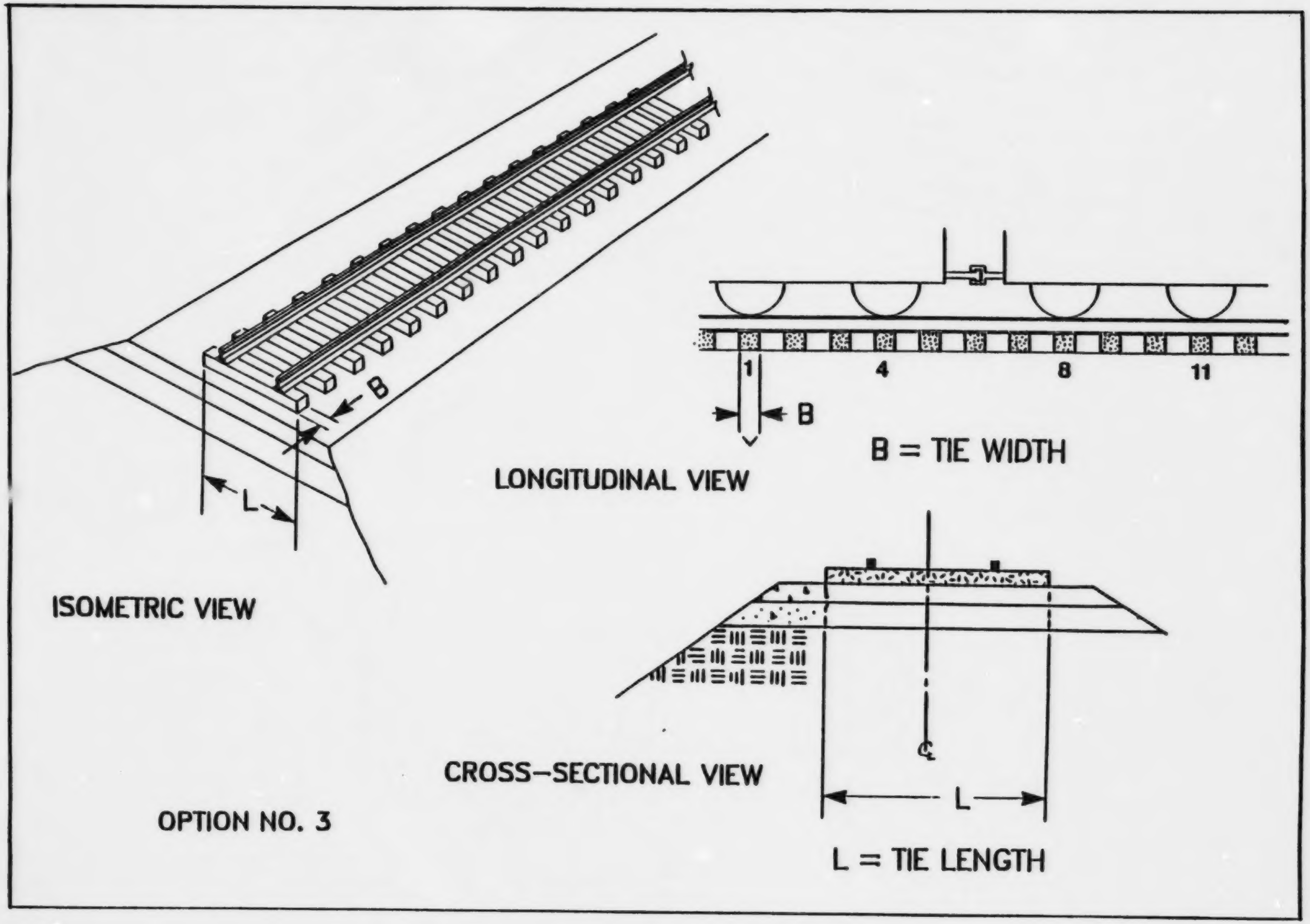
B
L
ISOMETRIC VIEW
1
4
8
11
B
B = TIE WIDTH
LONGITUDINAL VIEW
℄
L
CROSS-SECTIONAL VIEW
L = TIE LENGTH
OPTION NO. 3

Fig. 5.35 Option 3 "Bearing Capacity Configuration"

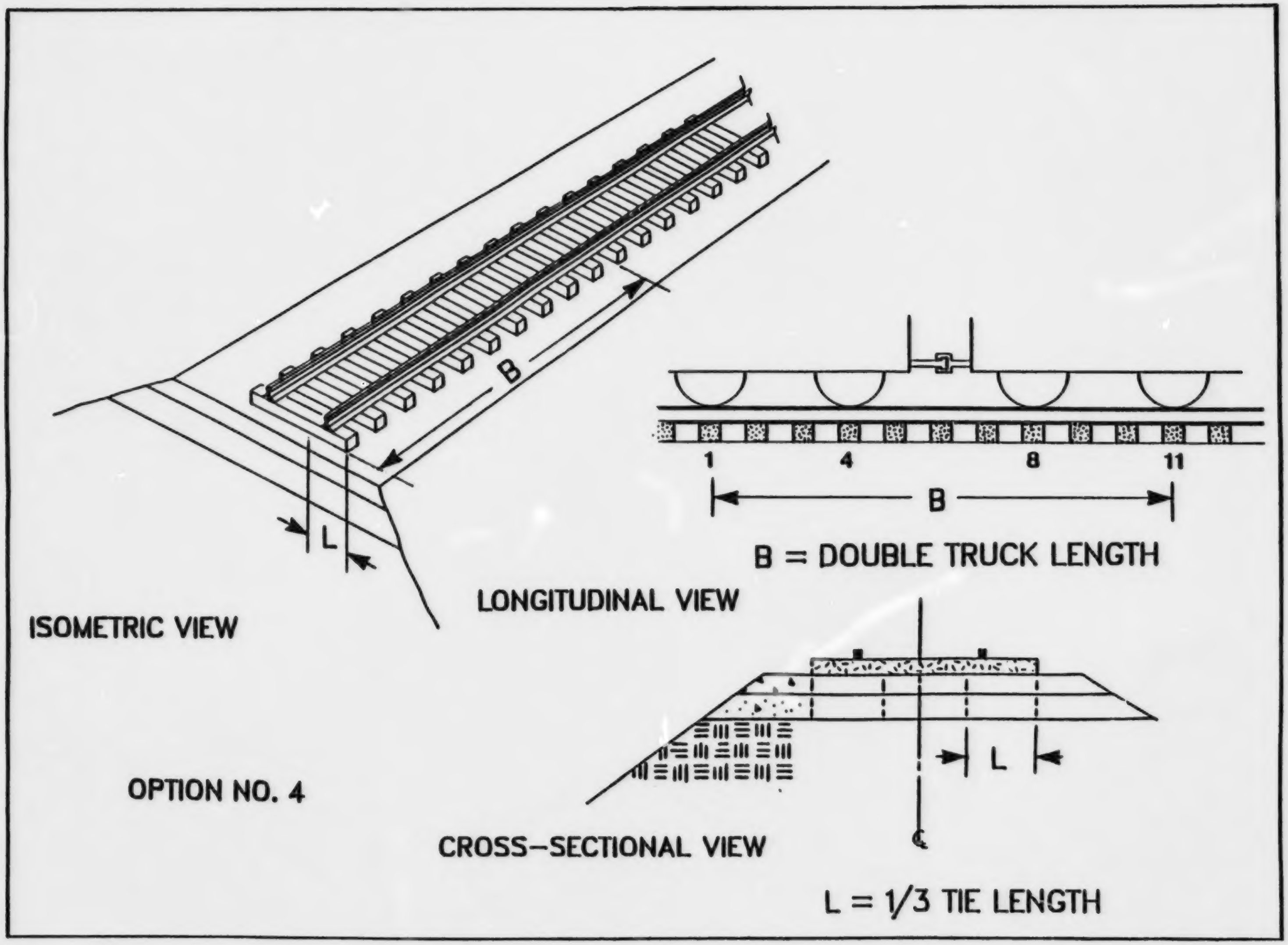
B
L
ISOMETRIC VIEW
1
4
8
11
B
B = DOUBLE TRUCK LENGTH
LONGITUDINAL VIEW
L
℄
OPTION NO. 4
CROSS–SECTIONAL VIEW
L = 1/3 TIE LENGTH

Fig. 5.36 Option 4 "Bearing Capacity Configuration"

corresponds to a width, B, equal to the double truck length, and a length, L, equal to 1/3 of the tie length.

The computer program, BEARING was developed to facilitate the computation of bearing capacity. If it is undesireable to interpolate for values within the charts presented in this section, the program BEARING can be used interactively to compute bearing capacity by either Broms approach or the Hanna and Meyerhof approach. A complete user's manual for the computer program BEARING is presented under separate cover.

Using Option 1 to compute the subgrade bearing capacity by Broms method results in Figures 5.37 through 5.39. Figure 5.37 shows a plot of the subgrade bearing capacity for various values of the design total cohesion for ϕ' angles of 10, 15, 20, and 25 degrees (i.e., a range which would be reasonable for a clay subgrade). Figure 5.38 shows a plot of typical subgrade bearing capacities for reasonable soil parameters for a glacial till material whereas Figure 5.39 presents typical subgrade bearing capacities for reasonable soil parameters for a silt or sand.

The bearing capacity computations show that whether the material is referred to as a sand, clay or glacial till is irrelevant if the material parameters (i.e., c', ϕ', ϕ^b and soil suction) are the same. Therefore, a stiff clay may reasonably exhibit the same soil parameters as a weak glacial till. In this case, the bearing capacity for a stiff clay would be equal to the bearing capacity for a weak glacial till. This observation is evident from the bearing capacity charts presented in Figures 3.37 through 5.39. The charts have been presented as bearing capacity charts for different soil types in order that the user will not be misled into using unreasonable soil parameters for any particular

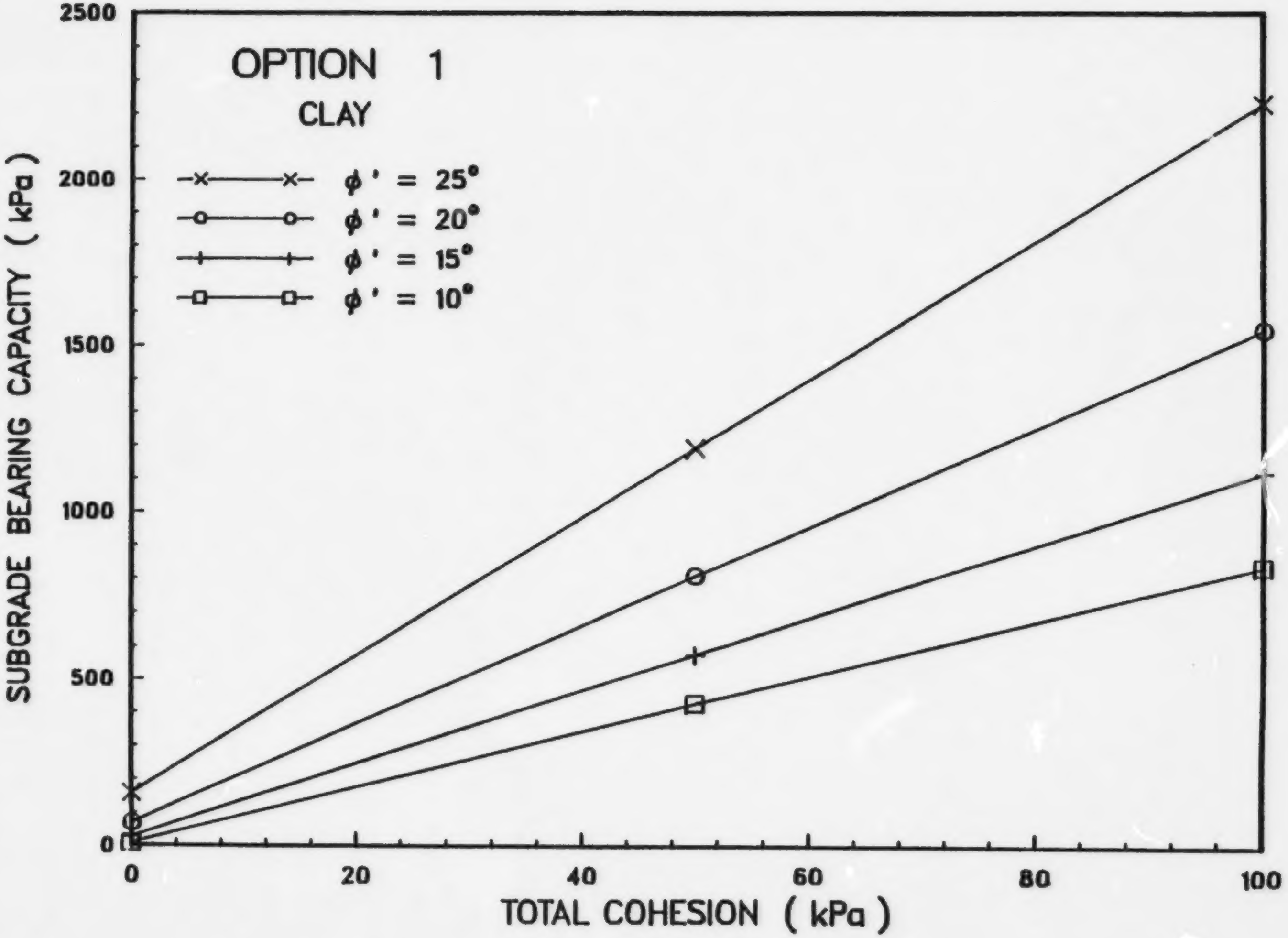

Fig. 5.37 Bearing capacity by Option 1 for typical clay subgrades

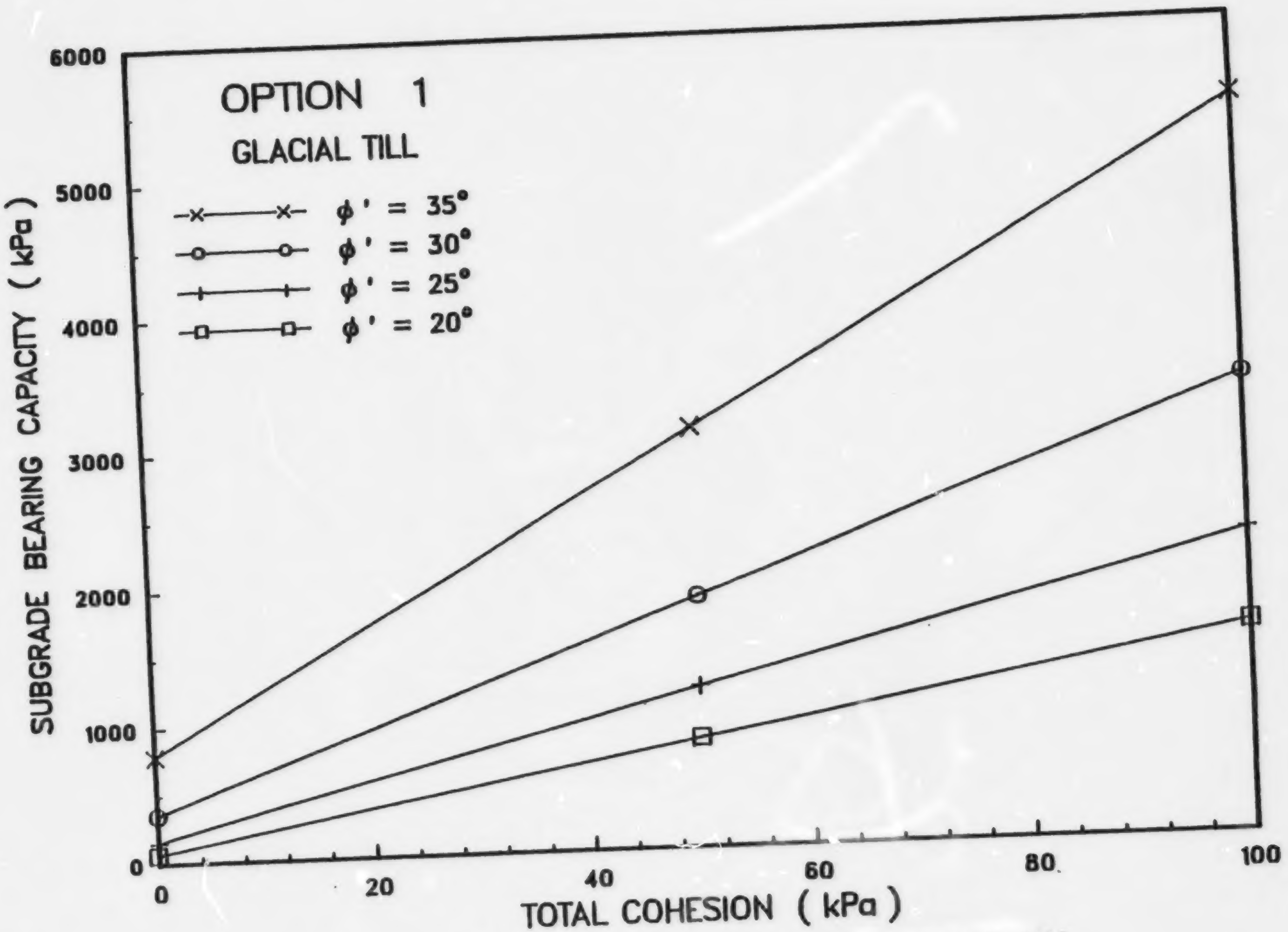

Fig. 5.38 Bearing capacity by Option 1 for typical glacial till subgrades

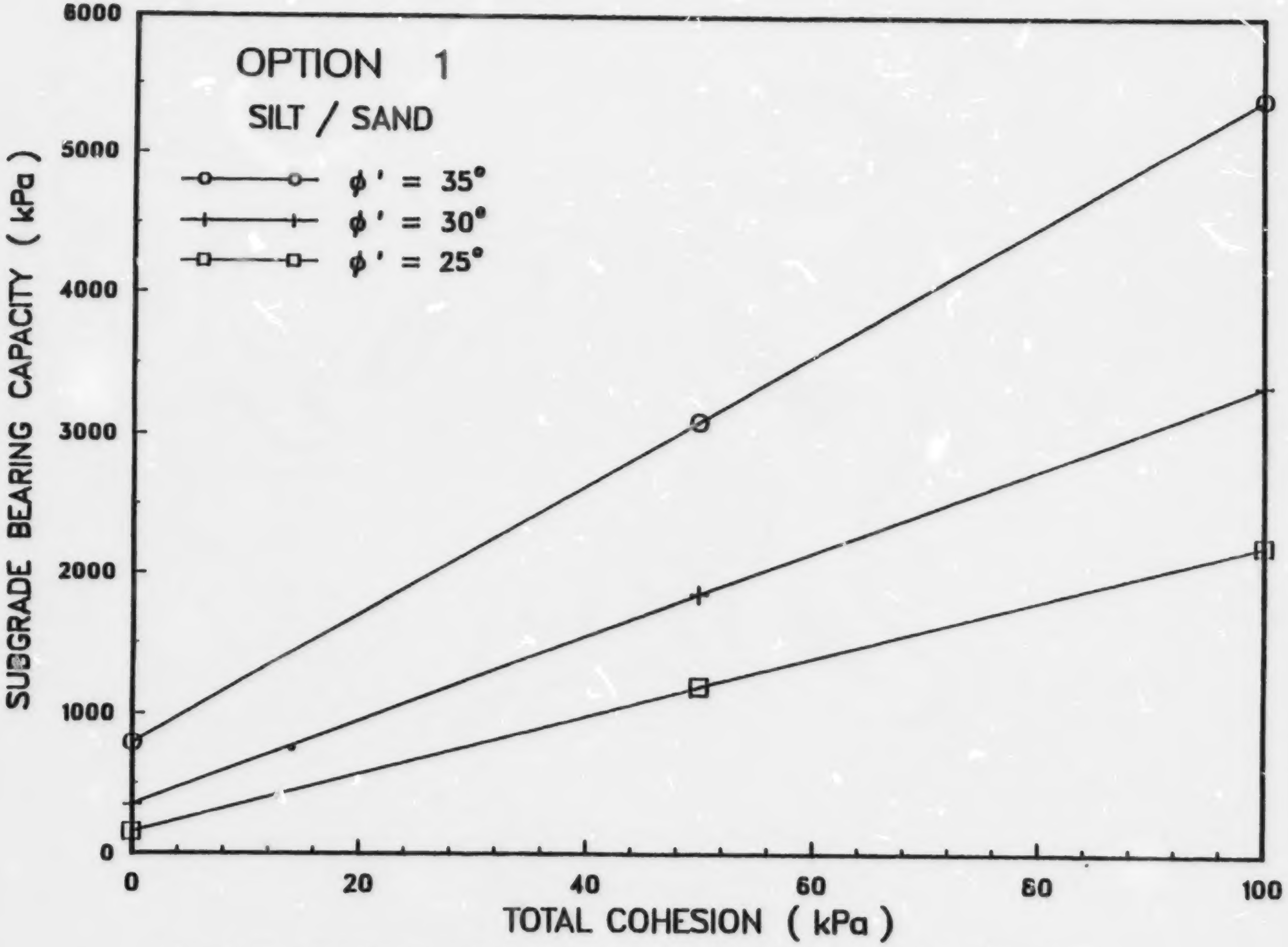

Fig. 5.39 Bearing capacity by Option 1 for typical silt/sand subgrades

material type.

Figures 5.40 through 5.42 present bearing capacity charts for each of the clay, glacial till and silt/sand subgrade systems respectively for computation of bearing capacity by Broms method and Option 2. Since the results of Option 2 have been emphasized in the stress analysis, the bearing capacity charts presented in Figures 5.40 through 5.42 are expected to be used more frequently than the other bearing capacity charts.

Figure 5.43 presents a bearing capacity chart which would be compared to Option 3 of the "Stress Averaging Techniques". The format of the chart in Figure 5.43 is different from the others presented in this section because this chart was developed using the Hanna and Meyerhof bearing capacity approach. The chart was developed using a width, B equal to 0.229 m, a length, L equal to infinity and four different depths H of: 1) 0.406 m , 2) 0.610 m, 3) 0.813 m and 4) 1.106 m. The ballast parameter ϕ' was fixed at 45 degrees to develop the chart shown in Figure 5.43.

Figures 5.44 through 5.46 present bearing capacity charts computed by the Broms approach and Option 4. At negligible cohesions, the bearing capacities computed by this method are actually less than zero. At greater cohesions, the bearing capacities computed by Option 4 are extremely large and therefore not critical. This would suggest that a failure depicted by Option 4 would only occur under extremely wet conditions.

Since the bearing capacity charts are based upon total cohesion, three additional plots have been included which illustrate the relationships between matric suction, the various soil parameters and the

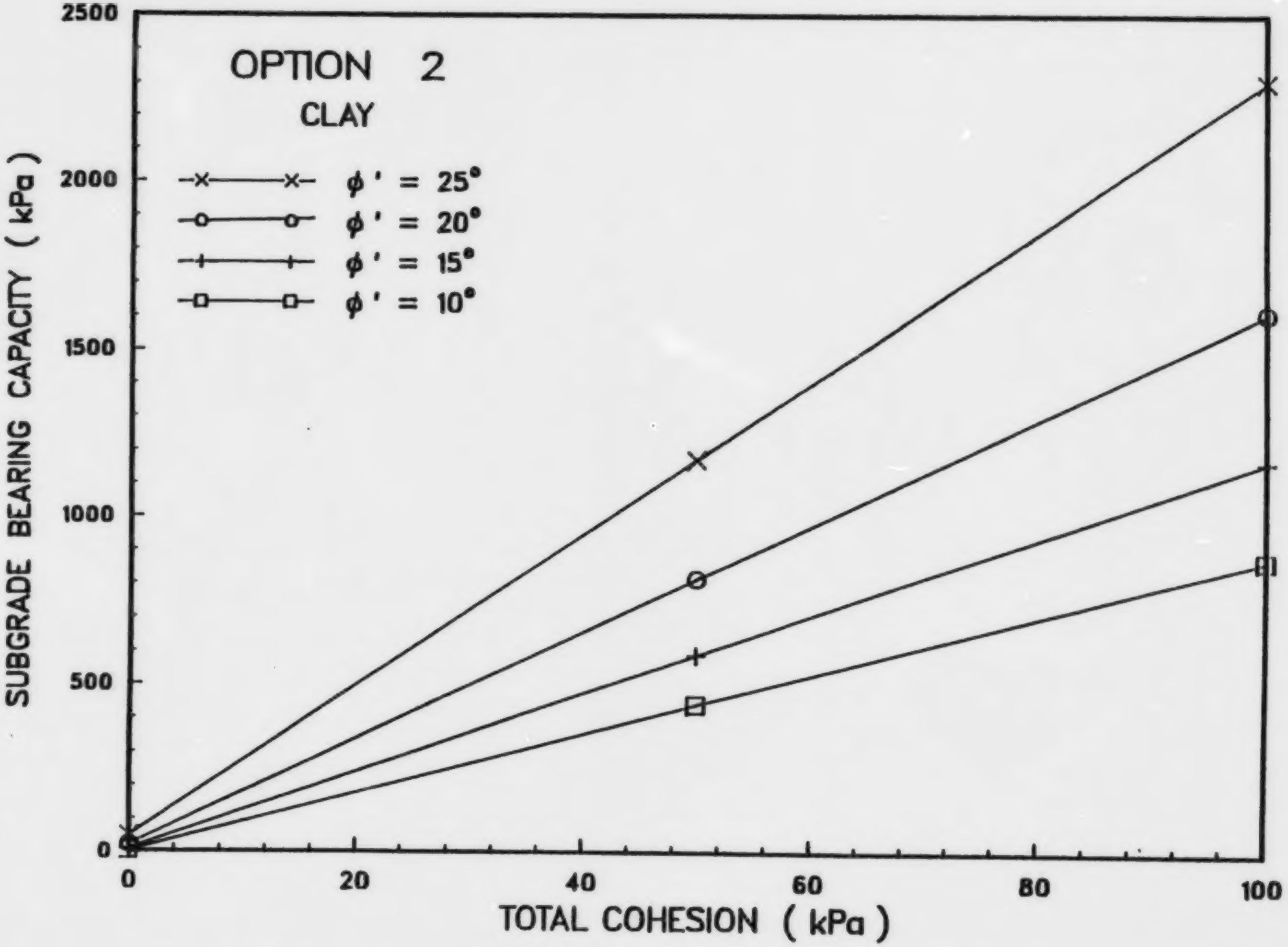

Fig. 5.40 Bearing capacity by Option 2 for typical clay subgrades

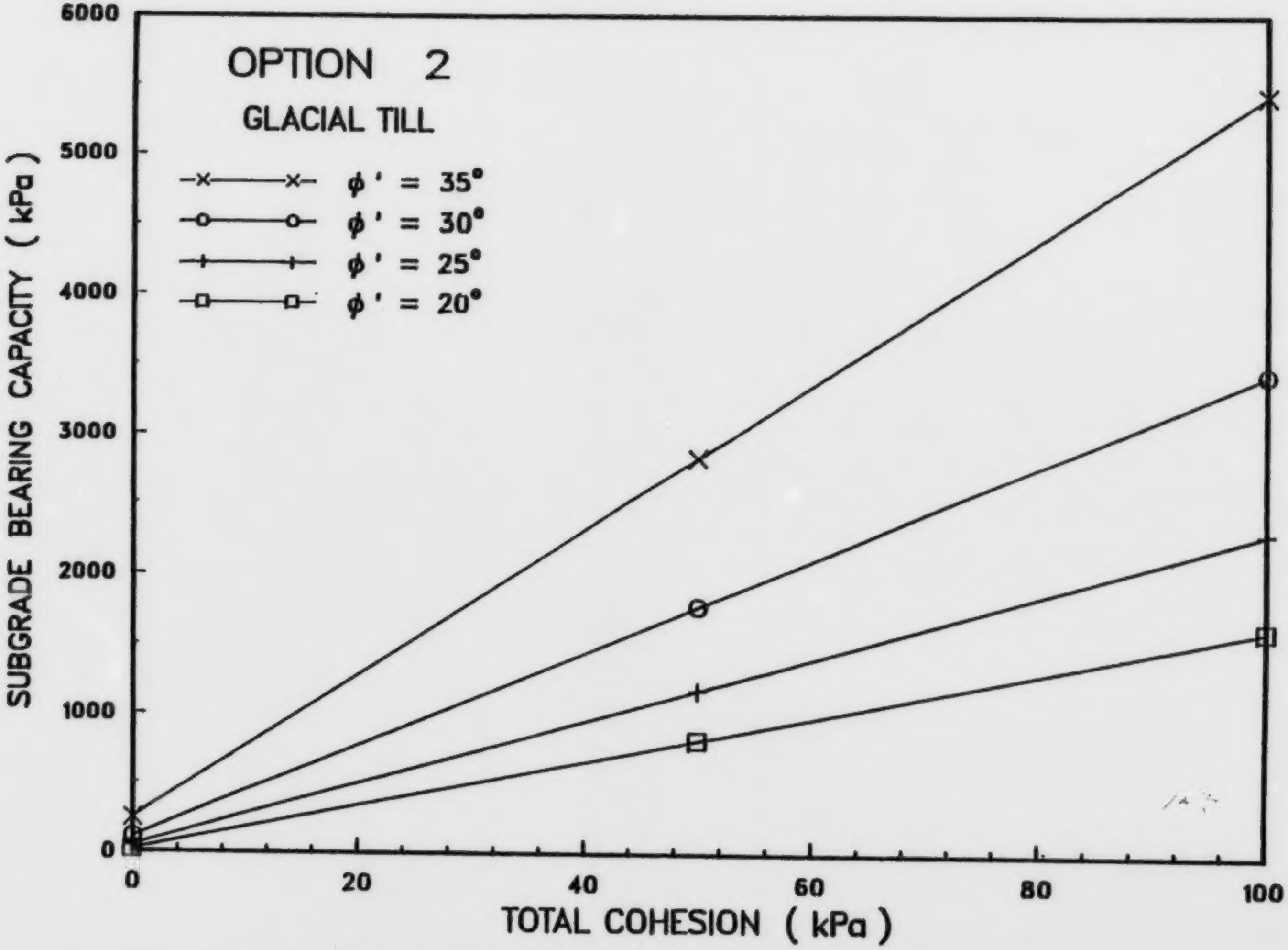

Fig. 5.41 Bearing capacity by Option 2 for typical glacial till subgrades

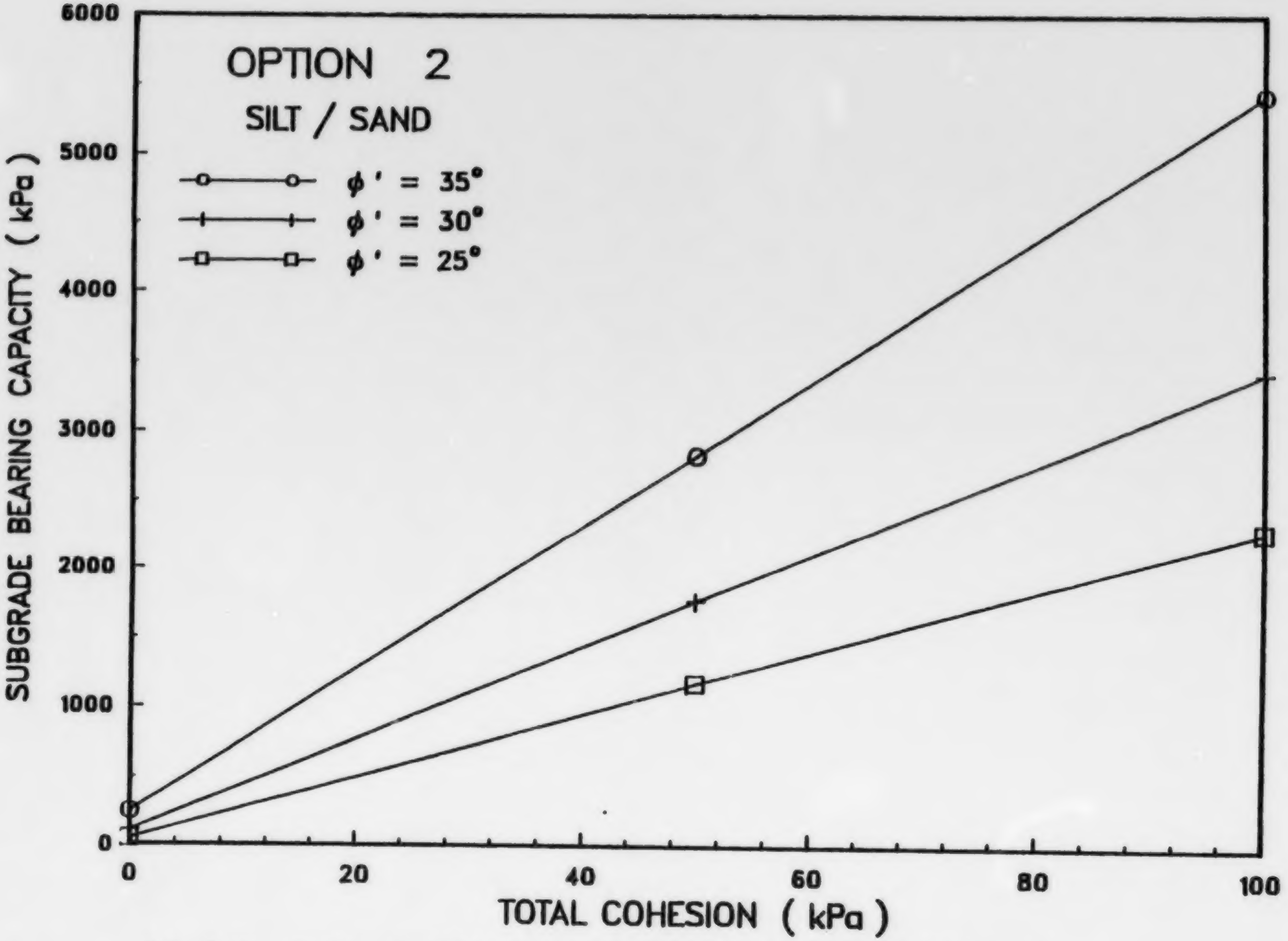

Fig. 5.42 Bearing capacity by Option 2 for typical silt/sand subgrades

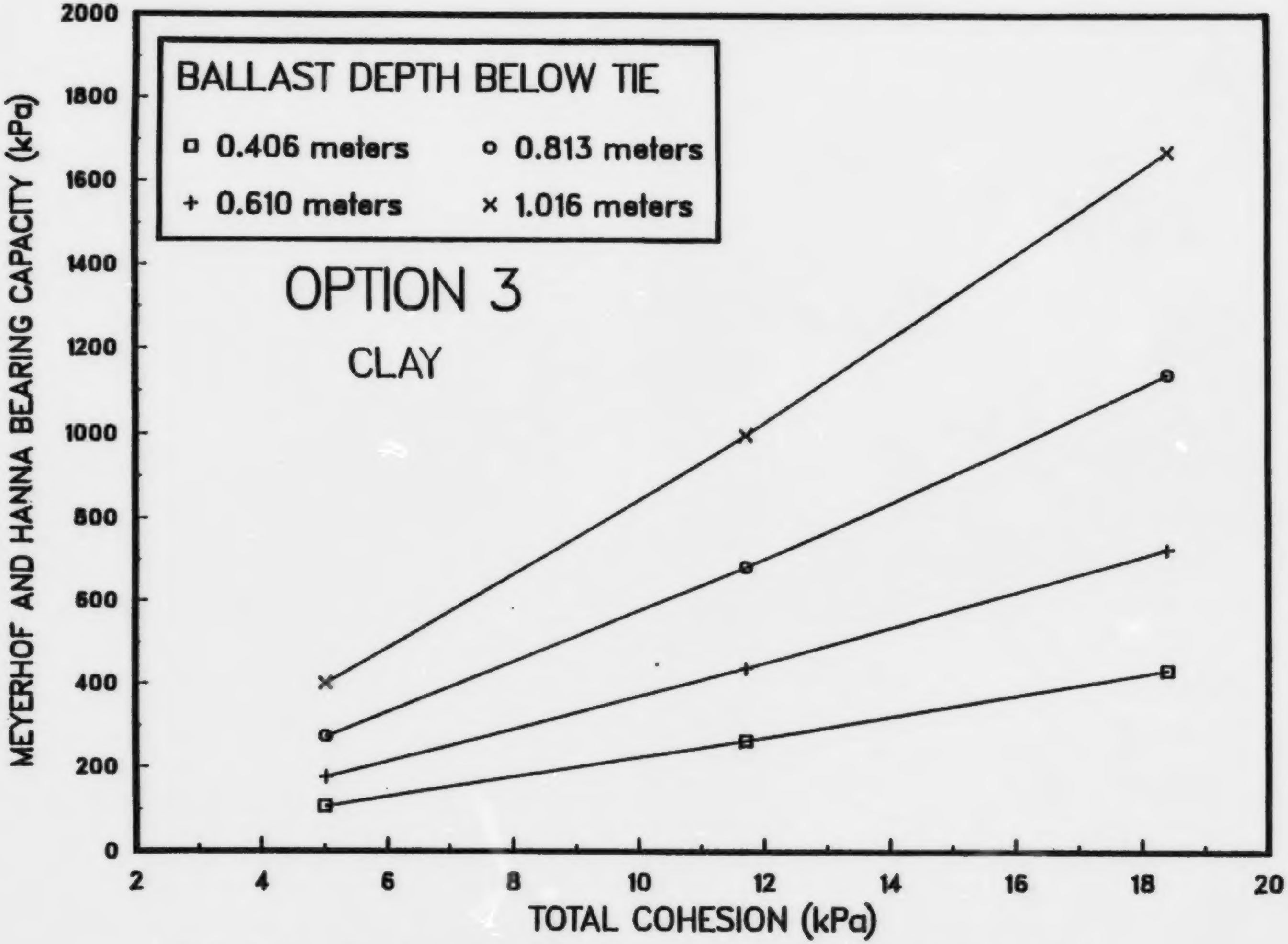

Fig. 5.43 Bearing capacity by Option 3 for a weak clay subgrade and the absence of subballast

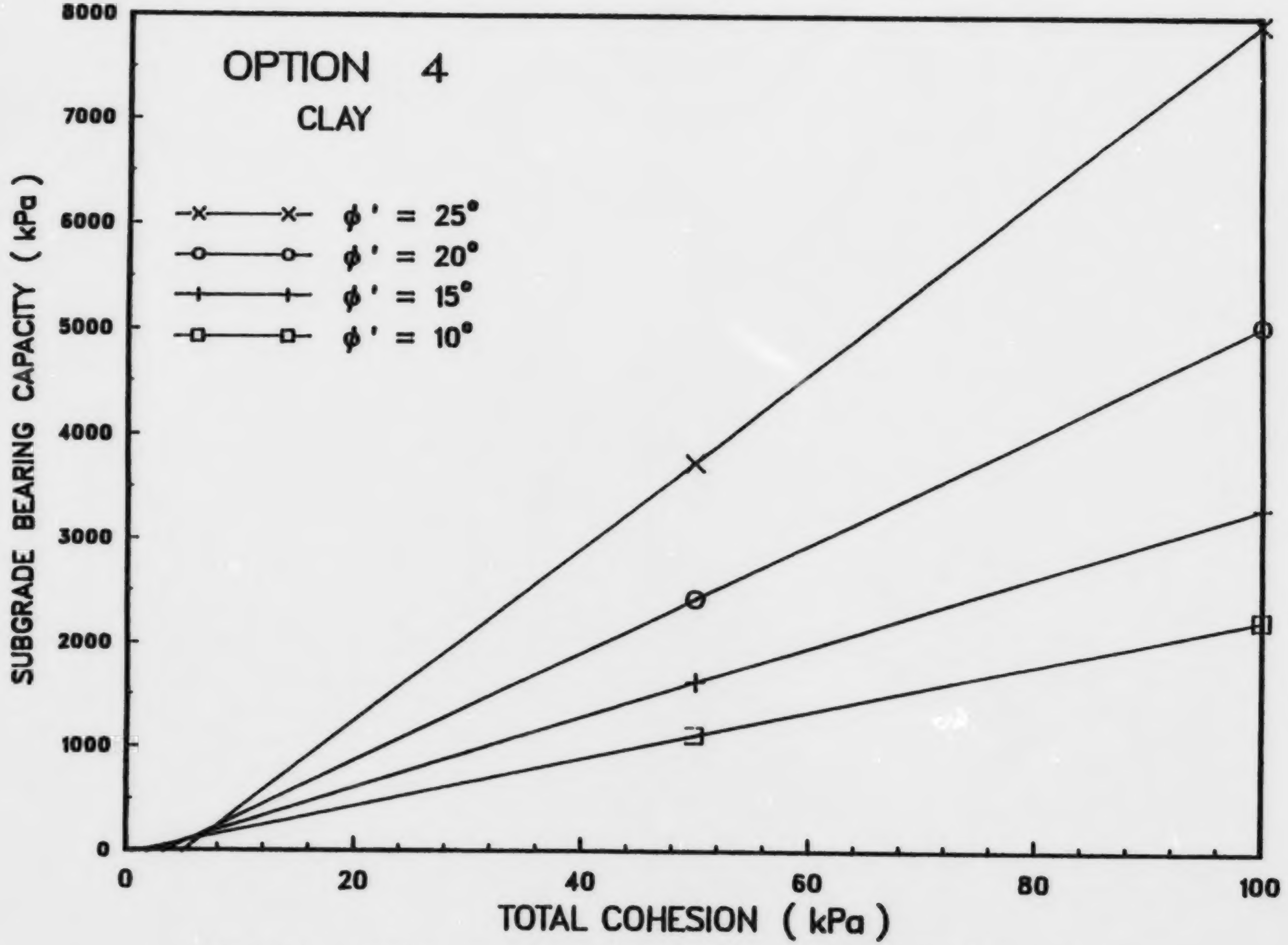

Fig. 5.44 Bearing capacity by Option 4 for typical clay subgrades

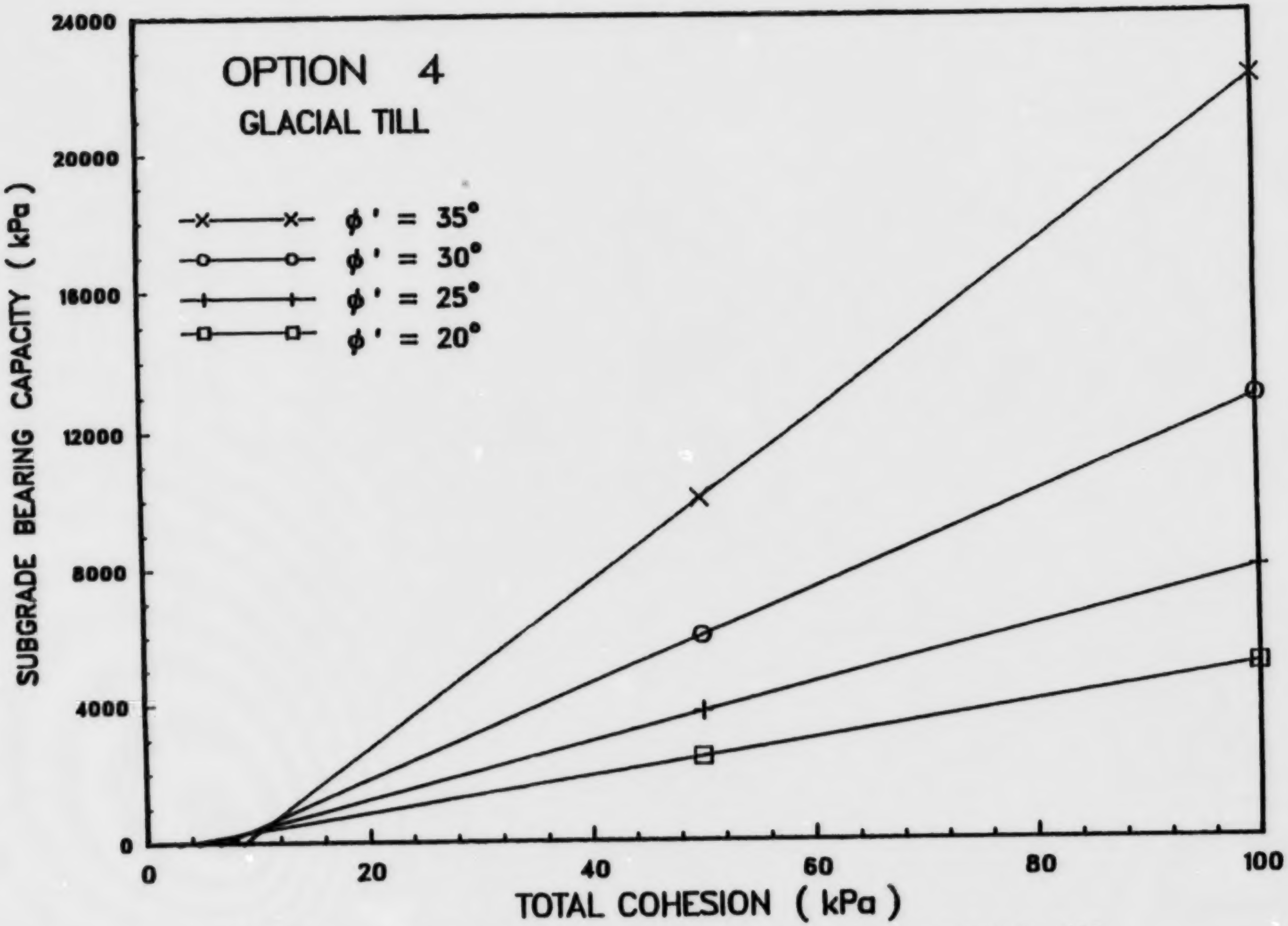

Fig. 5.45 Bearing capacity by Option 4 for typical glacial till subgrades

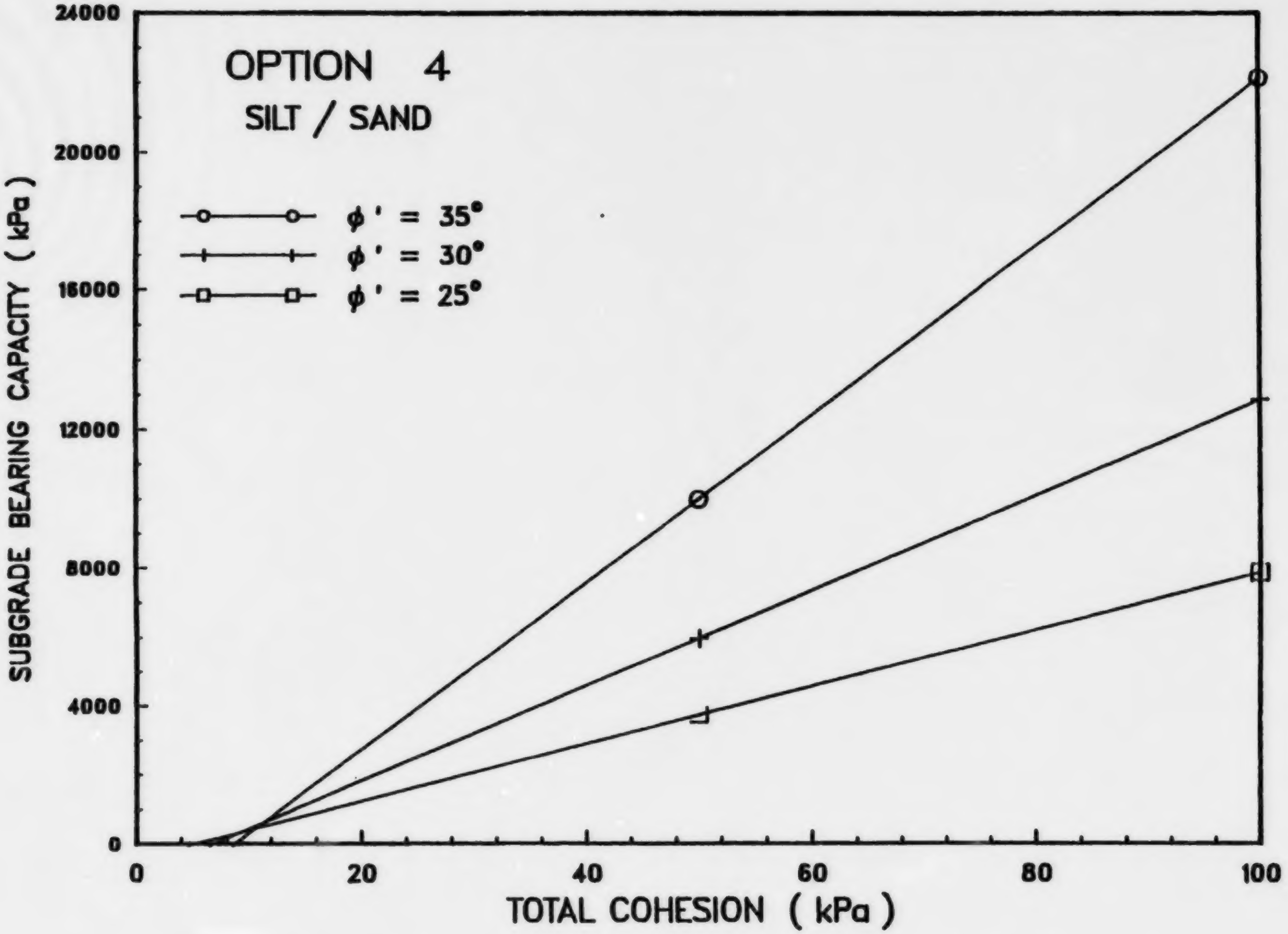

Fig. 5.46 Bearing capacity by Option 4 for typical silt/sand subgrades

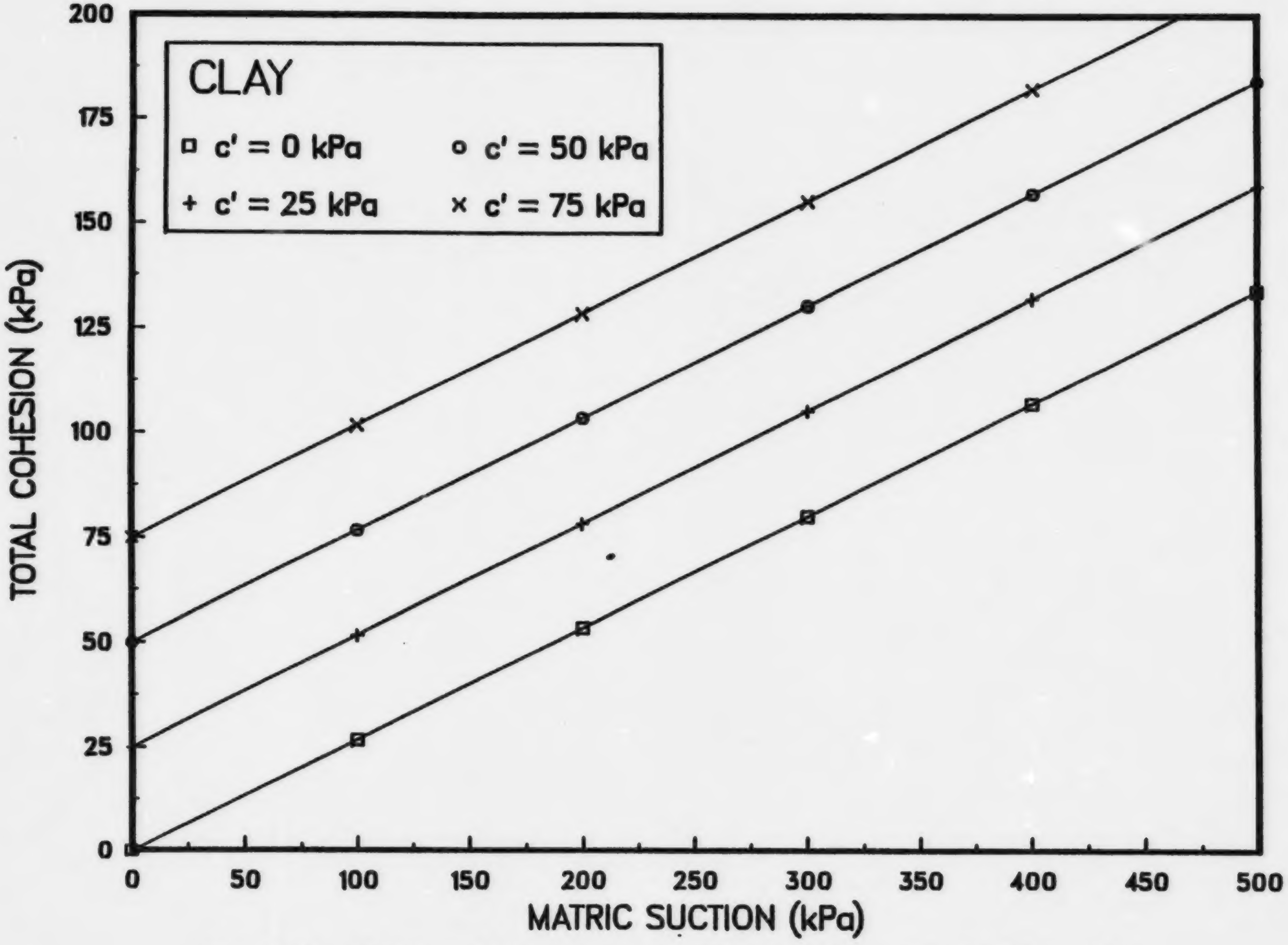

Fig. 5.47 Total cohesion versus matric suction for typical clay parameters

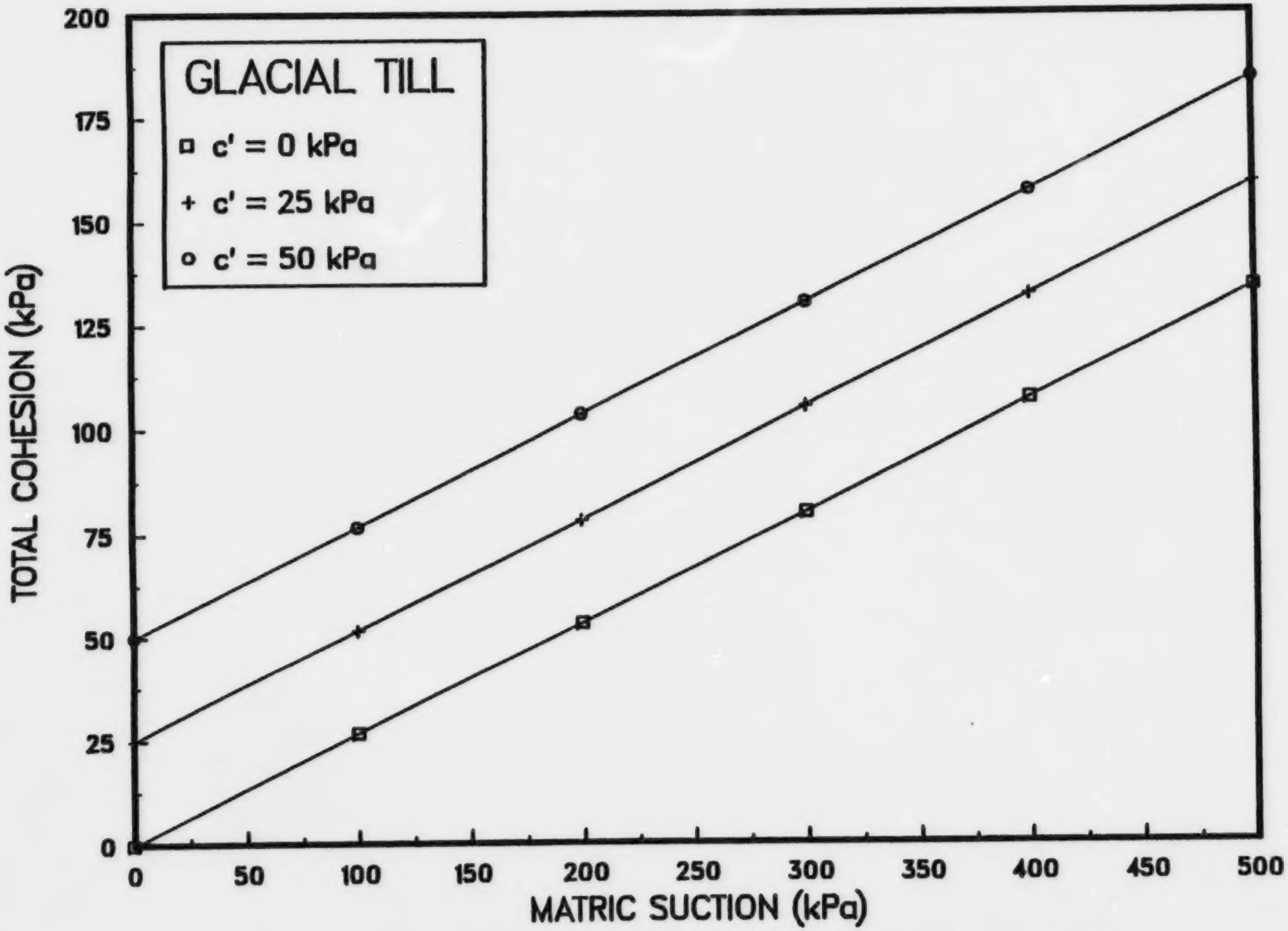

Fig. 5.48 Total cohesion versus matric suction for typical glacial till parameters

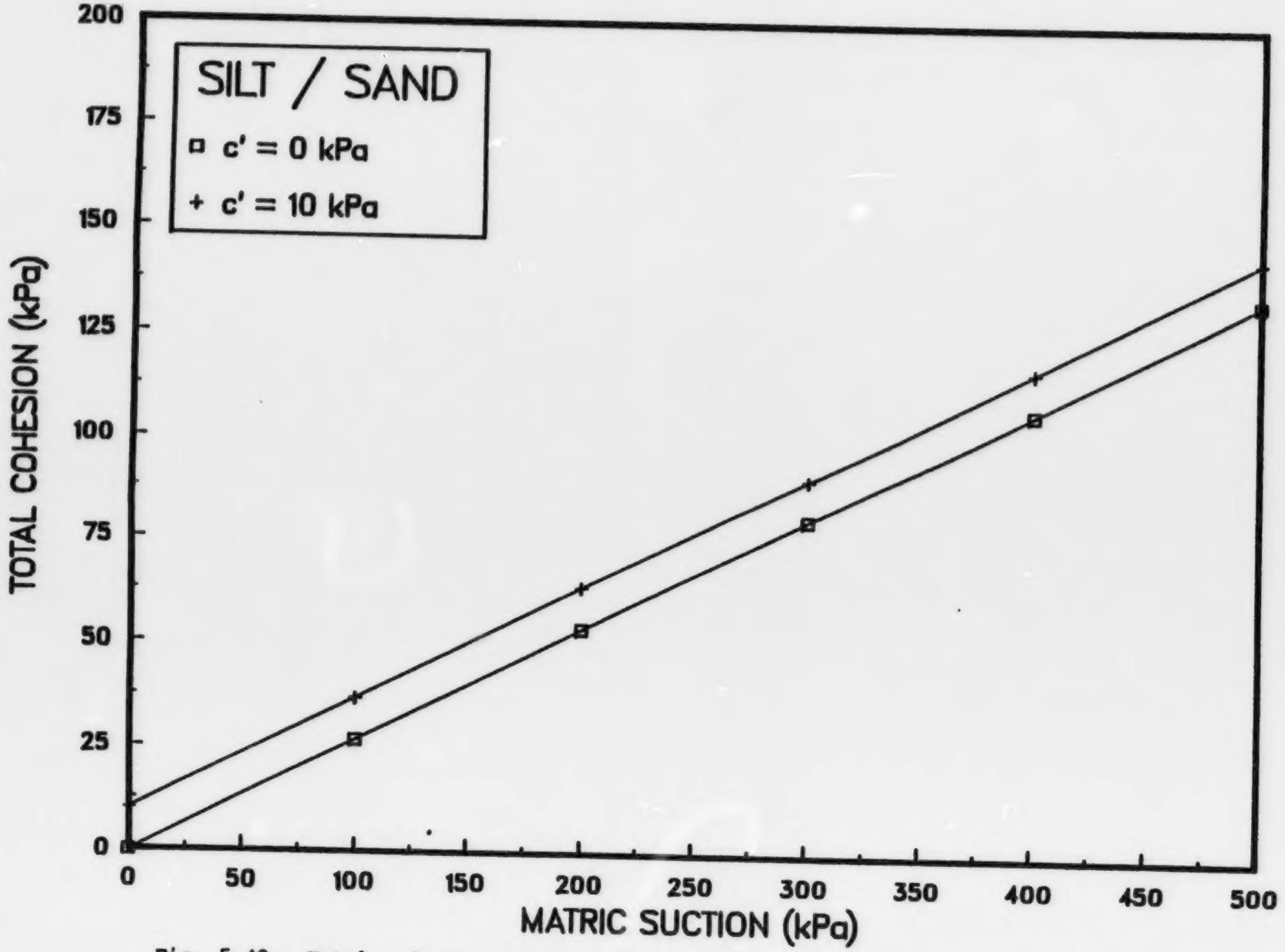

Fig. 5.49 Total cohesion versus matric suction for typical silt/sand parameters

total cohesion for a ϕ^b angle of 15° For an initial analysis, it may be advantageous to use Figures 5.47 through 5.49 to quickly estimate the total cohesion for a clay, glacial till or silt/sand, respectively.

The design approach omits the effect of pore-water pressures generated due to dynamic loading. The design loads have been increased by 50% as described in Section 4.1. The 50% increase in the static design load to represent the dynamic load accounts for build up of pore-water pressures under repeated dynamic loading. An investigation into the build-up of pore-water pressures under dynamic loading could be a topic of further research.

Example problems using the charts are presented in Section 5.5.

5.4 Presentation of the Bearing Capacity Factor of Safety Charts

This section presents the bearing capacity factor of safety charts which have been developed from the stress charts and bearing capacity charts. A computer program, COMPARE was developed to combine the STRESS output files and the BEARING output files and compute the bearing capacity factor of safety. Each point on a bearing capacity factor of safety chart represents the results of a GEOTRACK computer run, a STRESS computer run, a BEARING computer run, plus a COMPARE computer run. Although the charts cannot possibly present results for all the different combinations of bearing capacity which may be desireable to compare to a typical stress, Section 5.5 suggests a method which can be used to interpolate between the design charts.

Figures 5.50 and 5.51 present two bearing capacity factor of safety design charts which have been derived from the stress charts presented in Figures 5.6 and 5.7, respectively. Both correspond to an Option 1 type

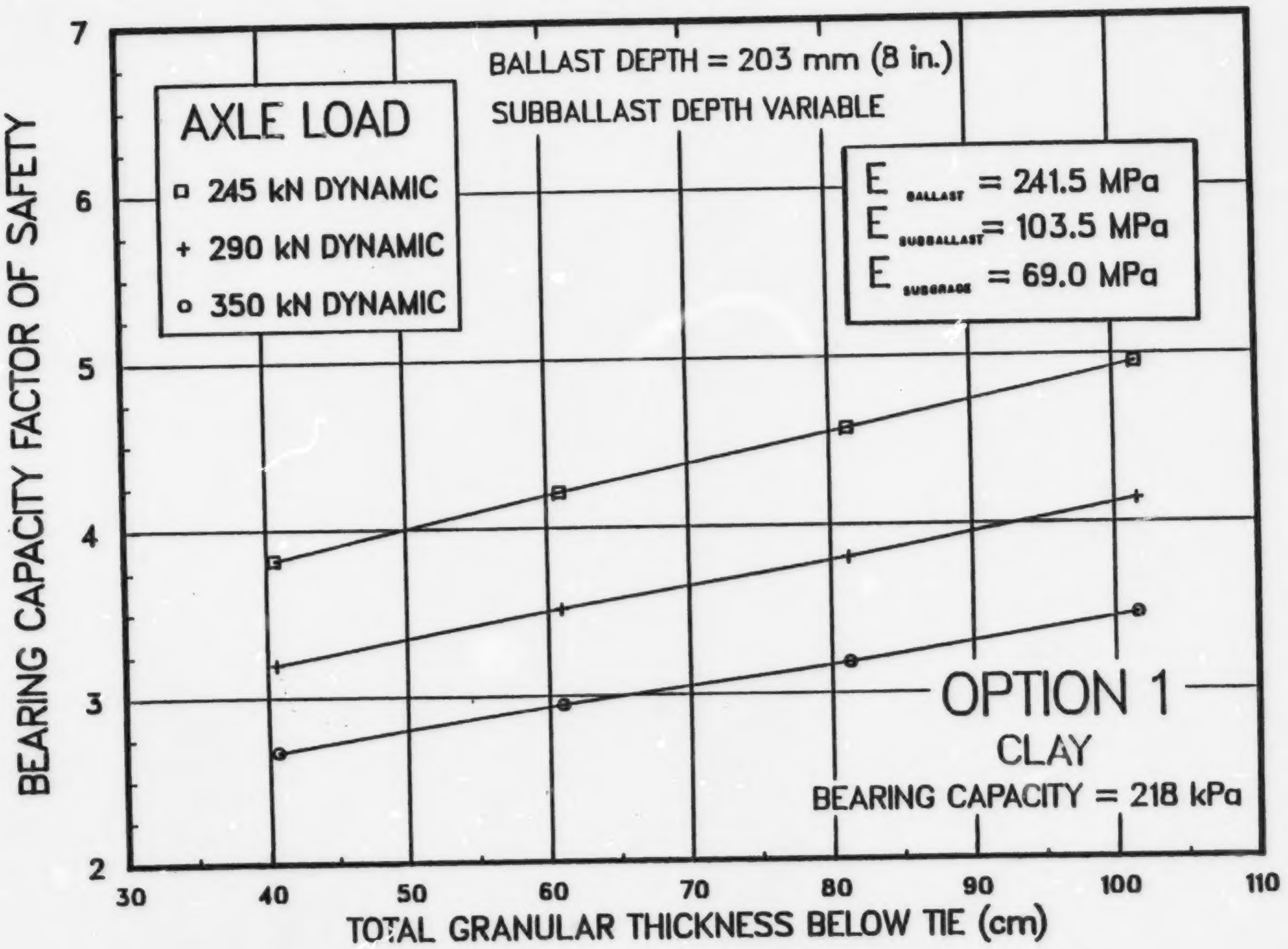

Fig. 5.50 Factor of safety for Option 1, Subgrade E = 69.0 MPa, Subballast E = 103.5 MPa

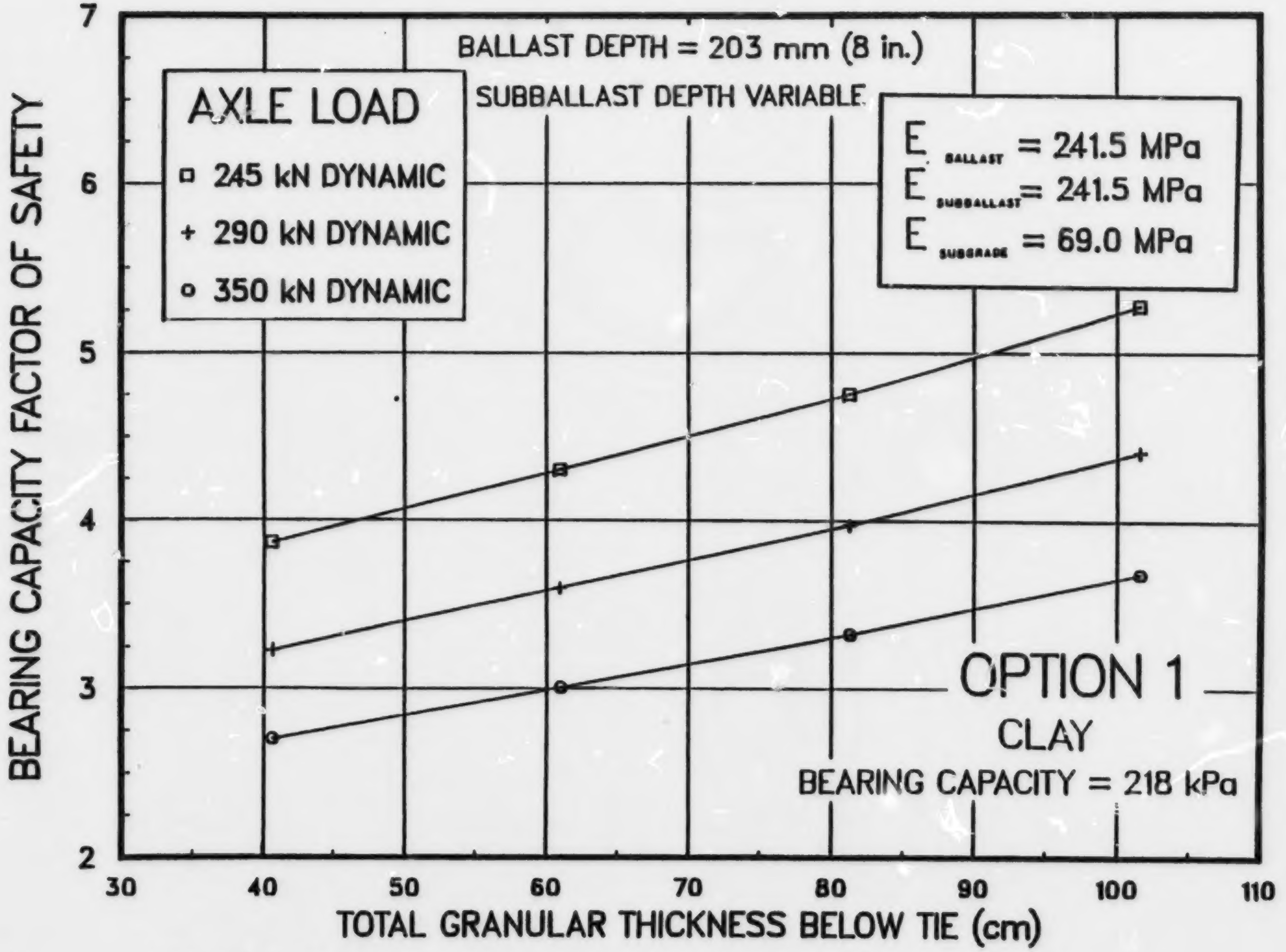

Fig. 5.51 Factor of safety for Option 1, Subgrade E = 69.0 MPa, Subballast E = 241.5 MPa

of bearing capacity failure. Both portray the results for a ballast thickness of 203 mm and E modulus of 241.5 MPa. The subgrade E modulus is 69.0 MPa. For Figure 5.50, the subballast E modulus is 103.5 MPa whereas for Figure 5.51, the subballast E modulus is 241.5 MPa.

The bearing capacity factors of safety plotted in Figures 5.50 were computed by dividing each of the stresses in the corresponding stress chart (i.e., Figure 5.6) by a typical Option 1 bearing capacity of 218 kPa (i.e., which would be representative of a medium clay material, possessing a total cohesion of 25 kPa and a ϕ' of 10 degrees). Similarly, the bearing capacity factors of safety plotted in Figure 5.51 were computed by dividing the stresses in Figure 5.7 by the same typical Option 1 bearing capacity. The charts are not limited to the one typical bearing capacity which was presented because multiplying the bearing capacity factor of safety by the ratio of the desired bearing capacity to the chart bearing capacity will provide a bearing capacity factor of safety for any desired bearing capacity. Example problems illustrating this interpolation are presented in Section 5.5.

Figures 5.52 through 5.59 present bearing capacity factor of safety charts for an Option 1 typical bearing capacity of 218 kPa (i.e., corresponding to a medium clay subgrade, $c = 25$ kPa and $\phi' = 10$ degrees). Figures 5.60 through 5.67 present typical bearing capacity factor of safety charts for an Option 1 typical bearing capacity of 675 kPa (i.e., corresponding to a competent glacial till, $c = 25$ kPa and $\phi' = 25$ degrees). Figures 5.68 through 5.75 present typical bearing capacity factor or safety charts for an Option 1 bearing capacity of 351 kPa (i.e., corresponding to a silt, $c = \phi$ and $\phi' = 30$ degrees). All charts were derived by dividing the bearing capacities by the stresses in the corresponding stress charts for an Option 1 "Stress Averaging Technique" (i.e., Figures 5.8 through 5.15).

In each series, the first two charts corresponding to a subgrade E modulus of 6.9 MPa should probably not be used other than for illustrative purposes. The significant non-linearity exhibited by the stress analysis suggests that alternative methods of analysis should be used for extremely weak subgrades. Fortunately, even subgrades which exhibit severe bearing capacity failures generally produce repeated loading moduli greater than 6.9 MPa (27).

The next series of bearing capacity factor of safety charts correspond to Option 2. The first 3 sets correspond to a ballast depth of 203 mm (8") while the next 3 sets correspond to a ballast depth of 305 mm (12"). Typical bearing capacities chosen to represent Option 2 are: 1) 222 kPa for a medium clay with c = 25 kPa and $\phi' = 10$ degrees, 2) 612 kPa for a competent glacial till with c = 25 kPa and $\phi' = 25$ degrees, and 3) 109 kPa for a silt with c = 0 and $\phi' = 30$ degrees. Although the soil parameters chosen to represent each material are the same, the resulting bearing capacities are different due to the failure configuration differences between Options 1 and 2. The difference is most significant for the silt in which the cohesion was assumed to be zero.

Figures 5.76 through 5.83 show the computed bearing capacity factors of safety for a typical Option 2 bearing capacity of 222 kPa for a ballast depth of 203 mm. Figures 5.84 through 5.91 show the computed bearing capacity factors of safety for a typical Option 2 bearing capacity of 612 kPa and a ballast depth of 203 mm. Similarly, Figures 5.92 through 5.99 show the computed bearing capacity factors of safety for a typical Option 2 bearing capacity of 109 kPa.

Comparison of the stress charts in Section 5.2 suggested that there was a negligible effect on the stress output caused by increasing the ballast depth to 305 mm (12") from 203 mm (8"). However, both sets of figures have been included so that the individual user may easily use design values specified by his/her agency.

Figures 5.100 through 5.107 show the computed bearing capacity factors of safety for a typical Option 2 bearing capacity of 222 kPa and a ballast depth of 305 mm (12"). Figures 5.108 through 5.115 are for an Option 2 bearing capacity of 612 kPa and a ballast depth of 305 mm (12") whereas Figures 5.116 through 5.123 are for a bearing capacity of 109 kPa.

Bearing capacity factor of safety charts for Option 3 are presented in Figures 5.124, 5.125, and 5.126. The format of the diagrams is different due to the use of the Hanna and Meyerhof bearing capacity approach. These charts are not intended to cover all possible ranges of failure by the Hanna and Meyerhof method. Rather, it is suggested that if these charts do not represent the design parameters chosen for a Hanna and Meyerhof type analysis, then it is up to the user to use the series of computer programs which have been documented in a separate report.

Figures 5.124 through 5.126 show computed bearing capacity factors of safety as a function of total cohesion of the subgrade material. Four representative ballast depths are portrayed by the four lines on each graph. All three figures correspond to a ballast friction angle of 45 degrees and a ballast E modulus of 241.5 MPa. The subgrade E modulus for all three figures was represented by 6.9 MPa. A width, $B = 0.229$ m, and a length, $L = \infty$ infinity were chosen to compute the bearing capacity.

Figure 5.124 shows the bearing capacity factor of safety for a 245 kN Dynamic load (i.e., a 220,000 lb. car). Figure 5.125 shows the bearing capacity factor of safety for a 290 kN Dynamic load (i.e., a 263,000 lb. car) and Figure 5.126 shows the bearing caapcity factor of safety for a 350 kN Dynamic load (i.e., a 315,000 lb. car).

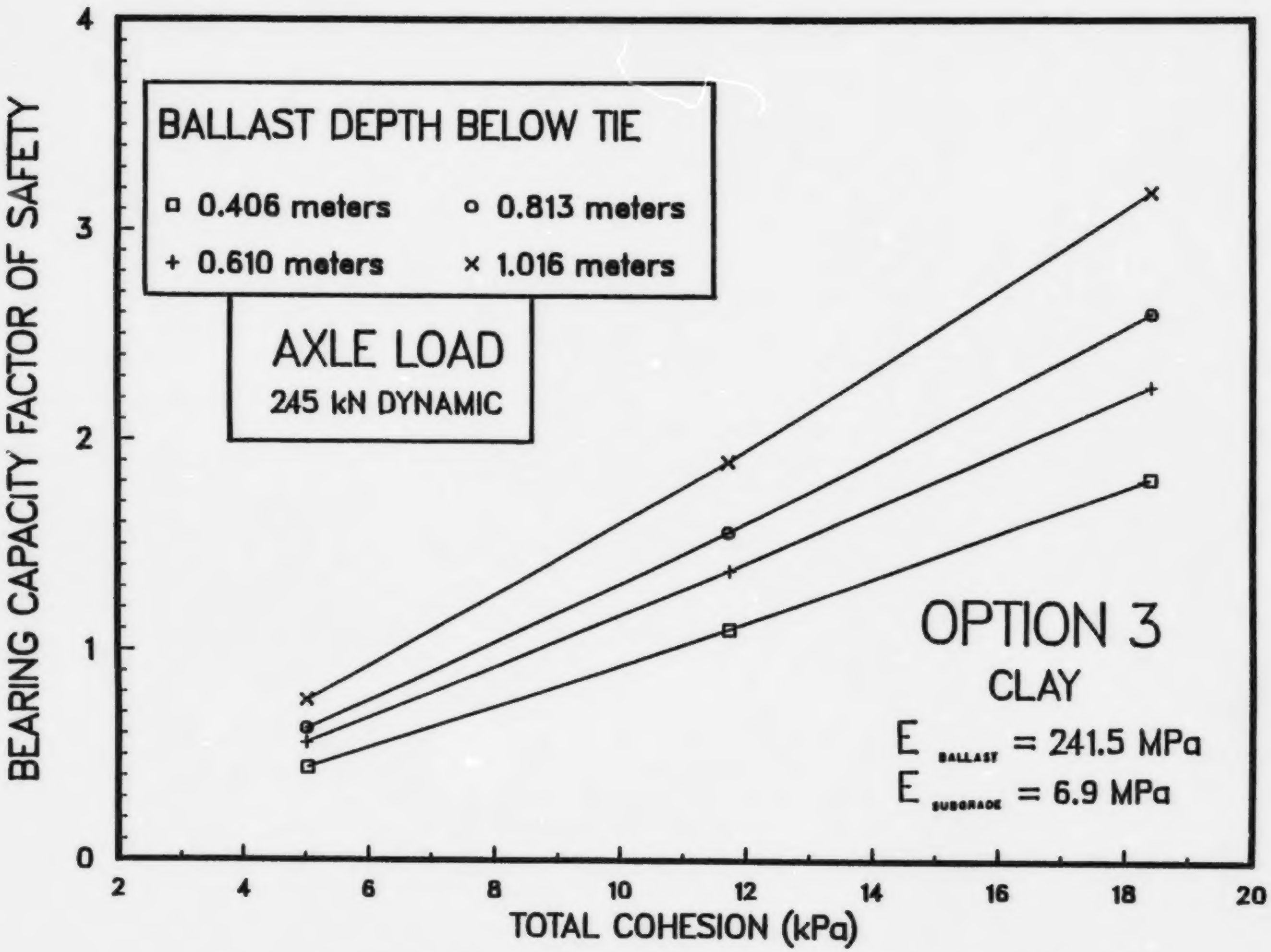

Fig. 5.124 Factor of safety for Option 3, Weak Clay by Hanna and Meyerhof Approach

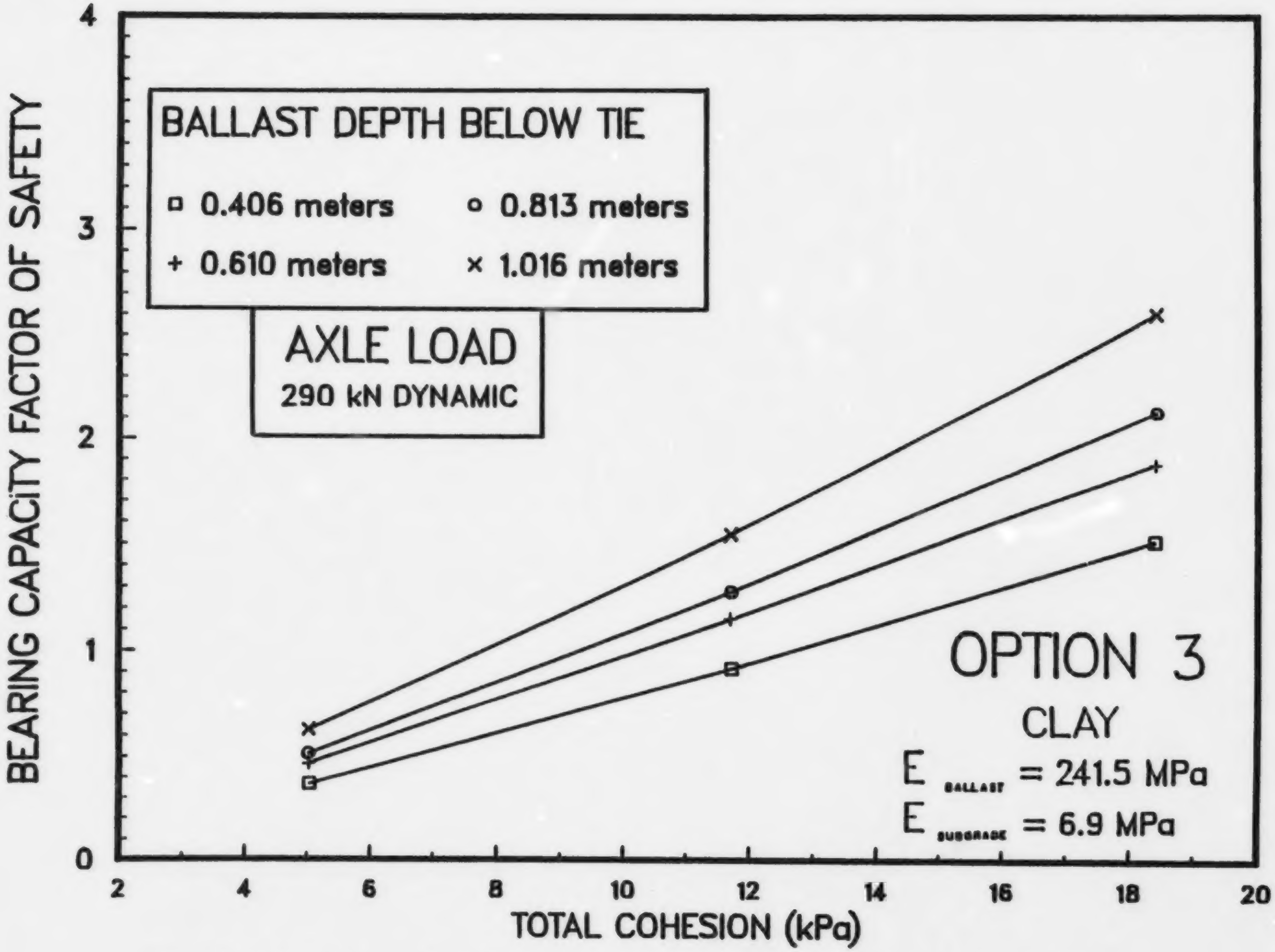

Fig. 5.125 Factor of safety for Option 3, Weak Clay by Hanna and Meyerhof Approach

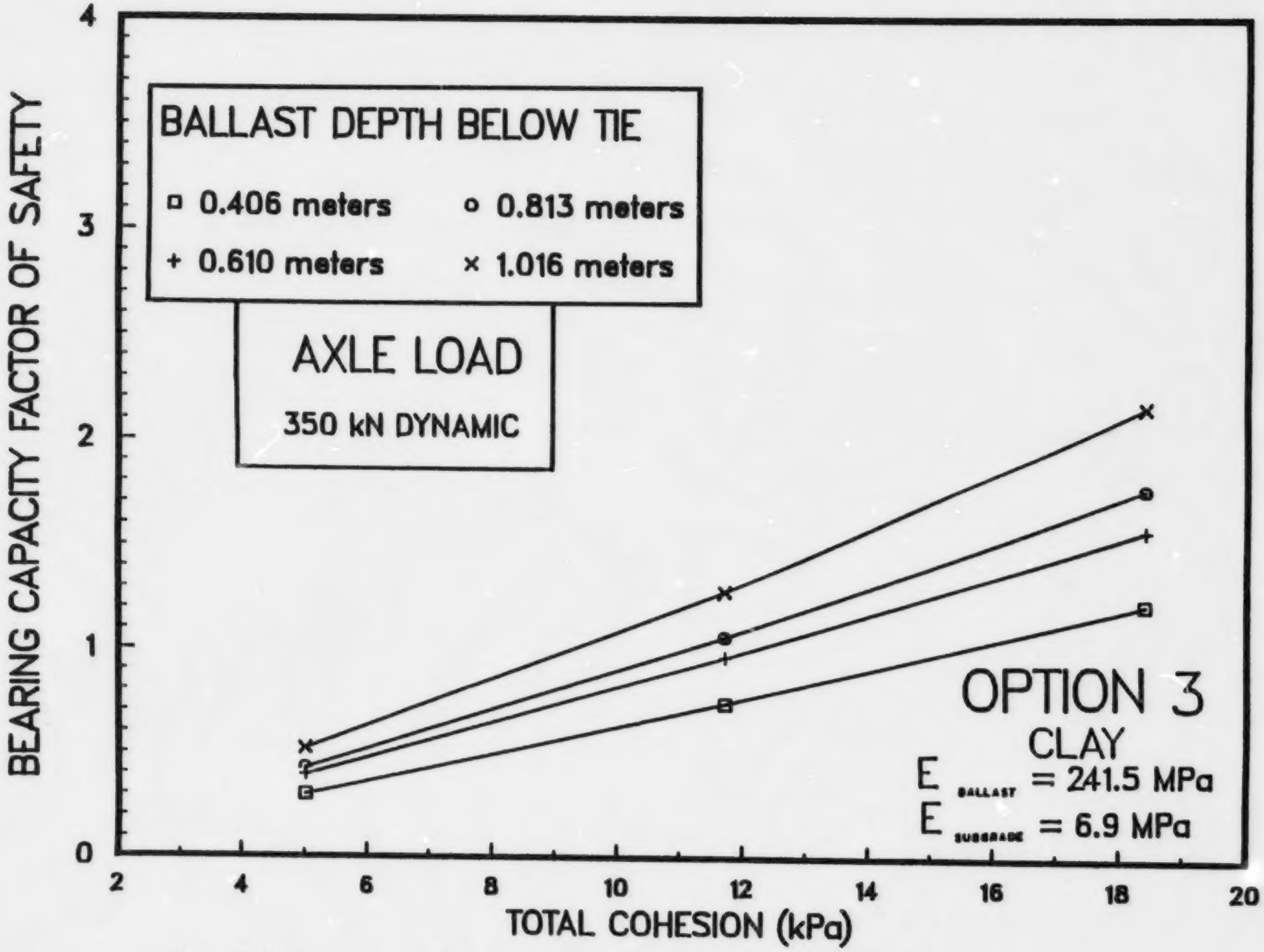

Fig. 5.126 Factor of safety for Option 3, Weak Clay by Hanna and Meyerhof Approach

Since the "Stress Averaging Technique" for Option 2 produces the same average stresses as for Option 4, the bearing capacity factor of safety charts presented for Option 2 may also be used for Option 4. The bearing capacities for Option 4 are usually significantly greater than for Option 2, therefore, it is not likely that the user would often be concerned about checking Option 4. Nonetheless, the use of the charts for an Option 4 type bearing capacity is described in the next section.

5.5 Use of the Design Charts for Example Problems

The following four example problems illustrate the use of the design charts in a bearing capacity approach to railway subgrade design. The example problems serve to illustrate the purpose for each of the various computer programs and the interactions between the programs. User's manuals for the computer programs, GEOTRACK, GEOPLOT, STRESS, BEARING, and COMPARE are presented in another separate document.

Example Problem No. 1:

Determine if the given set of design parameters will be "safe" for an Option 1 Bearing Capacity Loading Configuration for dynamic loading conditions. The design ballast-subballast-subgrade parameters are:

Subgrade Material Type: Clay

$c' = 25$ kPa

$\phi' = 10$ degrees

$\phi^b = 10$ degrees

Design Suction = 0 kPa

E Modulus = 69.0 MPa

Subballast:

E Modulus = 103.5 MPa

Depth = 250 mm

Ballast:

E Modulus = 241.5 MPa

Depth = 203 mm

ϕ' = 45 degrees

All material unit weights are 18 kN/m_3. The design loading configuration is for a 100,000 kg car (i.e., 220,000 lb. car).

Solution:

Step 1: Determine the bearing capacity by Broms method for an Option 1 Loading Configuration.

The preferable method is to use the computer program, BEARING, to compute the subgrade bearing capacity by a Broms approach for Option 1 and the design parameters given above. A value for the width B will be requested. An appropriate tie length to input for the width, B, is 2.59 meters. The resulting bearing capacity produced by BEARING is 238 kPa. The output file from the bearing program is presented in Appendix A under the file name EX1.BRG. The user's manual for the BEARING computer program is provided in a separate document.

Equations [1], [2], [3], [4], [5], [6], and [7] could also be used to manually compute the total cohesion, the bearing capacity factors, and the ultimate bearing capacity by a Broms approach.

Alternatively, the design charts may be used to graphically estimate the bearing capacity by a Broms approach. Figures 5.47 and 5.37 are used together to compute the bearing capacity of the clay subgrade. First, Figure 5.47 is used to estimate the total cohesion from the given design matric suction and effective cohesion. Note that Figures 5.47 through 5.49 are based on a ϕ^b angle of 15 degrees; however, when the design suction value is zero, the ϕ^b angle is insignificant and the total cohesion always equals the effective cohesion. For a design matric suction equal to zero and an effective cohesion of 25 kPa, the total cohesion is 25 kPa. (Note: Computation of the total cohesion is usually made using Equation [2]). Next, Figure 5.37 is used to determine the subgrade bearing capacity for a clay by an Option 1 Broms approach for a total cohesion of 25 kPa and a friction angle of 10 degrees. The graphical estimate obtained from Figure 5.37 is about 230 kPa.

Step 2: Determine the bearing capacity factor of safety for the given design parameters.

Figure 5.50 corresponds to an Option 1 bearing capacity of 218 kPa for the ballast, subballast, and subgrade moduli given and the ballast depth of 203 mm. The 100,000 kg car is represented by the 245 kN Dynamic line in Figure 5.50. The total granular thickness below the tie is equal to the depth of ballast (i.e., 203 mm) plus the depth of subballast (i.e., 250 mm). The total granular thickness is equal to 453 mm.

Using 453 mm or 45.3 cm as the value on the x-axis of Figure 5.50 and for the 245 kN Dynamic line, the bearing capacity factor of safety is about 3.85.

Step 3: Correct the bearing capacity factor of safety for the design bearing capacity. The chart bearing capacity was 218 kPa. The computed bearing capacity for this loading configuration was 238 kPa.

The correction is done as follows:

Actual Bearing Capacity Factor of Safety

= Actual Bearing Capacity/Chart Bearing Capacity

* Chart Bearing Capacity Factor of Safety

= 238 kPa/218 kPa * 3.85

Bearing Capacity Factor of Safety = 4.2

Present research indicates that a bearing capacity factor of safety greater than 2.5 to 3.0 is considered safe.

Example Problem No. 2:

Consider an Option 2 Bearing Capacity for a clay subgrade. Railway specifications call for a ballast depth of 305 mm (12"). What depth of subballast should be utilized to create a "safe" design for the following material and loading paramters?

Subgrade Material Type: Clay

$c' = 5$ kPa

$\phi' = 15$ degrees

$\phi^b = 15$ degrees

Design Suction = 25 kPa

E Modulus = 69.0 MPa

Subballast:

E Modulus = 103.5 MPa

Ballast:

E Modulus = 241.5 MPa

Depth = 305 mm

$\phi' = 45$ degrees

All material unit weights are 18 kN/m3. The design loading configuration is for a 143,000 kg car (i.e., 315,000 lb. car) under dynamic loading.

Solution:

Step 1: First compute the subgrade bearing capacity using the computer program, BEARING or the equations for a Broms type approach or the design charts.

Compute the bearing capacity from the computer program, BEARING. Assuming a 2.75 meter (9 foot) tie, one-third of the tie length is 914 mm. An appropriate double truck length is 5.87 meters. The resulting bearing capacity computed by Broms method with the BEARING computer program is 168 kPa. The BEARING output file is presented in Appendix A. Note that the charts are based upon a tie length of 2.59 and double truck length of 5.87 m. Therefore, the choice to use the bearing capacity charts over the BEARING computer program will limit the user to these assumptions.

Note that the total combined ballast and subballast depth is not known for input into the computer program. A depth equal to only the ballast depth was used. The user may wish to recalculate the bearing capacity, adding the required depth of subballast which is calculated in Step 5 and then proceeding in an iterative manner until a converged solution is obtained.

Step 2: Assume a bearing capacity factor of safety for use with the design charts.

Assume a bearing capacity factor of safety of 2.75 will be the minimum "safe" value.

Step 3: Find the bearing capacity factor of safety design chart for the given material moduli, ballast depth and material type. Figure 5.104 corresponds to a clay subgrade with a bearing capacity of 222 kPa. Figure 5.104 matches the design E moduli and ballast depth of 305 mm. However, since the chart bearing capacity differs from the computed bearing capacity for the design parameters, the chosen bearing capacity factor of safety will have to be converted to a chart bearing capacity factor of safety.

Step 4: Determine the bearing capacity factor of safety on the chart which will correspond to the desired bearing capacity factor of safety for the computed bearing capacity of 168 kPa.

Chart Bearing Capacity Factor of Safety =

= Chart Bearing Capacity / Actual Bearing Capacity

* Actual Bearing Capacity Factor of Safety

= 222 kPa / 168 kPa * 2.75 Chart Bearing Capacity Factor of Safety = 3.63

Step 5: Determine from the design chart the required depth of subballast.

Figure 5.104 is used with a chart bearing capacity factor of safety equal to 3.63 (i.e., corresponding to a bearing capacity factor of safety of 2.75 for the computed bearing capacity of 168 kPa). The total granular thickness required for the 315,000 kg car (i.e., 350 kN Dynamic Axle Load) is determined graphically. The total required granular thickness is 82 cm or 820 mm.

Of the total granular thickness, 305 mm is ballast material. The required subballast to ensure a bearing capacity factor of safety equal to 2.75 is the difference between the total granular thickness and the depth of ballast. The required depth of subballast is 515 mm.

Example Problem No. 3:

Consider an Option 2 Bearing Capacity Failure Geometry for a railway subgrade. Two subballast materials are available for the design: Subballast One and Subballast Two. Will the use of either material cause a significant increase in the bearing capacity?

Subgrade Material Type: Clay

$c' = 2.5$ kPa

$f' = 15$ degrees

$f^b = 15$ degrees

Design Suction = 5 kPa

E Modulus = 41.4 MPa

Subballast One:

E Modulus = 103.5 MPa

Depth = 400 mm

Subballast Two:

E Modulus = 241.5 MPa

Depth = 400 mm

Ballast:

E Modulus = 241.5 MPa

Depth = 203 mm

$f' = 45$ degrees

All material unit weights are 18 kN/m_3. The design loading configuration is for a 143,000 kg car (i.e., 315,000 lb. car) under dynamic loading.

Solution:

Step 1: Determine the bearing capacity for the subgrade.

Using the computer program, BEARING with the subgrade material parameters and a total depth of 603 mm, a bearing width of 914 mm and a bearing length of 5.87 meters yields a bearing capacity of 99 kPa. The output file is presented in Appendix A.

Step 2: Determine which charts can be used for the problem.

Figures 5.78 and 5.79 correspond to the ballast depth of 203 mm (8") for the subgrade and two different subballast moduli.

Step 3: Determine the bearing capacity factor of safety for Subballast One.

The required chart for Subballast One is depicted in Figure 5.78. For a total granular thickness of 603 mm, the bearing capacity factor of safety is 2.45.

Adjusting the chart bearing capacity factor of safety for the chart bearing capacity results in:

Actual Bearing Capacity Factor of Safety

= Actual Bearing Capacity/Chart Bearing Capacity

* Chart Bearing Capacity Factor of Safety

= 99 kPa/222 kPa * 2.45

Bearing Capacity Factor of Safety = 1.09

Step 4: Determine the bearing capacity factor of safety for

Subballast Two.

The required chart for Subballast Two is depicted in Figure 5.79. For a total granular thickness of 603 mm, the bearing capacity factor of safety is 2.50.

Adjusting the chart bearing capacity factor of safety for the chart bearing capacity results in:

Actual Bearing Capacity Factor of Safety

= Actual Bearing Capacity/Chart Bearing Capacity

* Chart Bearing Capacity Factor of Safety

= 99 kPa/222 kPa * 2.50

Bearing Capacity Factor of Safety = 1.11

Step 5: Is the difference significant?

The difference would not be considered significant because the bearing capacity factor of safety is not significant to two decimal places even though it is often represented to two decimal places.

This problem shows that the need to interpolate between the charts for the various subballast E moduli should never arise. To interpolate between charts for the subgrade moduli, simply repeat the problem twice for a subgrade moduli greater than the design value and for a subgrade moduli less than the design value. Then choose a bearing capacity factor of safety between the two computed factors of safety for the two different subgrade moduli.

Example Problem No. 4:

Consider an Option 3 Bearing Capacity Failure Geometry for a railway subgrade for the following parameters and loading configuration. What is the Hanna and Meyerhof bearing capacity and the resulting bearing capacity factor of safety?

Subgrade Material Type: Clay

$c' = 15$ kPa

$f' = 15$ degrees

$f^b = 15$ degrees

Design Suction = 25 kPa

E Modulus = 6.9 MPa

Subballast Absent

Ballast:

E Modulus = 241.5 MPa

Depth = 450 mm

$f' = 45$ degrees

All material unit weights are 18 kN/m_3. The design loading configuration is for a 143,000 kg car (i.e., 315,000 lb. car) under dynamic loading.

Solution:

Step 1: Determine the bearing capacity either through the design charts or through the computer program, BEARING for the Hanna and Meyerhof approach.

The computer program BEARING produces the output presented in Appendix A. The tie width was assumed equal to 0.229 meters and the depth of ballast above the tie was conservatively assumed to be zero. The resulting computed bearing capacity is 588 kPa and the computed total cohesion is 21.7 kPa.

Step 2: Determine which chart to use for the bearing capacity factor of safety.

Figure 5.126 corresponds to the subgrade and ballast E moduli given as design parameters. The design ballast depth of 450 mm lies between the charted lines for 406 mm abd 610 mm. However, the total cohesion value is greater than the chart x-axis.

It is possible to use the stress chart in Figure 5.32 to compute a ballast surface stress for comparison to the bearing capacity and hence the computation of a bearing capacity factor of safety.

Step 3: Determine the ballast surface stress by the Hanna and Meyerhof approach for the 350 kN Dynamic Axle Load.

Figure 5.32 is used to obtain a graphical estimate of the ballast surface stress. The ballast surface stress is 380 kPa.

Note that the stress charts can always be used to estimate the stress, either at the subgrade surface or at the ballast surface. Then the bearing capacity factor of safety charts are disregarded and the computed bearing capacity compared to the graphically determined stress to calculate a bearing capacity factor of safety.

Step 4: Compare the computed bearing capacity of 588 kPa to the ballast surface stress for a Hanna and Meyerhof approach as follows:

Bearing Capacity Factor of Safety =

Bearing Capacity by Hanna and Meyerhof/

Ballast Surface Stress

= 588 kPa/380 kPa

Bearing Capacity Factor of Safety = 1.55

6.0 Conclusions/Recommendations

A design procedure has been developed which can be used to predict the bearing capacity factor of safety for various axle loads, loading configurations and soil parameters. The user may choose to use the design charts or the user may choose to use the series of computer programs to compute the factor of safety against bearing capacity failure for the specific conditions of concern.

It is recommended that the user measure the relevant soil parameter values at a particular site. The design suction value should be based either on measurements or a reasonable estimate. Further research would be useful for determining reasonable estimates. The f' and f^b angles should be measured in the laboratory or estimated based on previous data. The repeated loading moduli for the ballast and the subgrade could be measured or based on previous experience. Published values for the soil parameters can be used as a guide.

A bearing capacity factor of safety greater than 1 does not imply that a bearing capacity failure could not occur. This results from the fact that the bearing capacity approach produces a single value to represent the strength of a heterogeneous subgrade system in which planes of weakness may exist. In addition, the choice of design values for the soil parameters, track structure, and loading configuration is subject to error which may be cumulative for each of the many design values which enter into the analysis.

Conventional use of the bearing capacity equation for shallow footings requires the use of a bearing capacity factor of 3.0. Present research indicates that a bearing capacity factor of safety of 2.5 to 3.0 would be reasonable for use with the design charts presented for railway systems. However, further research is necessary to develop confidence in the use of a particular value for the bearing capacity factor of safety.

The value of the bearing capacity may be dependent upon the conditions at a site. Therefore, when the soil and water content conditions can be expected to be extremely variable, it is recommended to use a greater design value for the bearing capacity factor of safety.

Inherent within the computer program GEOTRACK is the assumption that the soil layers act as plates which are infinite in lateral extent. Consequently, when the slope of the ballast-subballast-subgrade system is large, error may be introduced into the computed stress distribution and hence the averaged stress. This inherent error must be taken into consideration when choosing an appropriate bearing capacity factor of safety. Further research (in the proposal stage) would provide an estimate of the error involved and a means for circumventing this error.

Design of the railway ballast-subballast-subgrade system cannot be completed on the basis of a bearing capacity approach alone. It is essential that the user also analyze the embankments to ensure the stability of the overall slope. In addition, the final railway subgrade design must not exclude drainage requirements. Design for drainage and slope stability will increase the bearing capacity of the tie-track system.

The bearing capacity charts should be used to complement existing design procedures. It is only through use that the design procedure which has been developed can be assessed for approval or modification. Use of the procedure will provide feedback on an appropriate bearing capacity factor of safety for design, information on the reliability of the stress calculations and the reliability of the soil suction parameters.

REFERENCES

1. Hanna, A.M. and Meyerhof, G.G. (1980) Design charts for ultimate bearing capacity of foundations on sand overlying soft clay. Canadian Geotechnical Journal, Vol.17, pp. 300-303.

2. Broms, Bengt B. (1965) Effect of degree of saturation on bearing capacity of flexible pavements. Presented at the 43rd Annual Meeting of the Committee on Flexible Pavement Design, Ithaca, New York.

3. Talbot, A.N. (1918) First progress report of the Special Committee to Report on Stresses in Railroad Track. Transactions ASCE, Vol. 82 or Proceedings A.R.E.A., Vol. 19.

   Talbot, A.N. (1920) Second progress report. Transactions ASCE, Vol. 83 or Proceedings A.R.E.A., Vol.21.

   Talbot, A.N. (1923) Third progress report. Transactions ASCE, Vol. 86 or Proceedings A.R.E.A., Vol. 24.

   Talbot, A.N. (1925) Fourth progress report. Transactions ASCE, Vol. 88 or Proceedings A.R.E.A., Vol. 26.

   Talbot, A.N. (1930) Fifth progress report. Transactions ASCE, Vol. 93 or Proceedings A.R.E.A., Vol.31.

   Talbot, A.N. (1934) Sixth progress report. Transactions ASCE, Vol. 97 or Proceedings A.R.E.A., Vol. 35.

   Talbot, A.N. (1941) Seventh progress report. Transactions ASCE, Vol. 104 or Proceedings A.R.E.A., Vol. 42.

4. Terzaghi, K. and Peck, R.B. (1967) Soil Mechanics in Engineering Practice. John Wiley and Sons, Inc., New York.

5. Ireland, Herbert O. (1973) Railroad subgrade stresses. Proceedings of the American Railway Engineering Association, Bulletin No. 641, pp. 382-386.

6. Newmark, N.M. (1942) Influence charts for computation of stresses in elastic foundations. University of Illinois, Experiment Station, Bulletin Series No. 338, Vol. 61, No. 92.

7. Burmister, D.M. (1943) The theory of stresses and displacements in layered systems and applications to design of airport runways. Highway Research Board Proceedings, pp. 126-148.

8. Poulos, H.G. and Davis, E.H. (1974) Elastic Solutions for Soil and Rock Mechanics. John Wiley and Sons, Inc., New York.

9. So, W., Martin, G.C., Singh, B., Chang, I.C. and Chang, E.H. (1978) Mathematical Models for Track Structures. Final Report to U.S. DOT/FRA, Report No. DOT FR-30038, Association of American Railroads.

10. Turcke, D.J. and Raymond, G.P. (1979) Three dimensional analysis of rail track structures, Transportation Research Board, Transportation Research Record No. 733, Washington, D.C. pp. 1-6.

11. Tayabji, S.D. and Thompson, M.R. (1976) Program ILLITRACK: A Finite Element Analysis of Conventional Railway Support System - User's Manual and Program Listing. Federal Railroad Administration, Technical Report FRA-ORD 76/257.

12. Ballast-Subgrade Finite Element Model: Prismatic Solid Analysis Program. Report and Test Department, Association of American Railroads, Washington, D.C. Report 262-14, Vol. II.

13. Kennedy, J.C. and Prause, R.H. (1978) Development of multilayer analysis model for tie-ballast track structures. Railroad Track and Electrification Studies, Transportation Research Record 694, Transportation Research Board. Presented at the 57th Annual Meeting of the Transportation Research Board, Washington, D.C.

14. Chang, C.S., Adegoke, C.W. and Selig, E.T. (1980) GEOTRACK model for railroad track performance. Journal of the Geotechnical Engineering Division, ASCE, Vol. 106, pp. 1201-1218.

15. Stewart, Harry E. and Selig, Ernest T. (1982) Predicted and measured resilient response of track. Proceedings ASCE, Vol. 108, No. GT11, pp. 1423-1442.

16. Terzaghi, K. (1943) Theoretical Soil Mechanics. Johm Wiley and Sons, Inc., New York.

17. Meyerhof, G.G. (1951) The ultimate bearing capacity of foundations. Geotechnique, Vol. 2, pp. 301-332.

18. Meyerhof, G.G. (1953) The bearing capacity of foundations under eccentric and inclined loads. Proceedings of the Third International Conference on Soil Mechanics, Vol. 1, pp. 440.

19. Meyerhof, G.G. (1955) Influence of roughness of base and ground-water conditions on the ultimate bearing capacity of foundations. Geotechnique, Vol. 5, pp. 227.

20. Brinch-Hansen, J. (1970) A revised and extended formula for bearing capacity. Danish Geotechnical Institute, Bulletin No. 28, Copenhagen, Denmark. pp. 5-11.

21. Vesic, A.S. (1973) Analysis of ultimate loads of shallow foundations. Proceedings ASCE, Journal of the Geotechnical Engineering Division, Vol. 99, pp. 45-73.

22. Canadian Foundation Engineering Manual, Second Edition. (1985) Canadian Geotechnical Society, Technical Committee on Foundations, Part 2: Shallow Foundations, pp. 155.

23. Kraft, Leland M. and Helfrich, Steven C. (1983) Bearing capacity of shallow footing, sand over clay. Canadian Geotechnical Journal, Vol. 20, pp. 182-185.

24. Baracos, A. (1969). Design of foundations on Winnipeg clays. Canadian Geotechnical Journal, Volume 6, pp. 197-208.

25. Baracos, A. and Graham, J. (1981). Landslide problems in Winnipeg. Canadian Geotechnical Journal, Volume 18, pp. 390-401.

26. Baracos, A., Graham, J. and Domaschuk, L. (1980). Yielding and rupture in a lacustrine clay. Canadian Geotechnical Journal, Volume 17, pp. 559-573.

27. Clifton Associates Ltd. (1980). Geotechnical investigation and analysis, embankment instability, Mile 7 to 9, Emerson Subdivision, Winnipeg, Manitoba. Report to Canadian Pacific Railways.

28. Clifton Associates Ltd. and University of Saskatchewan (1988). Embankment Instability, Investigation and Analysis, Emerson Subdivision, Winnipeg, Manitoba. Report to Canadian Pacific Railways.

29. Crawford, C.B. (1964). Some characteristics of Winnpeg clay. Canadian Geotechnical Journal, Volume 1, pp. 227-235.

30. Mishtak, J. (1964). Soil mechanics aspects of the Red River Floodway. Canadian Geotechnical Journal, Volume 1, pp. 133-146.

31. Freeman, W.S. and Sutherland, H.B. (1974). Slope stability analysis in anisotropic Winnipeg clays. Canadian Geotechnical Journal, Volume 11, pp. 59-71.

32. Widger, R.A. and Fredlund, D.G. (1979). Stability of swelling clay embankments. Canadian Geotechnical Journal, Volume 16, pp. 140-151.

33. Fredlund, D.G. (1975). Engineering properties of expansive clays. Presented to the Seminar on Shallow Foundations on Expansive Clays, Regina, Saskatchewan, October, 1975. Internal Report of the Transportation and Geotechnical Group, Department of Civil Engineering, University of Saskatchewan, Saskatoon, Saskatchewan. Internal Report IR-7.

34. Clifton, A.W., Yoshida, R.T. and Chursinoff, R.W. (1986). Regina Beach - a town on a landslide. Canadian Geotechnical Journal, Volume 23, pp. 60-68.

35. Krahn, J., Johnson, R.F., Fredlund, D.G. and Clifton, A.W. (1979). A highway cut failure in Cretaceous sediments at Maymont, Saskatchewan. Canadian Geotechnical Journal, Volume 16, pp. 703-715.

36. Insley, A.E., Chatterji, P.K. and Smith, L.B. (1977). Use of residual shear strength for stability analyses of embankment foundations containing pre-existing failure surfaces. Canadian Geotechnical Journal, Volume 14, pp. 408-428.

37. Thomson, S. and Hayley, D.W. (1975). The Little Smoky landslide. Canadian Geotechnical Journal, Volume 12, pp. 379-392.

38. Yoshida, R.T. and Krahn, J. (1985). Movement and stability analysis of the Beaver Creek landslide, Saskatchewan, Canada. Canadian Geotechnical Journal, Volume 22, pp. 277-285.

39. Sauer, E.K. (1983). The Denholm landslide, Saskatchewan. Part II: analysis. Canadian Geotechnical Journal, Volume 20, pp. 208-220.

40. Sauer, E.K. (1984). A landslide in clay shale in the North Saskatchewan River Valley, Canada. Engineering Geology, Volume 20, pp. 279-300.

41. Thomson, S. (1970). Riverbank stability study at the University of Alberta, Edmonton. Canadian Geotechnical Journal, Volume 17, pp. 157-168.

42. Thomson, S. and Yacyshyn, R. (1977). Slope instability in the city of Edmonton. Canadian Geotechnical Journal, Volume 14, pp. 1-16.

43. Thomson, S. and Tweedie, R.W. (1978). The Edgerton landslide. Canadian Geotechnical Journal, Volume 15, pp. 510-521.

44. Lidgren, R.A. and Sauer, E.K. (1982). The Gronlid crossing, Saskatchewan Provincial Highway No. 6 at the Saskatchewan River. Canadian Geotechnical Journal, Volume 19.

45. Thomson, S. and Mekechuk, J. (1982). A landslide in glacial lake clays in central British Columbia. Canadian Geotechnical Journal, Volume 19, pp. 296-306.

46. Lafleur, J., Lefebvre, G., Marcotte, M. and Silvestri, V. (1982). Shear strength of the weathered Champlain clay measured in a large diameter triaxial test. Canadian Geotechnical Journal, Volume 19, pp. 413-420.

47. Rivard, P.J. and Lu, Y. (1978). Shear strength of soft fissured clays. Canadian Geotechnical Journal, Volume 15, pp. 382-390.

48. Thomson, S. and Kjartanson, B.H. (1985). A study of delayed failure in a cut slope in stiff clay. Canadian Geotechnical Journal, Volume 22, pp. 286-297.

49. Brzezinski, L.S. (1971). A review of the 1924 Kenogami landslide. Canadian Geotechnical Journal, Volume 8, pp. 1-6.

50. La Rochelle, P., Lefebvre, G. and Bilodeau, P.M. (1977). The stabilization of a slide in Saint-Jerome, Lac Saint-Jean. Canadian Geotechnical Journal, Volume 14, pp. 340-356.

51. Sangrey, D.A. and Paul, M.J. (1971). A regional study of landsliding near Ottawa. Canadian Geotechnical Journal, Volume 8, pp. 315-335.

52. Quigley, R.M., Matich, M.A.J., Horvath, R.G. and Hawson, H.H. (1971). Swelling clay in two slope failures at Toronto, Canada. Canadian Geotechnical Journal, Volume 8, pp. 417-424.

53. Haug, M.D., Sauer, E.K. and Fredlund, D.G. (1977). Retrogressive slope failures at Beaver Creek, south of Saskatoon, Saskatchewan, Canada. Canadian Geotechnical Journal, Volume 14, pp. 288-301.

54. EBA Engineering Consultants Ltd. (1982). CP Rail Rogers Pass, Grade Improvement Project, Surface Route Conceptual Design Evaluations. Report to Canadian Pacific Railways, Special Projects.

55. Conlon, R.J., Tanner, R.G., and Coldwell, K.L. (1971). The geotechnical design of the townline road-rail tunnel. Canadian Geotechnical Journal, Volume 8, pp. 299-314.

56. MacDonald, A.B. (1969). Drift stratigraphy in terrain evaluation. M.Sc. Thesis, Department of Civil Engineering, University of Saskatchewan, Saskatoon, Saskatchewan.

57. Christiansen, E.A., Editor (1970). Physical Environment of Saskatoon, Canada. Published by Saskatchewan Research Council in cooperation with The National Research Council of Canada. NRC Publication Number 11378. pp. 53-55.

58. Radhakrishna, H.S. and Klym, T.W. (1974). Geotechnical properties of a very dense glacial till. Canadian Geotechnical Journal, Volume 11, pp. 396-408.

59. Sauer, E.K. and Christiansen, E.A. (1985). A landslide in till near Warman, Saskatchewan, Canada. Canadian Geotechnical Journal, Volume 22, pp. 195-204.

60. Terzaghi, K. and Peck, R.B. (1967). Soil Mechanics in Engineering Practice, Second Edition. John Wiley and Sons, Inc. New York.

61. Lambe, T.W. and Whitman, R.V. (1979). Soil Mechanics, SI Version. John Wiley and Sons, Inc. New York.

62. Van Dine, D.F. (1983). Drynoch landslide, British Columbia - a history. Canadian Geotechnical Journal, Volume 20, pp. 82-103.

63. Gan, K.J. and Fredlund, D.G. (1987) Multistage direct shear testing of unsaturated soils. American Society for Testing and Materials, Proceedings of the Geotechnical Testing Journal, American Society of Civil Engineers.

64. Gan, K. J. (1986) Direct Shear Strength Testing of Unsaturated Soils. M.Sc. Thesis, Department of Civil Engineering, University of Saskatchewan, Saskatoon, Saskatchewan, Canada.

65. Ho, D.Y.F. and Fredlund, D.G. (1982) The increase in shear strength due to soil suction for two Hong Kong soils. ASCE Geotechnical Conference on "Engineering and Construction in Tropical and Residual Soils", Honolulu, Hawaii. pp. 263-295.

66. Fredlund, D.G., Rahardjo, H. and Gan, J.K.M. (1987) Non-linearity of strength envelope for unsaturated soils. Proceedings of the Sixth International Conference on Expansive Soils, New Delhi, India.

67. Wong, D.K.H. and Ho, A. (1987) An Evaluation of a Thermal Conductivity Sensor for the Measurement of Soil Matric Suction. The Geotechnical Group, Department of Civil Engineering, University of Saskatchewan, Saskatoon, Saskatchewan, Canada, S7N 0W0.

68. Fredlund, D.G. and Wong, D.K.H. (1988) Calibration of AGWA-II thermal conductivity sensors for measuring soil suction. Submitted for review to ASTM Geotechnical Testing Journal.

69. Wong, D.K.H., Fredlund, D.G., Imre, E. and Putz, G. (1988) Difficulties associated with the use of AGWA-II thermal conductivity sensors to measure suction. Submitted to the Transportation Research Board, Washington, D.C.

70. Sattler, P. and Fredlund, D.G. (1988) Use of thermal conductivity sensors to measure matric suction in the laboratory. Submitted to the Canadian Geotechnical Journal.

71. van der Raadt, P., Fredlund, D.G., Clifton, A.W., Klassen, M.J. and Jubien, W.E. (1987) Soil suction measurements at several sites in Western Canada. Presented to the Session on Geotechnical Problems in Arid Regions, Transportation Research Board, Committee A2L06TRB, Washington, D.C.

72. van der Raadt, P. and Clifton, A.W. (1985) Soil Suction Measurement Final Report. A report prepared for CP Rail, CN Rail and the Transportation Development Center by Clifton Associates Ltd., Regina, Saskatchewan.

73. van der Raadt, P. (1988) Field Measurement of Soil Suction Using Thermal Conductivity Matric Potential Sensors. M.Sc. Thesis, Department of Civil Engineering, University of Saskatchewan, Saskatoon, Saskatchewan.

APPENDIX A

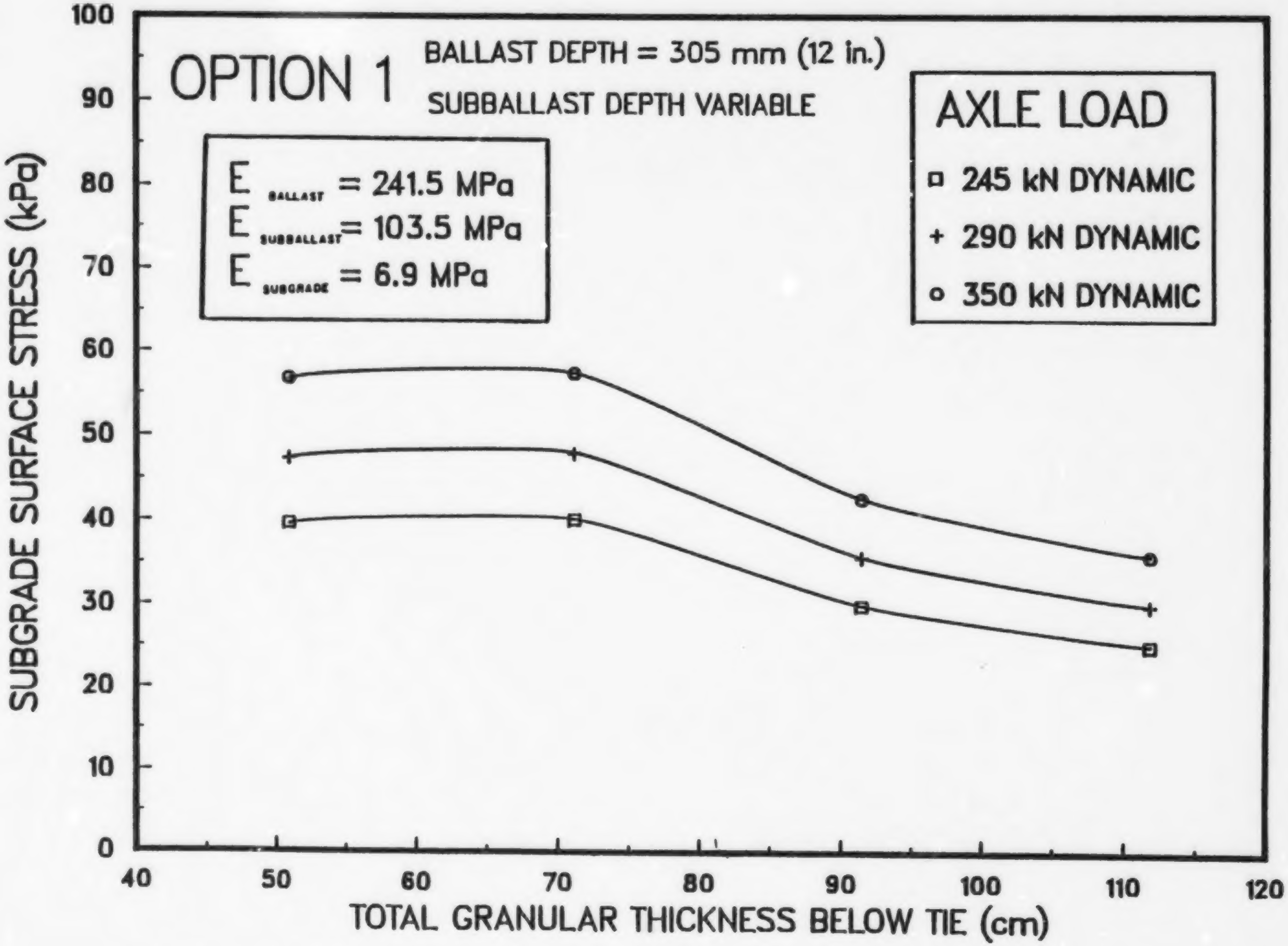

Fig. 5.8 Stress chart for Option 1, Subgrade E = 6.9 MPa, Subballast E = 103.5 MPa

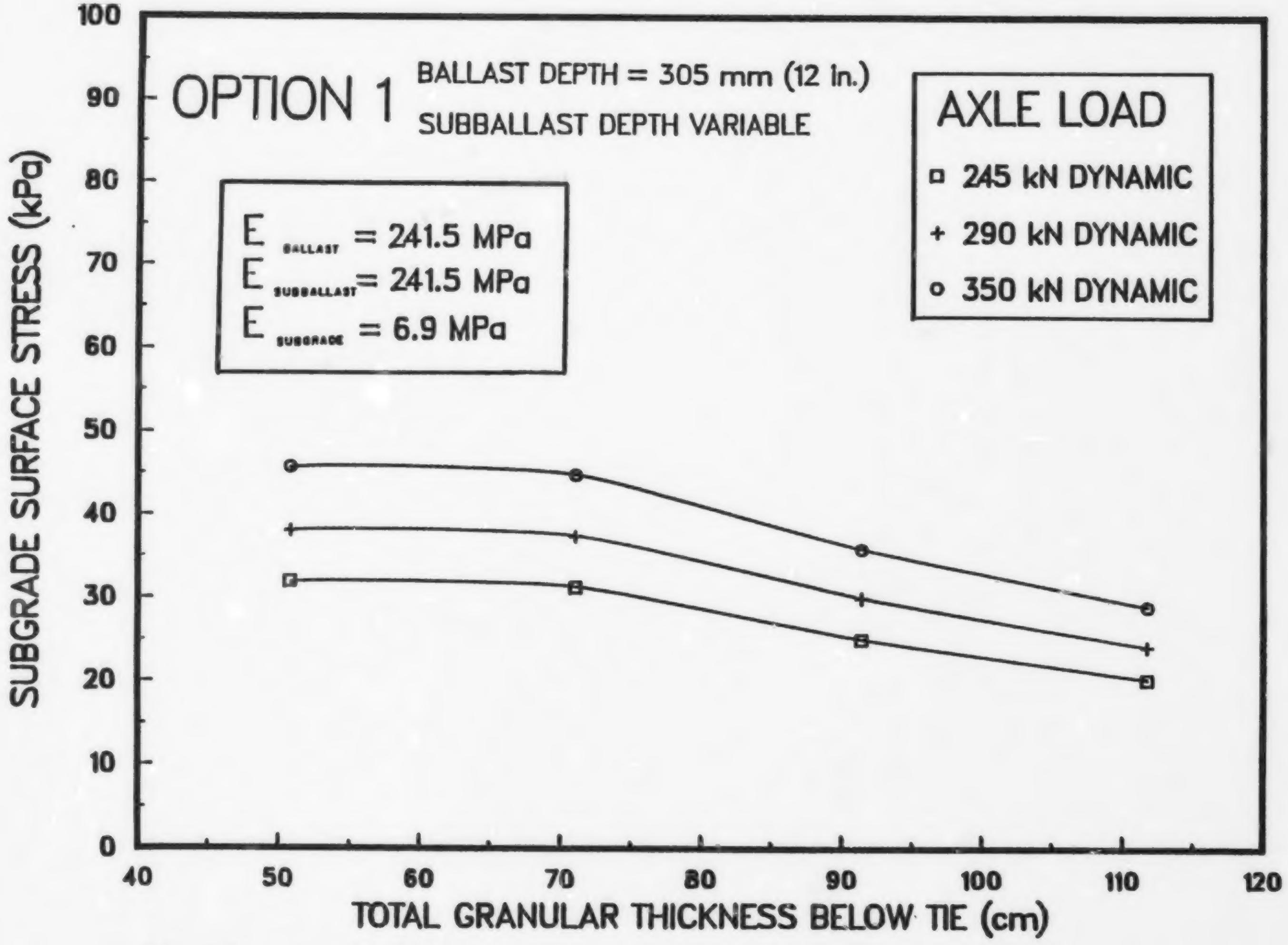

Fig. 5.9 Stress chart for Option 1, Subgrade E = 6.9 MPa, Subballast E = 241.5 MPa

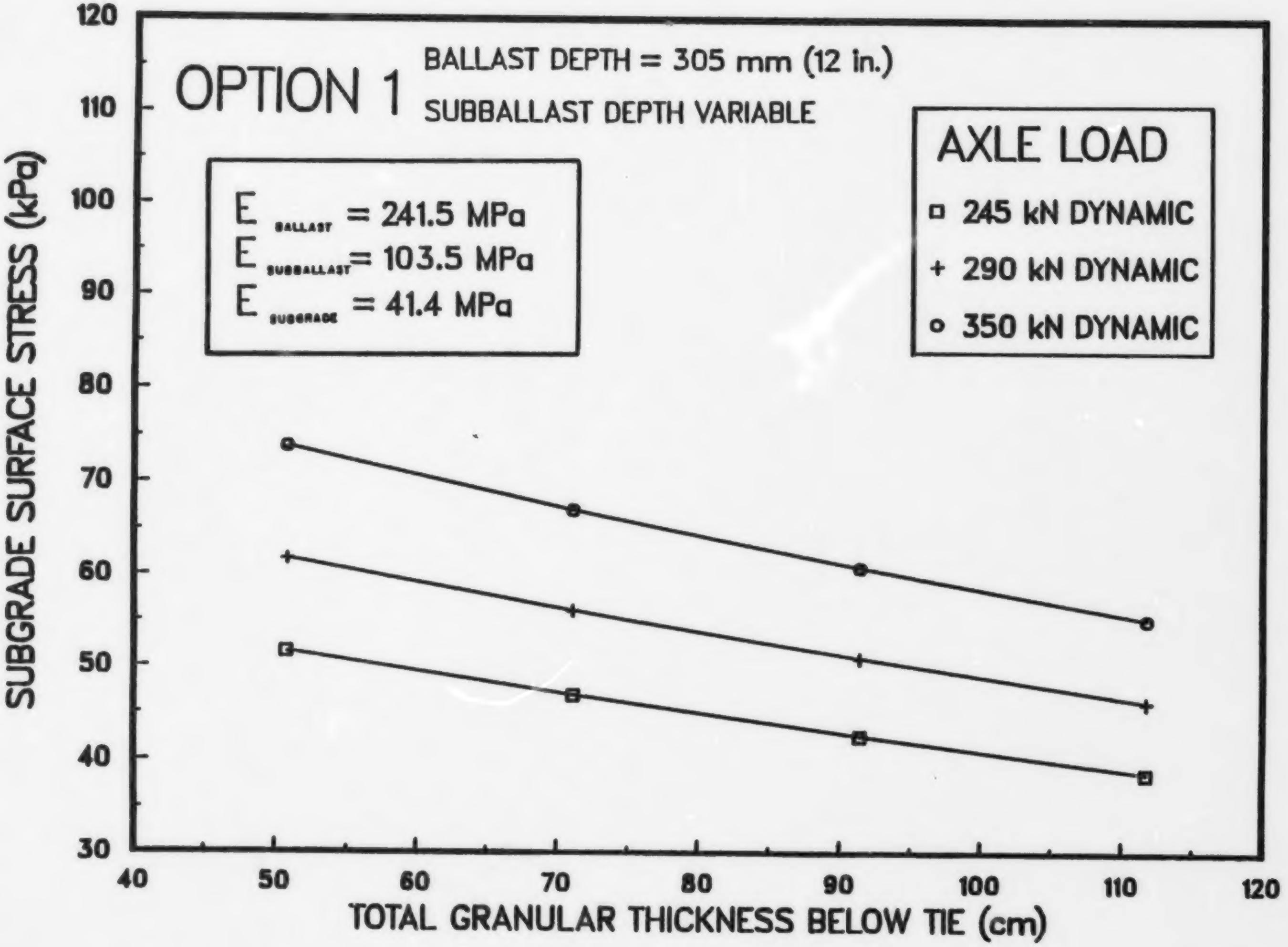

Fig. 5.10 Stress chart for Option 1, Subgrade E = 41.4 MPa, Subballast E = 103.5 MPa

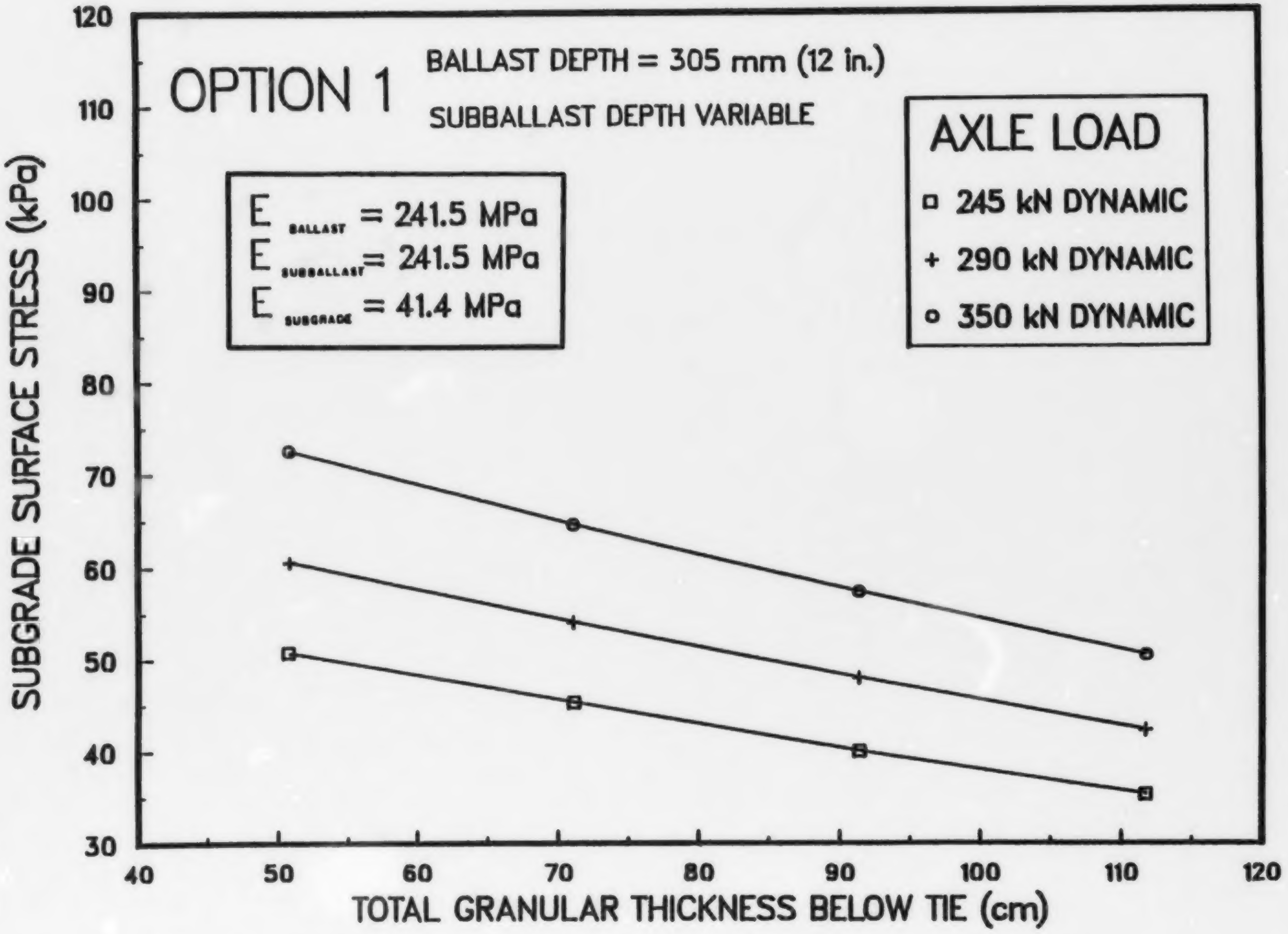

Fig. 5.11 Stress chart for Option 1, Subgrade E = 41.4 MPa, Subballast E = 241.5 MPa

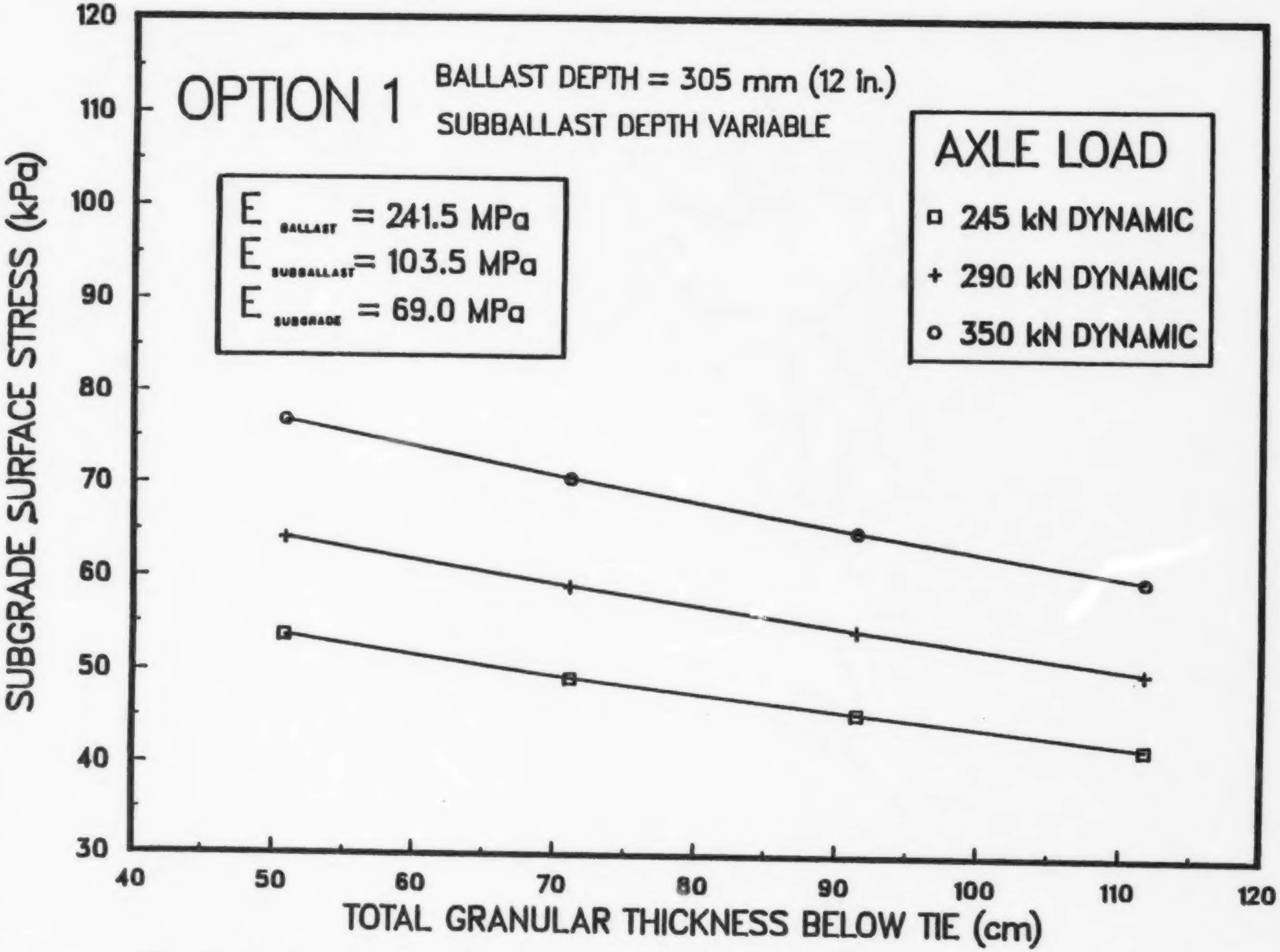

Fig. 5.12 Stress chart for Option 1, Subgrade E = 69.0 MPa, Subballast E = 103.5 MPa

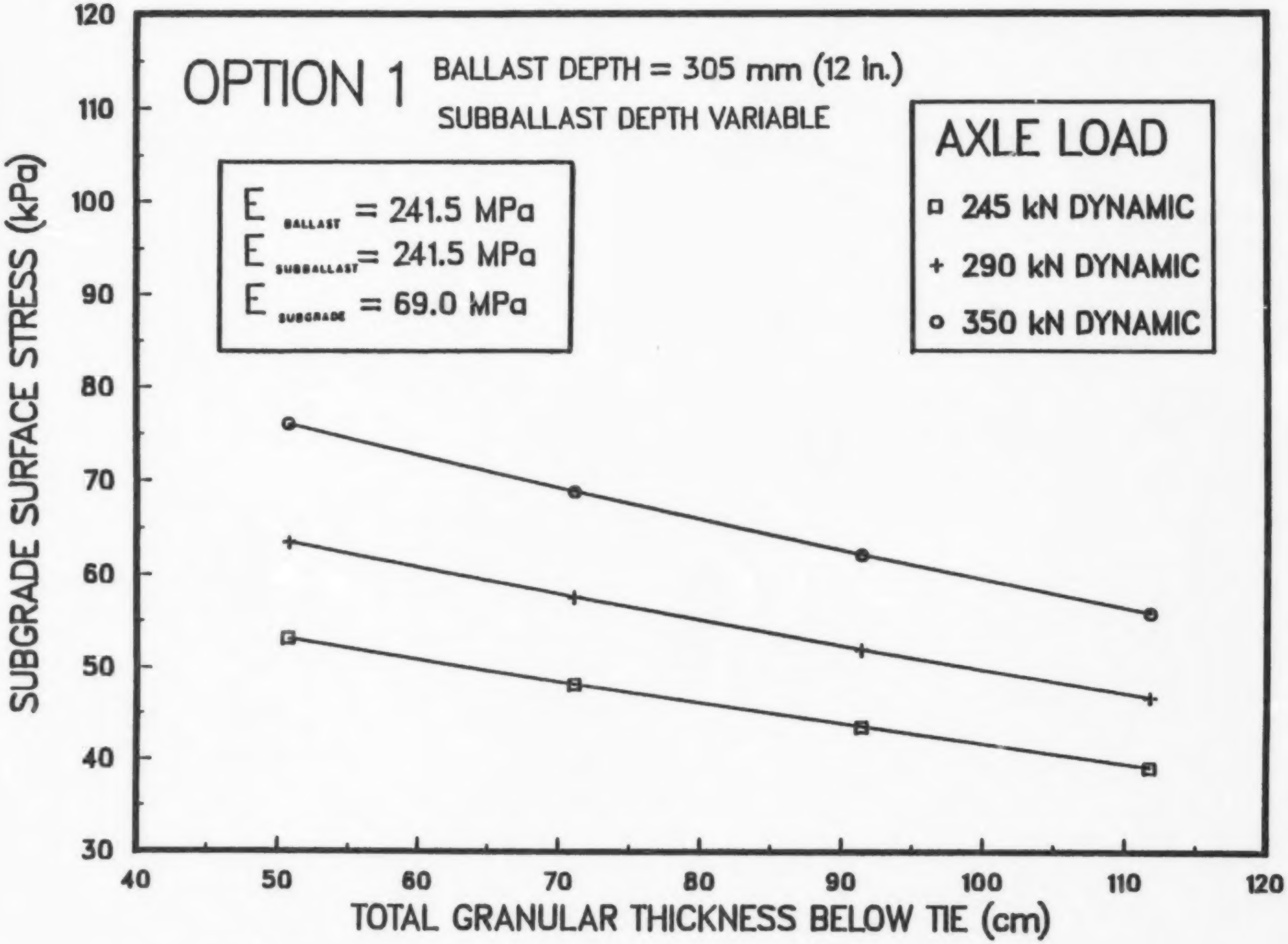

Fig. 5.13 Stress chart for Option 1, Subgrade E = 69.0 MPa, Subballast E = 241.5 MPa

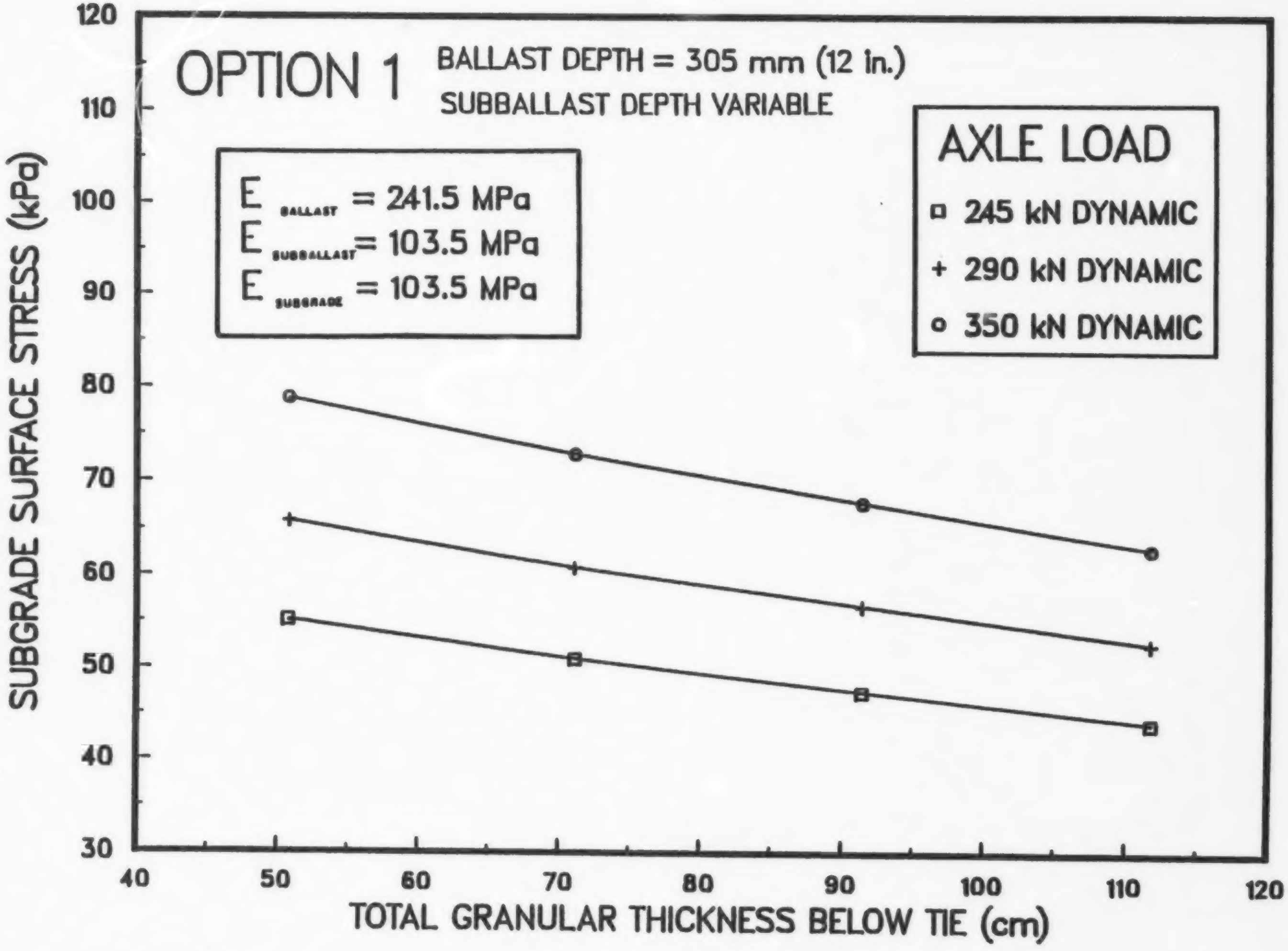

Fig. 5.14 Stress chart for Option 1, Subgrade E = 103.5 MPa, Subballast E = 103.5 MPa

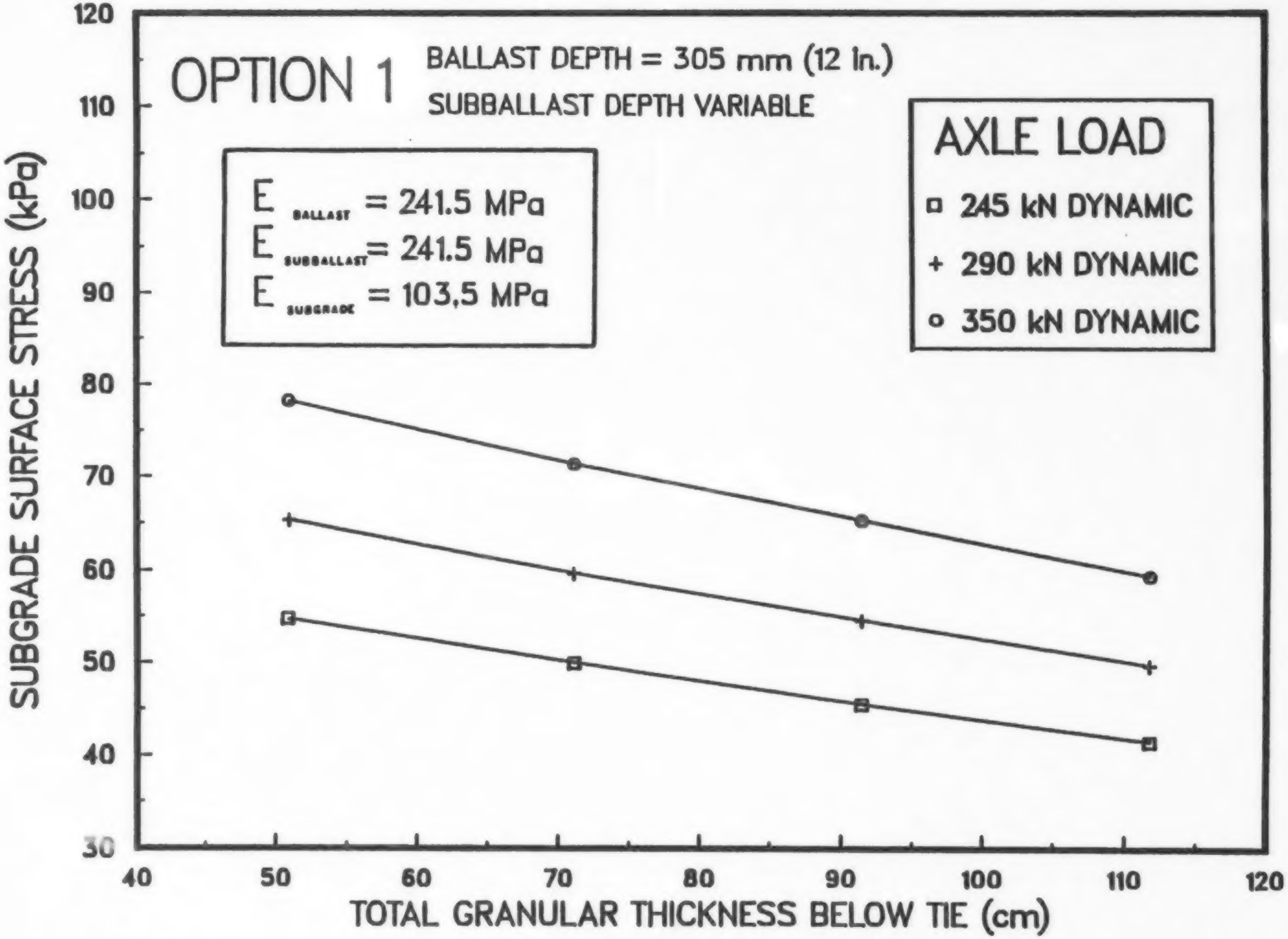

Fig. 5.15 Stress chart for Option 1, Subgrade E = 103.5 MPa, Subballast E = 241.5 MPa

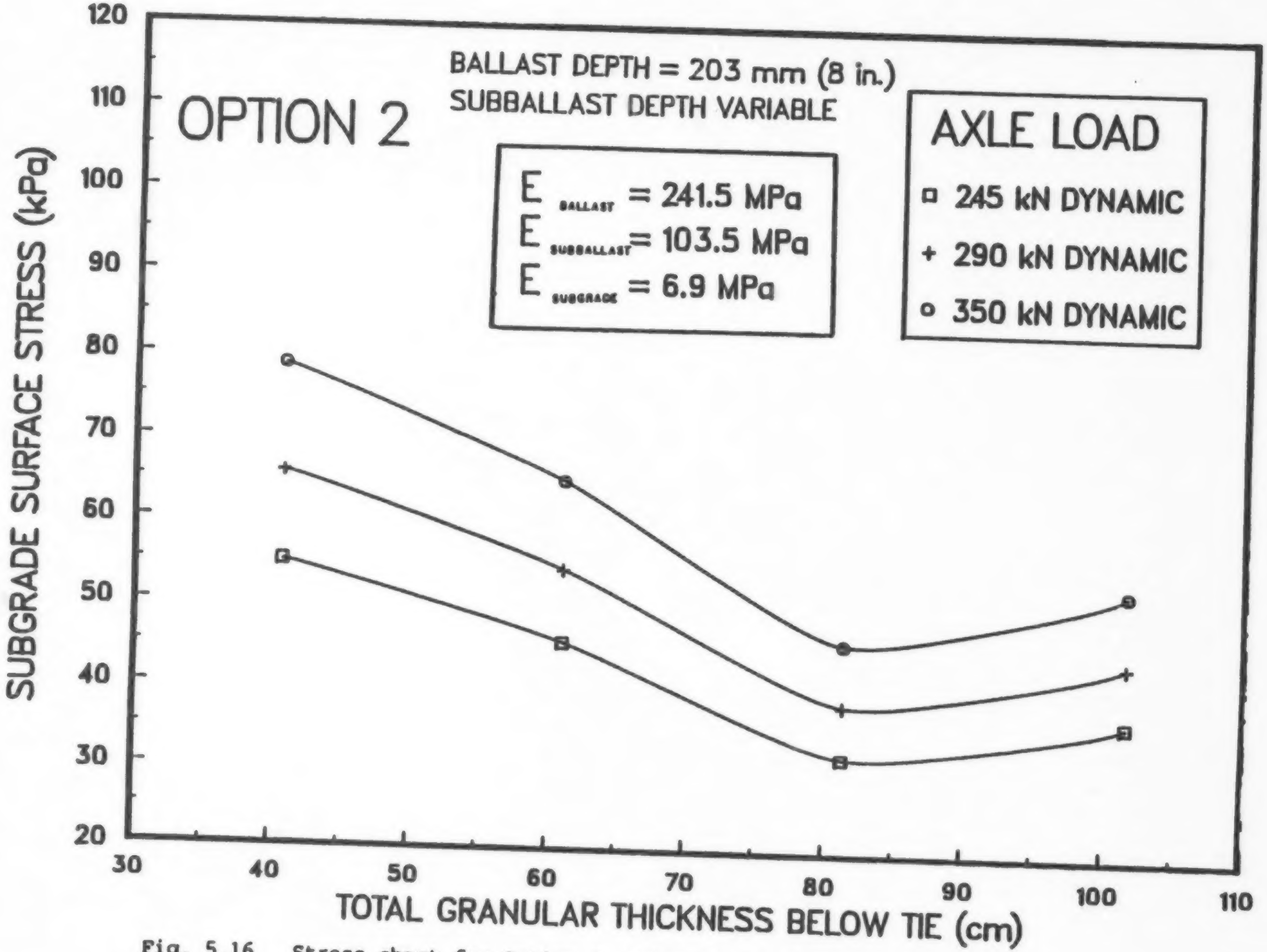

Fig. 5.16 Stress chart for Option 2, Subgrade E = 6.9 MPa, Subballast E = 103.5 MPa

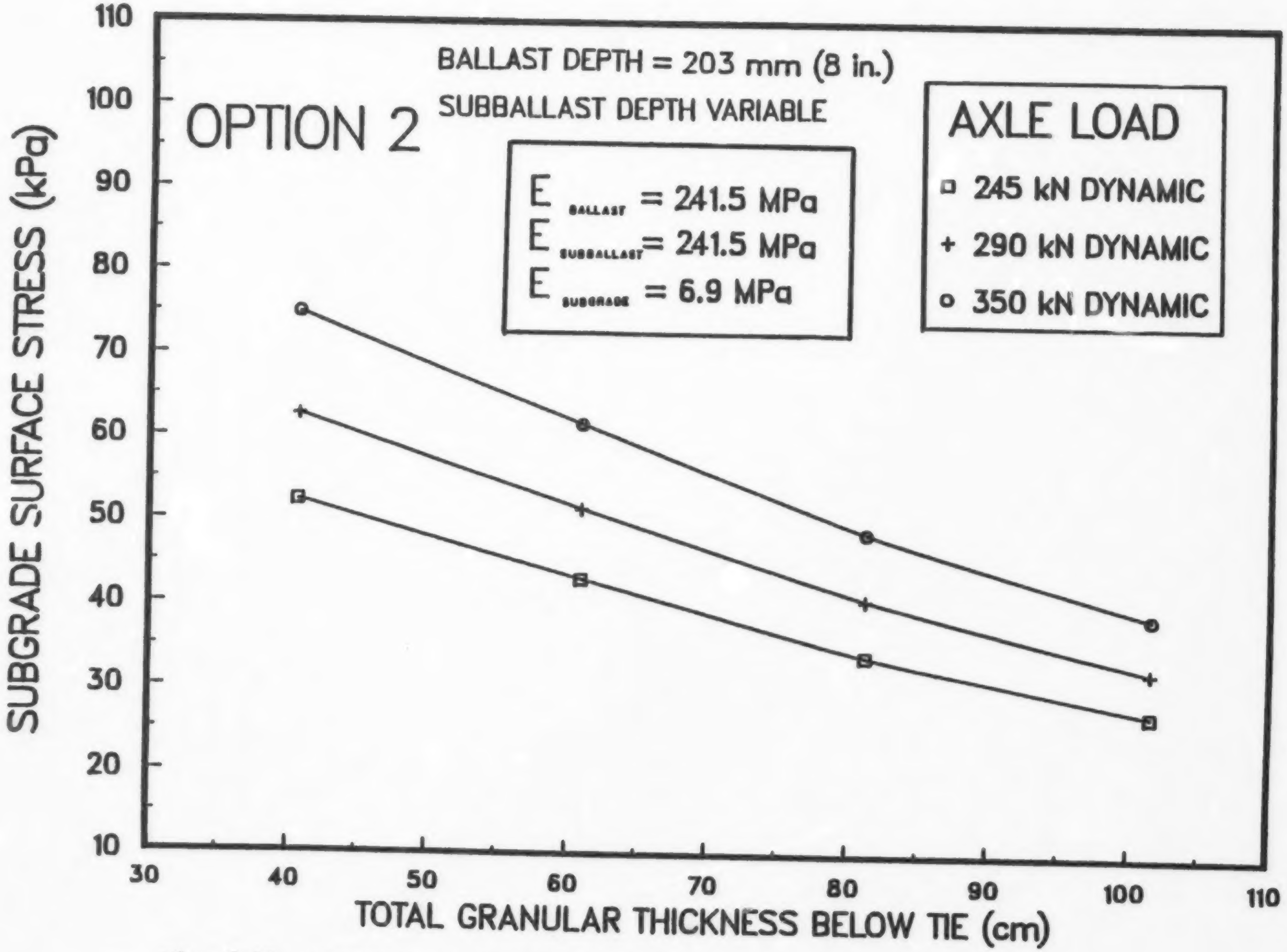

Fig. 5.17 Stress chart for Option 2, Subgrade E = 6.9 MPa, Subballast E = 241.5 MPa

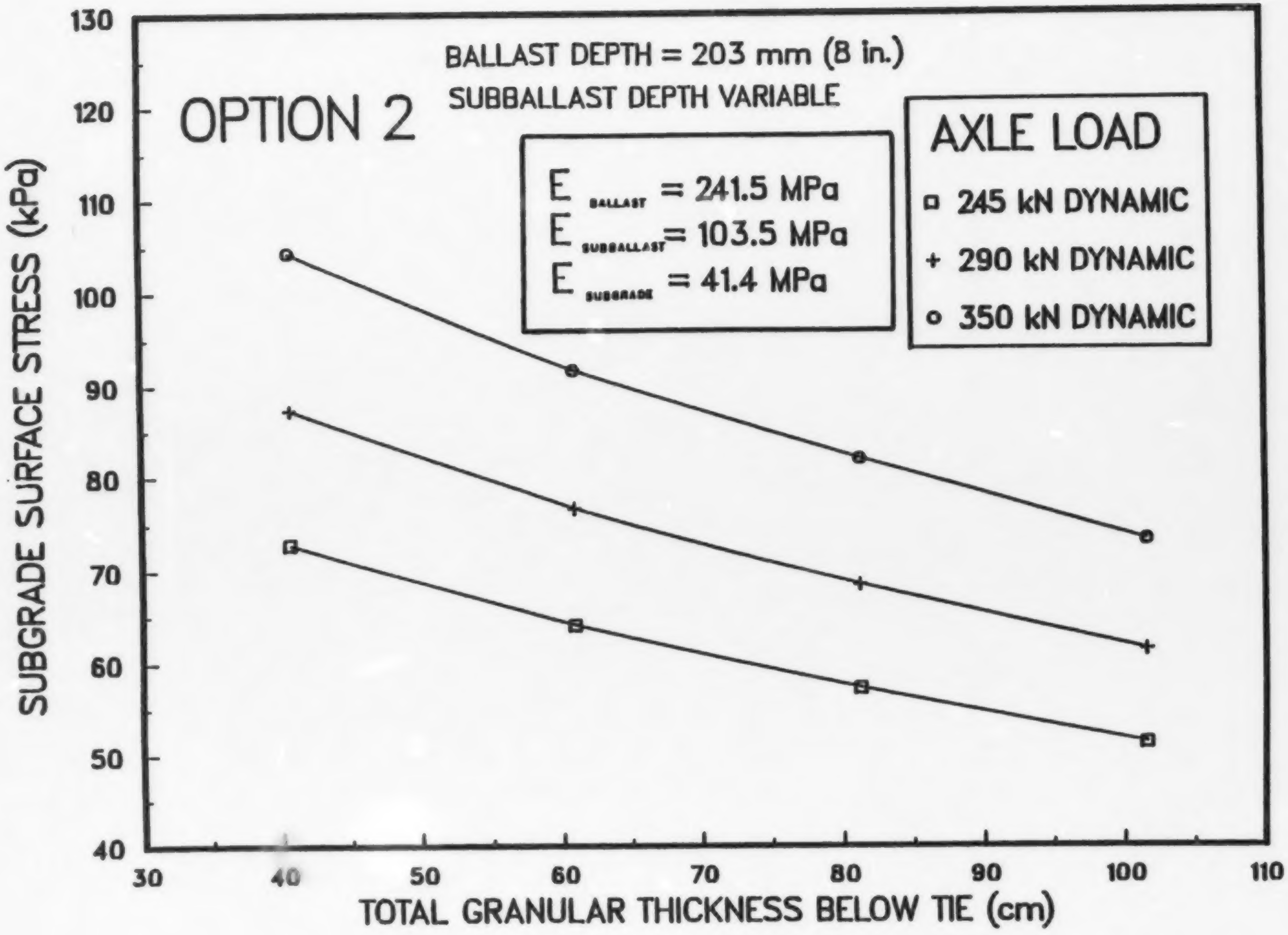

Fig. 5.18 Stress chart for Option 2, Subgrade E = 41.4 MPa, Subballast E = 103.5 MPa

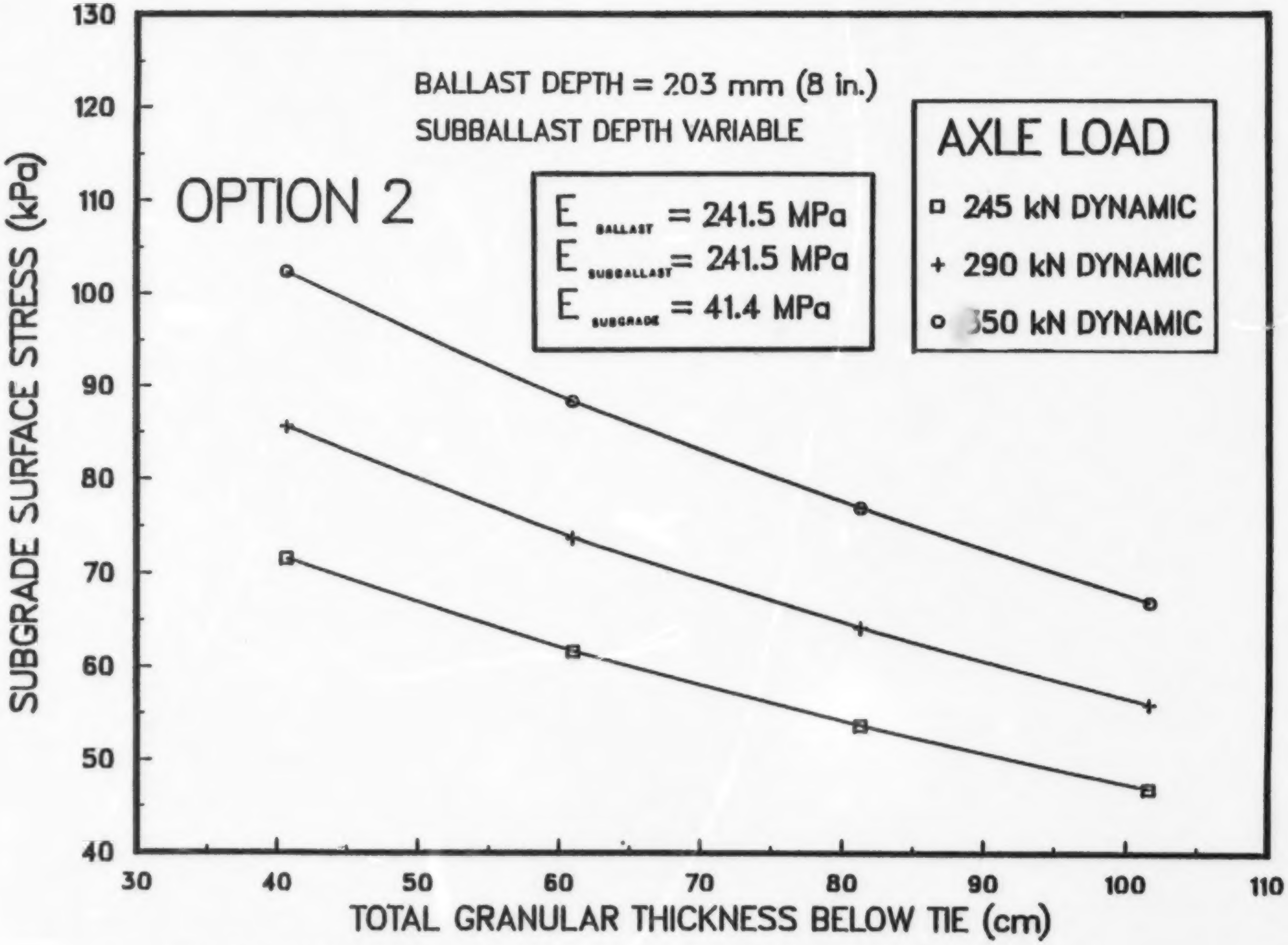

Fig. 5.19 Stress chart for Option 2, Subgrade E = 41.4 MPa, Subballast E = 241.5 MPa

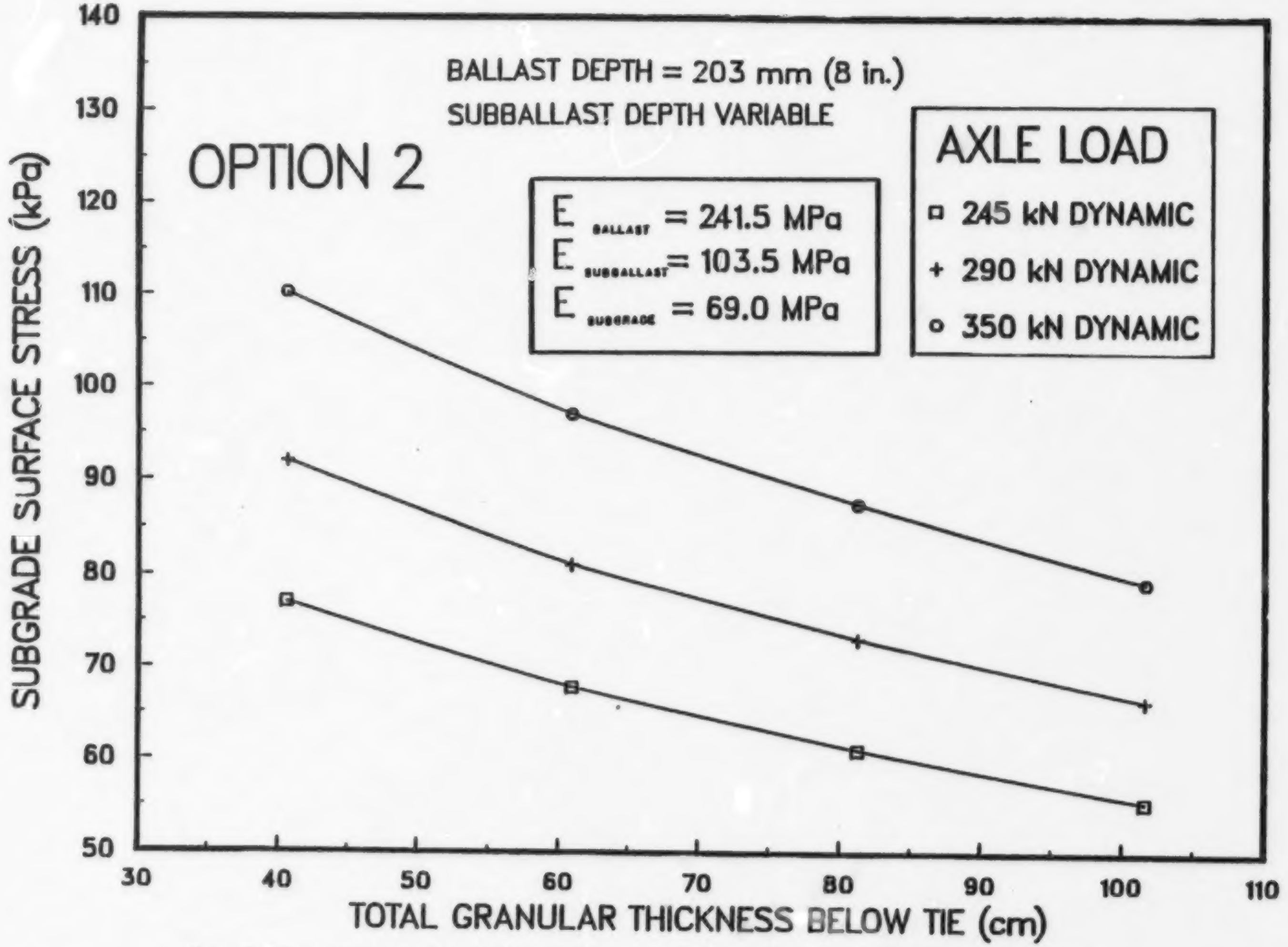

Fig. 5.20 Stress chart for Option 2, Subgrade E = 69.0 MPa, Subballast E = 103.5 MPa

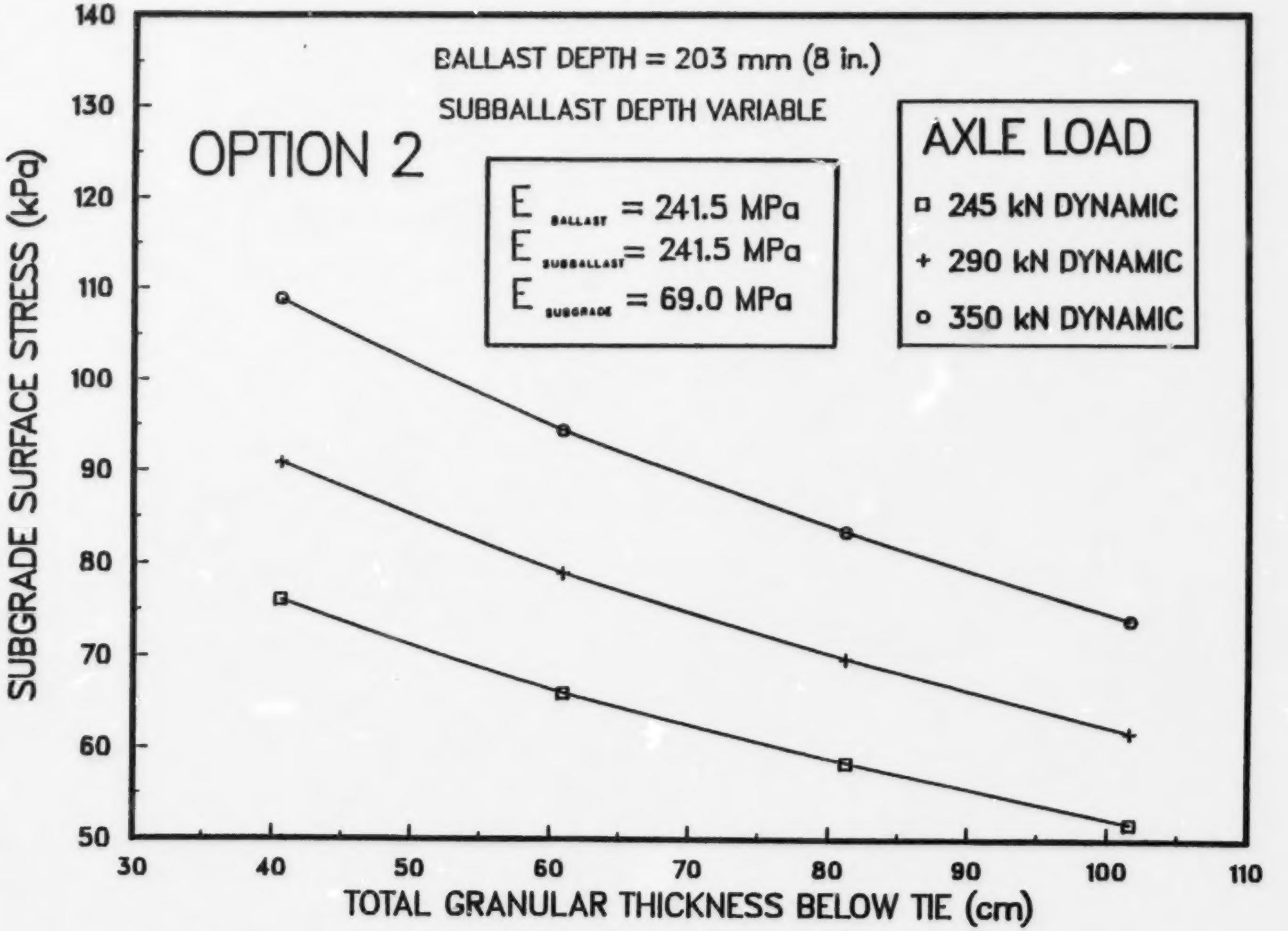

Fig. 5.21 Stress chart for Option 2, Subgrade E = 69.0 MPa, Subballast E = 241.5 MPa

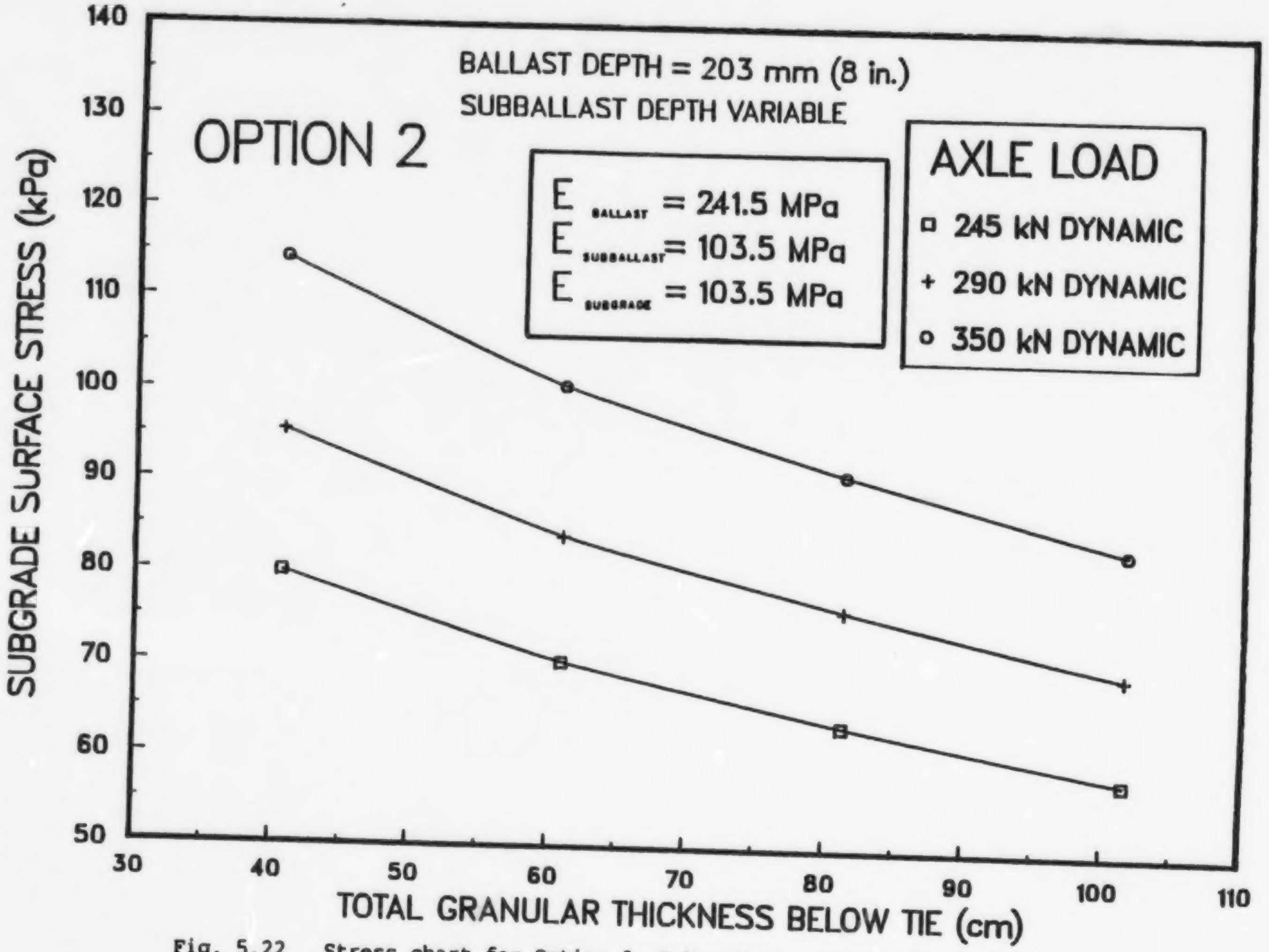

Fig. 5.22 Stress chart for Option 2, Subgrade E = 103.5 MPa, Subballast E = 103.5 MPa

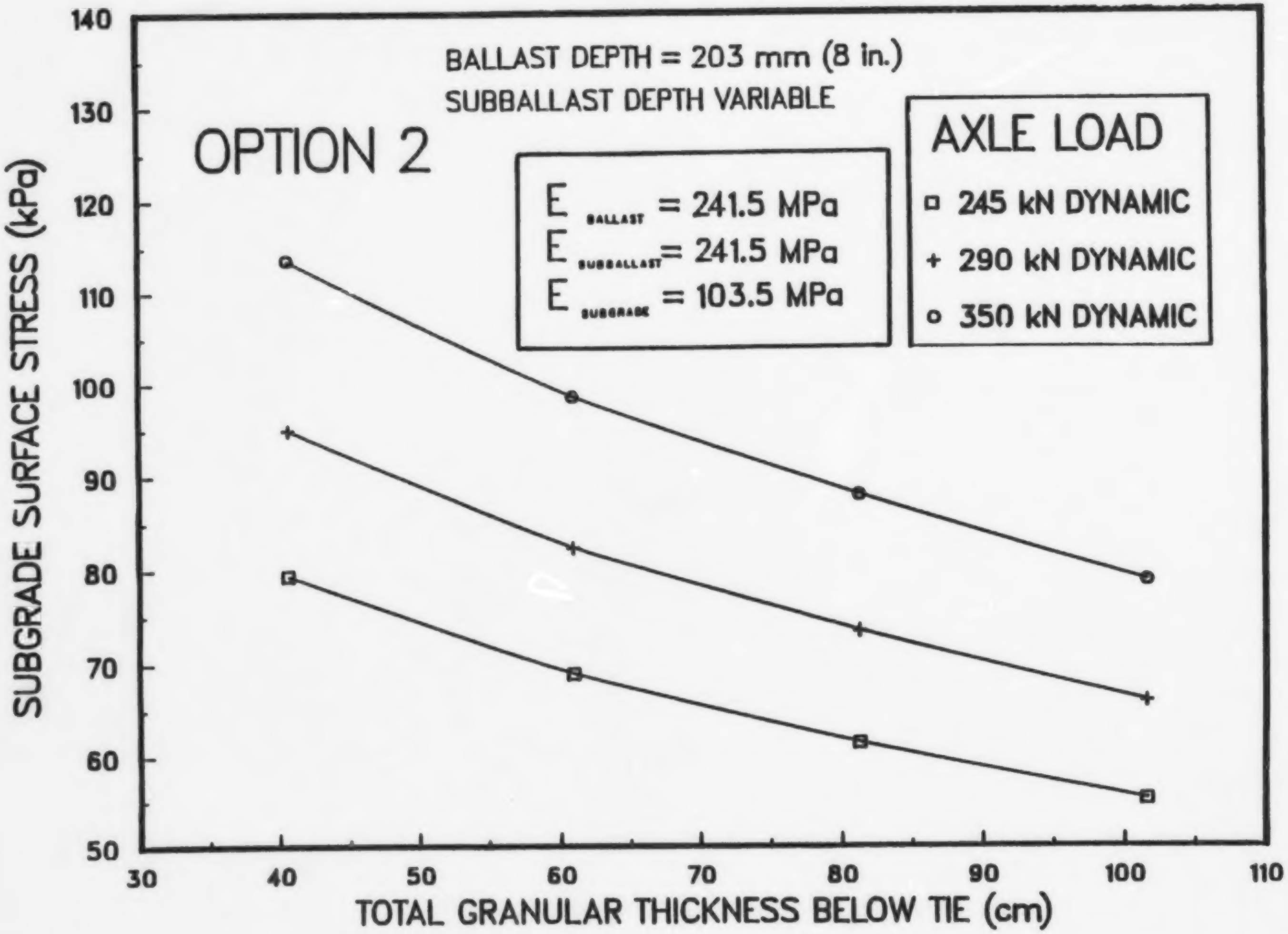

Fig. 5.23 Stress chart for Option 2, Subgrade E = 103.5 MPa, Subballast E = 241.5 MPa

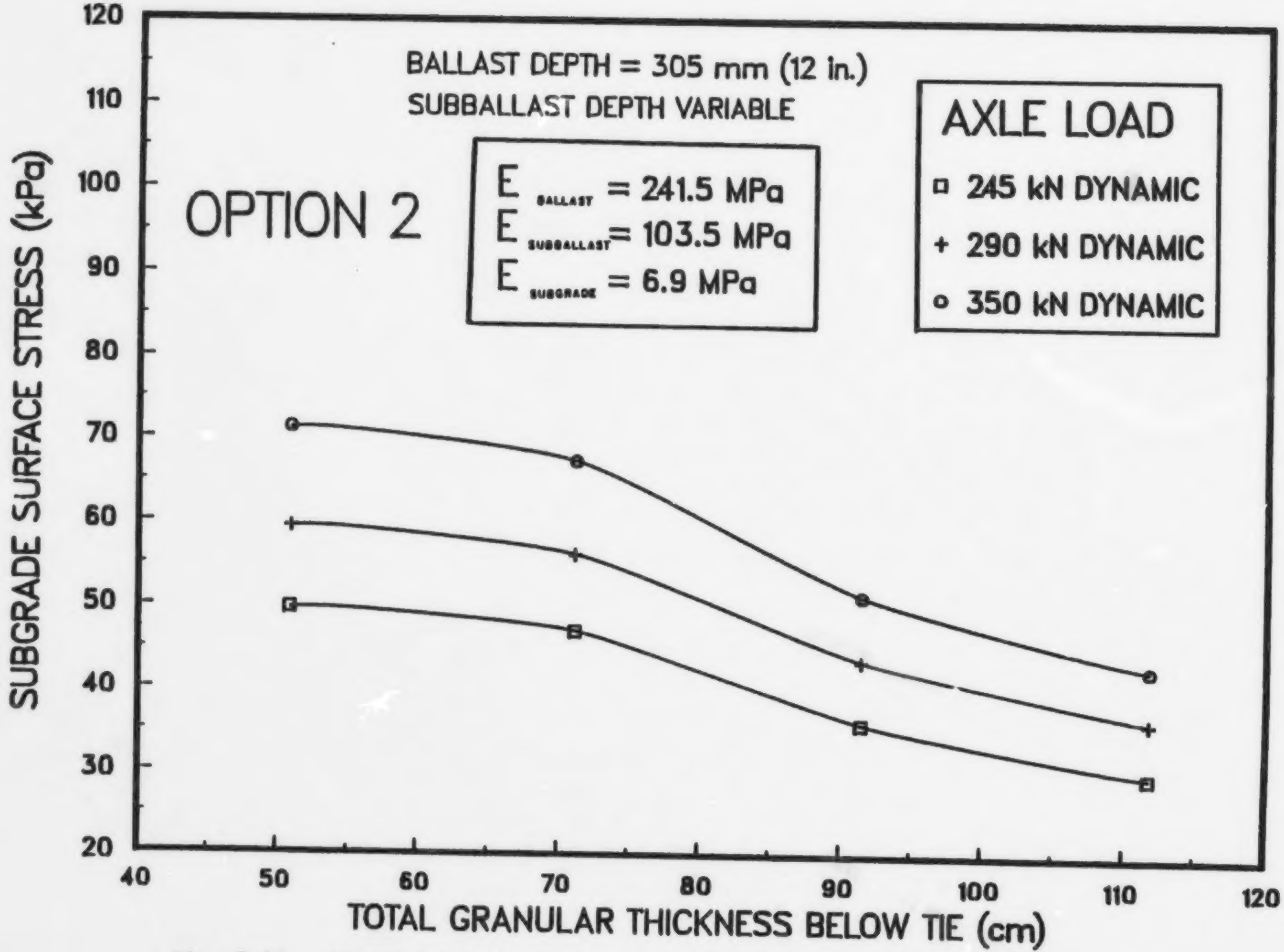

Fig. 5.24 Stress chart for Option 2, Subgrade E = 6.9 MPa, Subballast E = 103.5 MPa

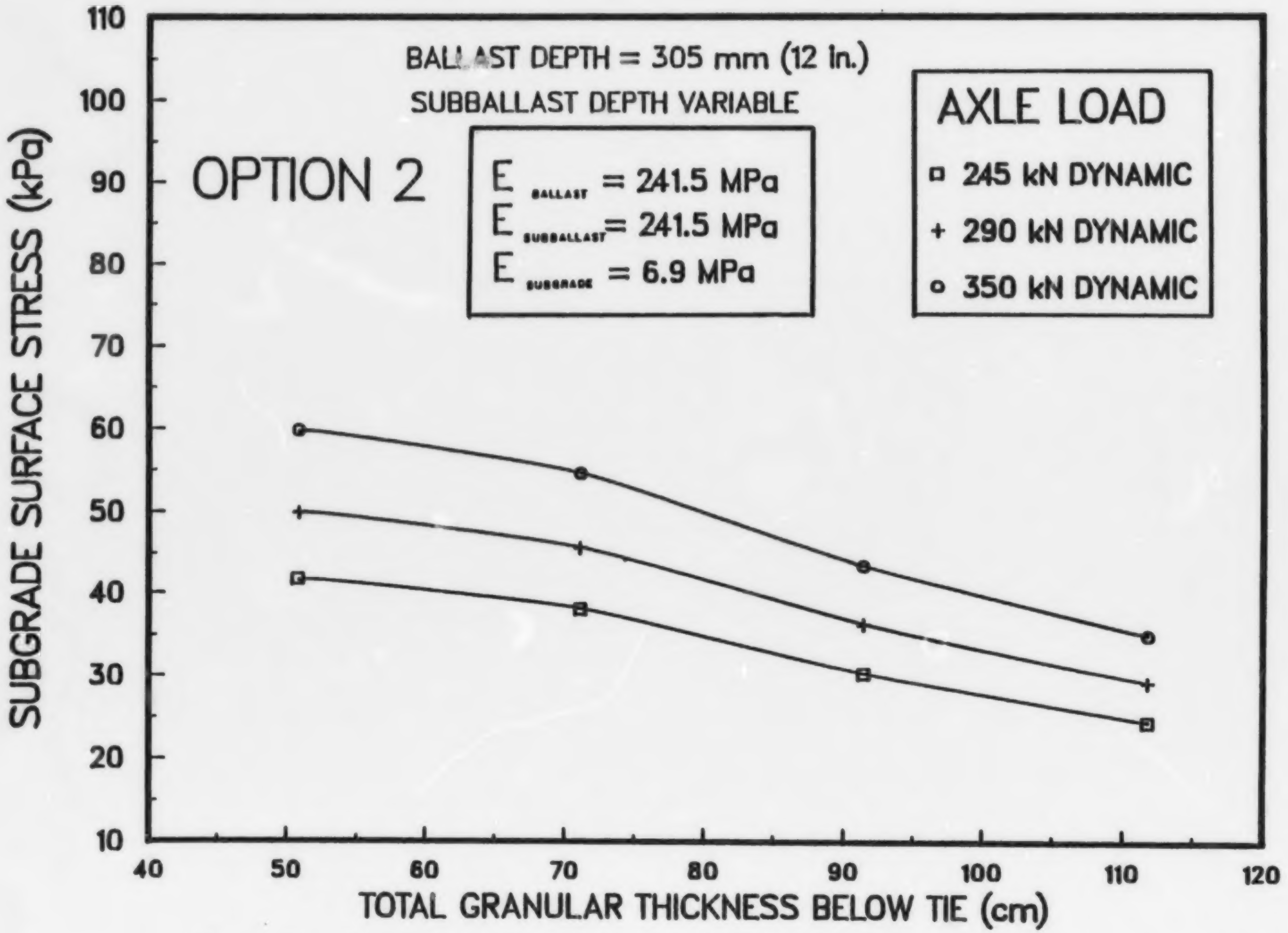

Fig. 5.25 Stress chart for Option 2, Subgrade E = 6.9 MPa, Subballast E = 241.5 MPa

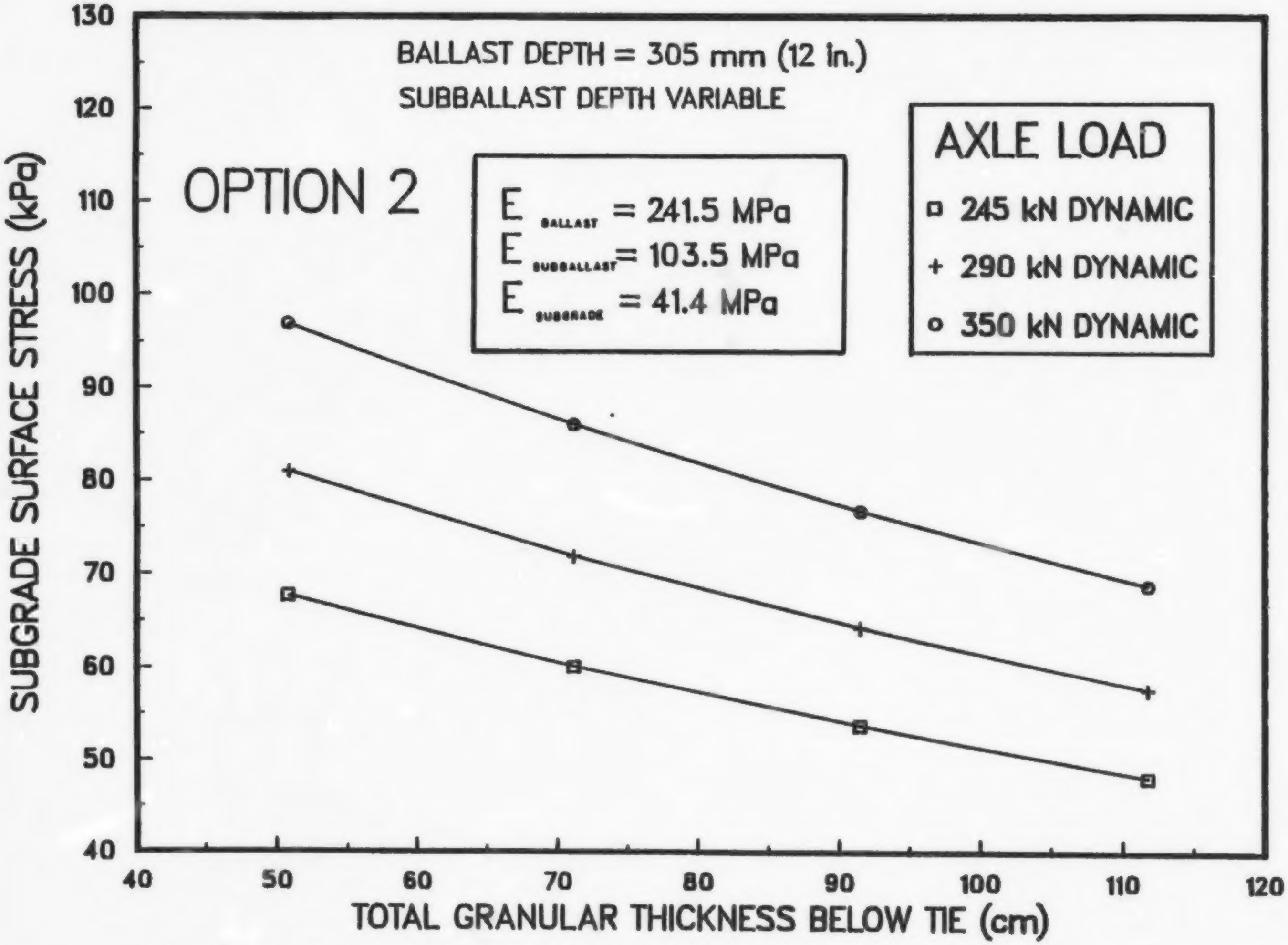

Fig. 5.26 Stress chart for Option 2, Subgrade E = 41.4 MPa, Subballast E = 103.5 MPa

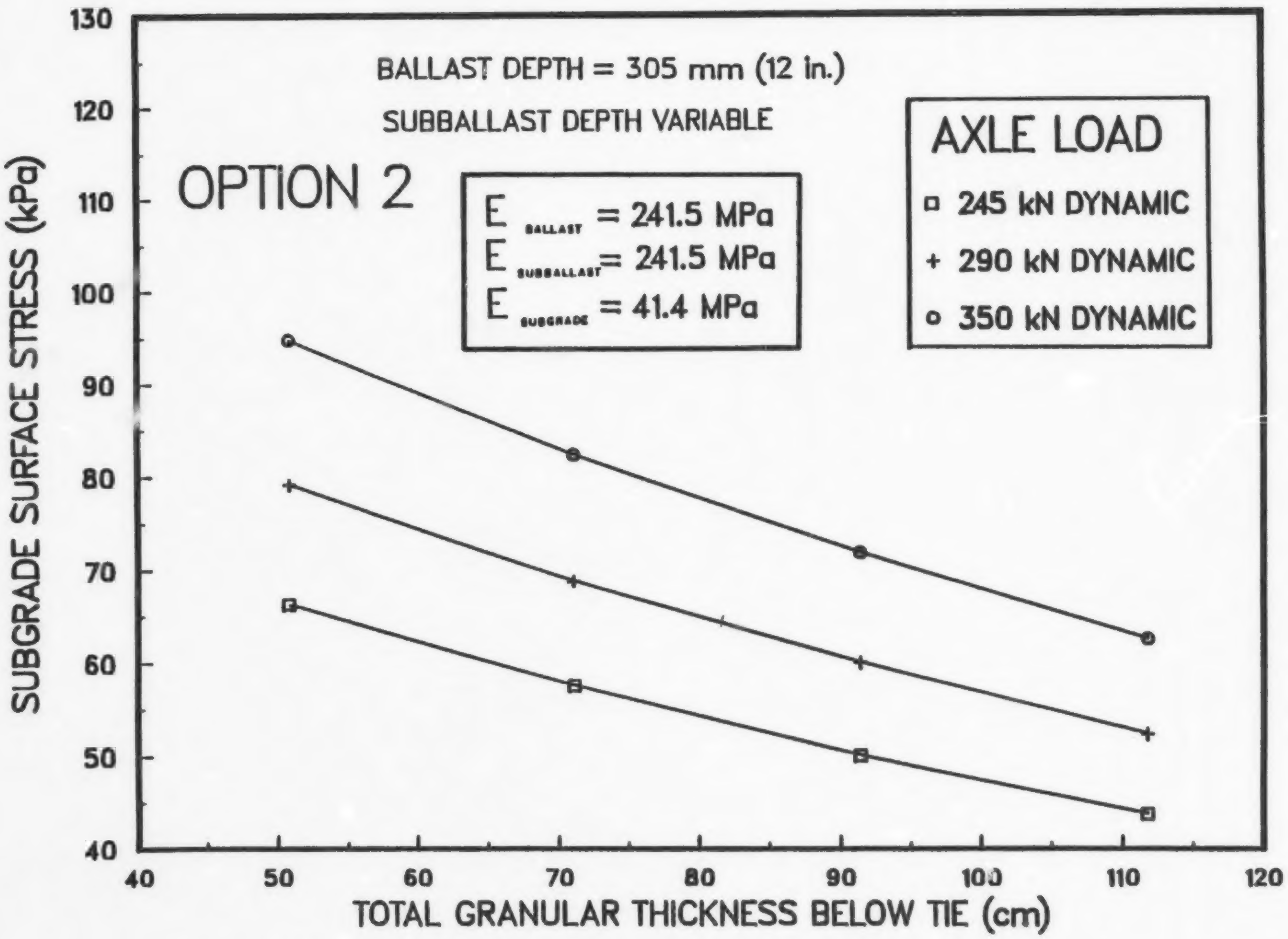

Fig. 5.27 Stress chart for Option 2, Subgrade E = 41.4 MPa, Subballast E = 241.5 MPa

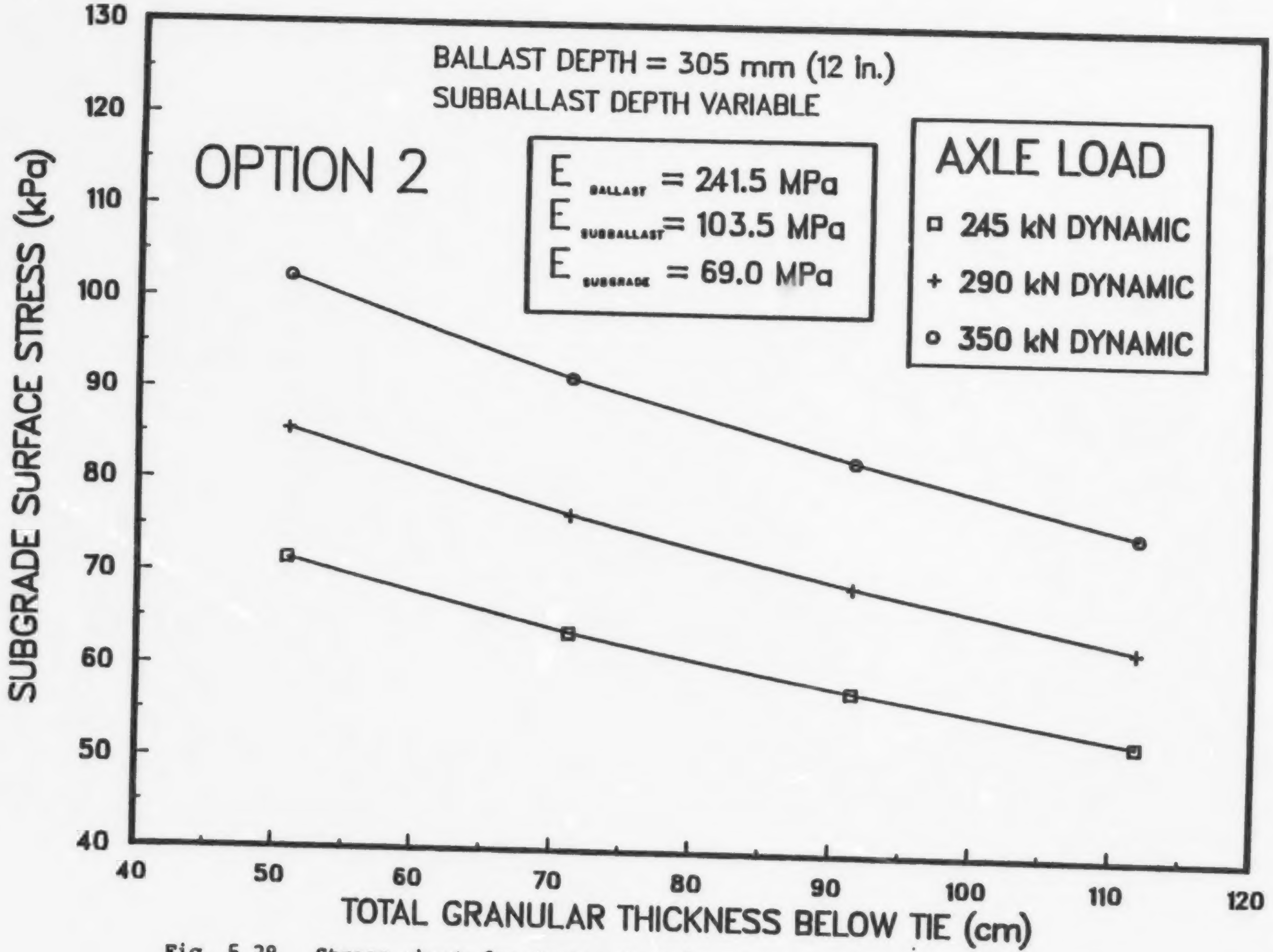

Fig. 5.28 Stress chart for Option 2, Subgrade E = 69.0 MPa, Subballast E = 103.5 MPa

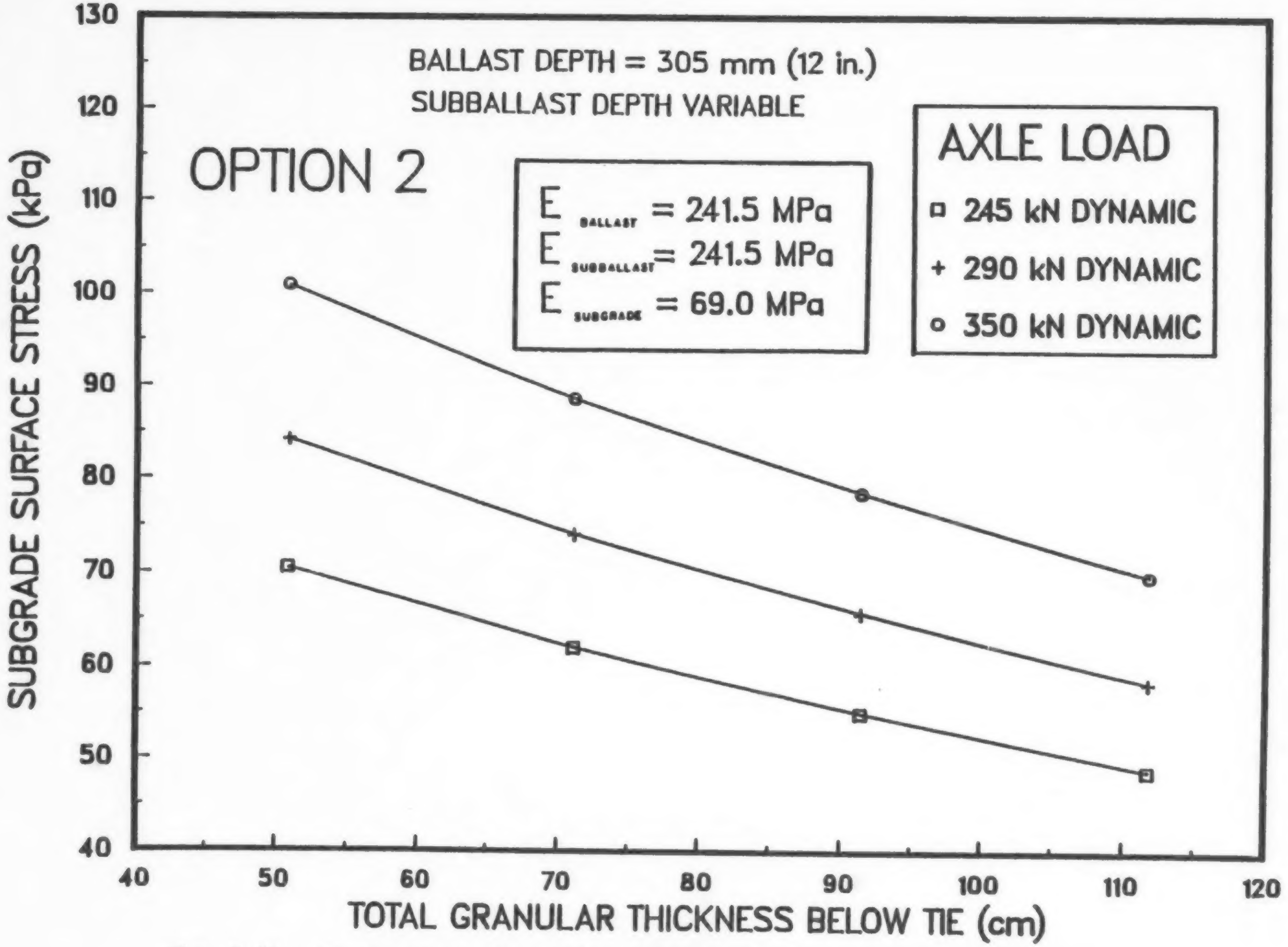

Fig. 5.29 Stress chart for Option 2, Subgrade E = 69.0 MPa, Subballast E = 241.5 MPa

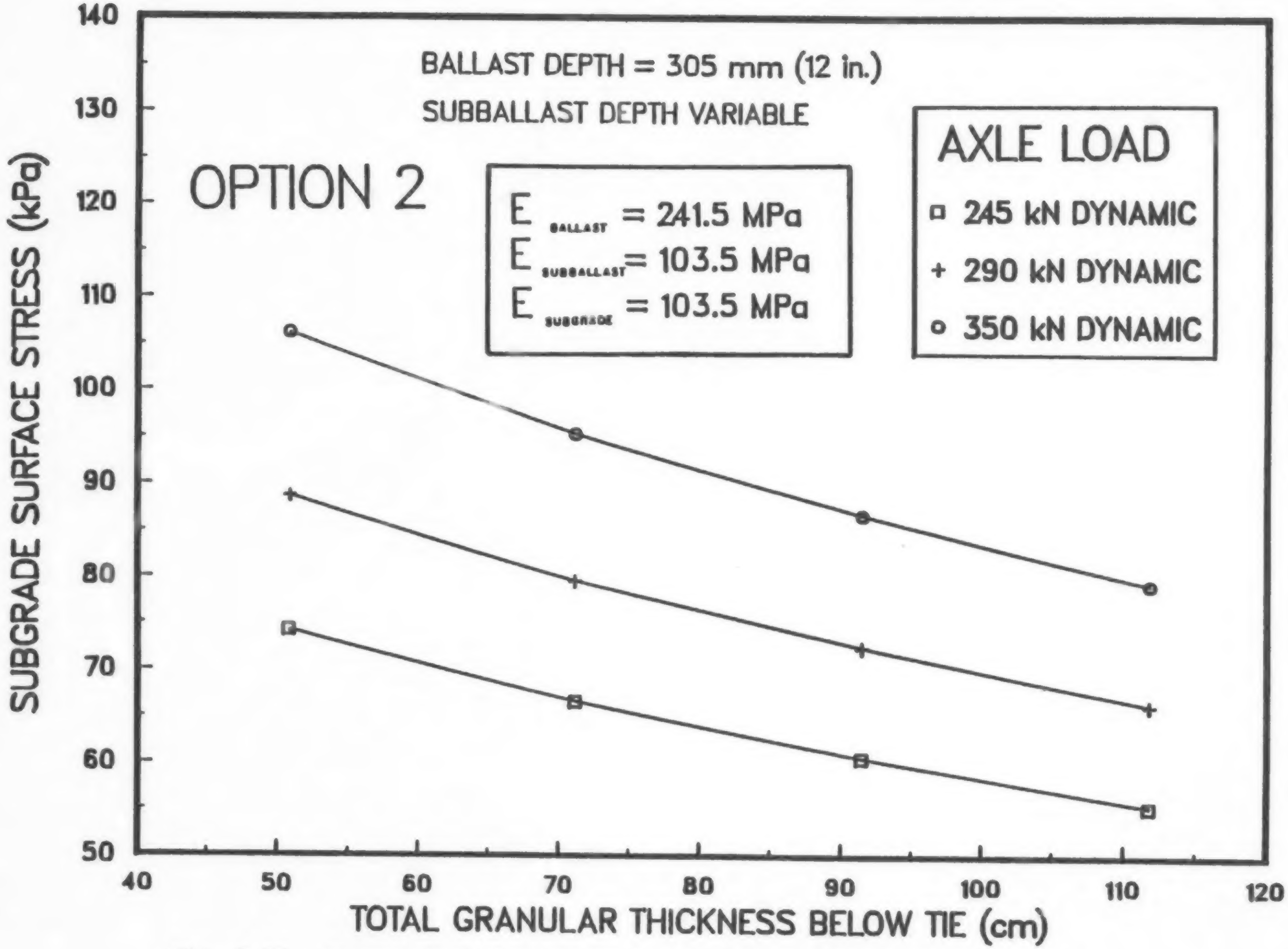

Fig. 5.30 Stress chart for Option 2, Subgrade E = 103.5 MPa, Subballast E = 103.5 MPa

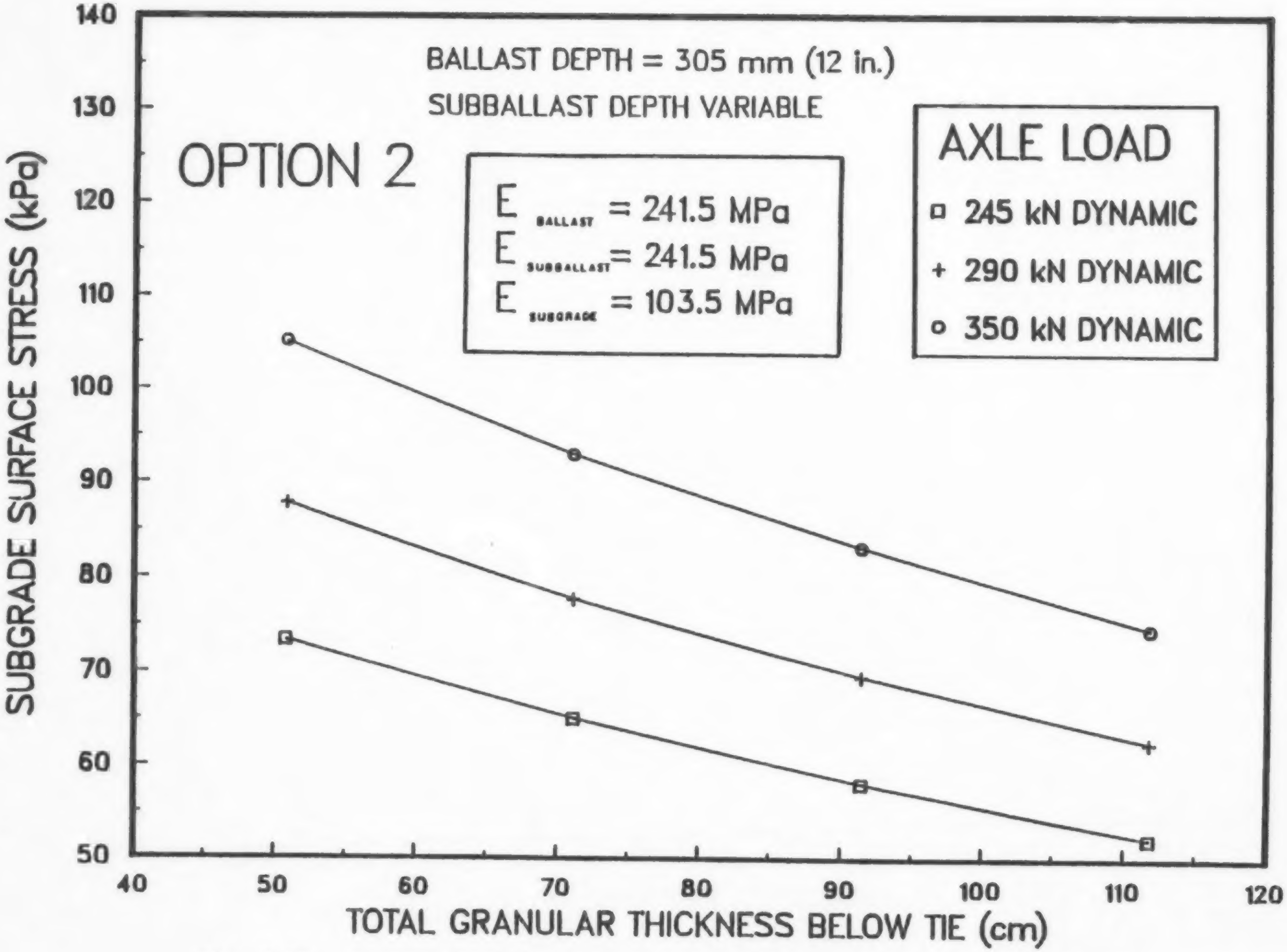

Fig. 5.31 Stress chart for Option 2, Subgrade E = 103.5 MPa, Subballast E = 241.5 MPa

APPENDIX B

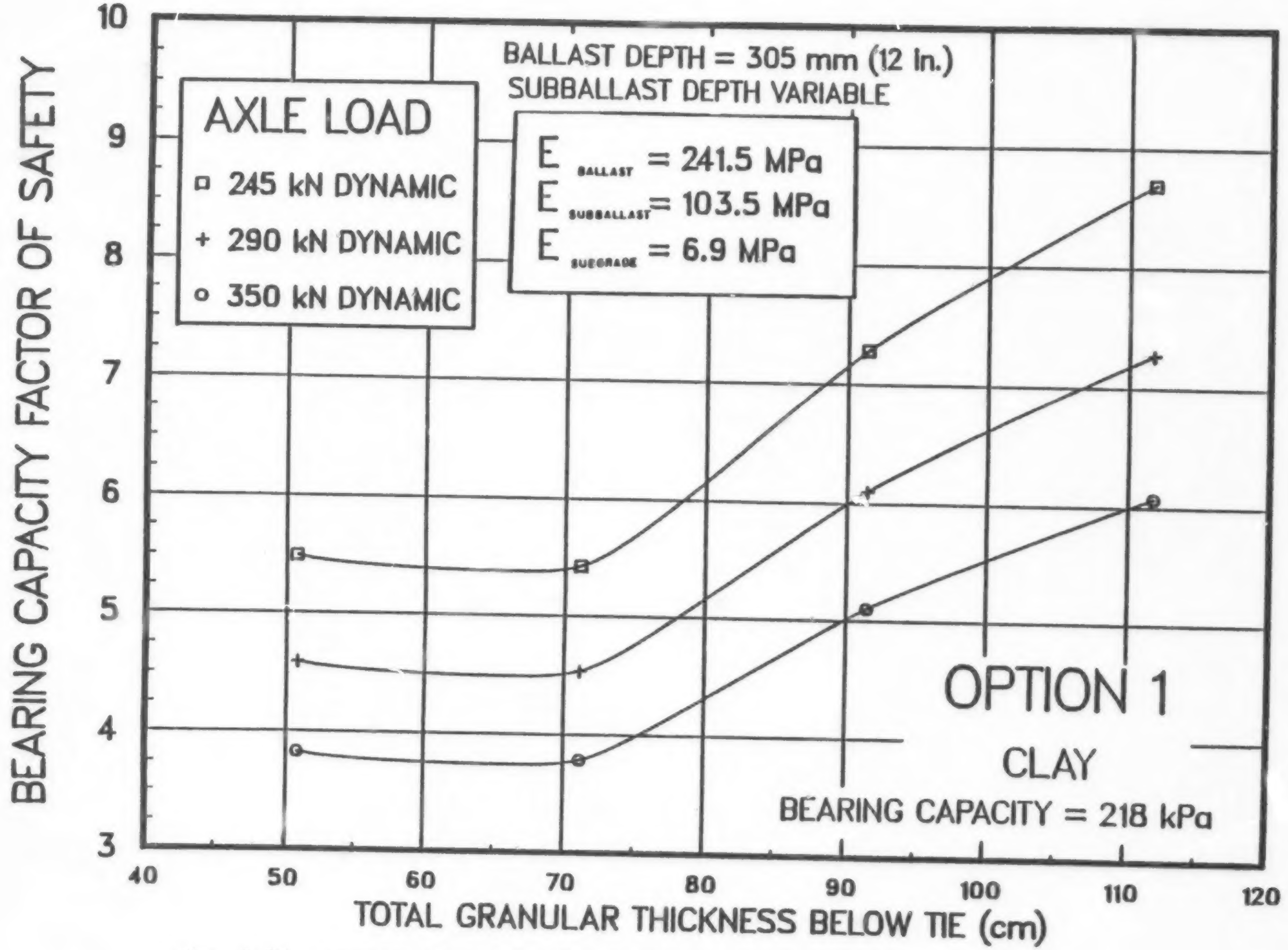

Fig. 5.52 Factor of safety for Option 1, Clay Subgrade E = 6.9 MPa, Subballast E = 103.5 MPa

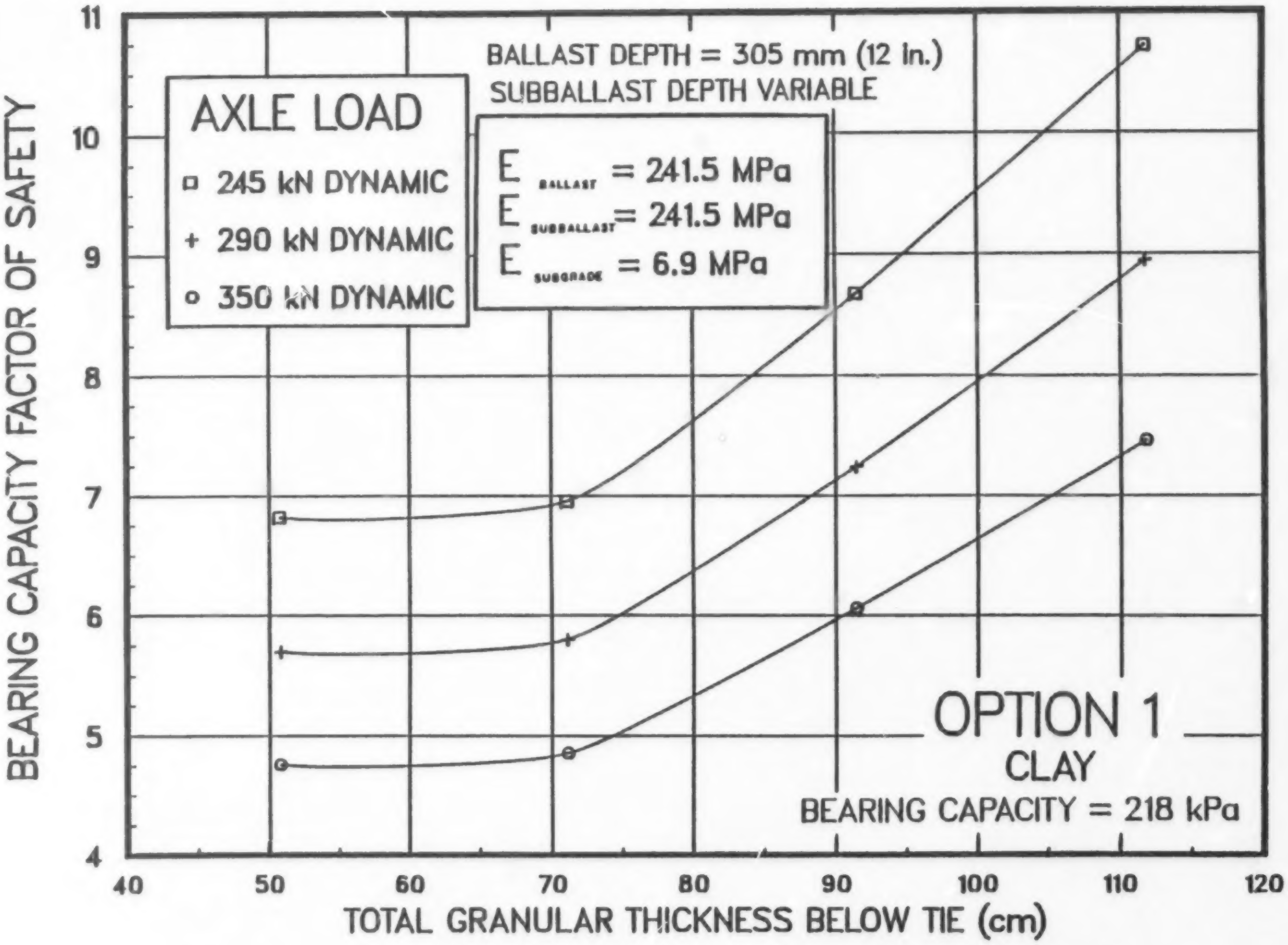

Fig. 5.53 Factor of safety for Option 1, Clay Subgrade E = 6.9 MPa, Subballast E = 241.5 MPa

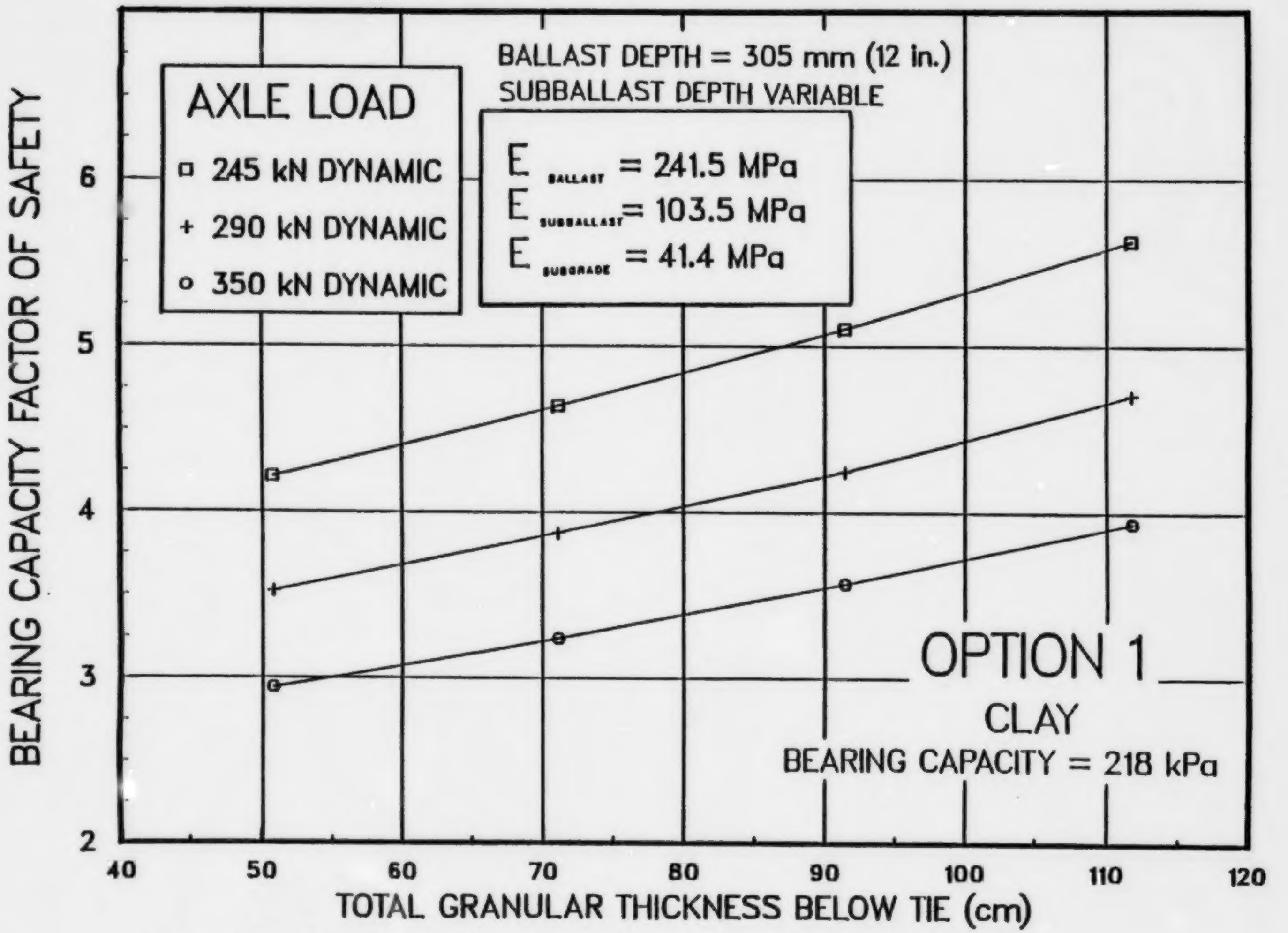

Fig. 5.54 Factor of safety for Option 1, Clay Subgrade E = 41.4 MPa, Subballast E = 103.5 MPa

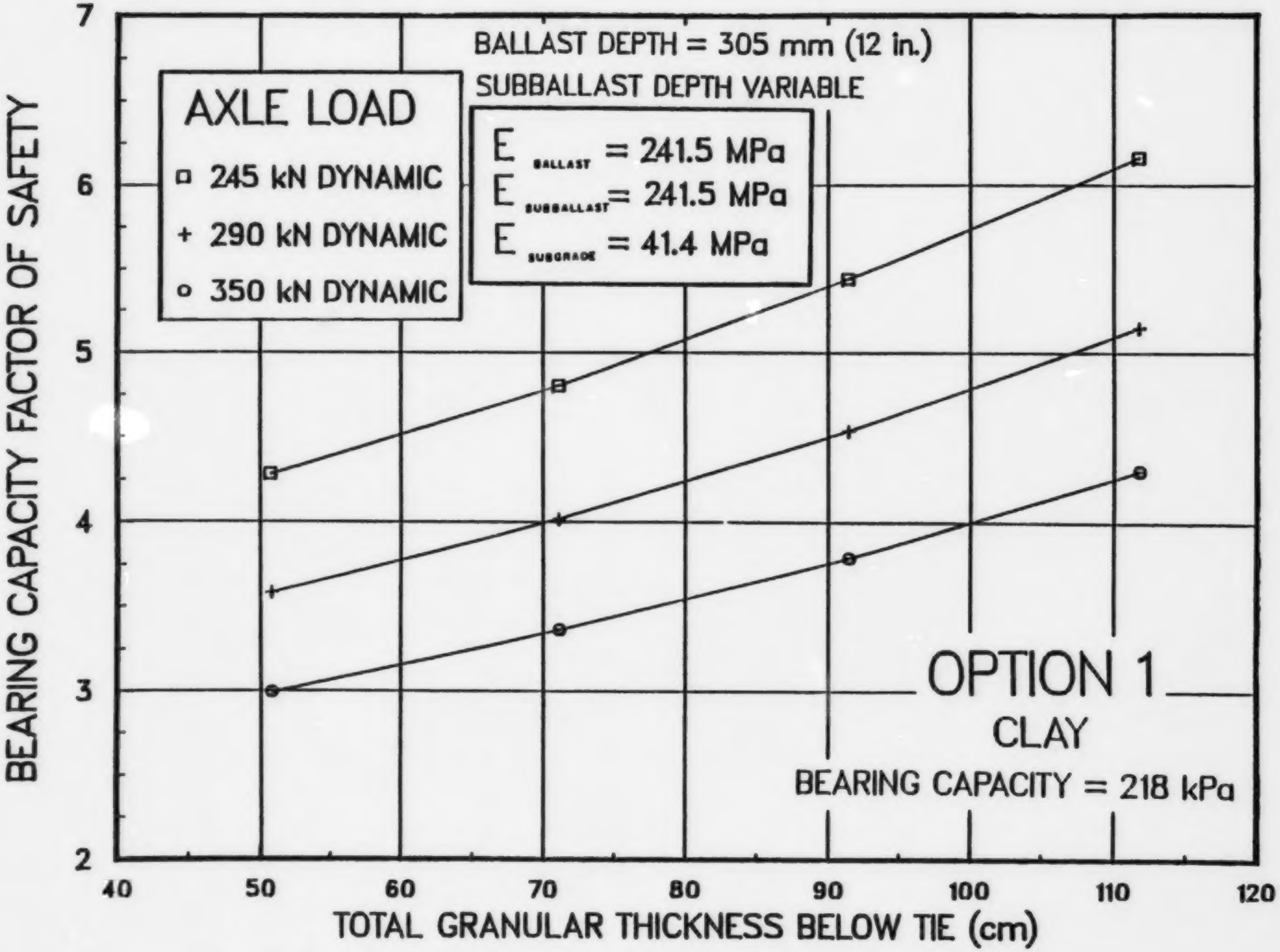

Fig. 5.55 Factor of safety for Option 1, Clay Subgrade E = 41.4 MPa, Subballast E = 241.5 MPa

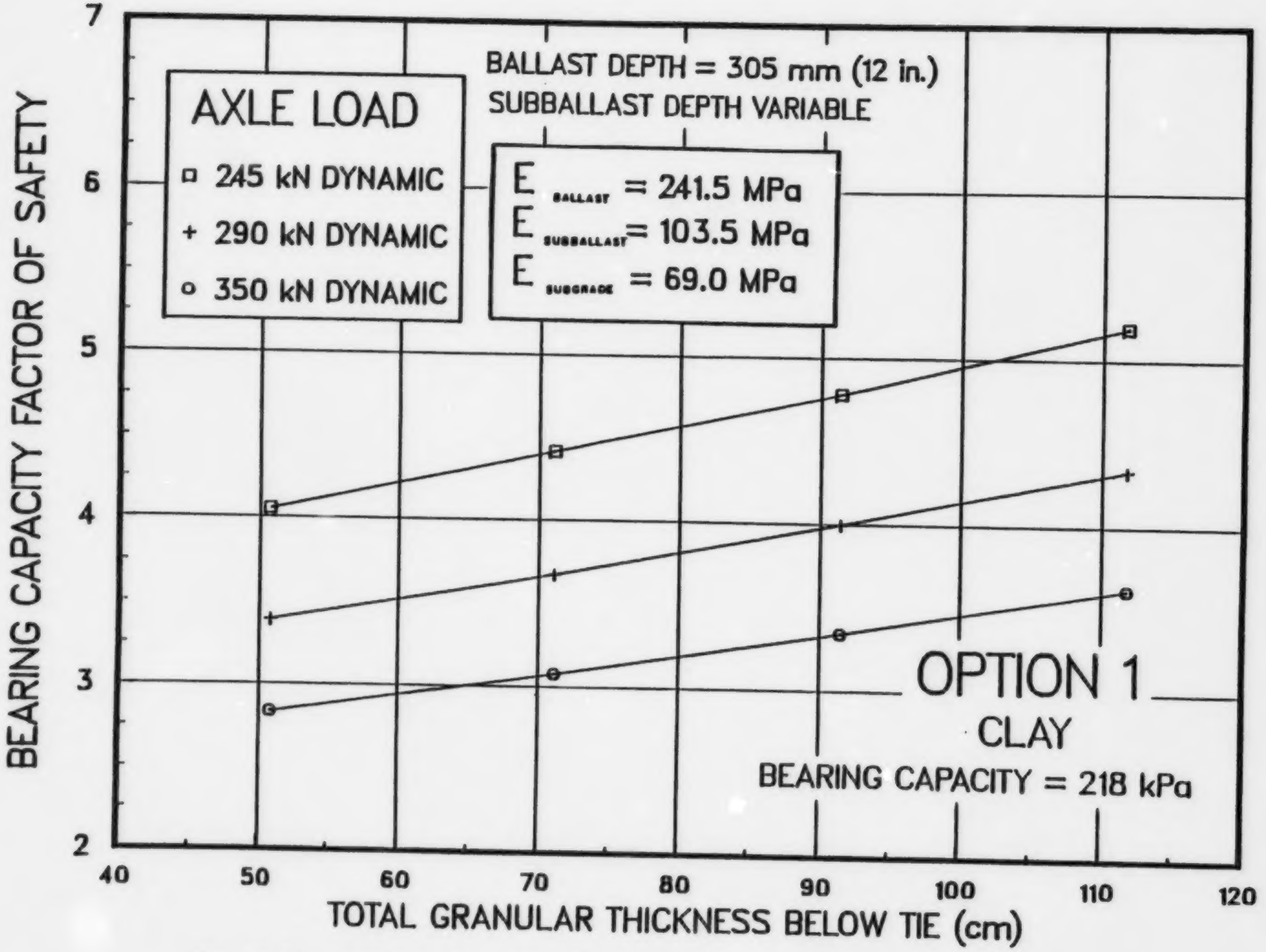

Fig. 5.56 Factor of safety for Option 1, Clay Subgrade E = 69.0 MPa, Subballast E = 103.5 MPa

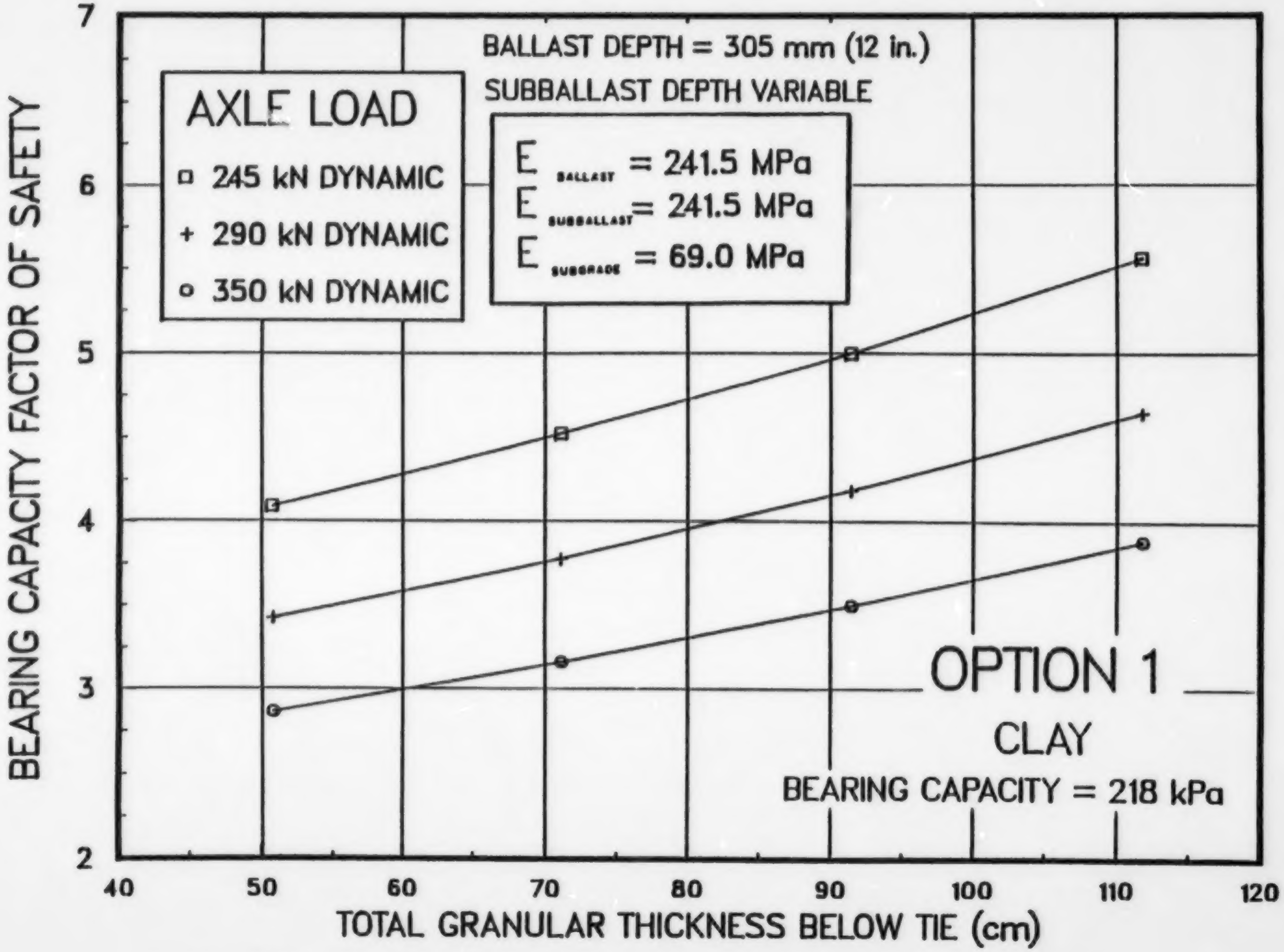

Fig. 5.57 Factor of safety for Option 1, Clay Subgrade E = 69.0 MPa, Subballast E = 241.5 MPa

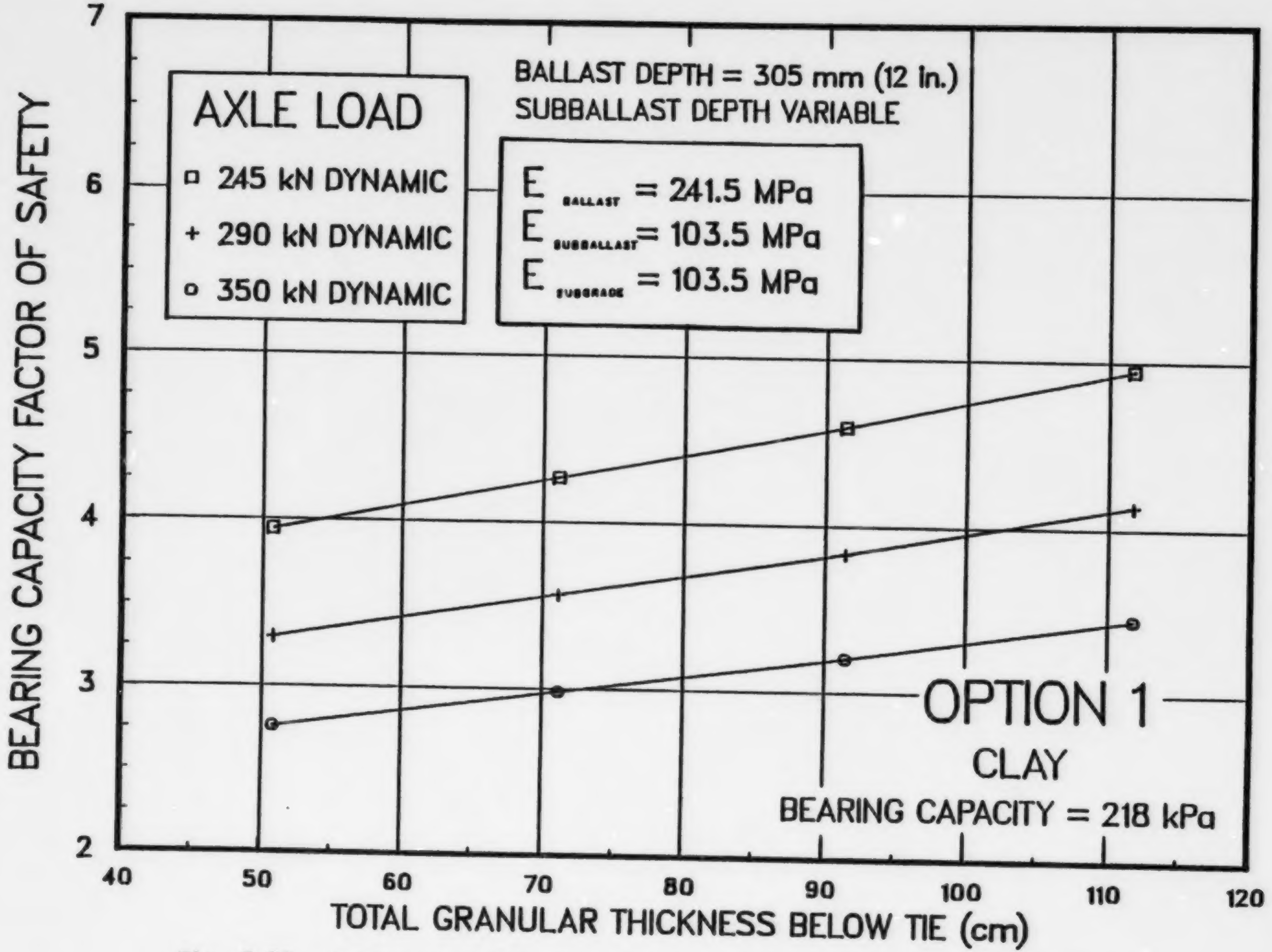

Fig. 5.58 Factor of safety for Option 1, Clay Subgrade E = 103.5 MPa, Subballast E = 103.5 MPa

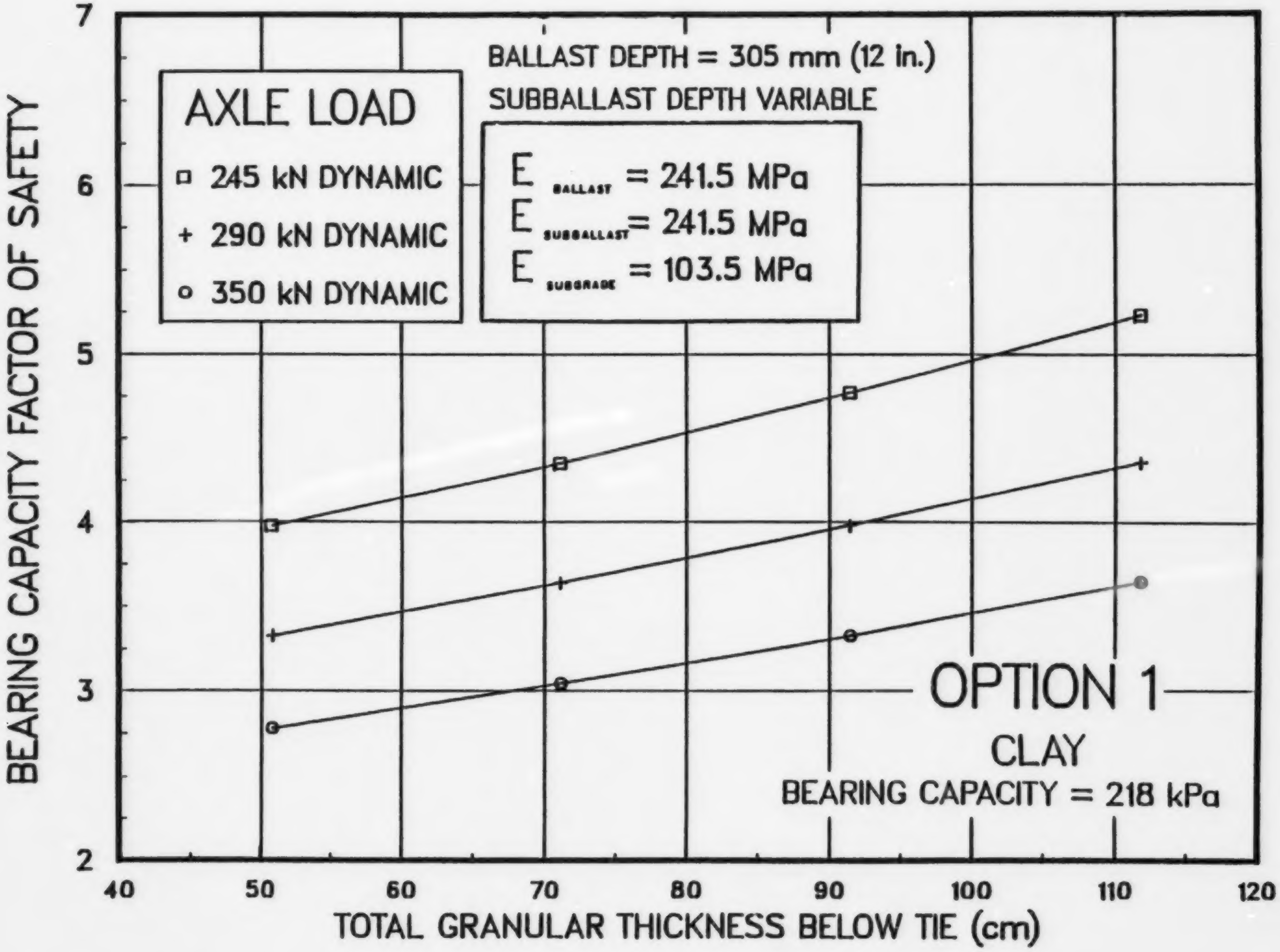

Fig. 5.59 Factor of safety for Option 1, Clay Subgrade E = 103.5 MPa, Subballast E = 241.5 MPa

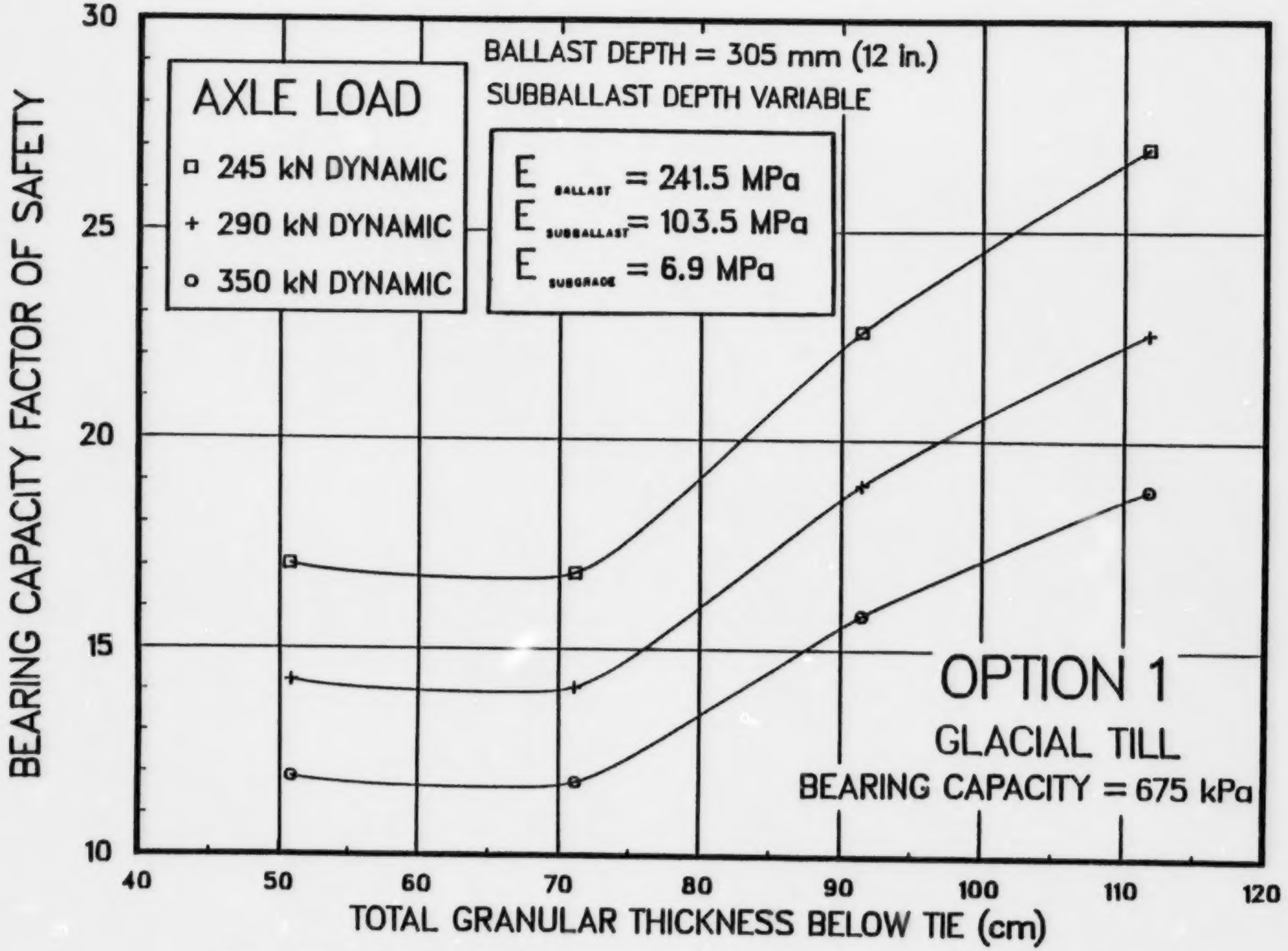

Fig. 5.60 Factor of safety for Option 1, Glacial Till Subgrade E = 6.9 MPa, Subballast E = 103.5 MPa

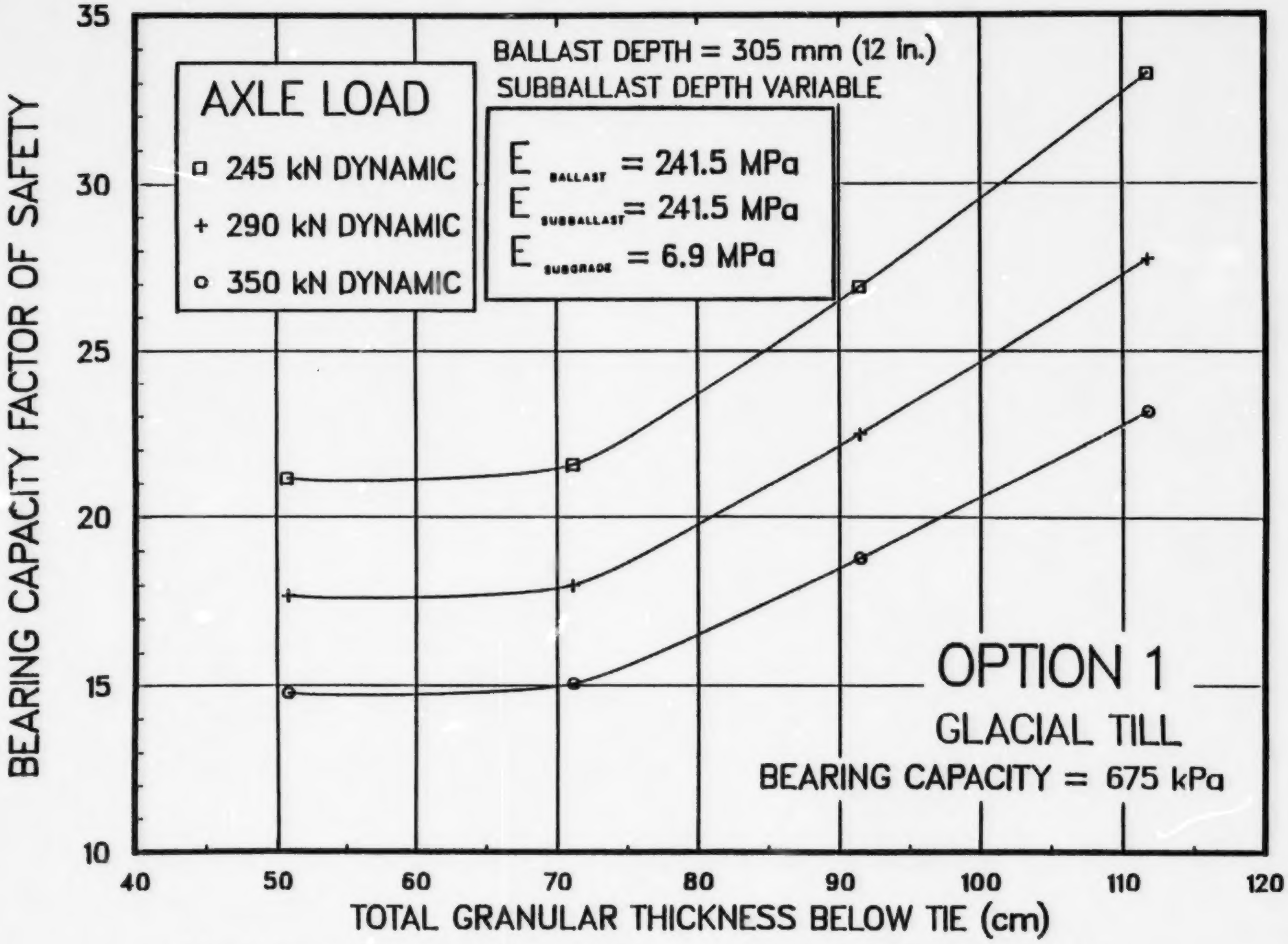

Fig. 5.61 Factor of safety for Option 1, Glacial Till Subgrade E = 6.9 MPa, Subballast E = 241.5 MPa

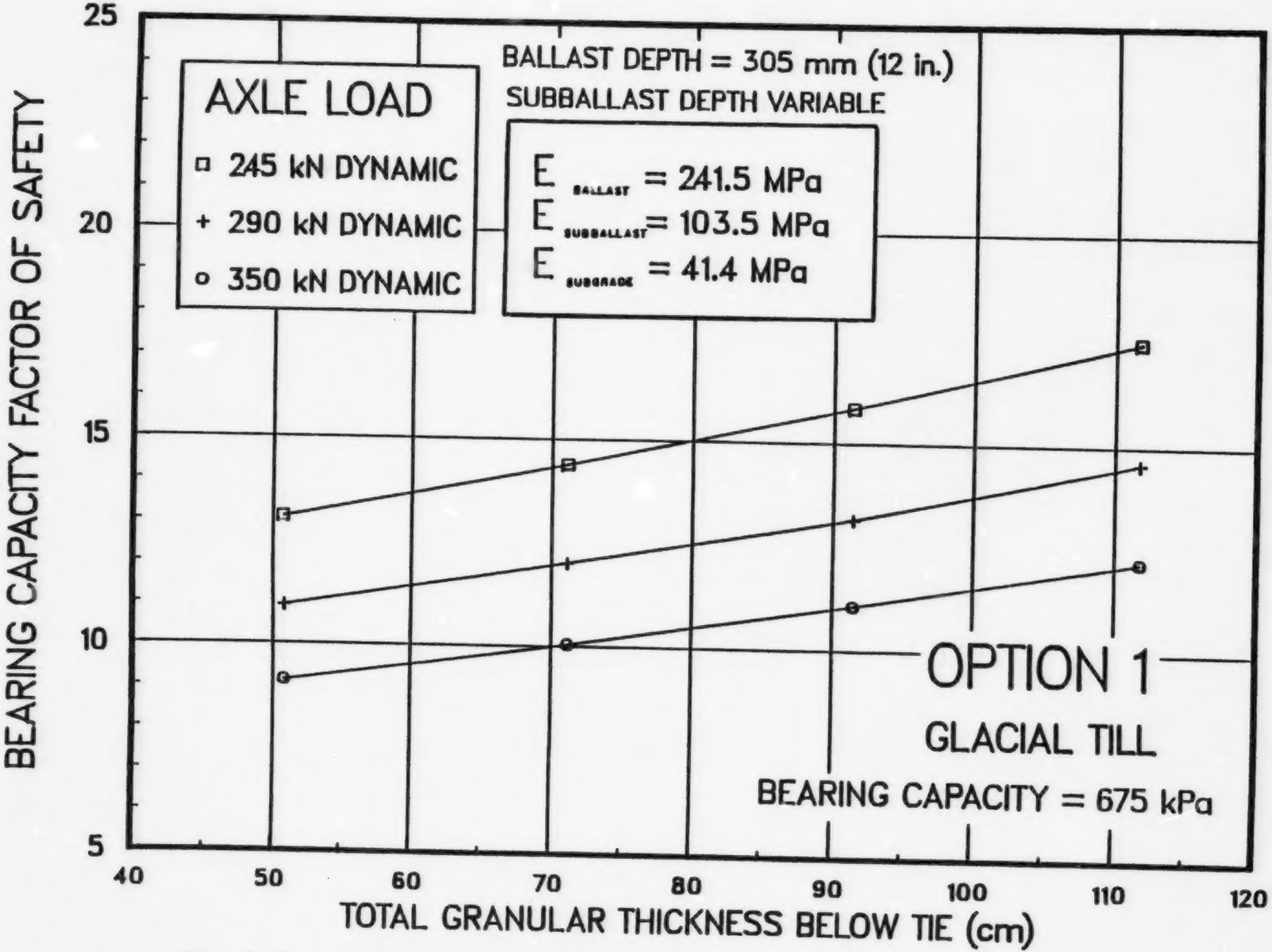

Fig. 5.62 Factor of safety for Option 1, Glacial Till Subgrade E = 41.4 MPa, Subballast E = 103.5 MPa

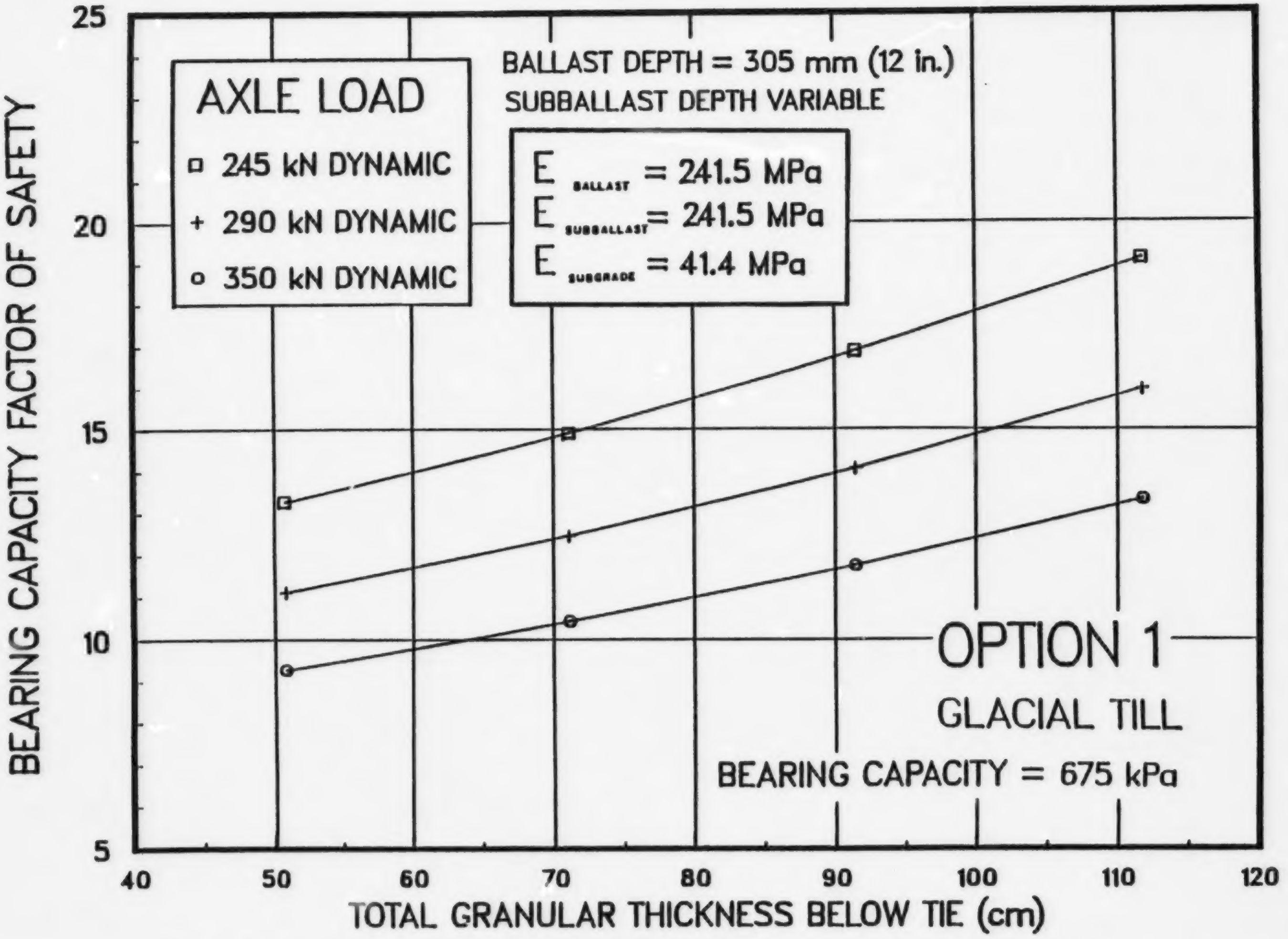

Fig. 5.63 Factor of safety for Option 1, Glacial Till Subgrade E = 41.4 MPa, Subballast E = 241.5 MPa

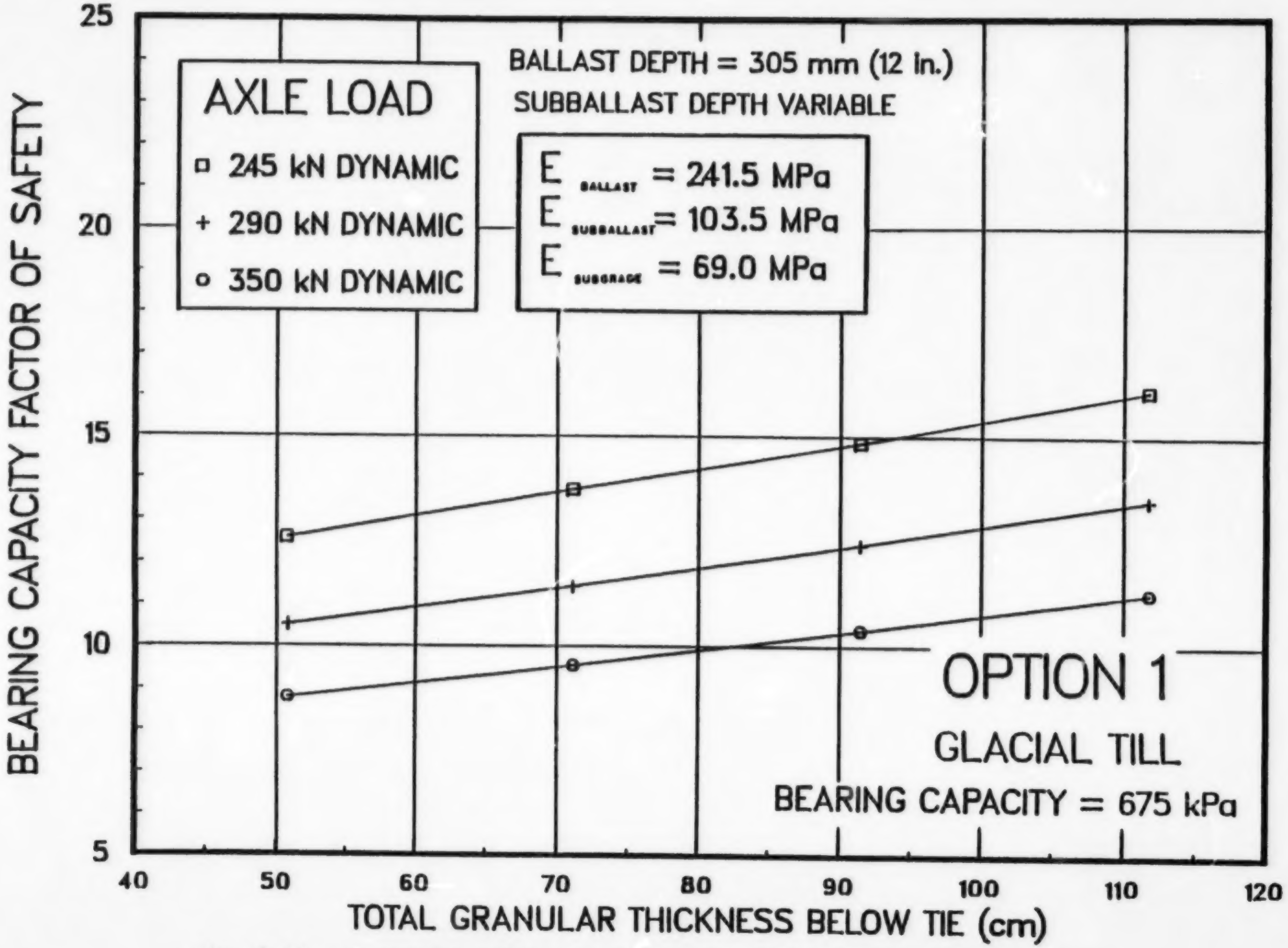

Fig. 5.64 Factor of safety for Option 1, Glacial Till Subgrade E = 69.0 MPa, Subballast E = 103.5 MPa

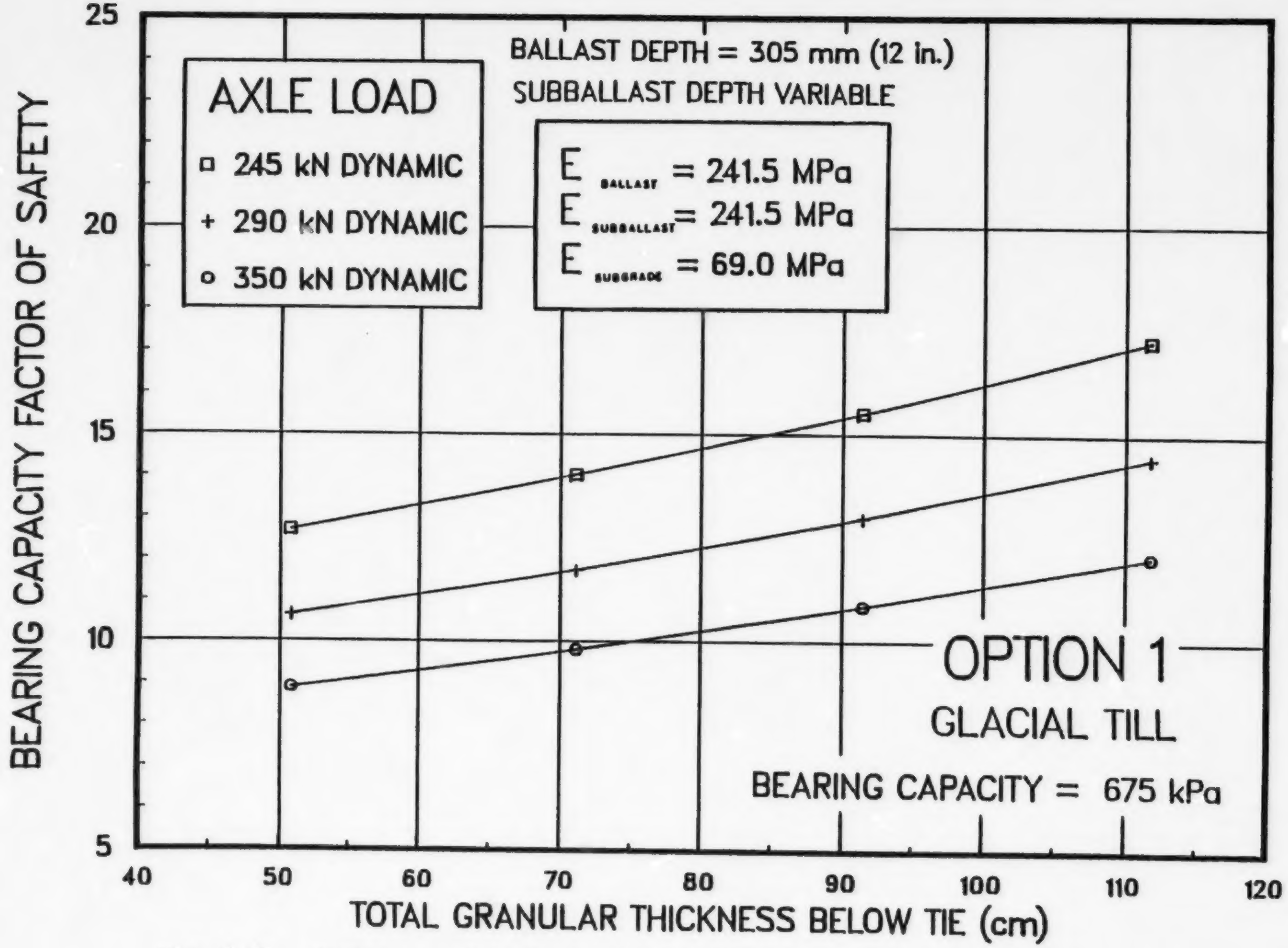

Fig. 5.65 Factor of safety for Option 1, Glacial Till Subgrade E = 69.0 MPa, Subballast E = 241.5 MPa

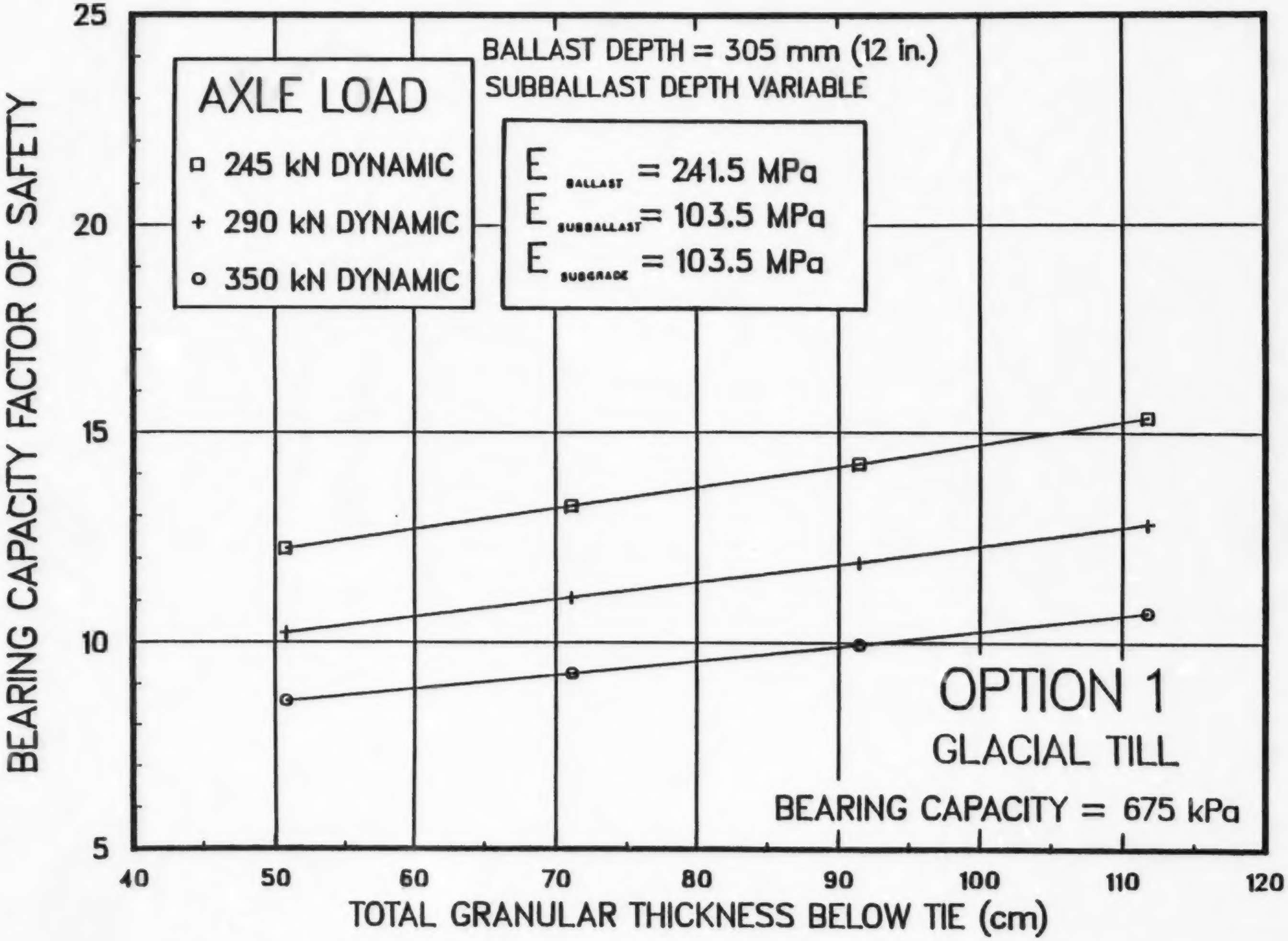

Fig. 5.66 Factor of safety for Option 1, Glacial Till Subgrade E = 103.5 MPa, Subballast E = 103.5 MPa

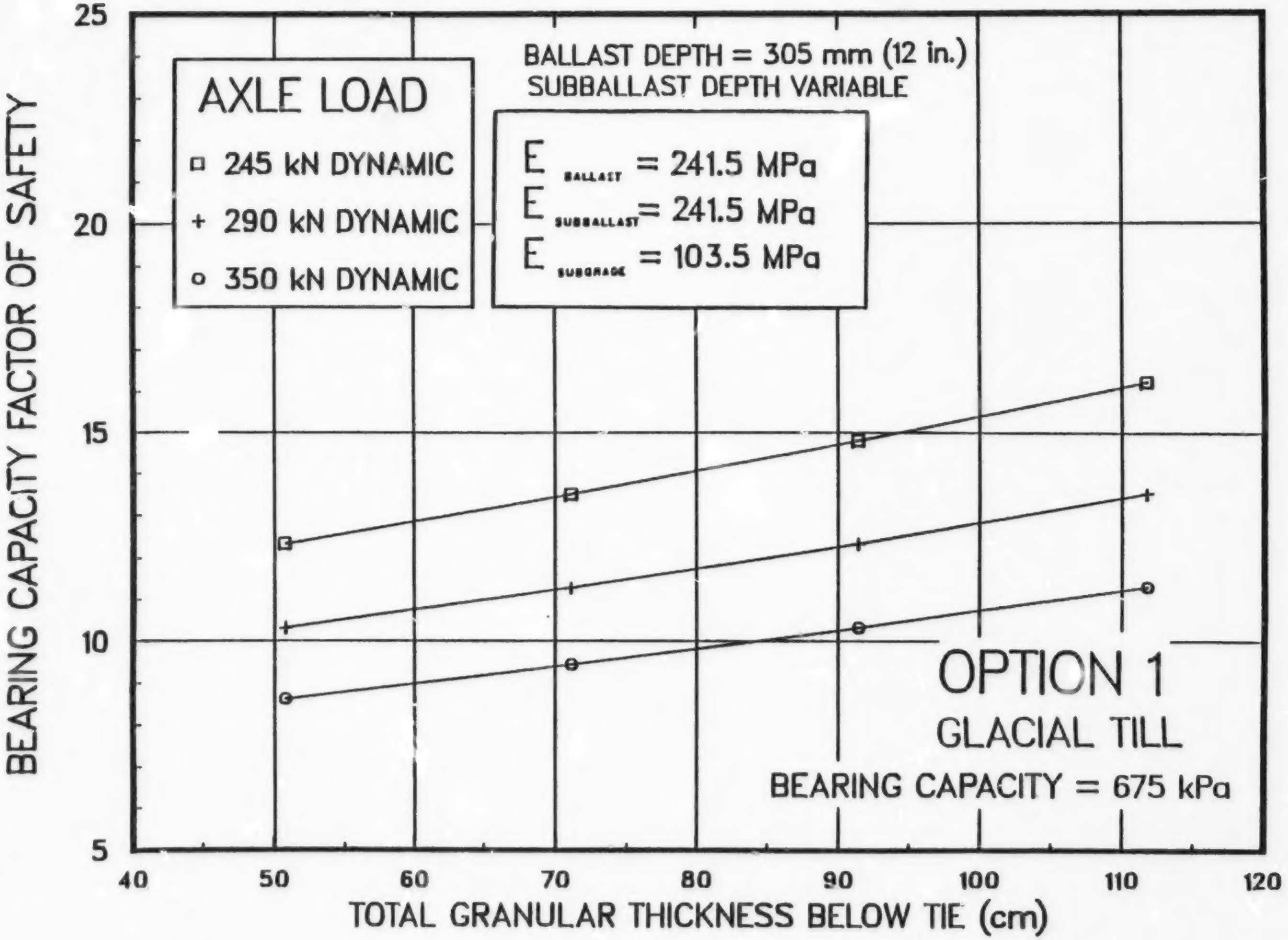

Fig. 5.67 Factor of safety for Option 1, Glacial Till Subgrade E = 103.5 MPa, Subballast E = 241.5 MPa

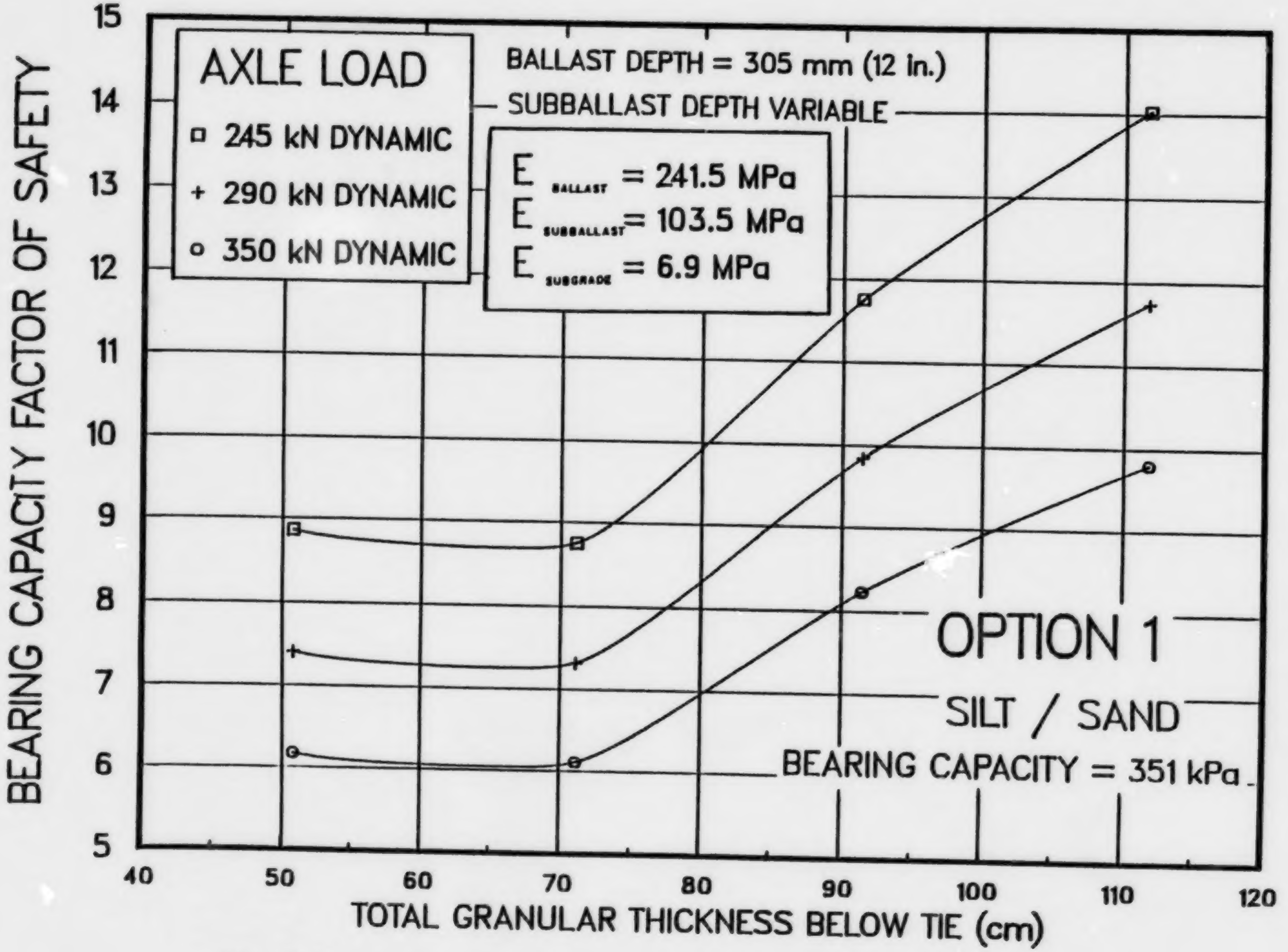

Fig. 5.68 Factor of safety for Option 1, Silt/Sand Subgrade E - 6.9 MPa, Subballast E - 103.5 MPa

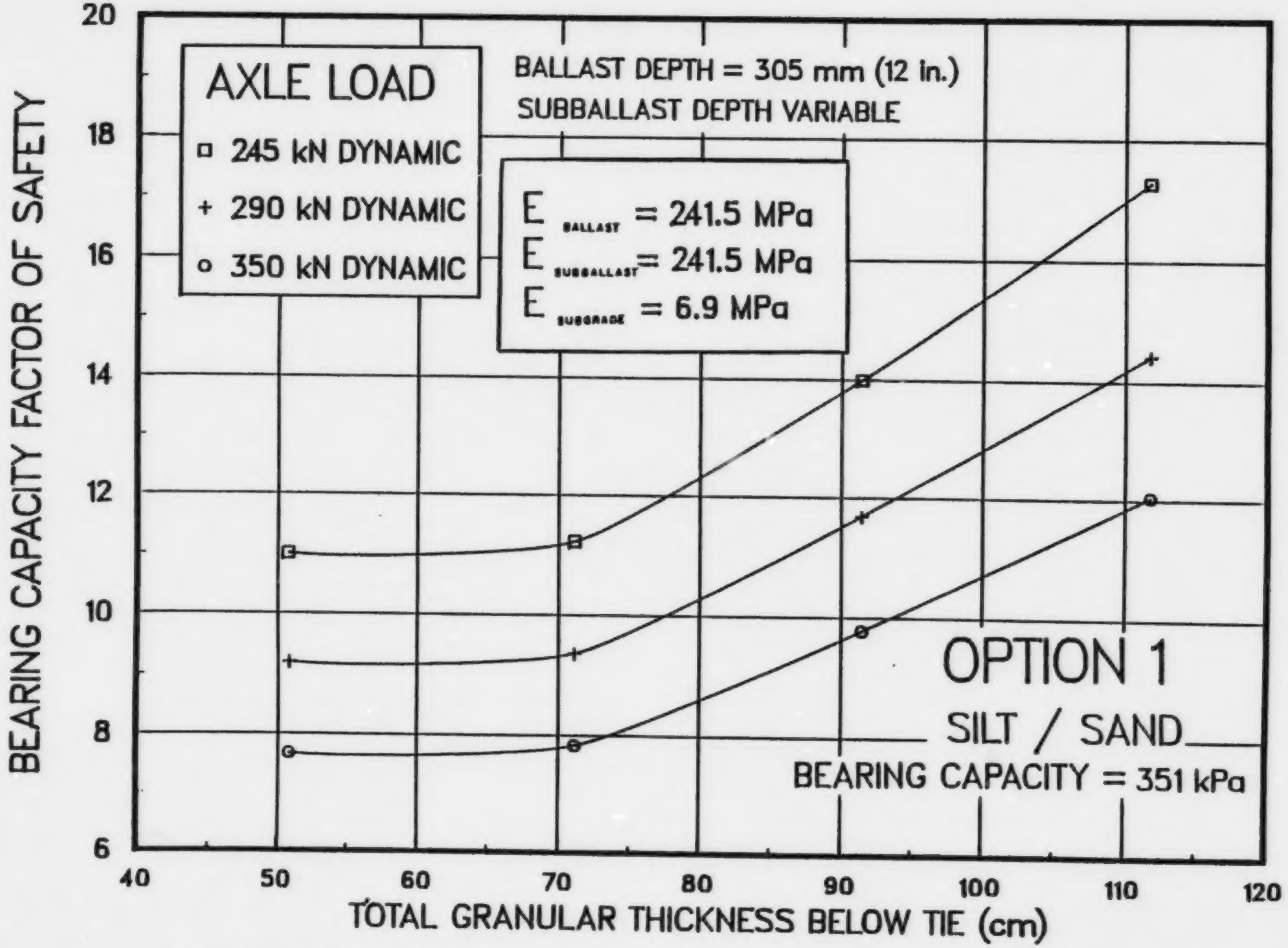

Fig. 5.69 Factor of safety for Option 1, Silt/Sand Subgrade E = 6.9 MPa, Subballast E = 241.5 MPa Fig.

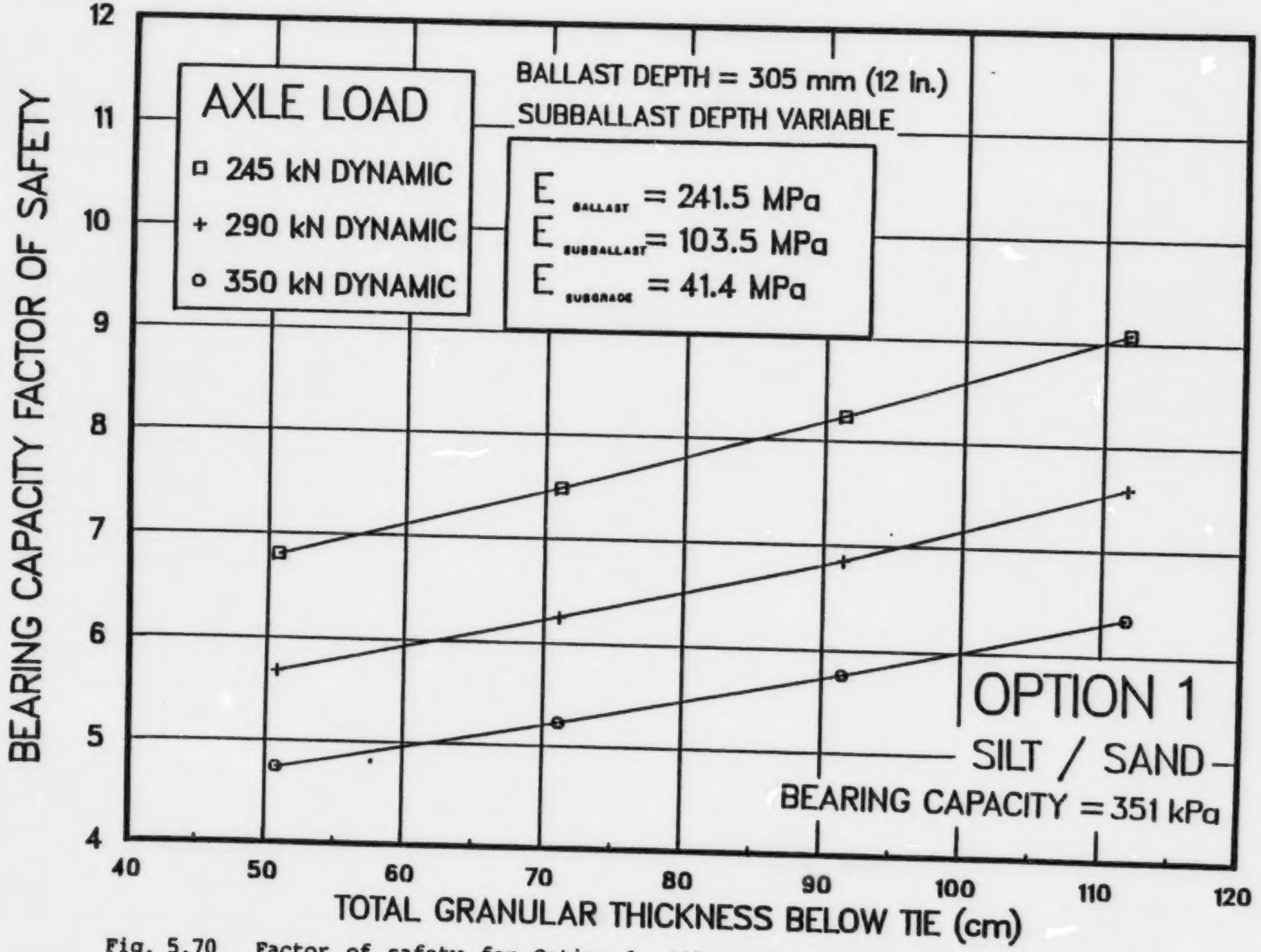

Fig. 5.70 Factor of safety for Option 1, Silt/Sand Subgrade E = 41.4 MPa, Subballast E = 103.5 MPa

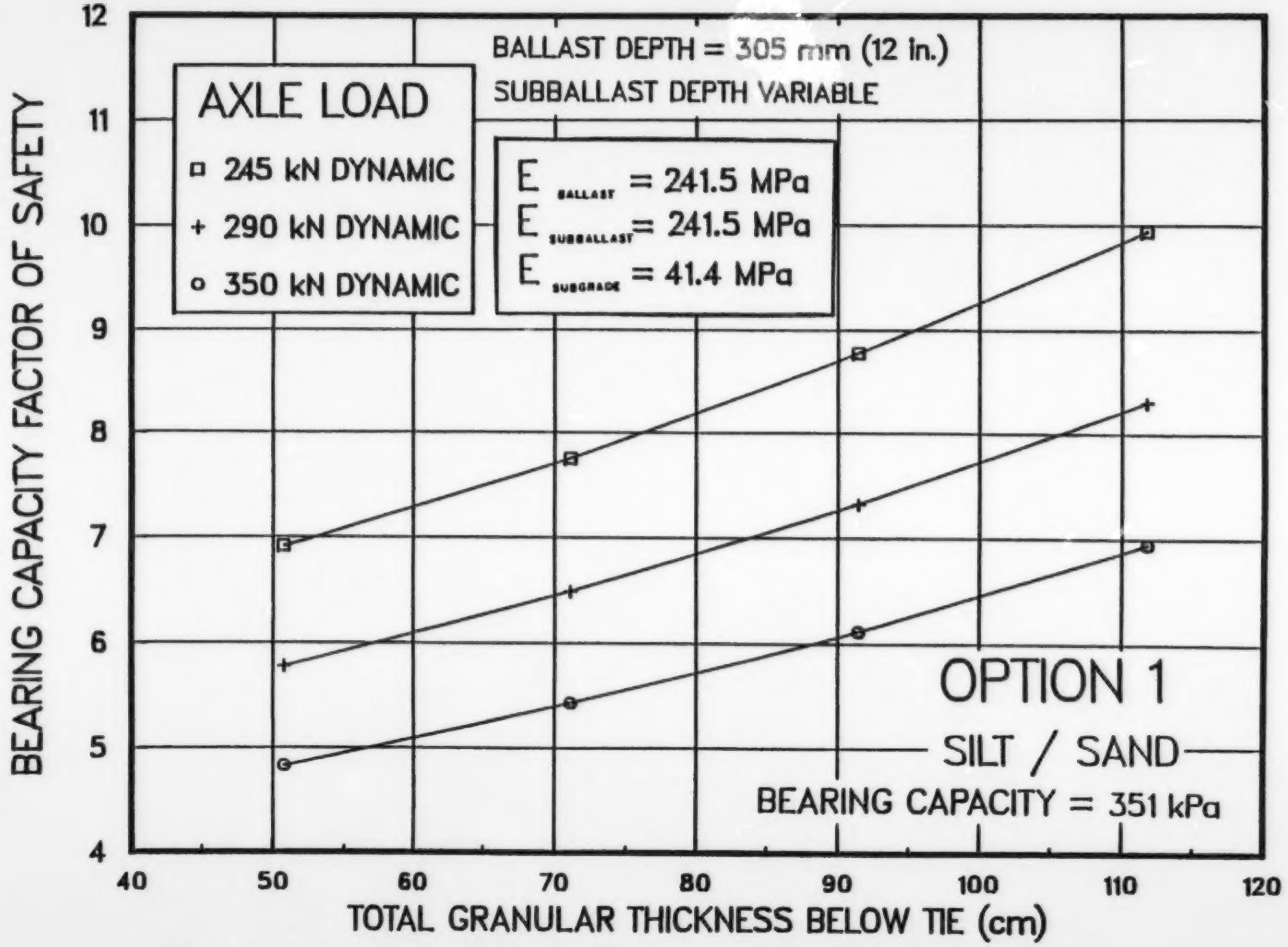

Fig. 5.71 Factor of safety for Option 1, Silt/Sand Subgrade E = 41.4 MPa, Subballast E = 241.5 MPa

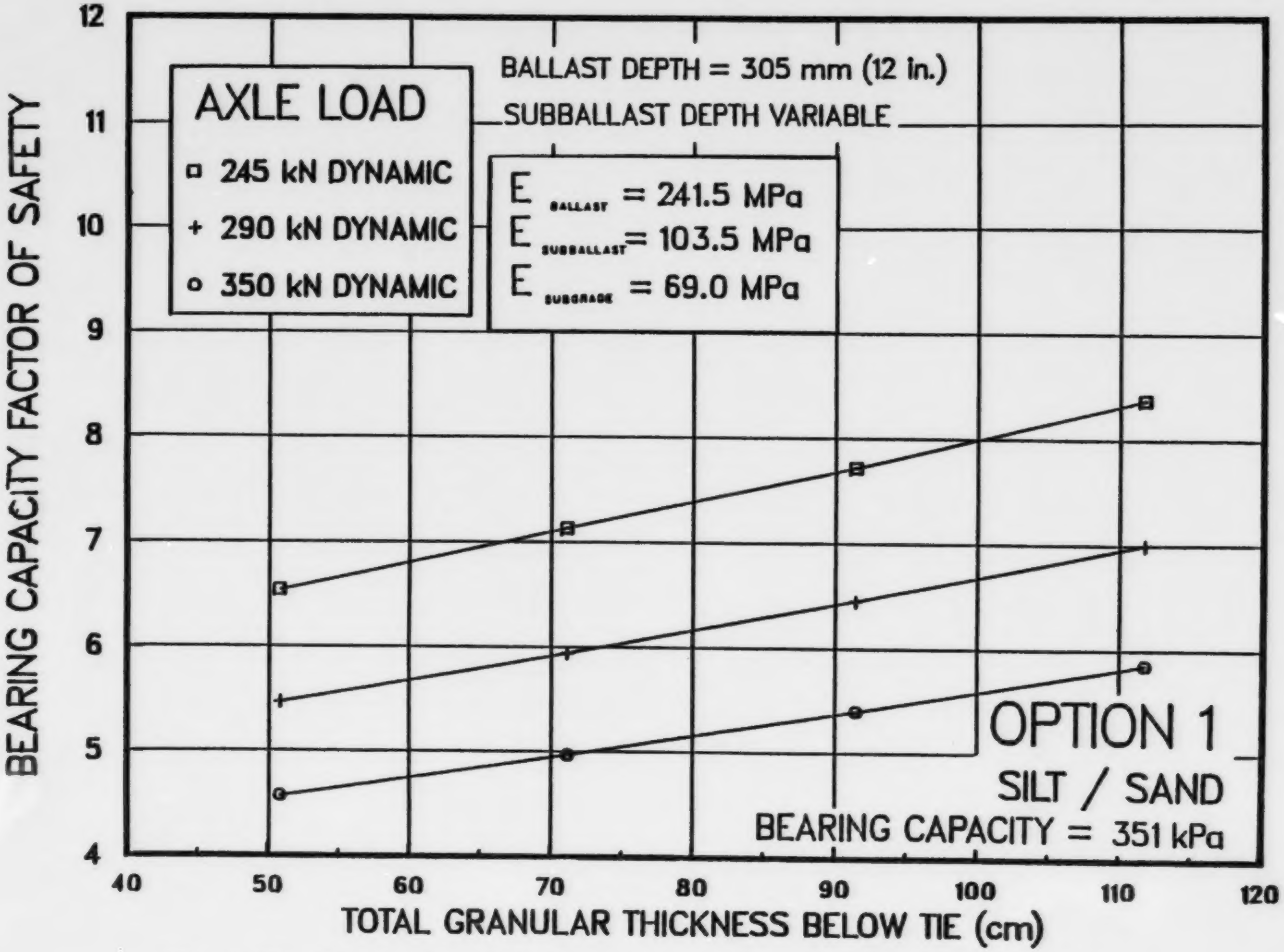

Fig. 5.72 Factor of safety for Option 1, Silt/Sand Subgrade E = 69.0 MPa, Subballast E = 103.5 MPa

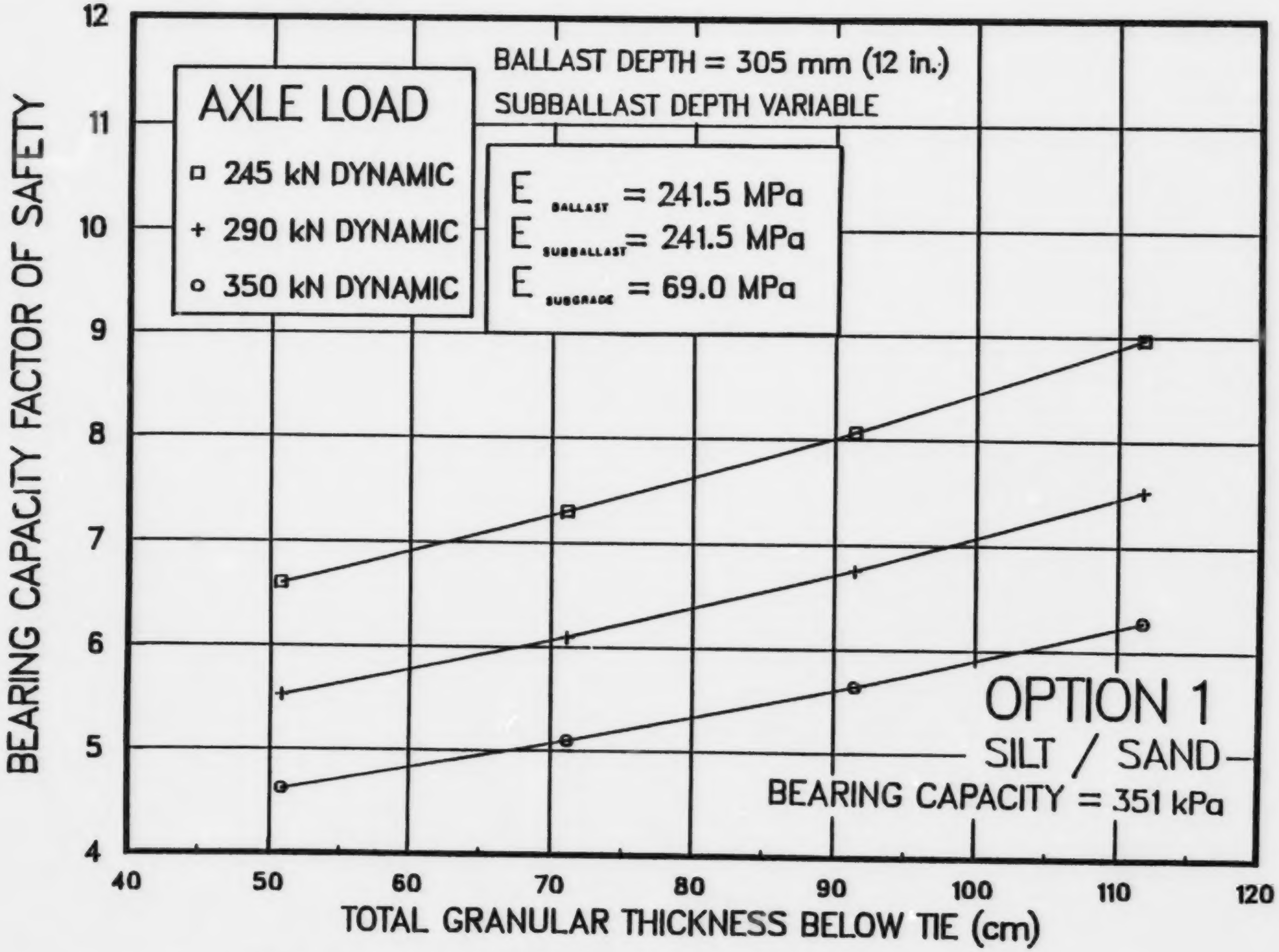

Fig. 5.73 Factor of safety for Option 1, Silt/Sand Subgrade E = 69.0 MPa, Subballast E = 241.5 MPa

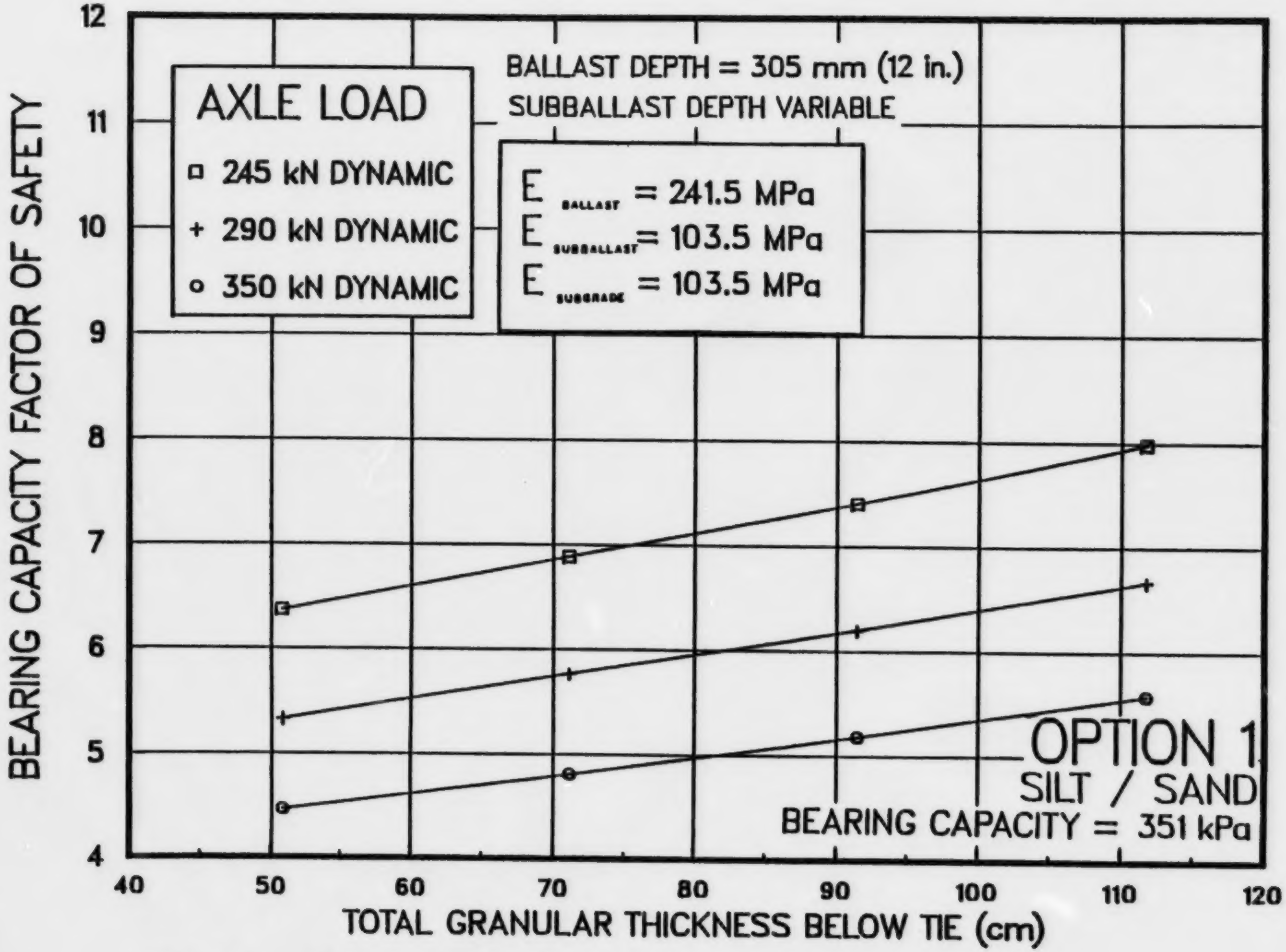

Fig. 5.74 Factor of safety for Option 1, Silt/Sand Subgrade E = 103.5 MPa, Subballast E = 103.5 MPa

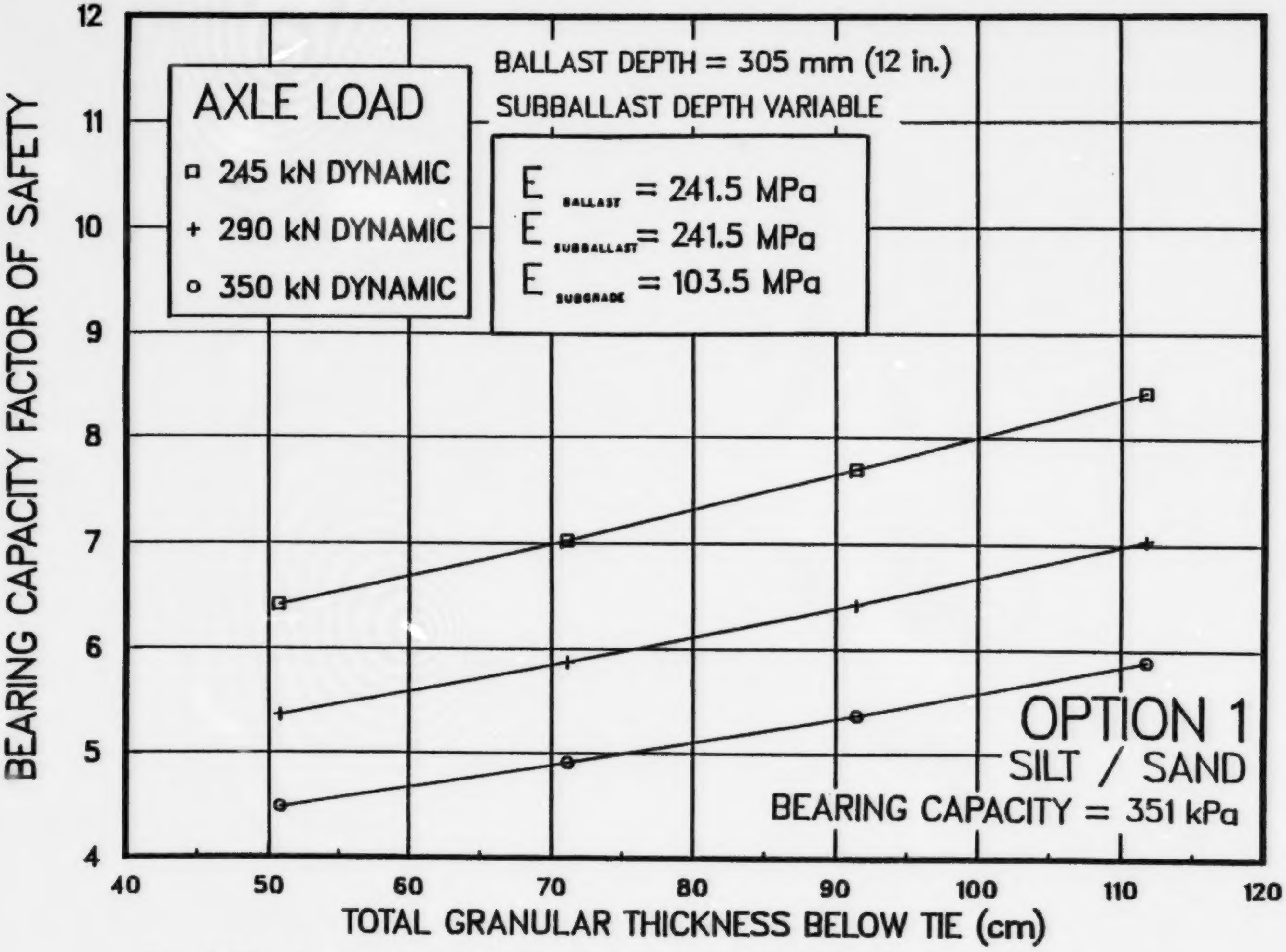

Fig. 5.75 Factor of safety for Option 1, Silt/Sand Subgrade E = 103.5 MPa, Subballast E = 241.5 MPa

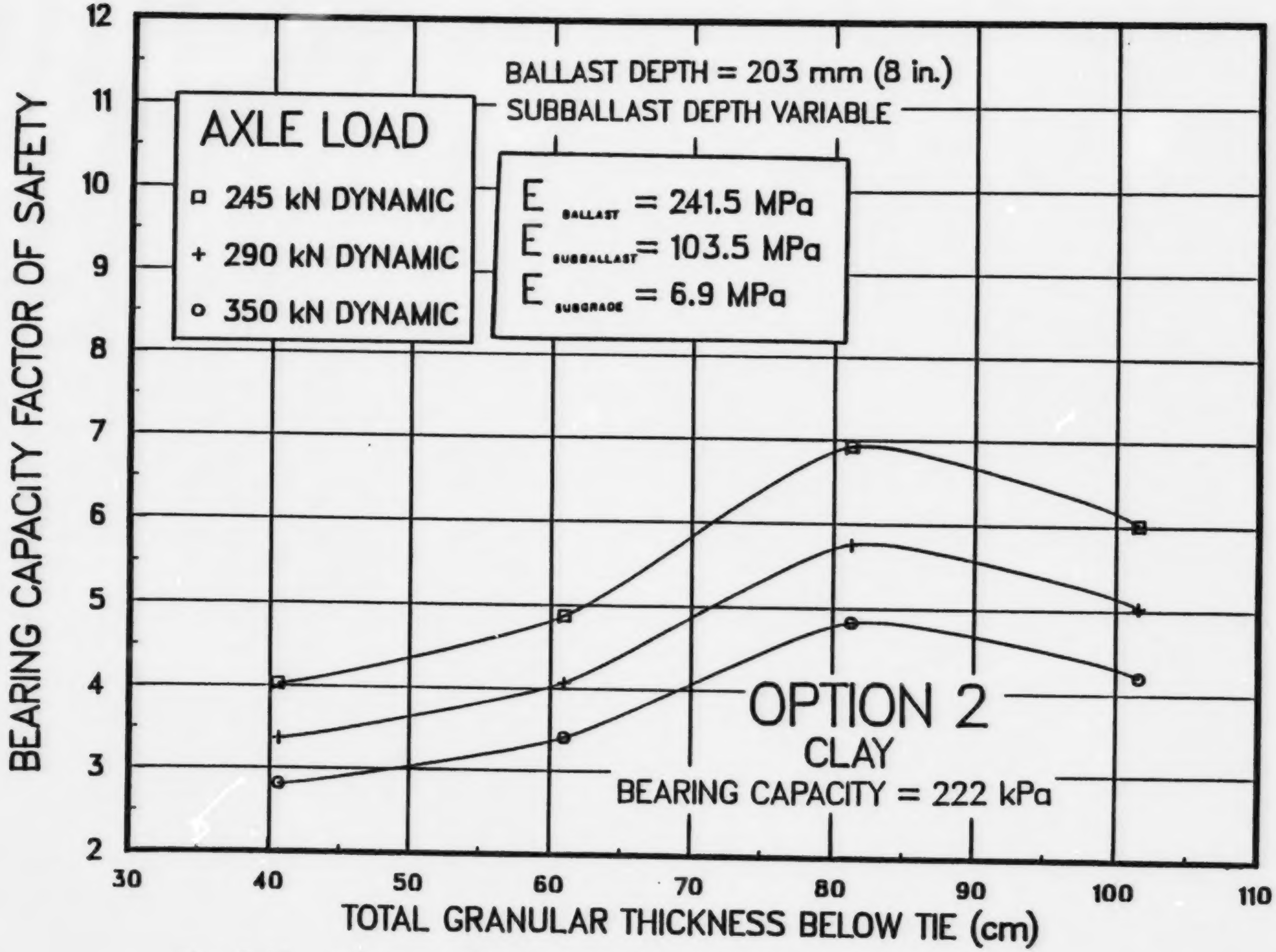

Fig. 5.76 Factor of safety for Option 2, Clay Subgrade E = 6.9 MPa, Subballast E = 103.5 MPa

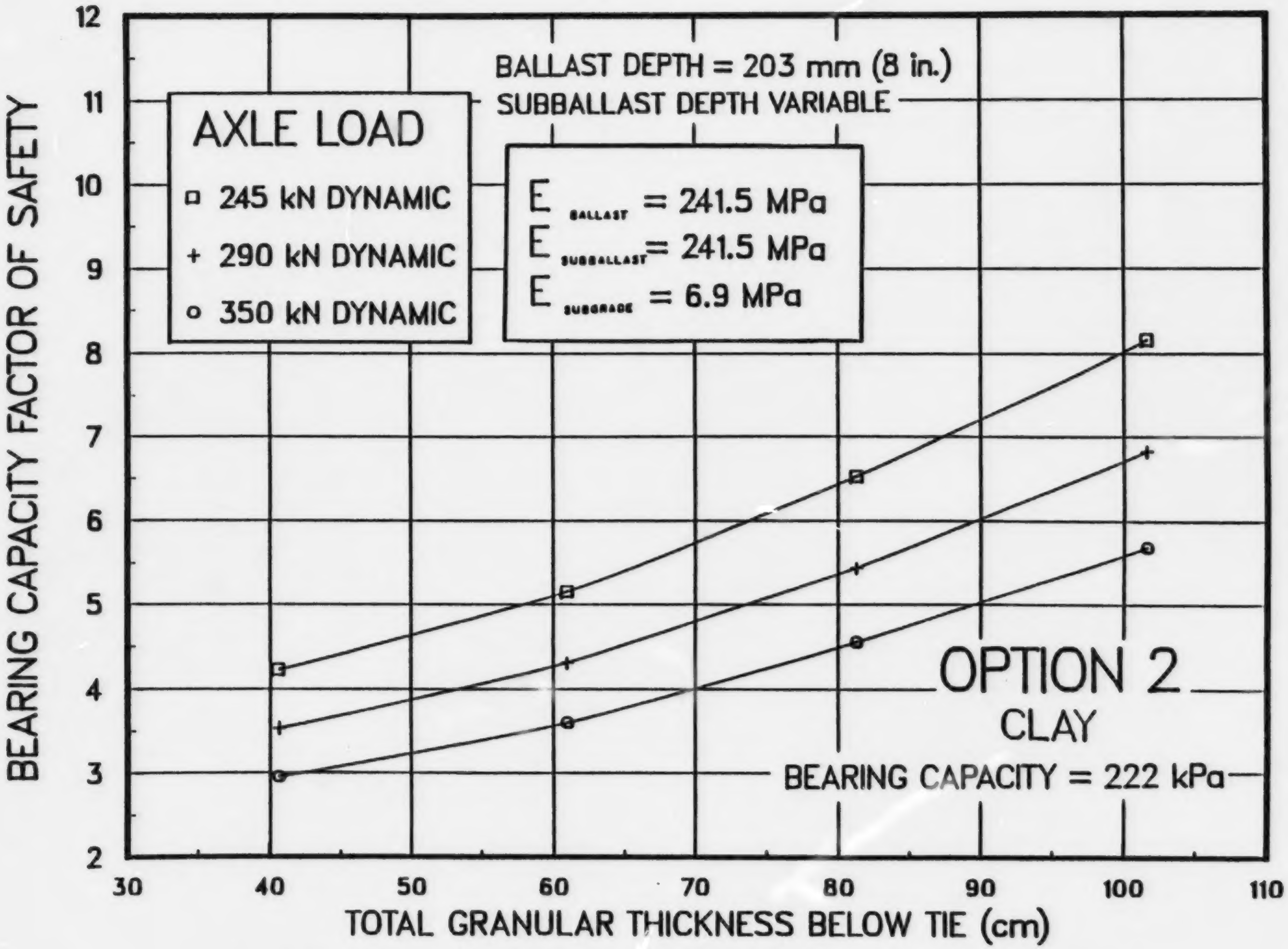

Fig. 5.77 Factor of safety for Option 2, Clay Subgrade E = 6.9 MPa, Subballast E = 241.5 MPa

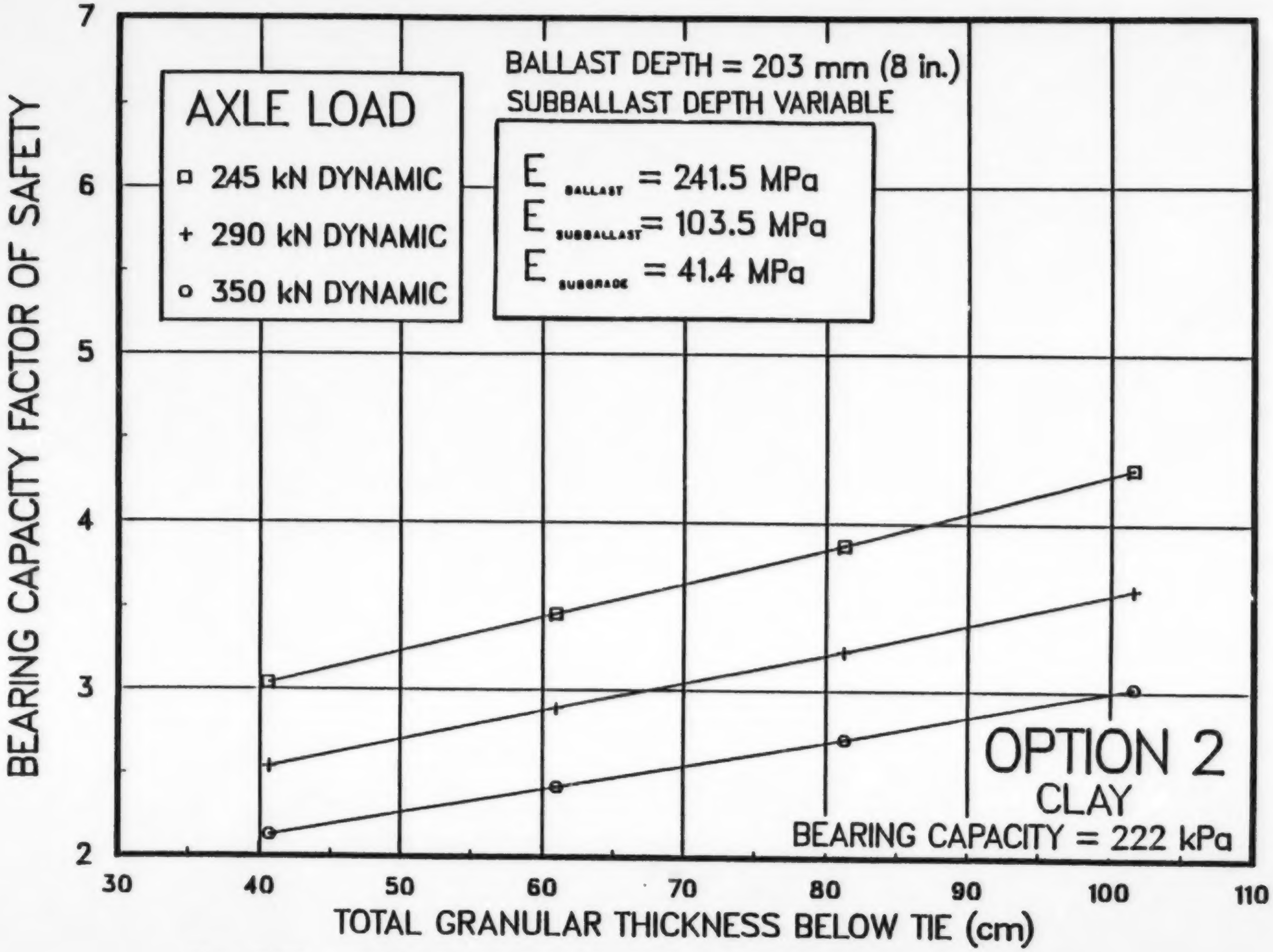

Fig. 5.78 Factor of safety for Option 2, Clay Subgrade E = 41.4 MPa, Subballast E = 103.5 MPa

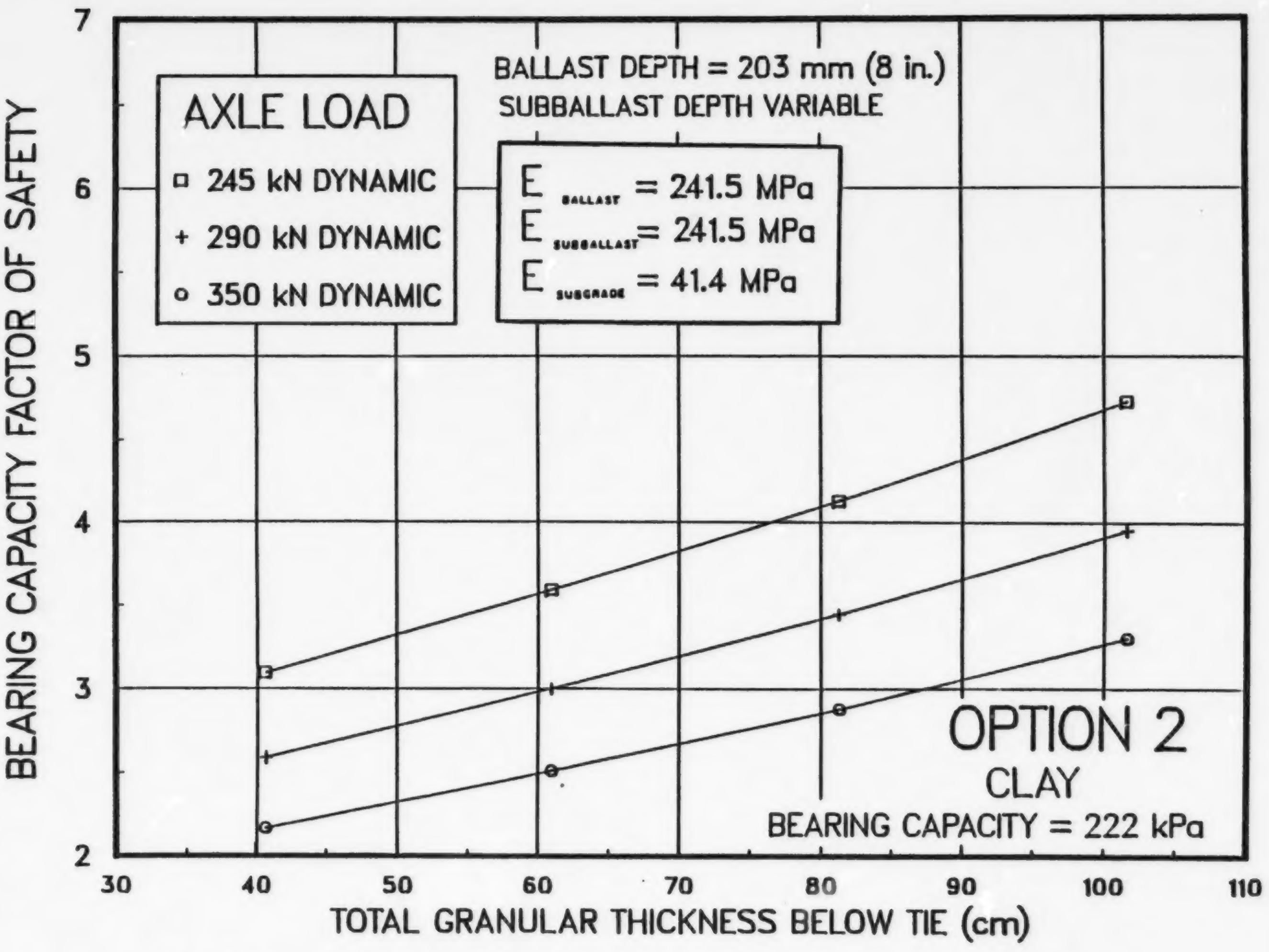

Fig. 5.79 Factor of safety for Option 2, Clay Subgrade E = 41.4 MPa, Subballast E = 241.5 MPa

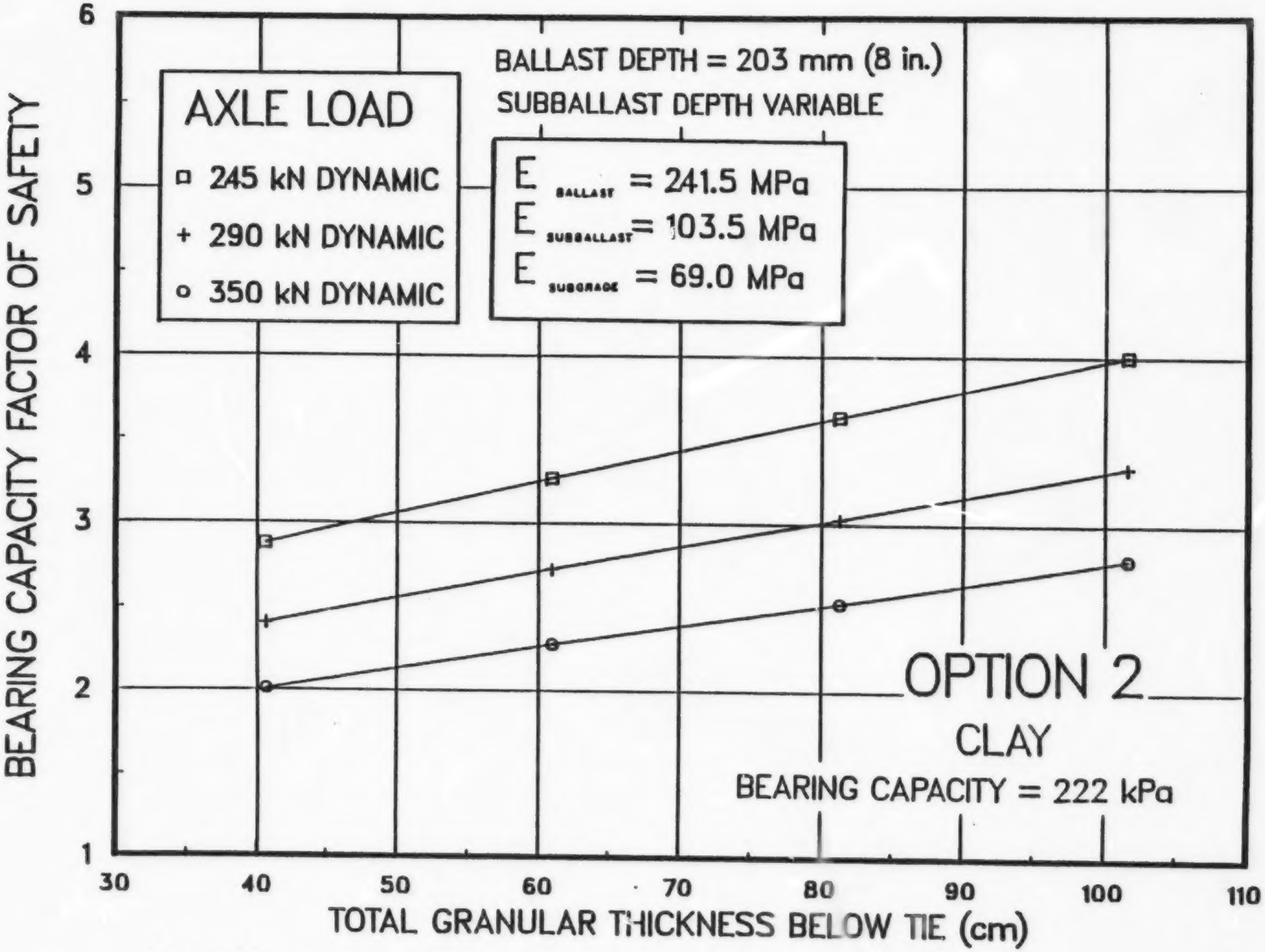

Fig. 5.80 Factor of safety for Option 2, Clay Subgrade E = 69.0 MPa, Subballast E = 103.5 MPa

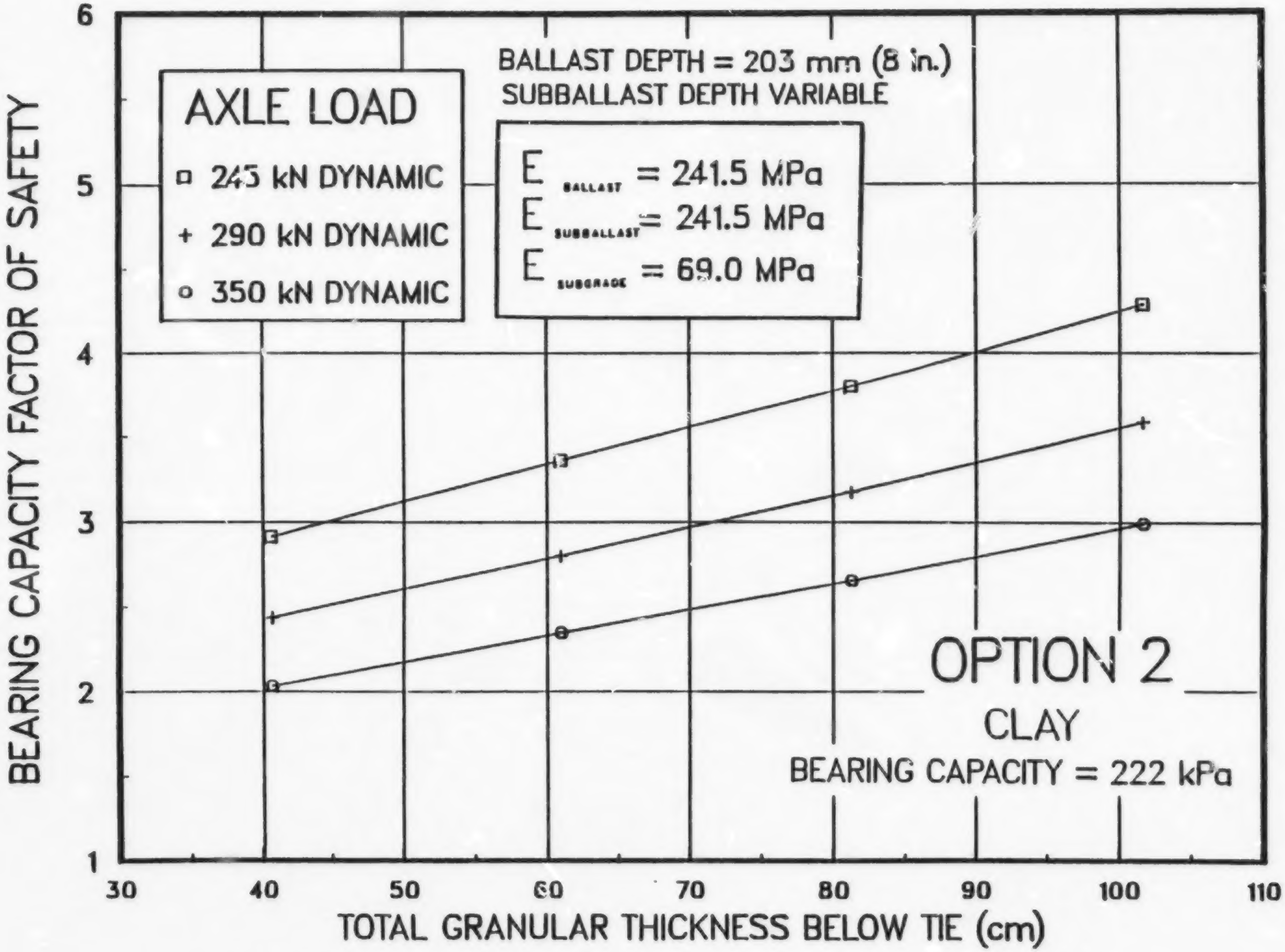

Fig. 5.81 Factor of safety for Option 2, Clay Subgrade E = 69.0 MPa, Subballast E = 241.5 MPa

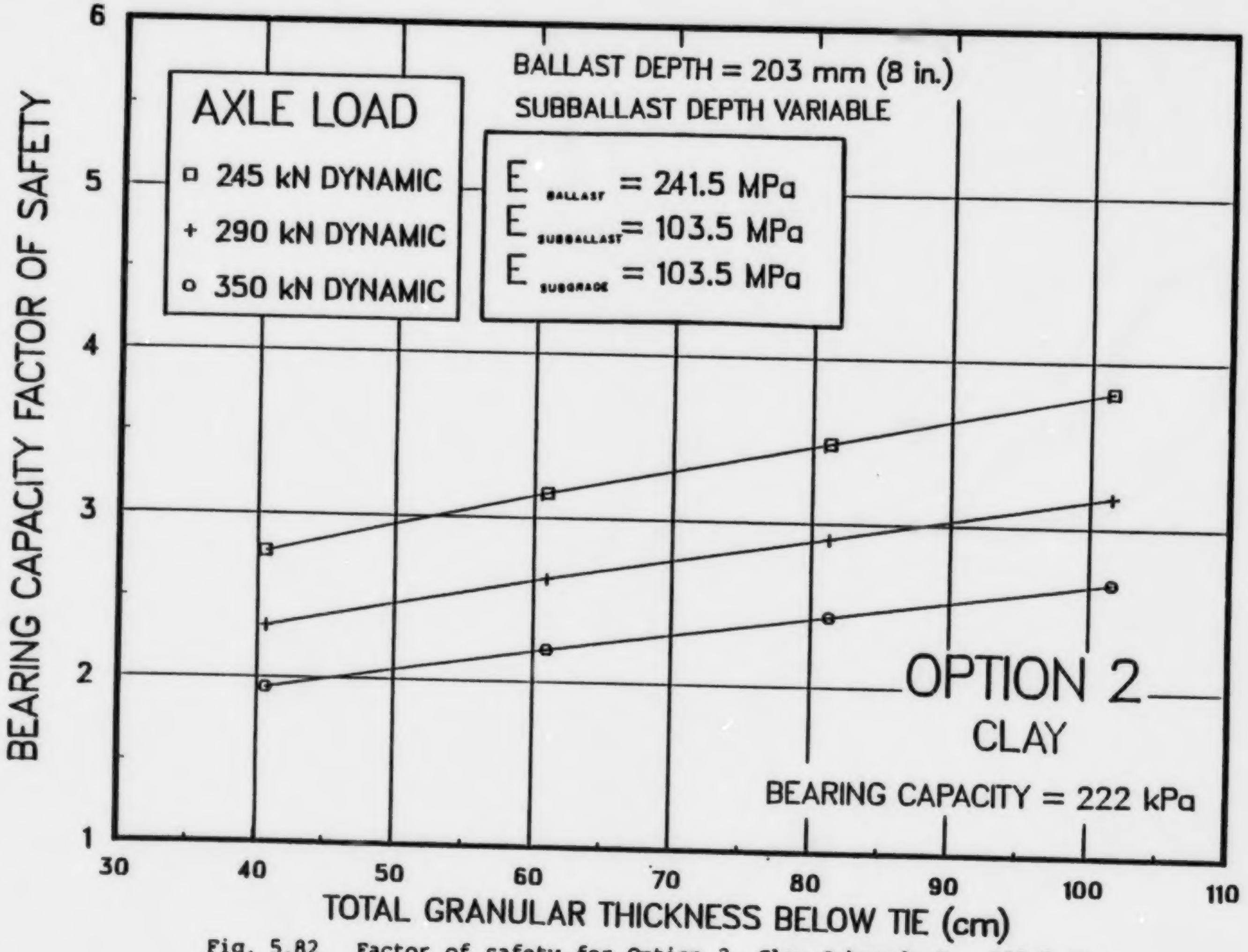

Fig. 5.82 Factor of safety for Option 2, Clay Subgrade E - 103.5 MPa, Subballast E - 103.5 MPa

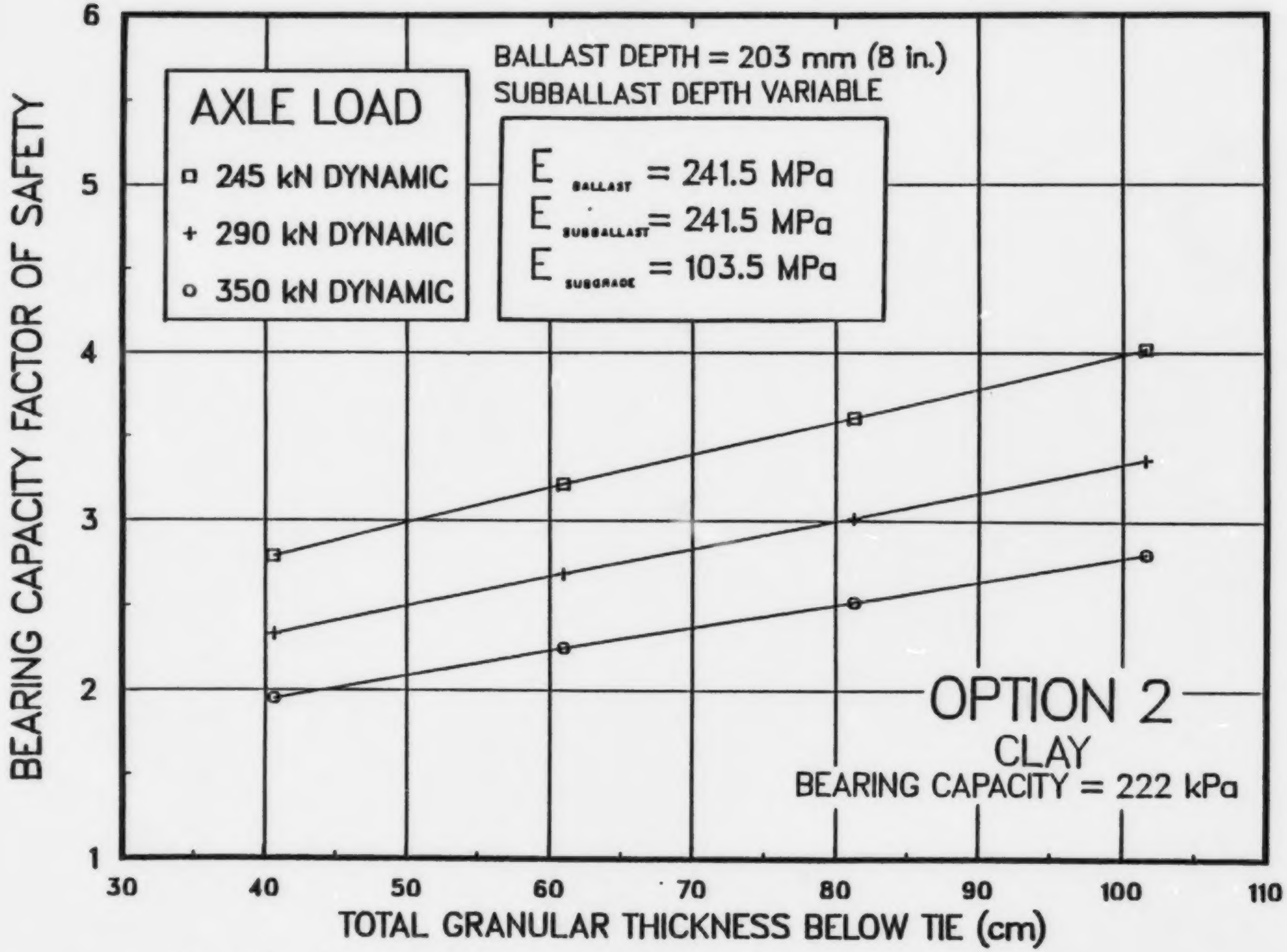

Fig. 5.83 Factor of safety for Option 2, Clay Subgrade E = 103.5 MPa, Subballast E = 241.5 MPa

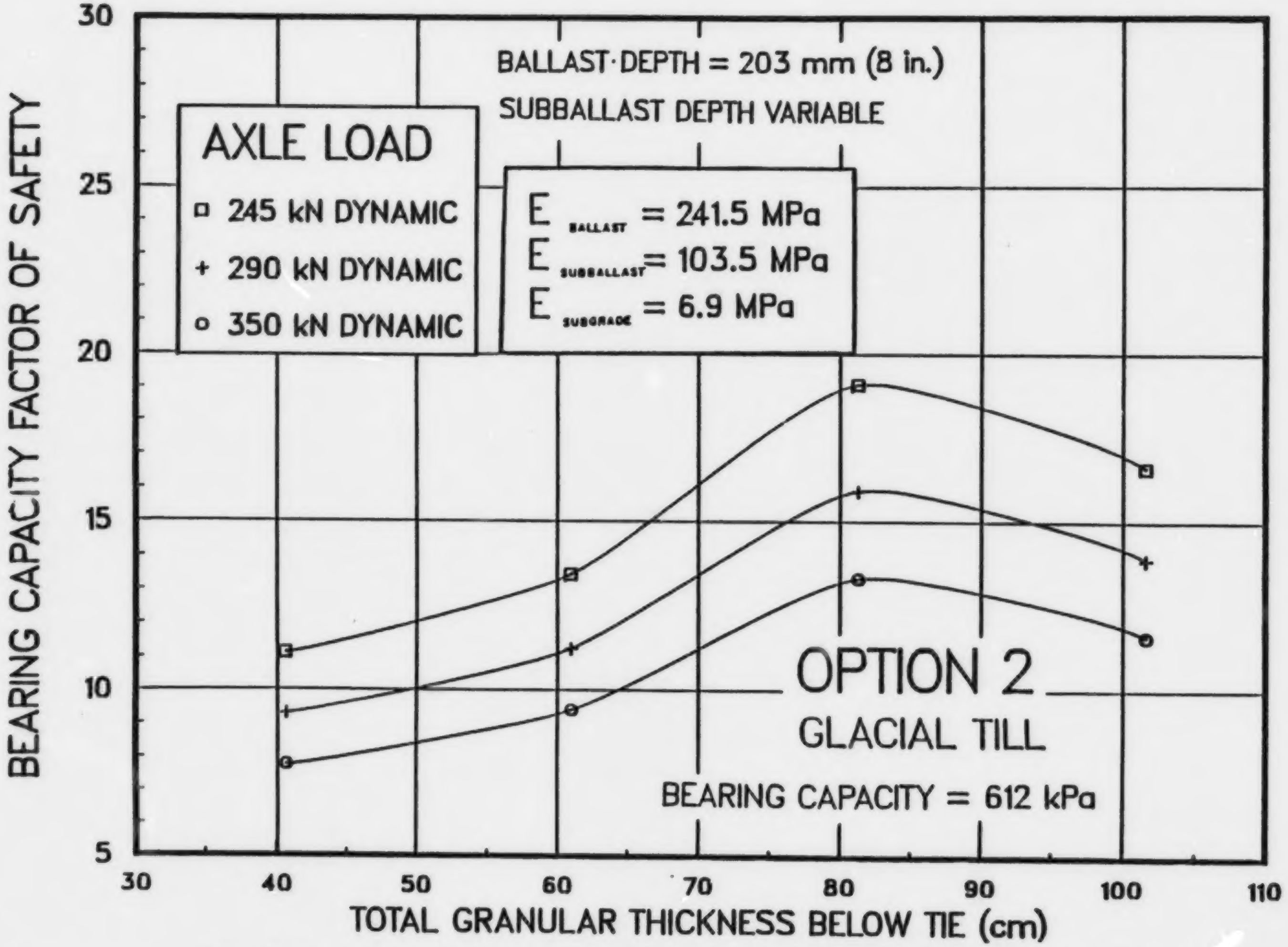

Fig. 5.84 Factor of safety for Option 2, Glacial Till Subgrade E = 6.9 MPa, Subballast E = 103.5 MPa

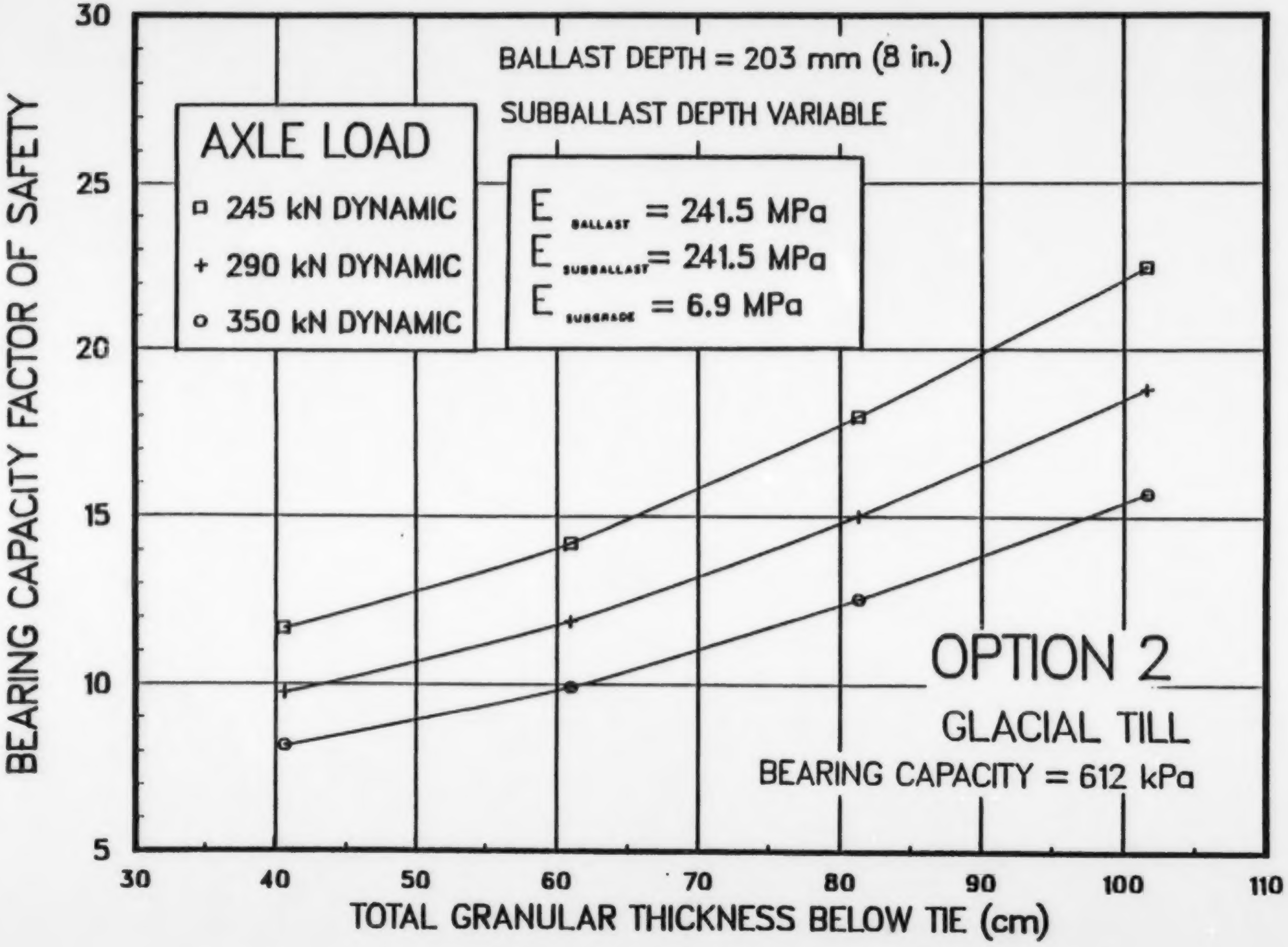

Fig. 5.85 Factor of safety for Option 2, Glacial Till Subgrade E = 6.9 MPa, Subballast E = 241.5 MPa

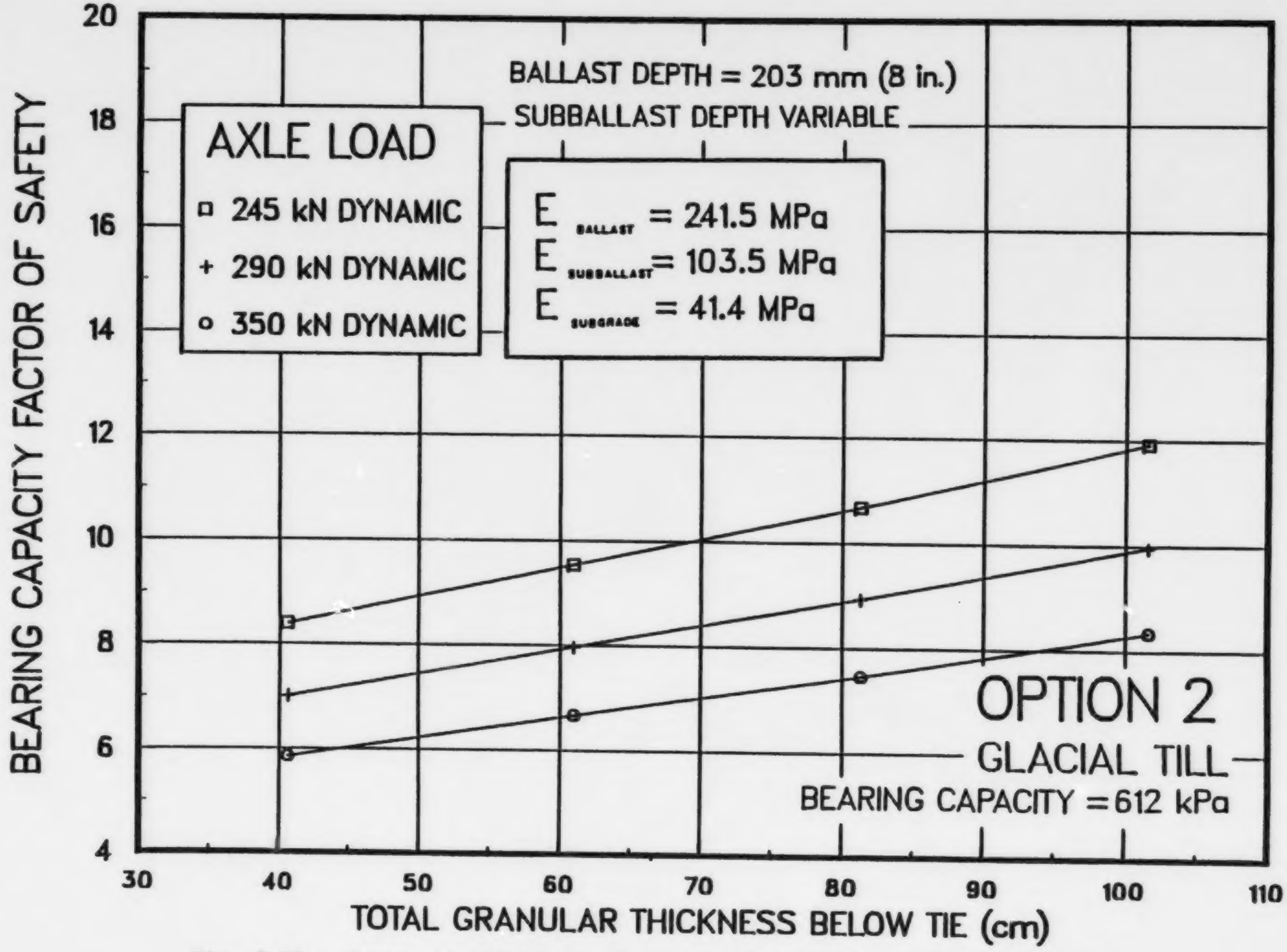

Fig. 5.86 Factor of safety for Option 2, Glacial Till Subgrade E = 41.4 MPa, Subballast E = 103.5 MPa

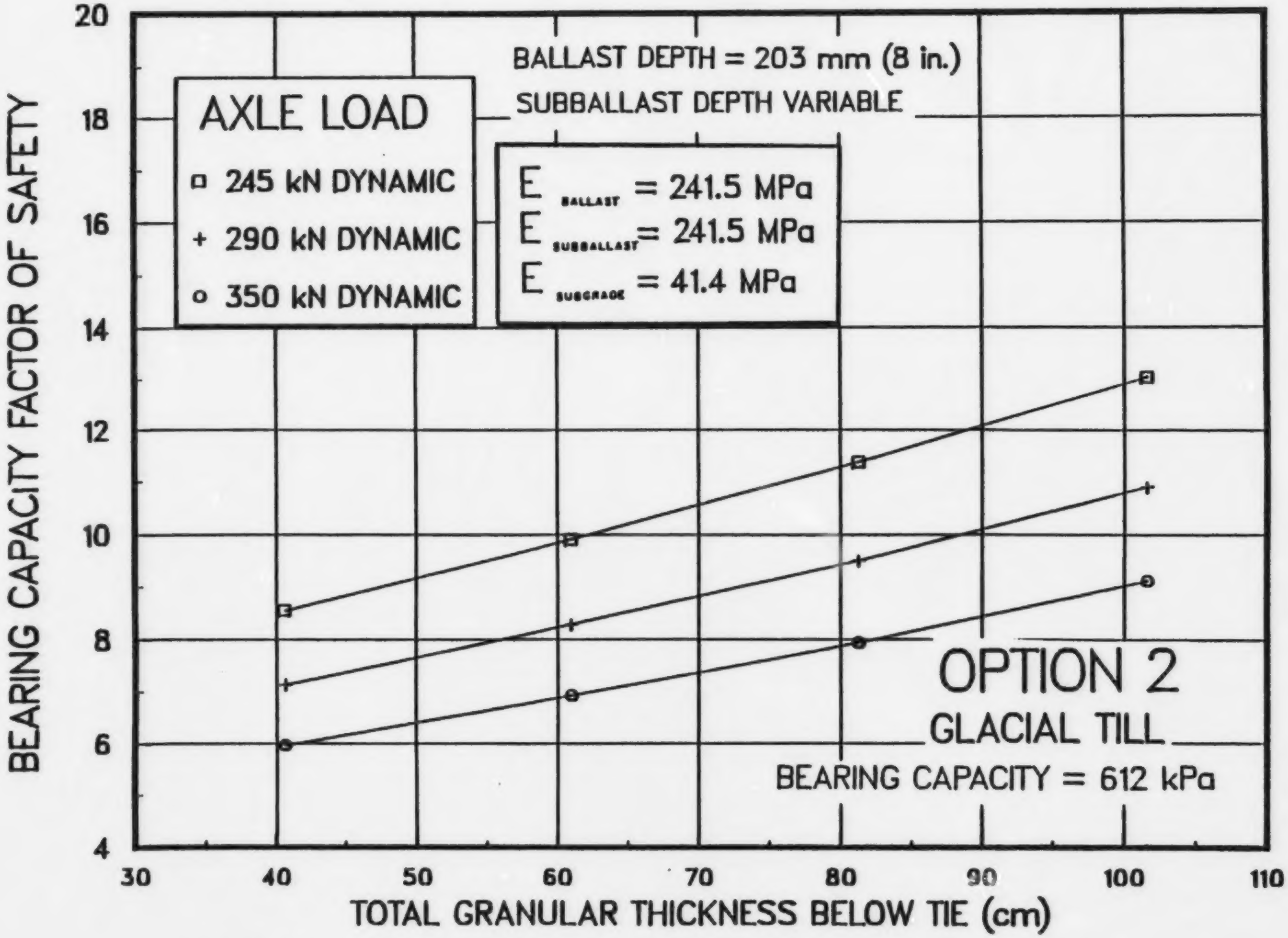

Fig. 5.87 Factor of safety for Option 2, Glacial Till Subgrade E = 41.4 MPa, Subballast E = 241.5 MPa

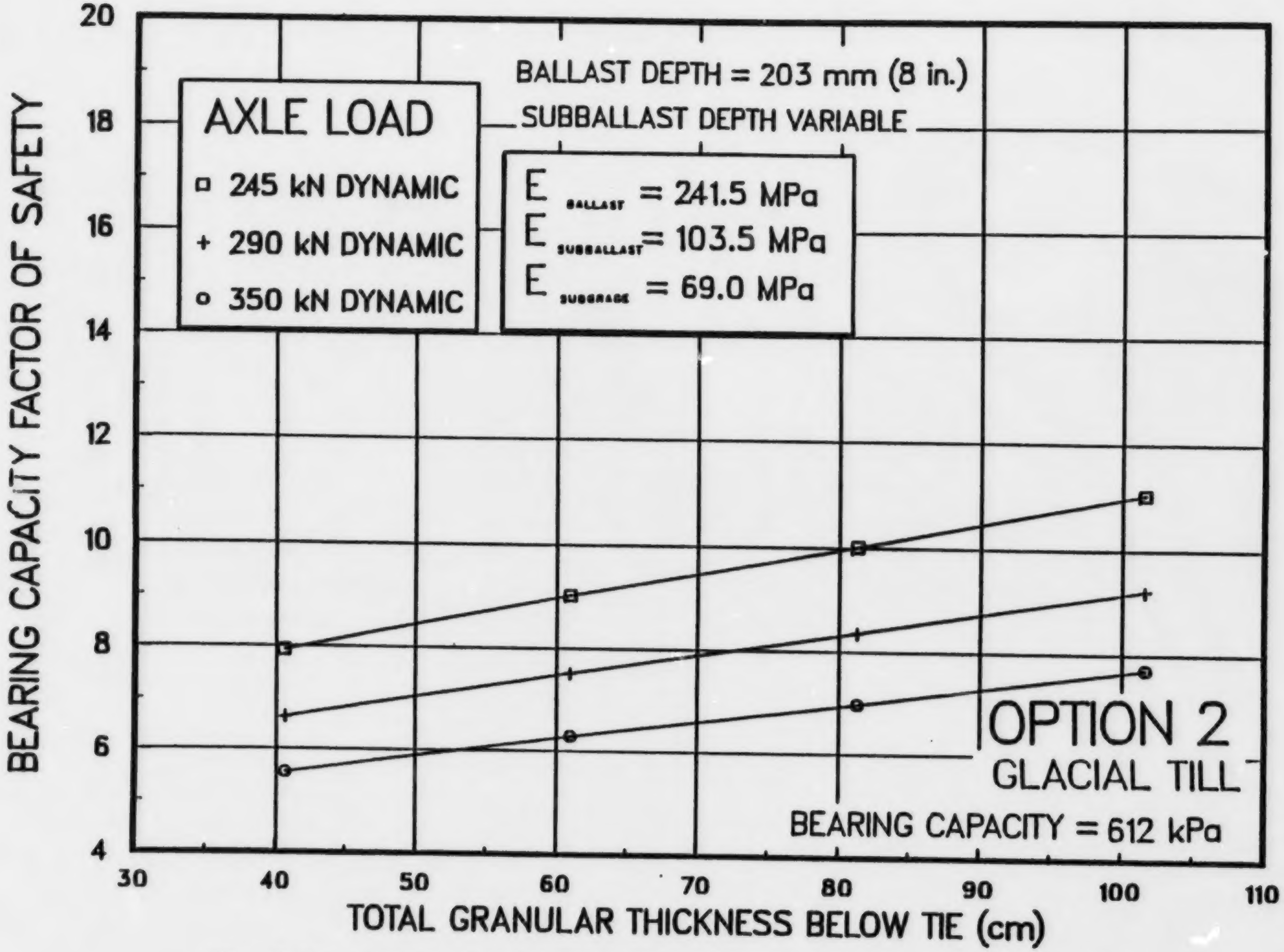

Fig. 5.88 Factor of safety for Option 2, Glacial Till Subgrade E = 69.0 MPa, Subballast E = 103.5 MPa

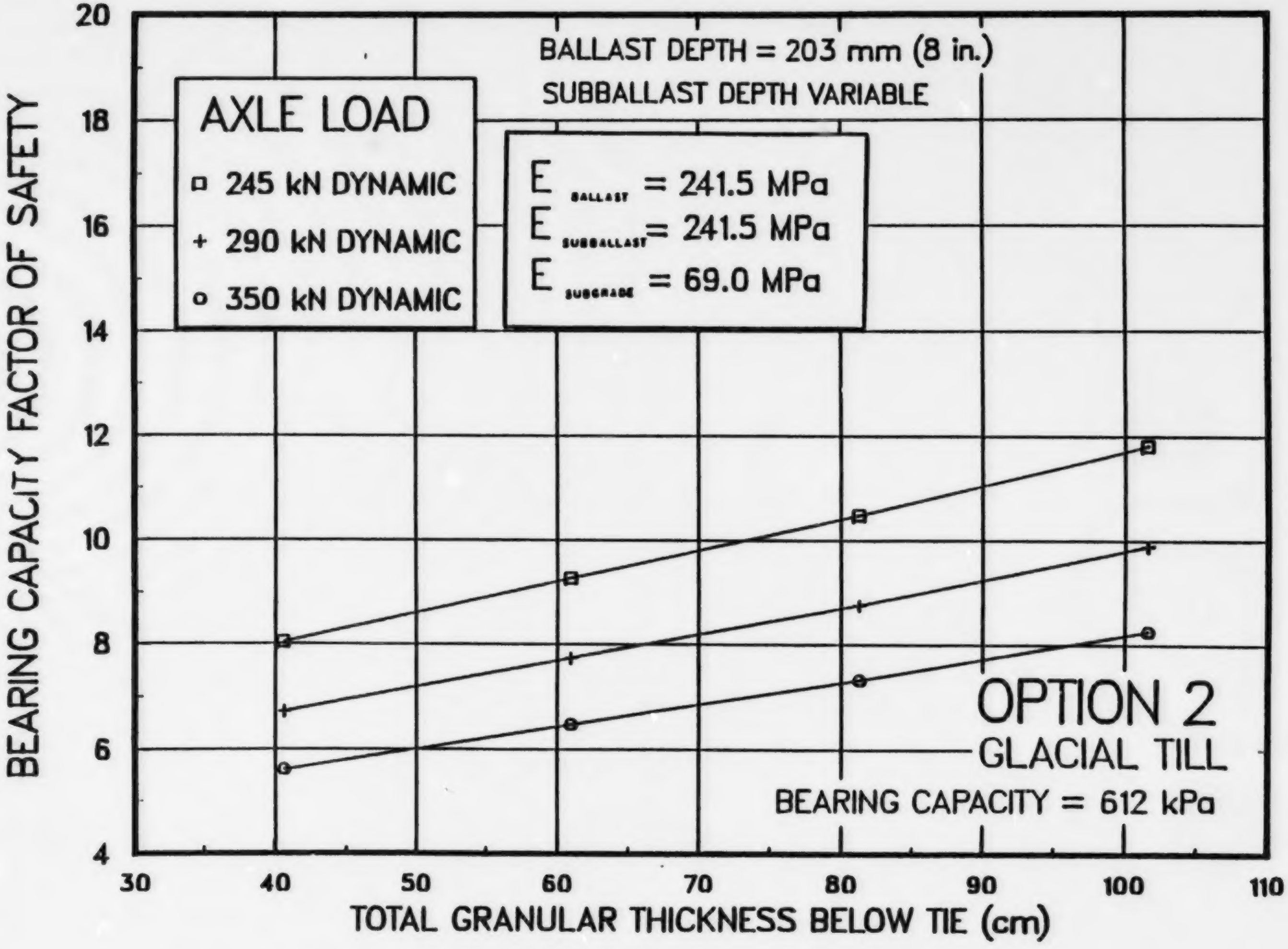

Fig. 5.89 Factor of safety for Option 2, Glacial Till Subgrade E = 69.0 MPa, Subballast E = 241.5 MPa

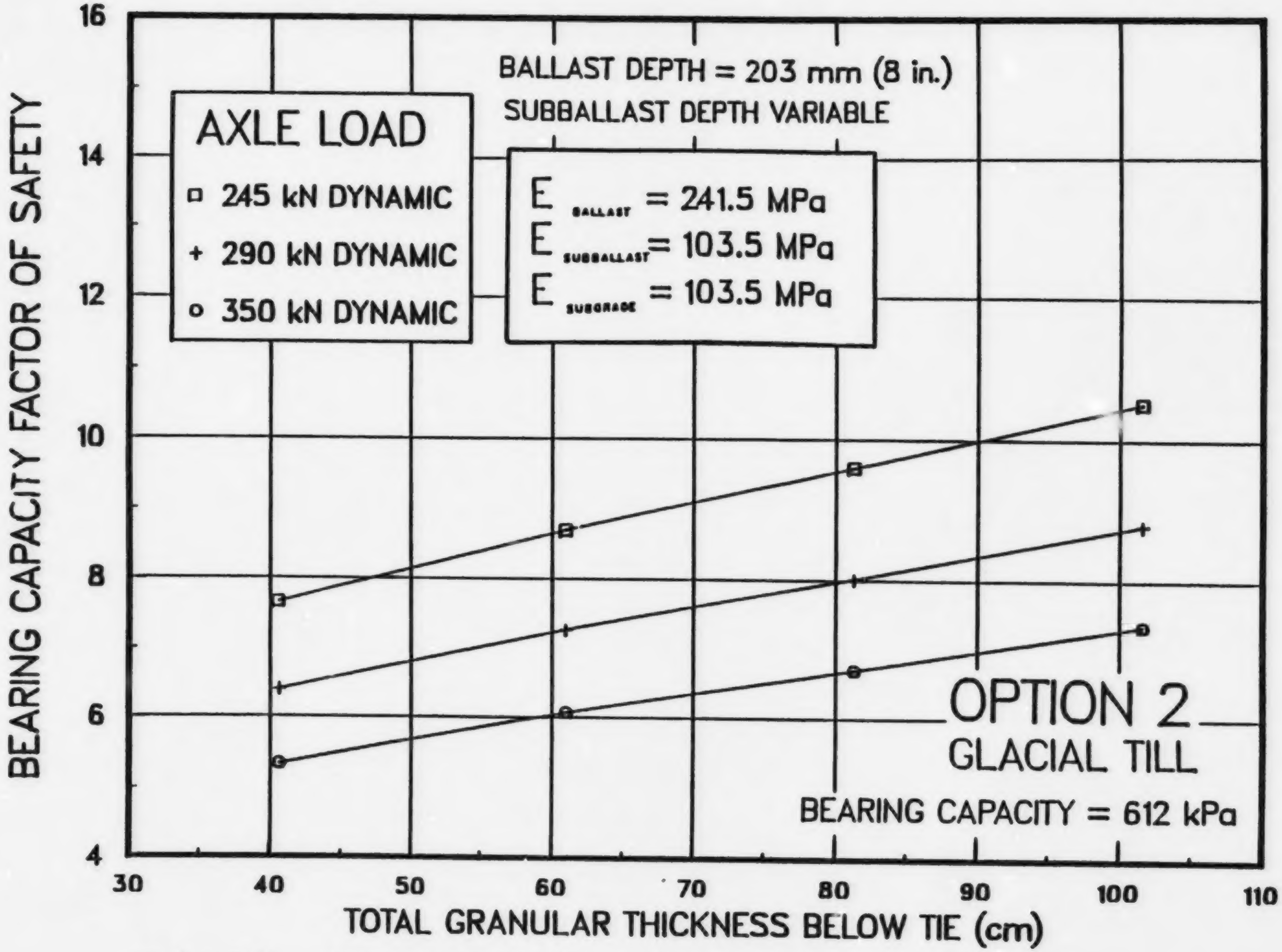

Fig. 5.90 Factor of safety for Option 2, Glacial Till Subgrade E = 103.5 MPa, Subballast E = 103.5 MPa

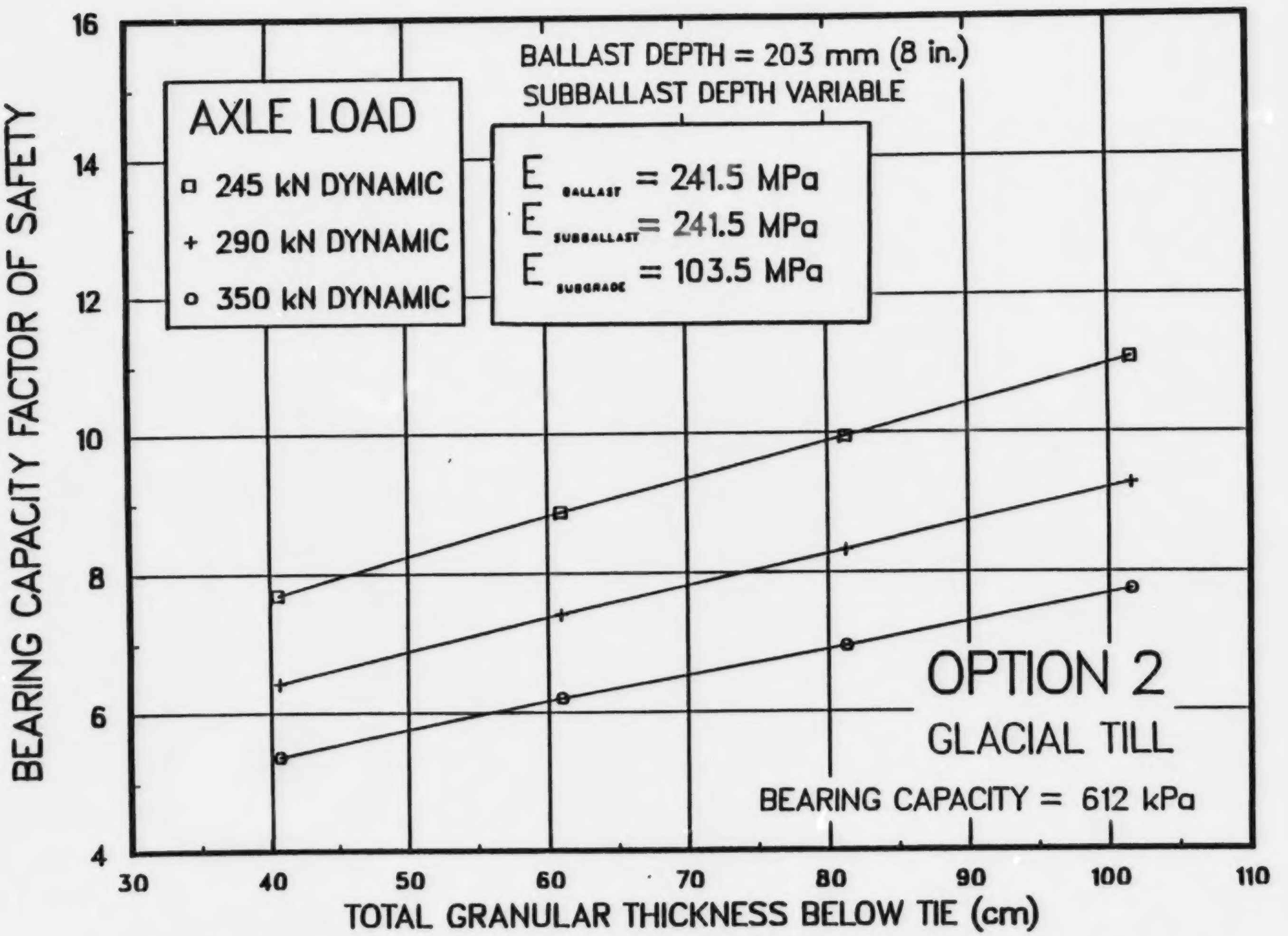

Fig. 5.91 Factor of safety for Option 2, Glacial Till Subgrade E = 103.5 MPa, Subballast E = 241.5 MPa

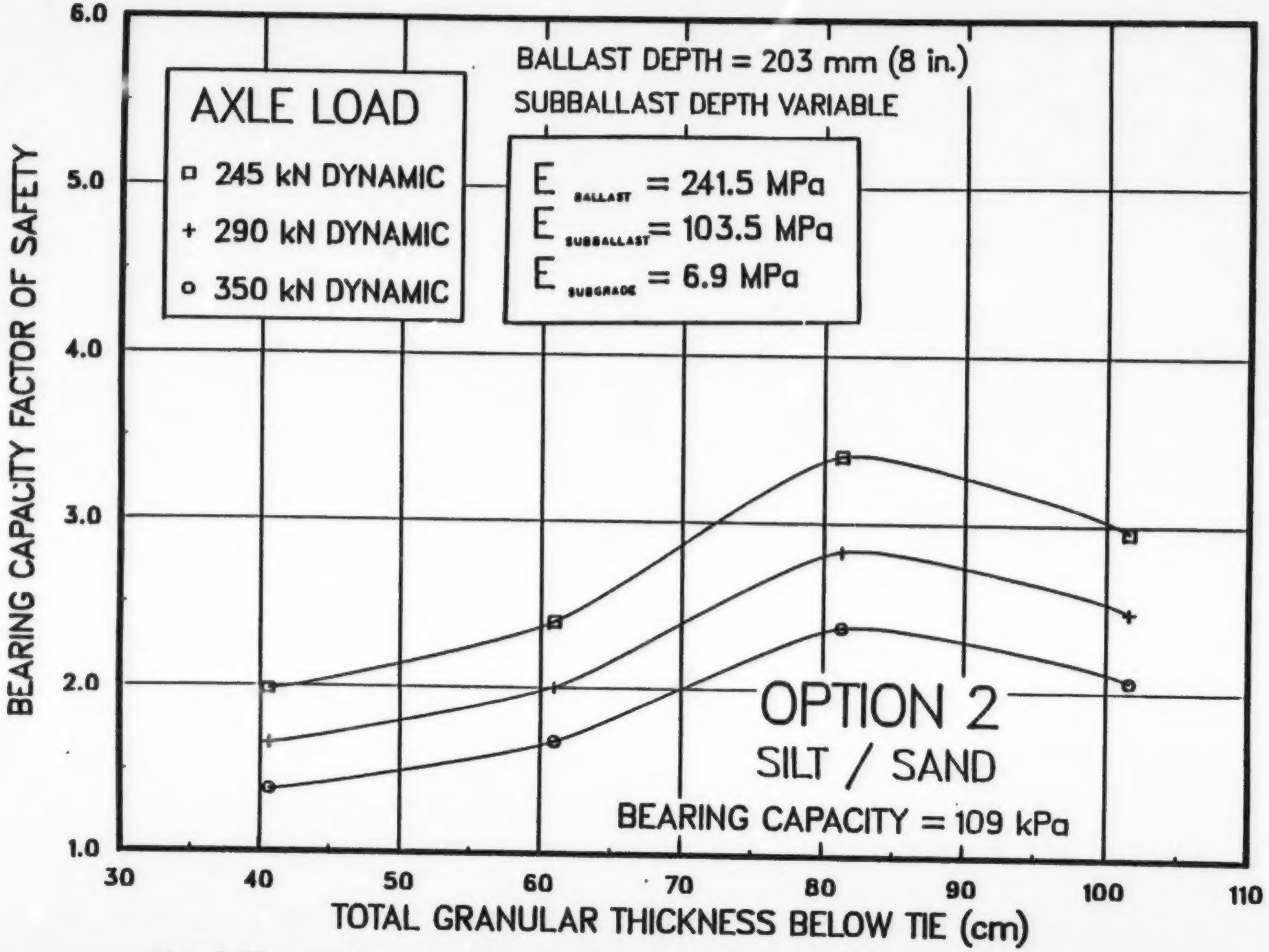

Fig. 5.92 Factor of safety for Option 2, Silt/Sand Subgrade E - 6.9 MPa, Subballast E - 103.5 MPa

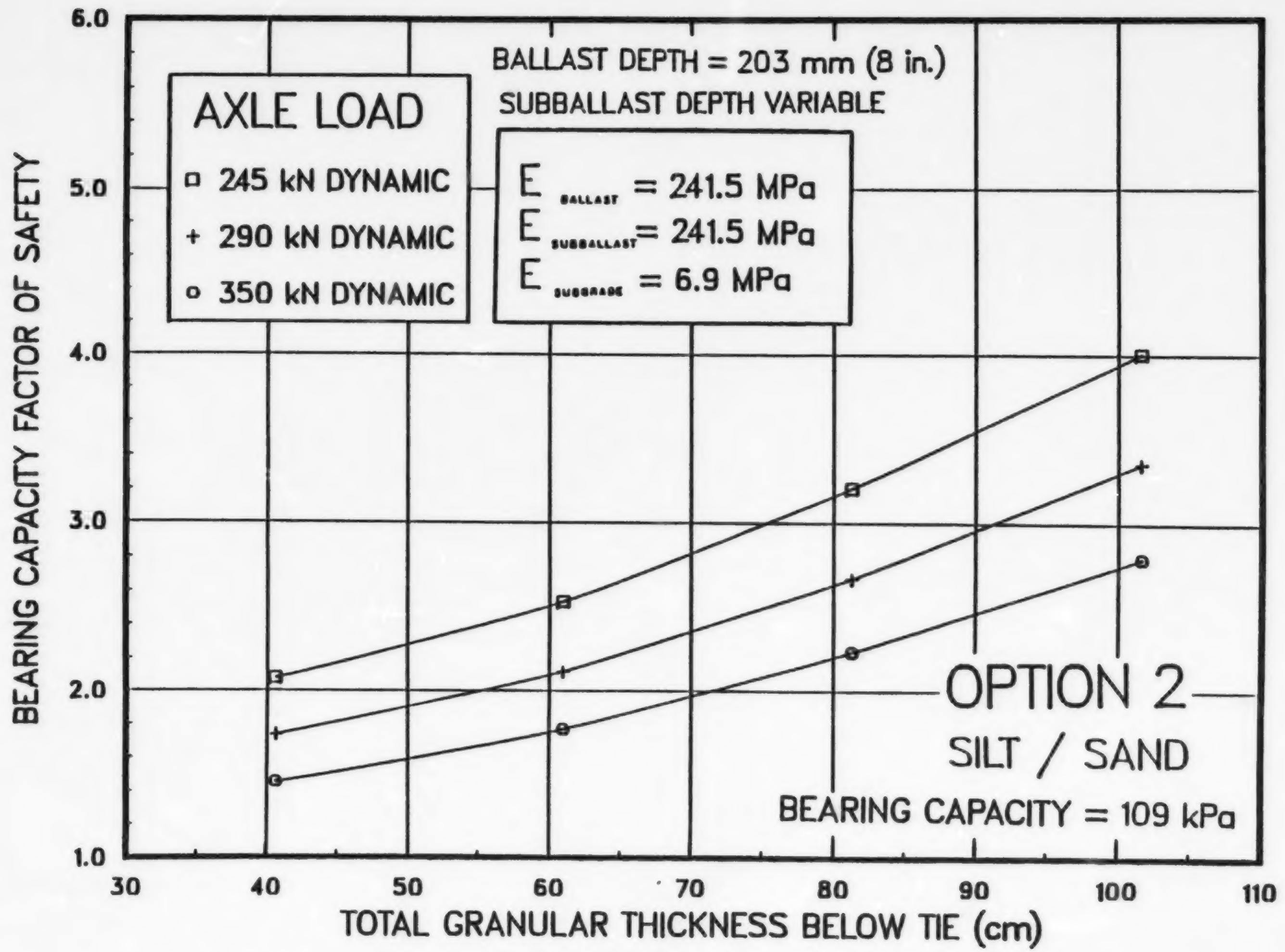

Fig. 5.93 Factor of safety for Option 2, Silt/Sand Subgrade E = 6.9 MPa, Subballast E = 241.5 MPa

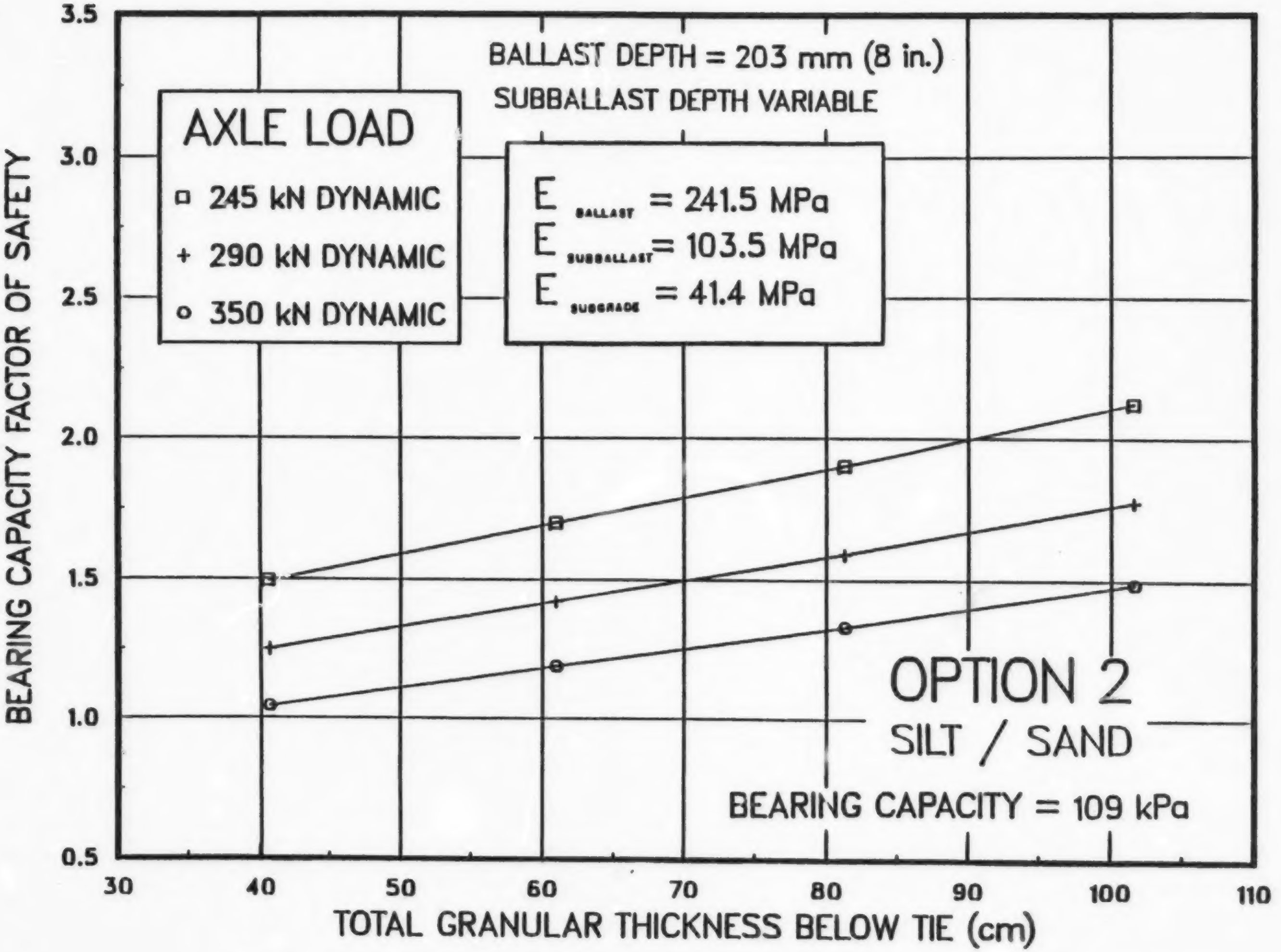

Fig. 5.94 Factor of safety for Option 2, Silt/Sand Subgrade E = 41.4 MPa, Subballast E = 103.5 MPa

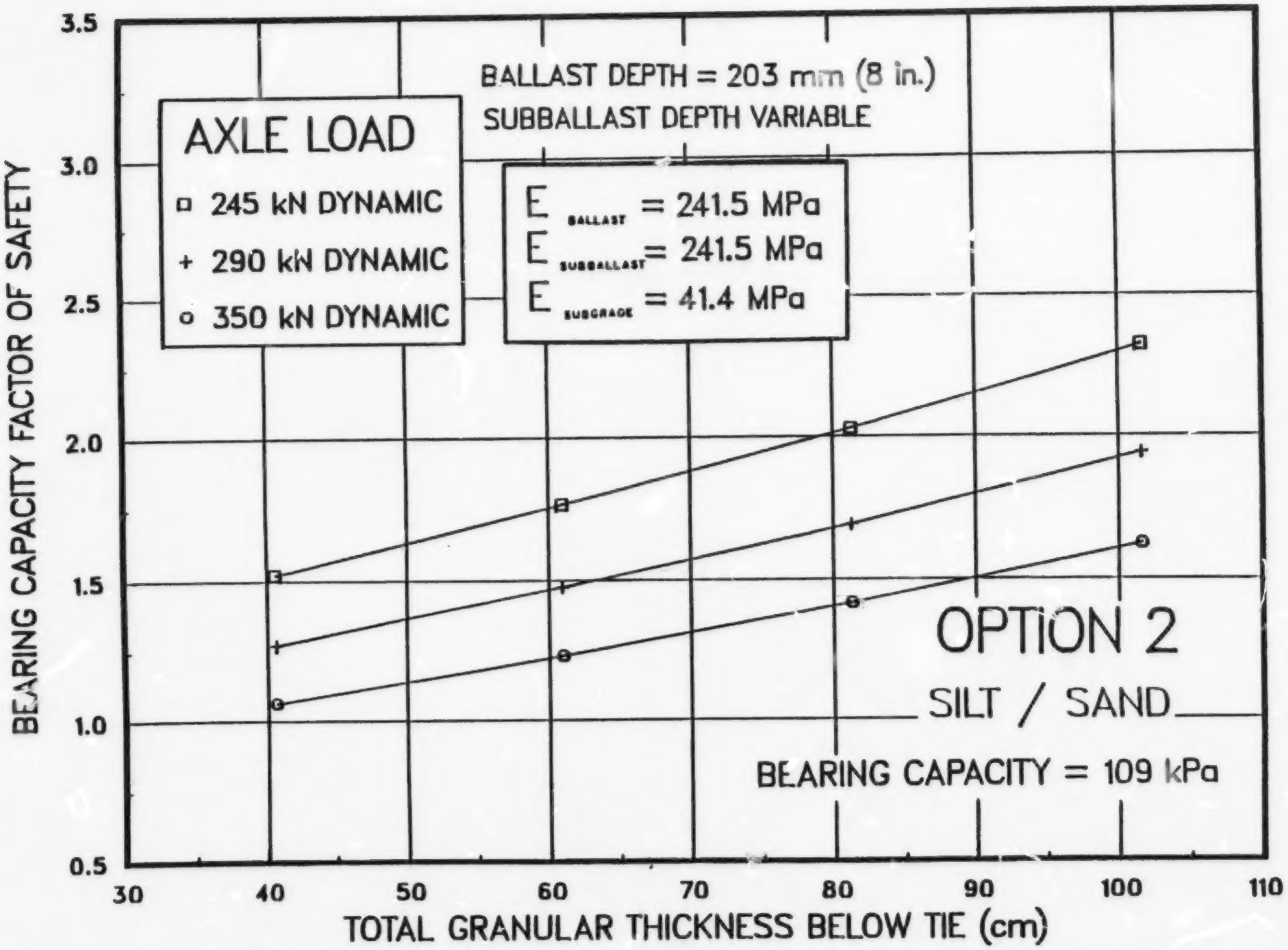

Fig. 5.95 Factor of safety for Option 2, Silt/Sand Subgrade E = 41.4 MPa, Subballast E = 241.5 MPa

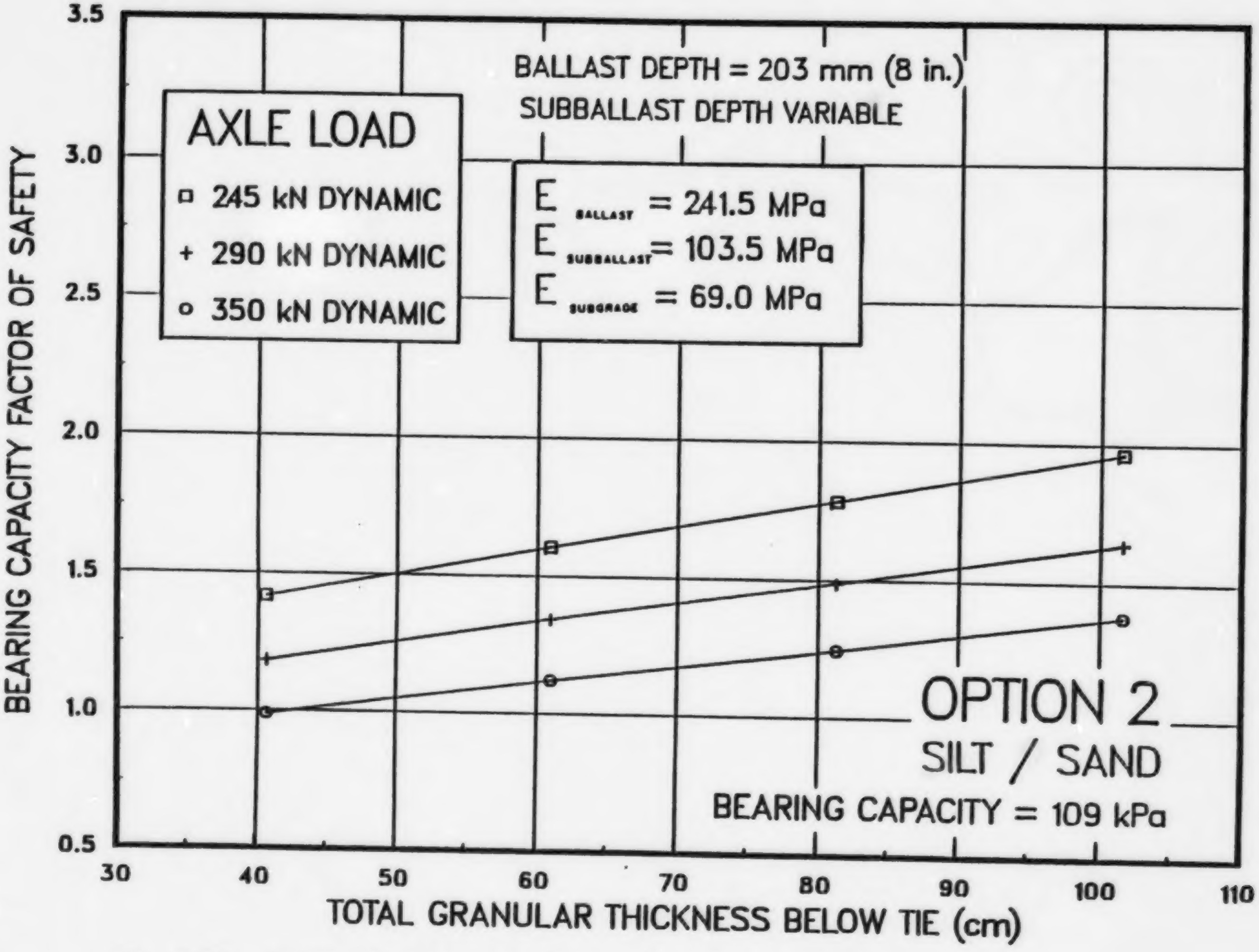

Fig. 5.96 Factor of safety for Option 2, Silt/Sand Subgrade E = 69.0 MPa, Subballast E = 103.5 MPa

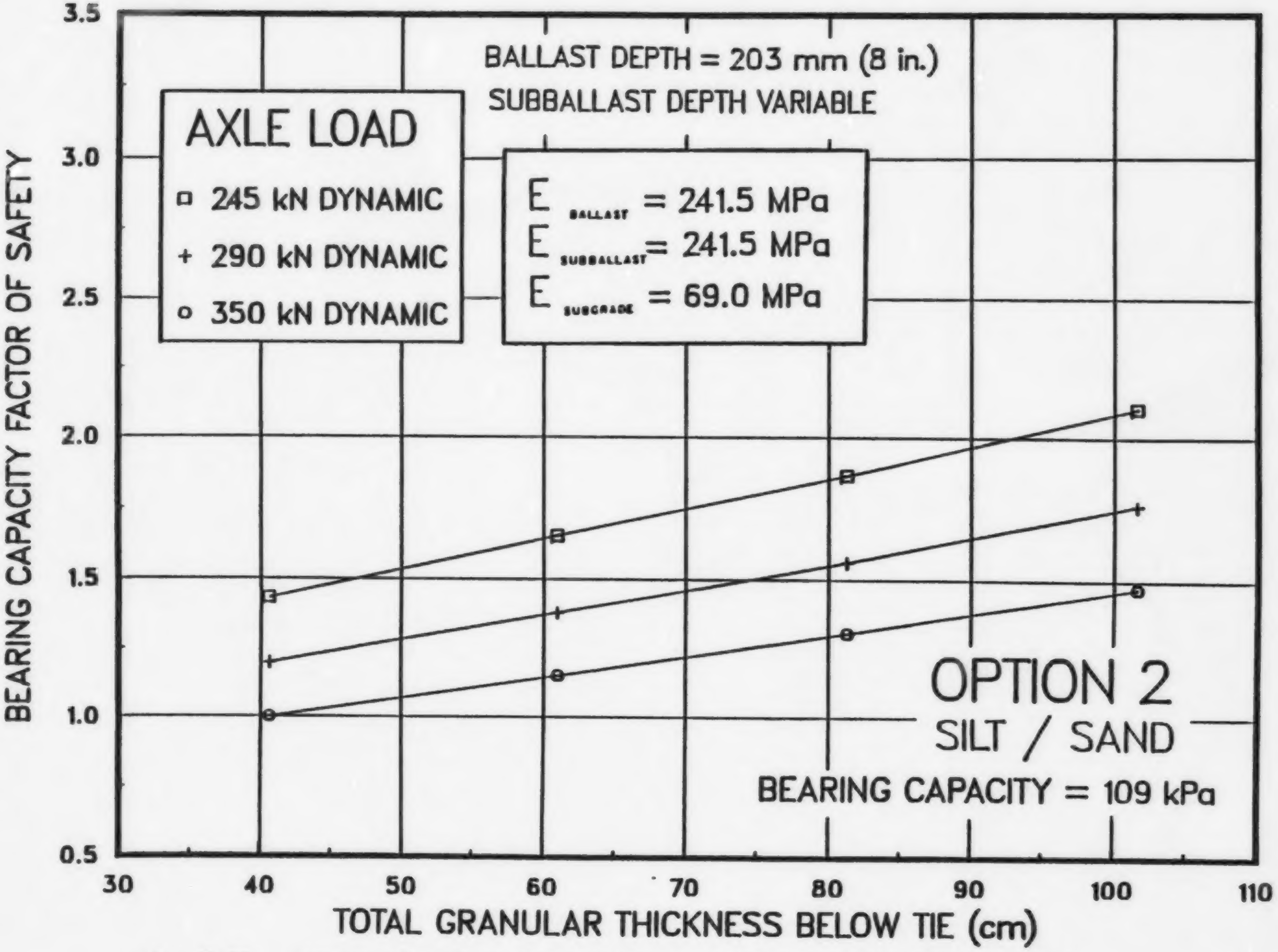

Fig. 5.97 Factor of safety for Option 2, Silt/Sand Subgrade E = 69.0 MPa, Subballast E = 241.5 MPa

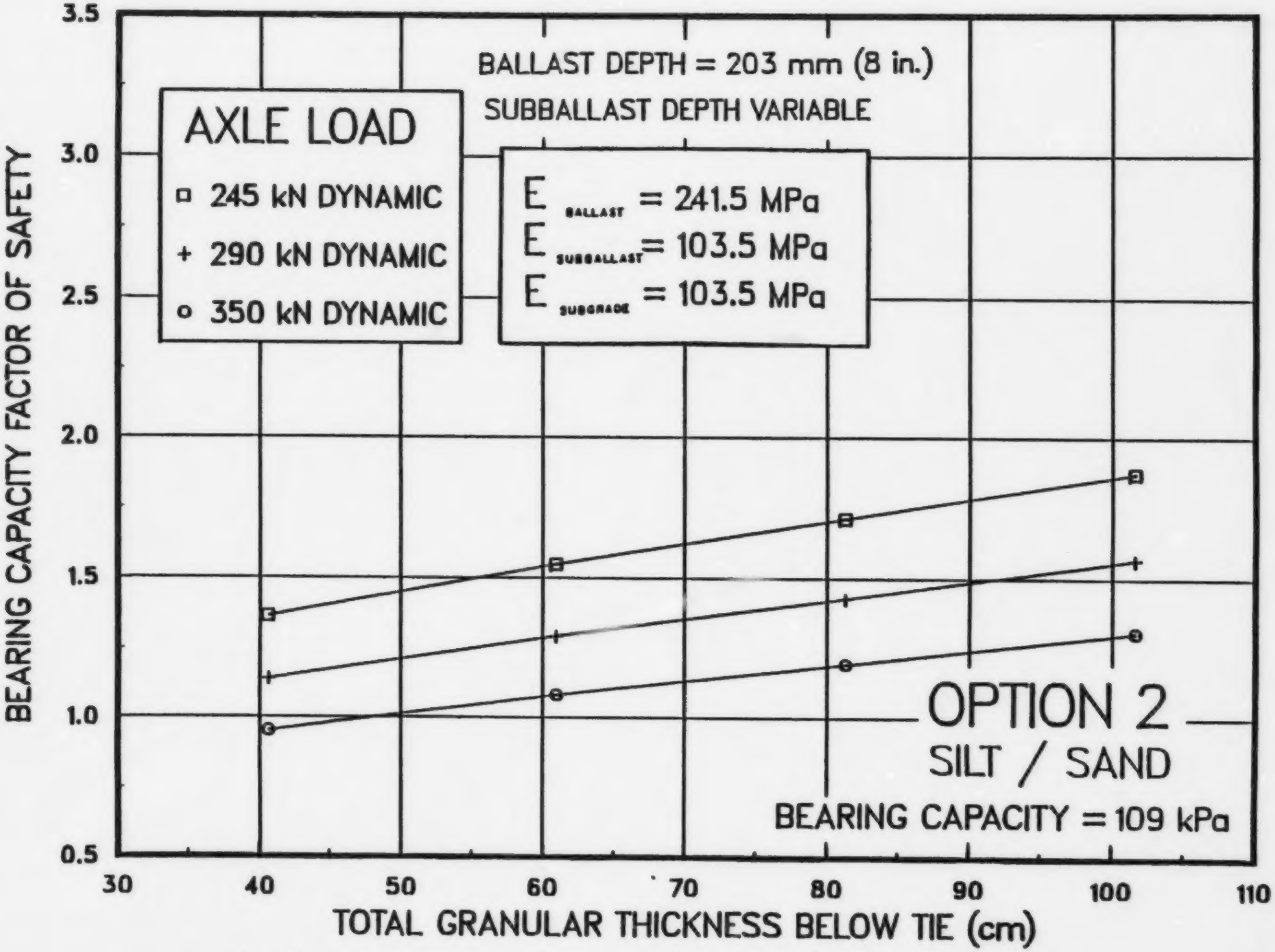

Fig. 5.98 Factor of safety for Option 2, Silt/Sand Subgrade E = 103.5 MPa, Subballast E = 103.5 MPa

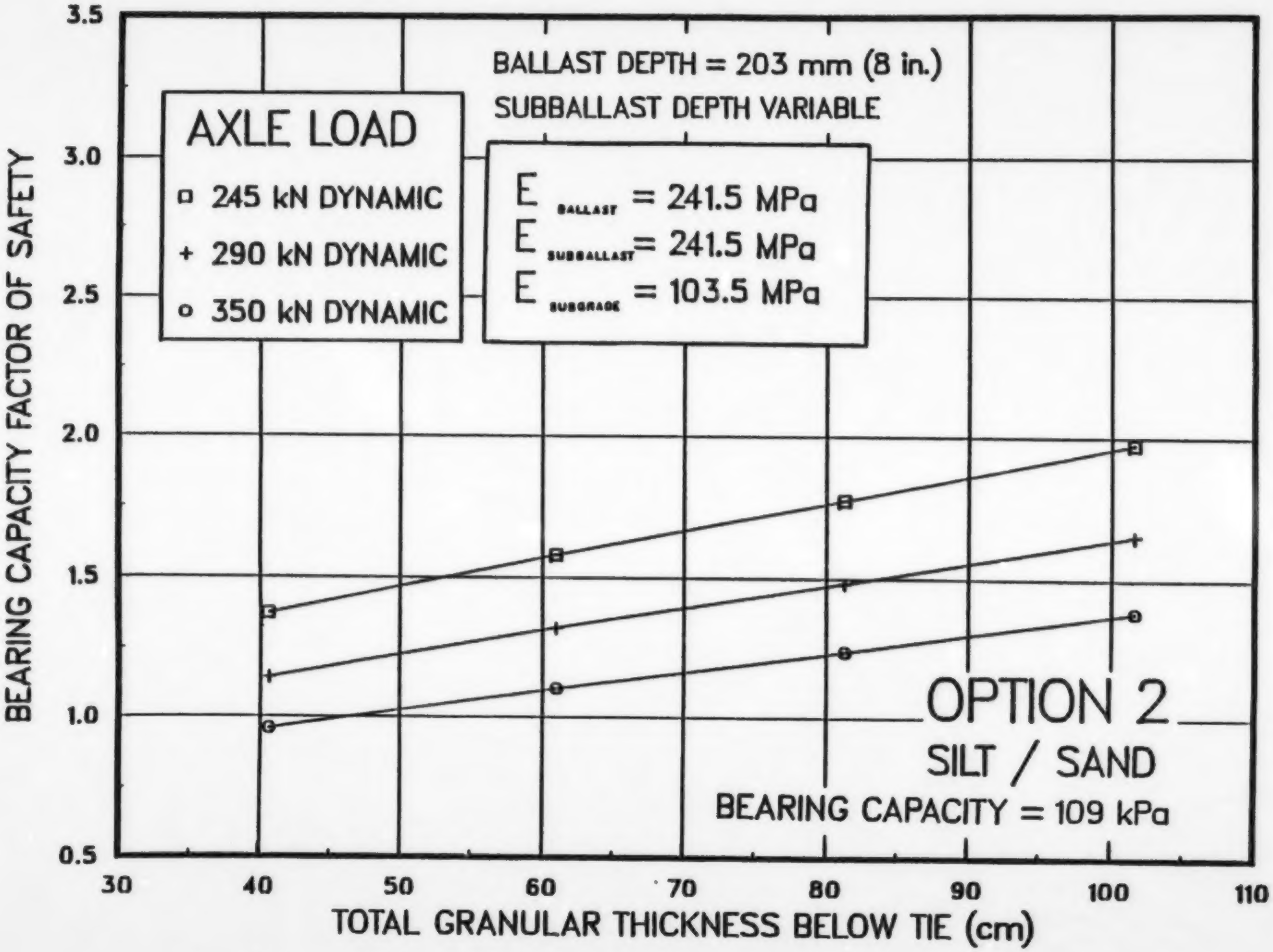

Fig. 5.99 Factor of safety for Option 2, Silt/Sand Subgrade E = 103.5 MPa, Subballast E = 241.5 MPa

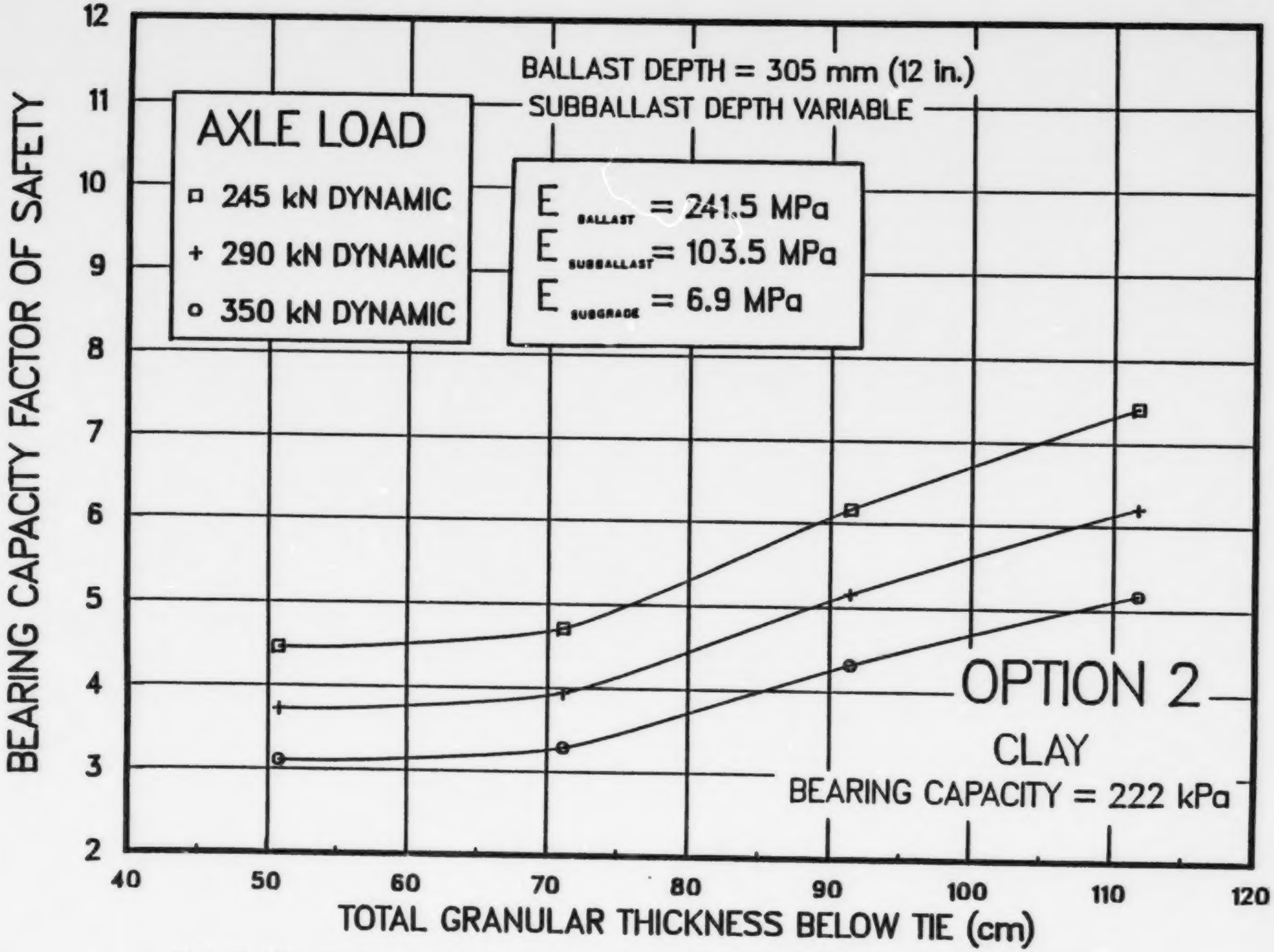

Fig. 5.100 Factor of safety for Option 2, Clay Subgrade E = 6.9 MPa, Subballast E = 103.5 MPa

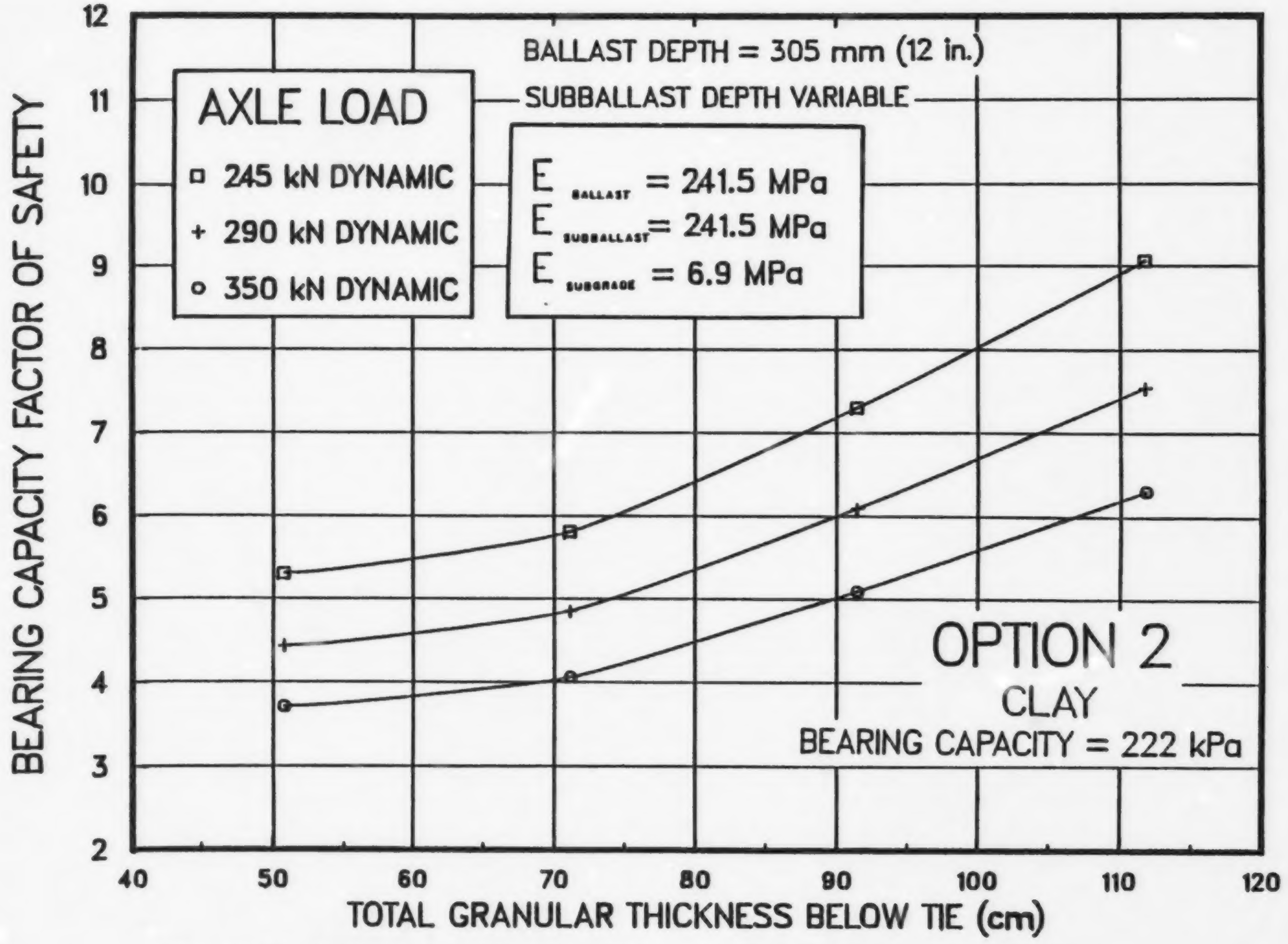

Fig. 5.101 Factor of safety for Option 2, Clay Subgrade E = 6.9 MPa, Subballast E = 241.5 MPa

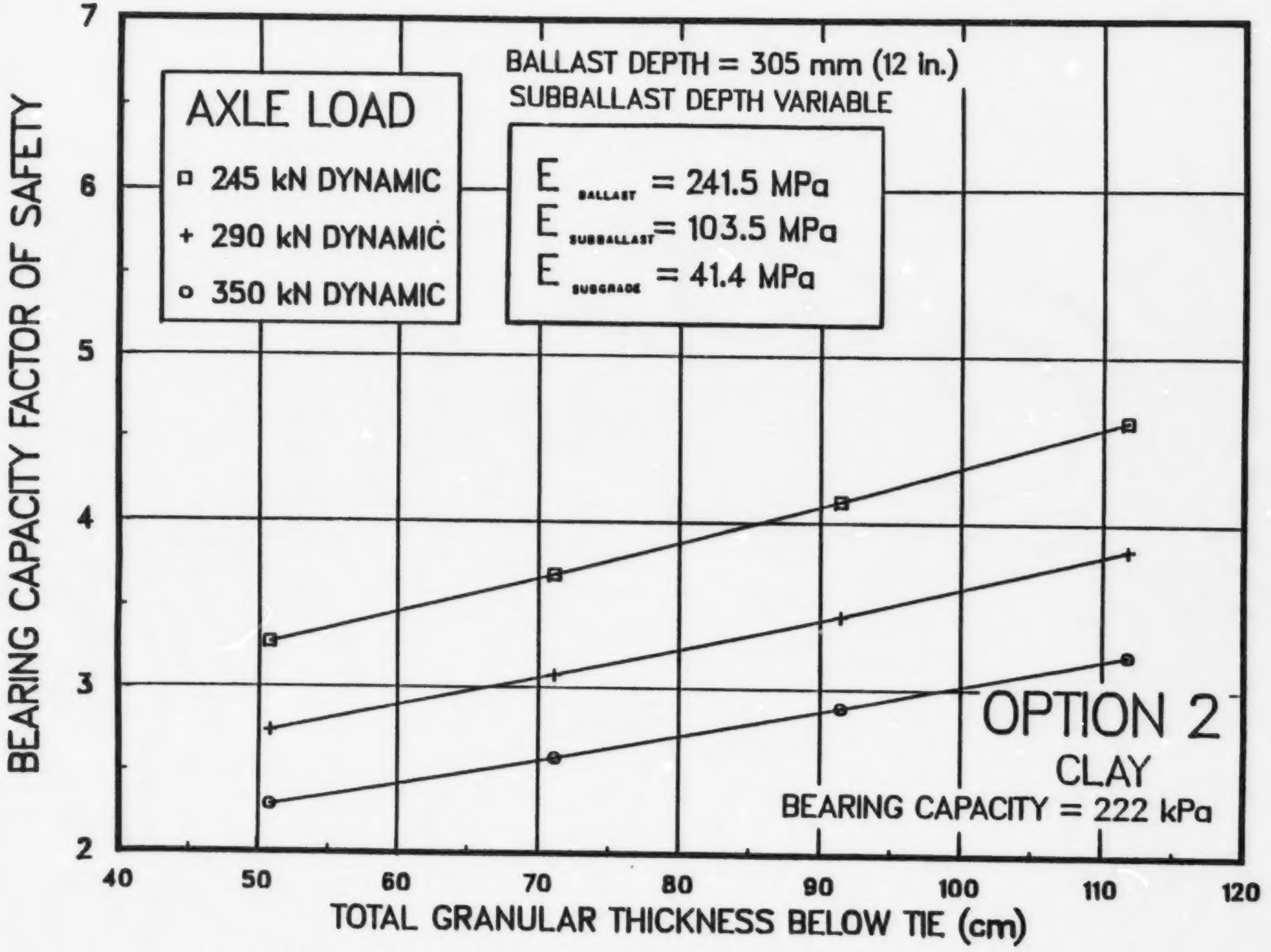

Fig. 5.102 Factor of safety for Option 2, Clay Subgrade E = 41.4 MPa, Subballast E = 103.5 MPa

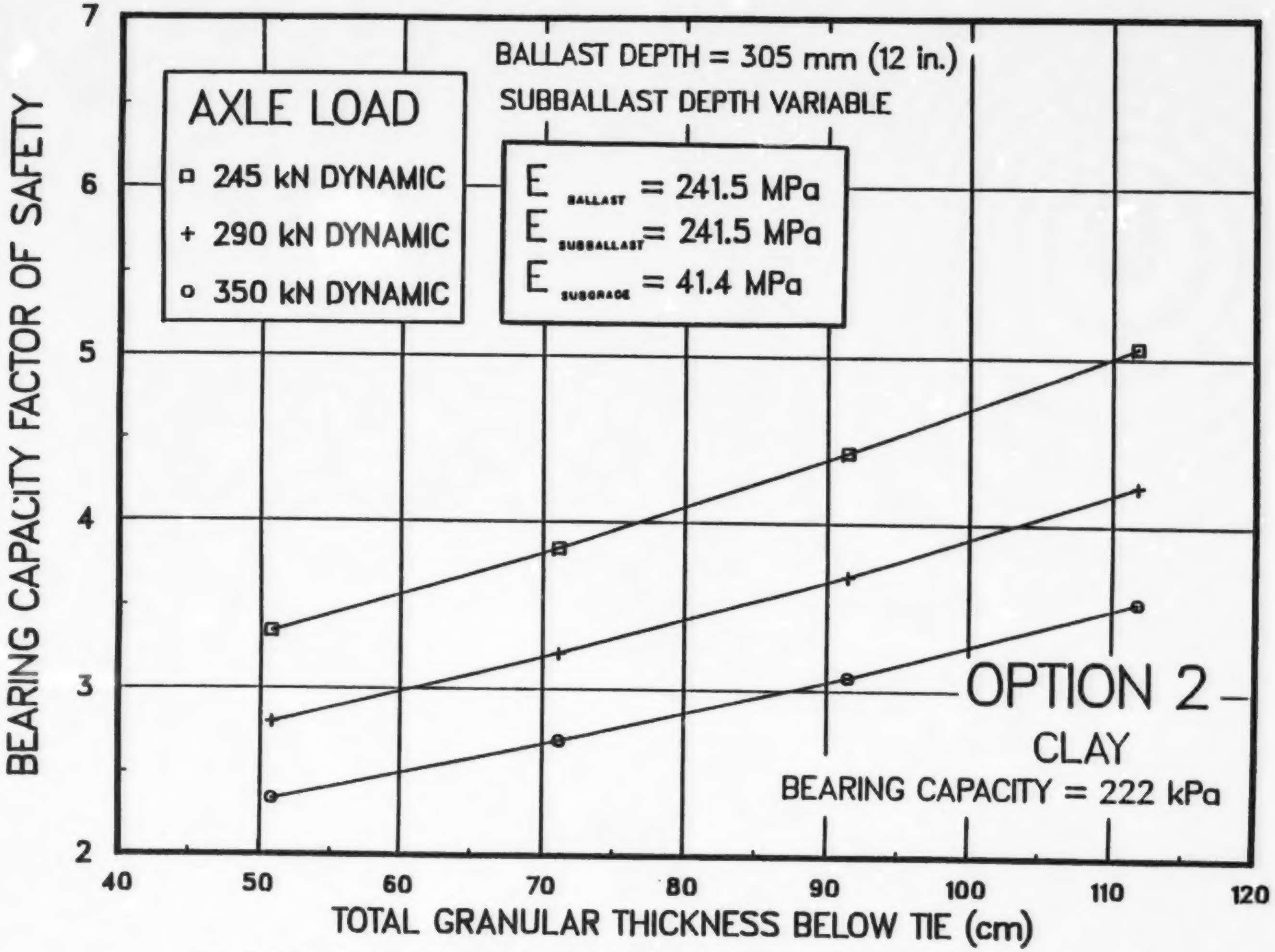

Fig. 5.103 Factor of safety for Option 2, Clay Subgrade E = 41.4 MPa, Subballast E = 241.5 MPa

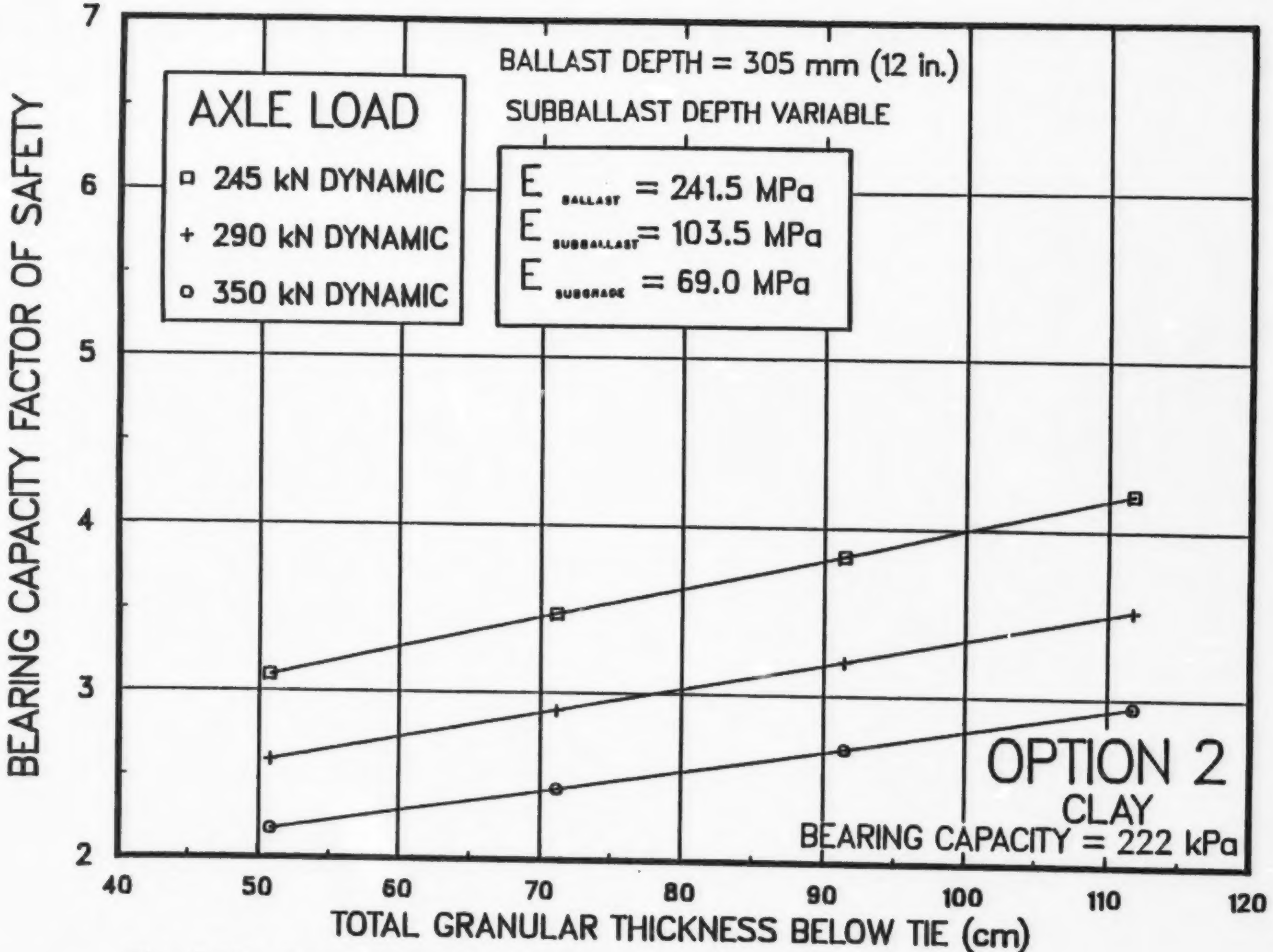

Fig. 5.104 Factor of safety for Option 2, Clay Subgrade E = 69.0 MPa, Subballast E = 103.5 MPa

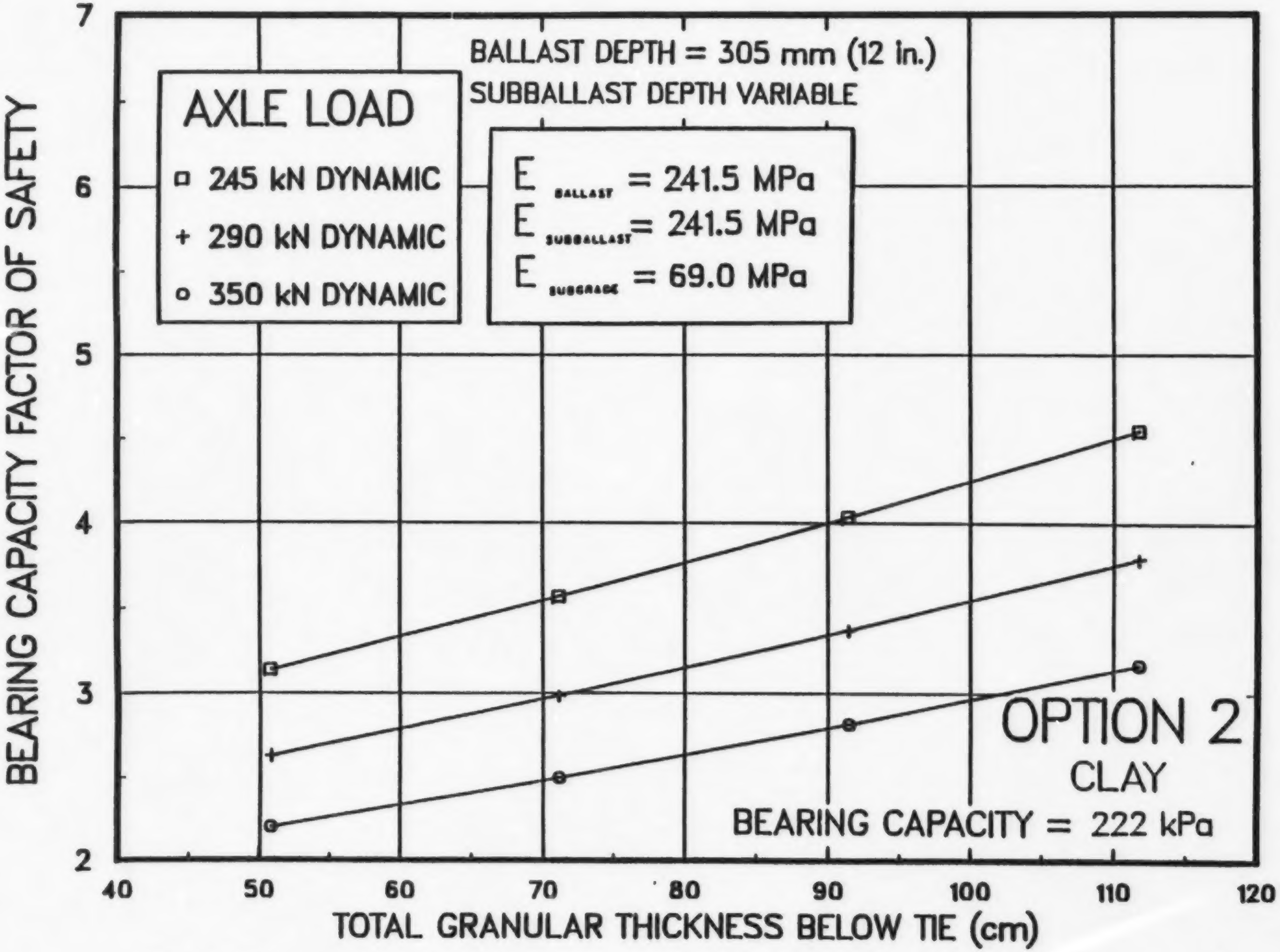

Fig. 5.105 Factor of safety for Option 2, Clay Subgrade E = 69.0 MPa, Subballast E = 241.5 MPa

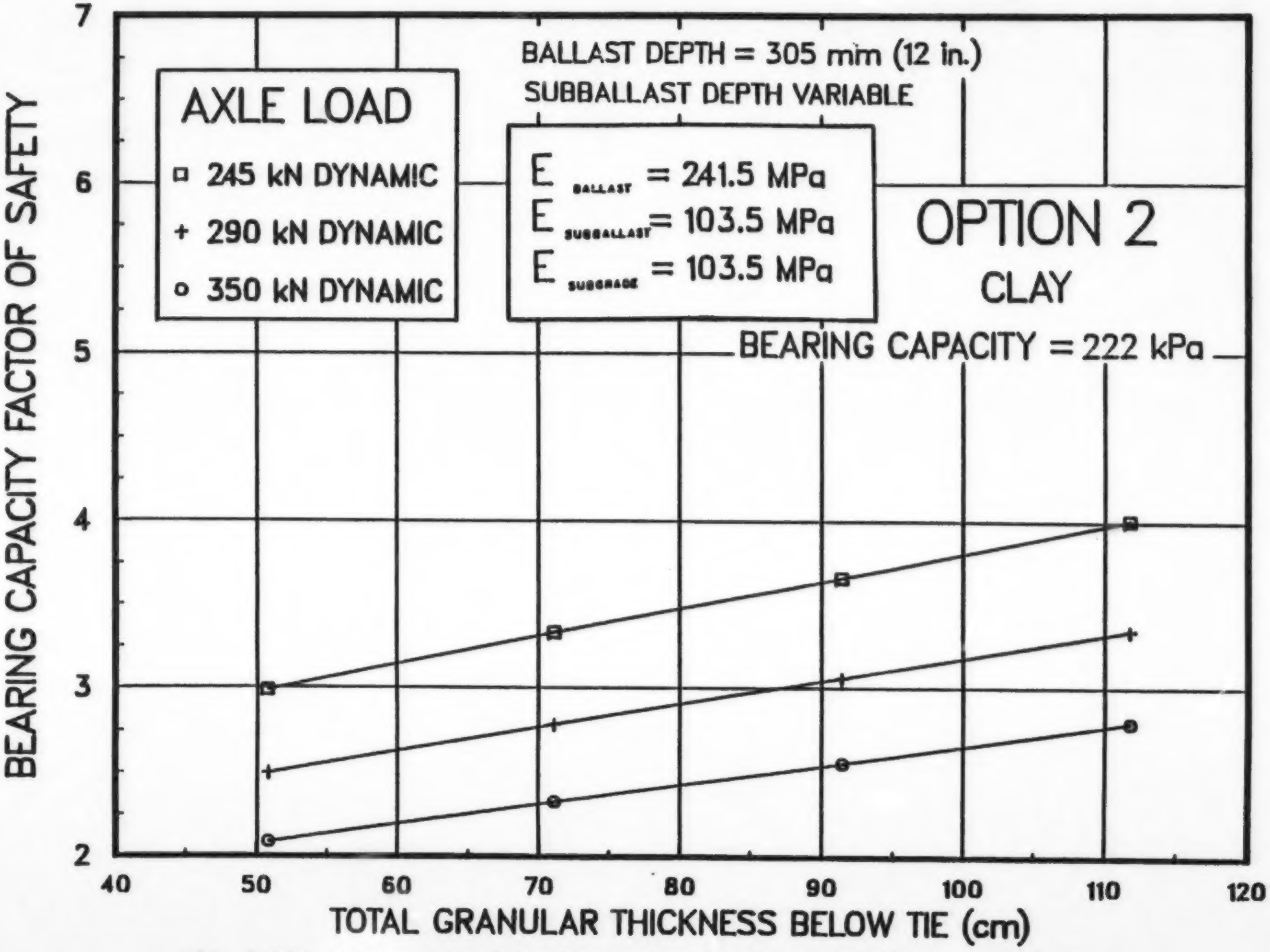

Fig. 5.106 Factor of safety for Option 2, Clay Subgrade E - 103.5 MPa, Subballast E - 103.5 MPa

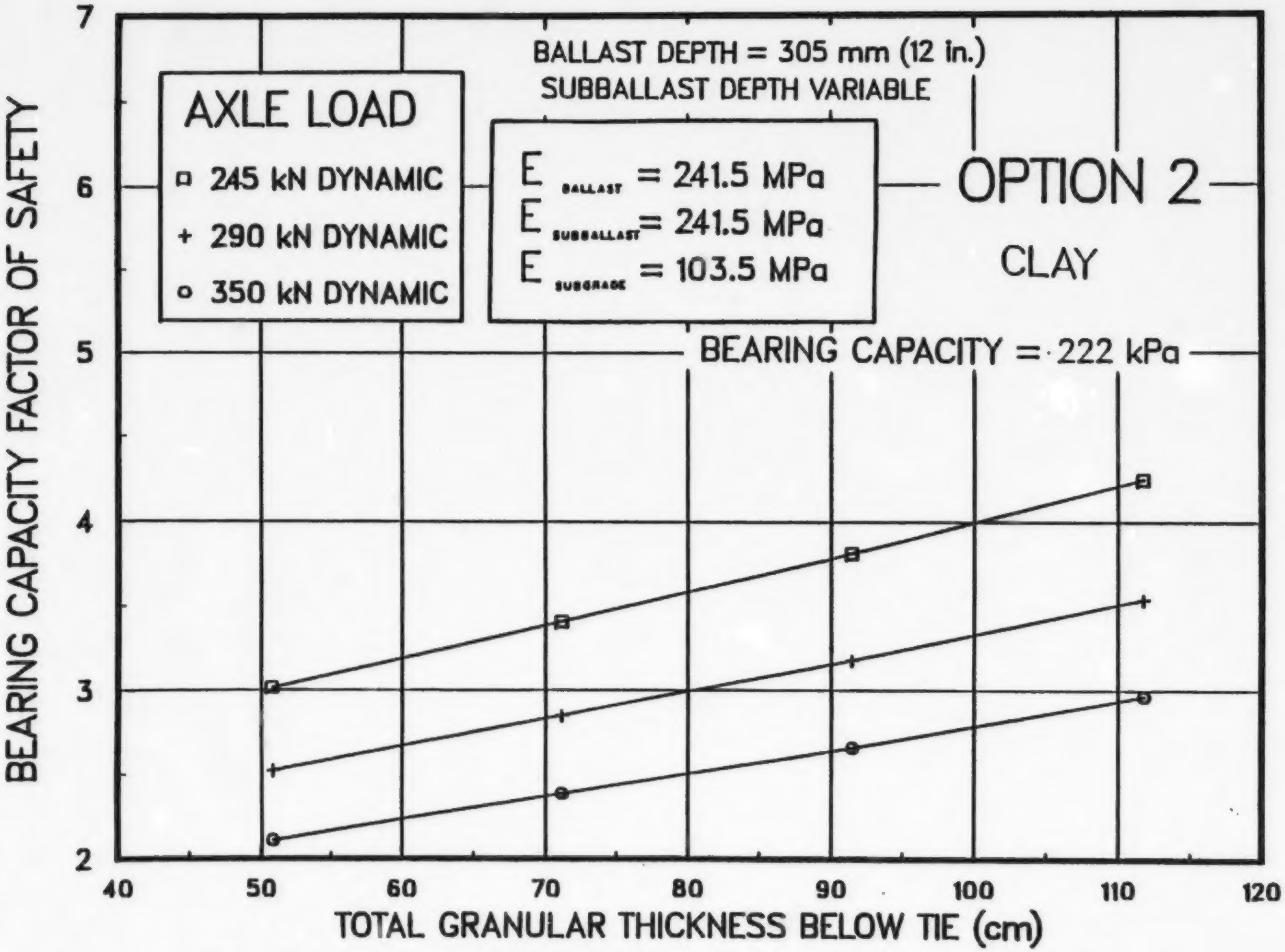

Fig. 5.107 Factor of safety for Option 2, Clay Subgrade E = 103.5 MPa, Subballast E = 241.5 MPa

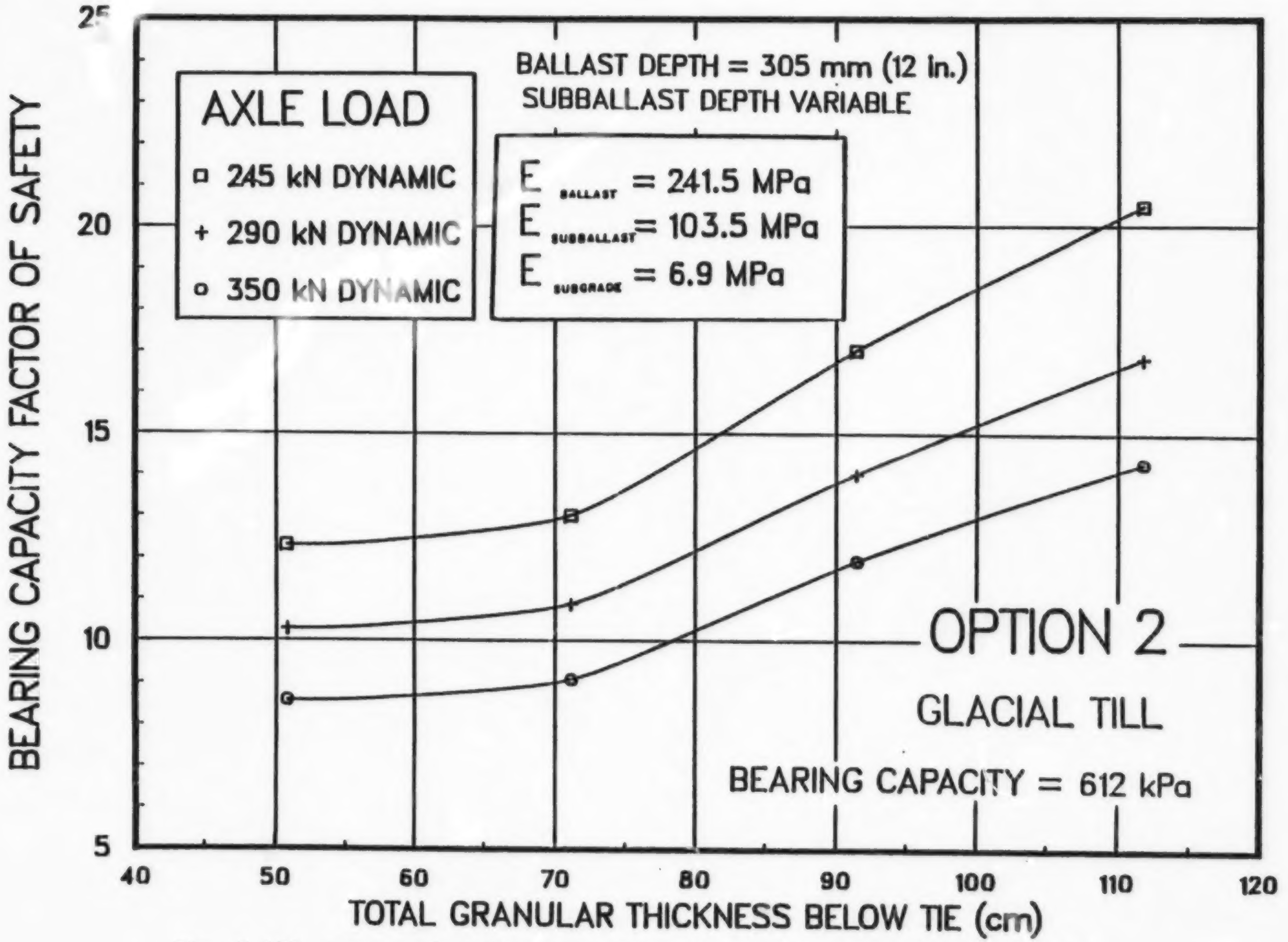

Fig. 5.108 Factor of safety for Option 2, Glacial Till Subgrade E = 6.9 MPa, Subballast E = 103.5 MPa

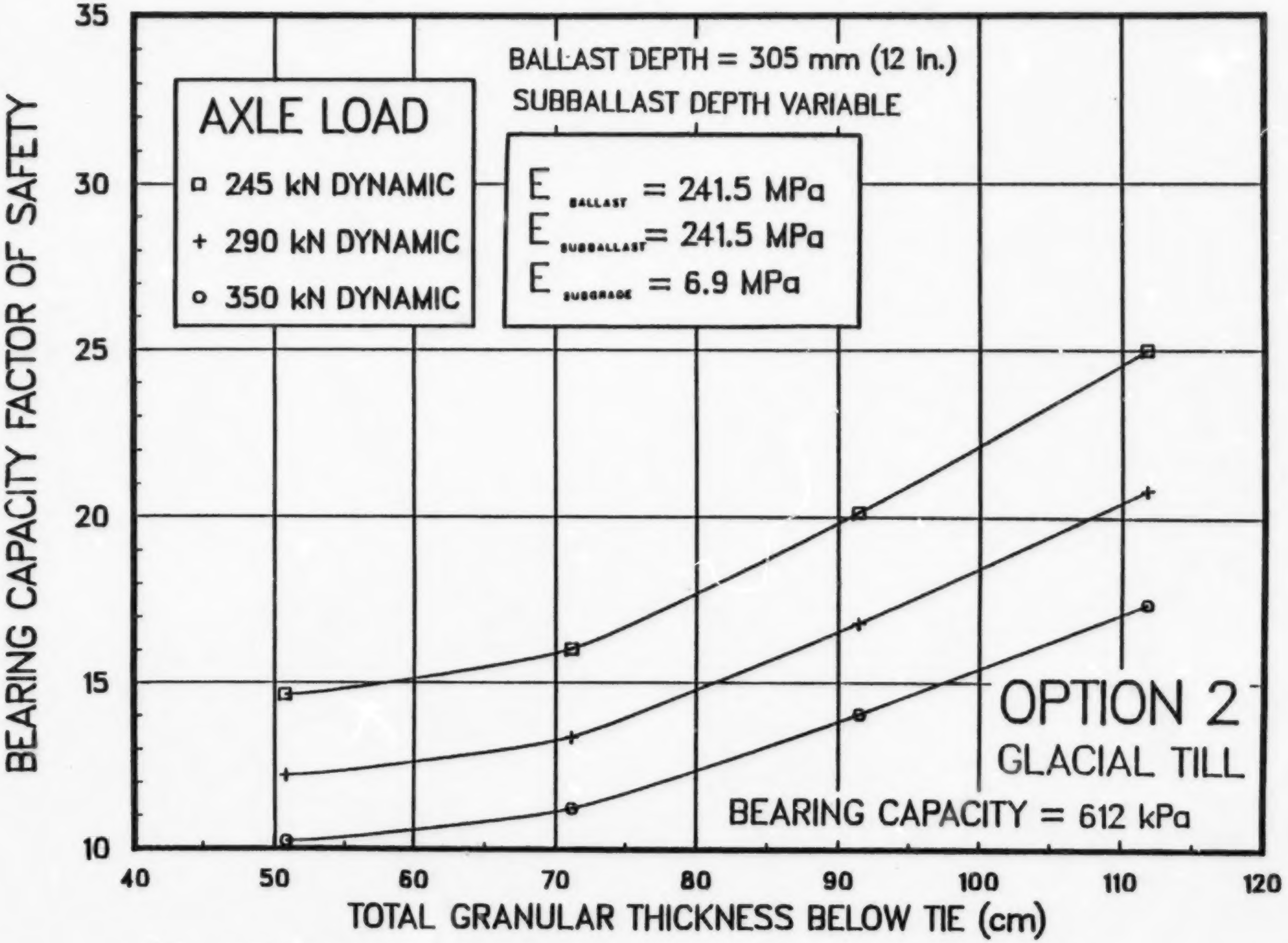

Fig. 5.109 Factor of safety for Option 2, Glacial Till Subgrade E = 6.9 MPa, Subballast E = 241.5 MPa

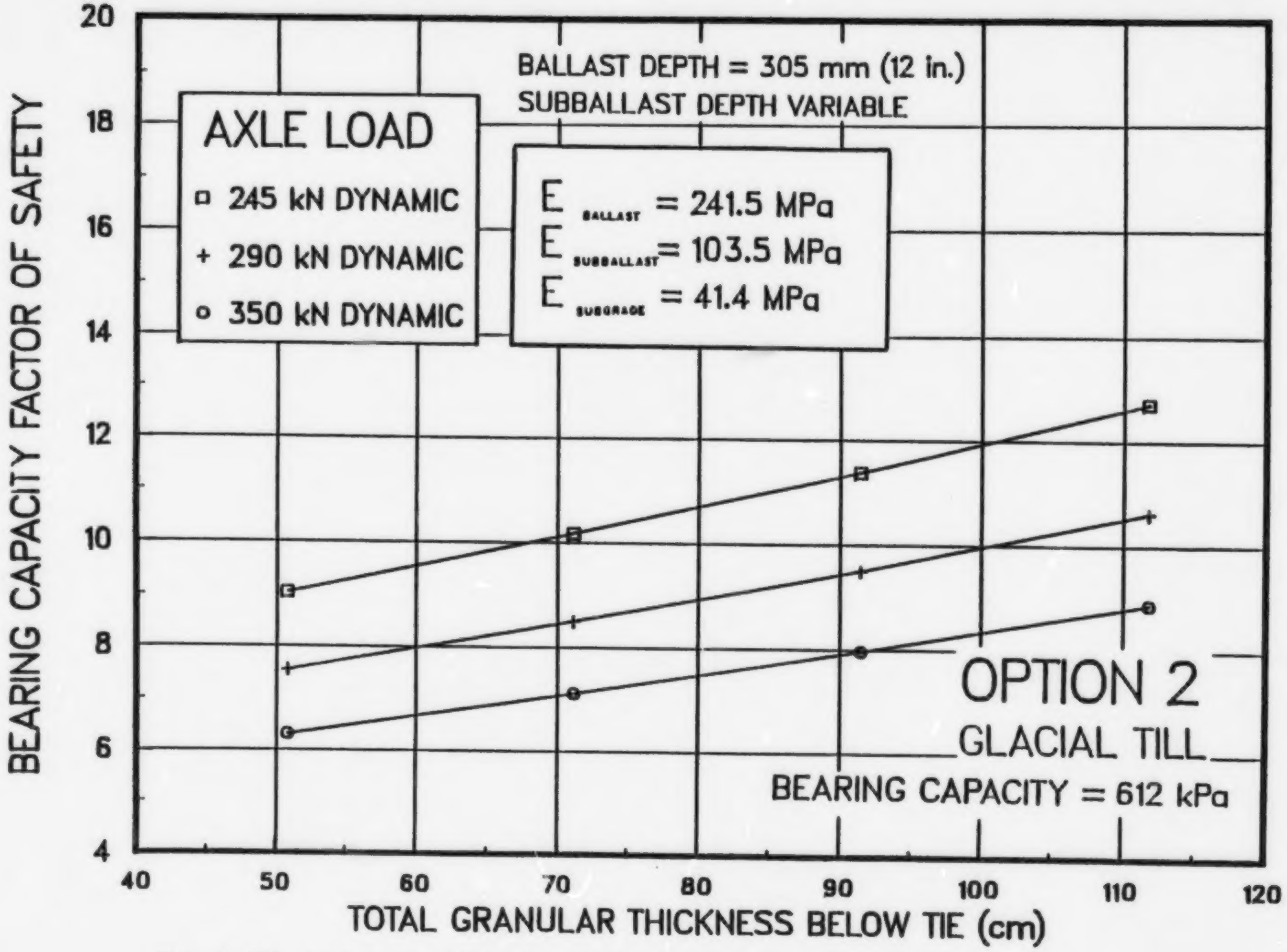

Fig. 5.110 Factor of safety for Option 2, Glacial Till Subgrade E = 41.4 MPa, Subballast E = 103.5 MPa

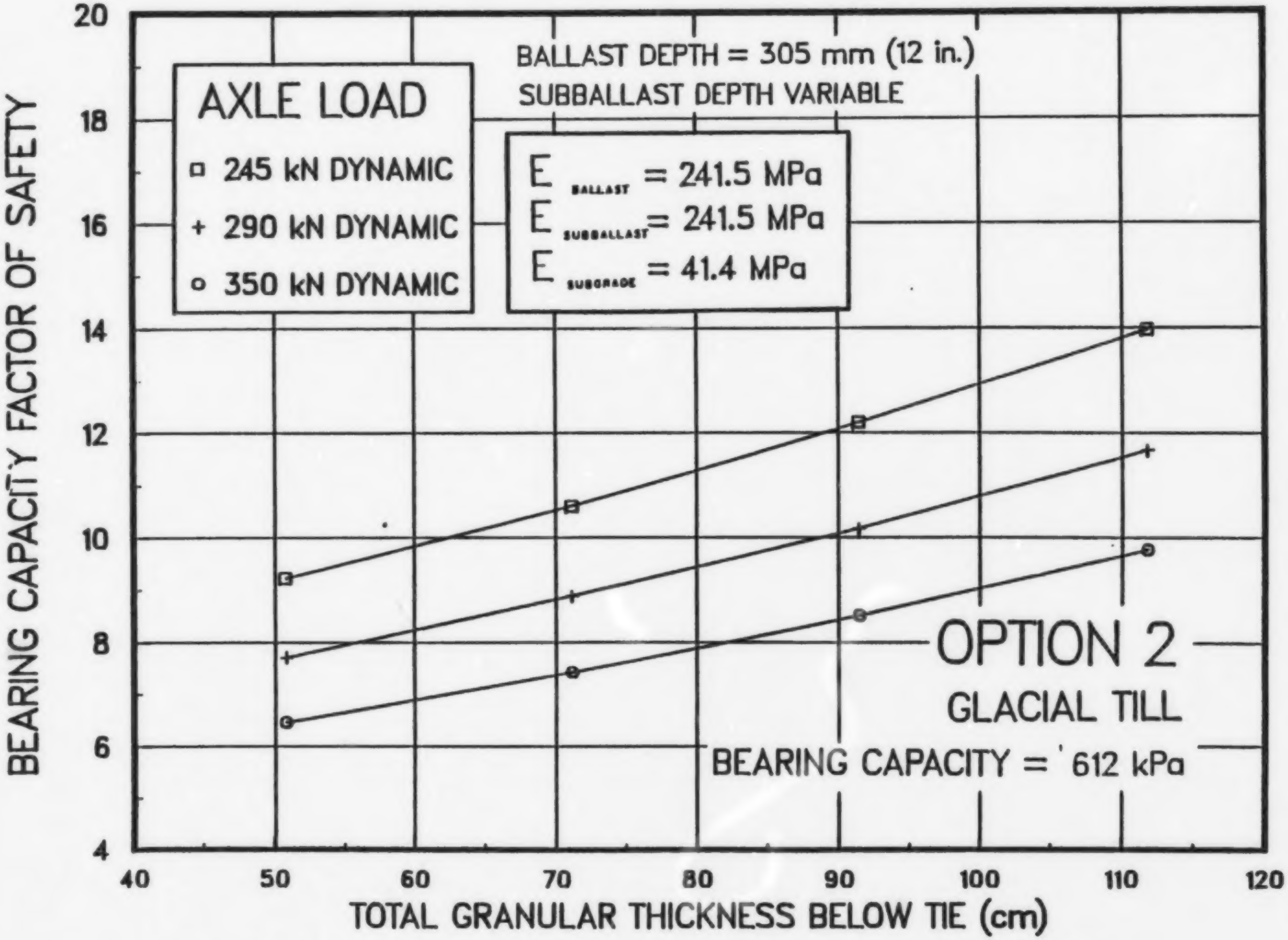

Fig. 5.111 Factor of safety for Option 2, Glacial Till Subgrade E = 41.4 MPa, Subballast E = 241.5 MPa

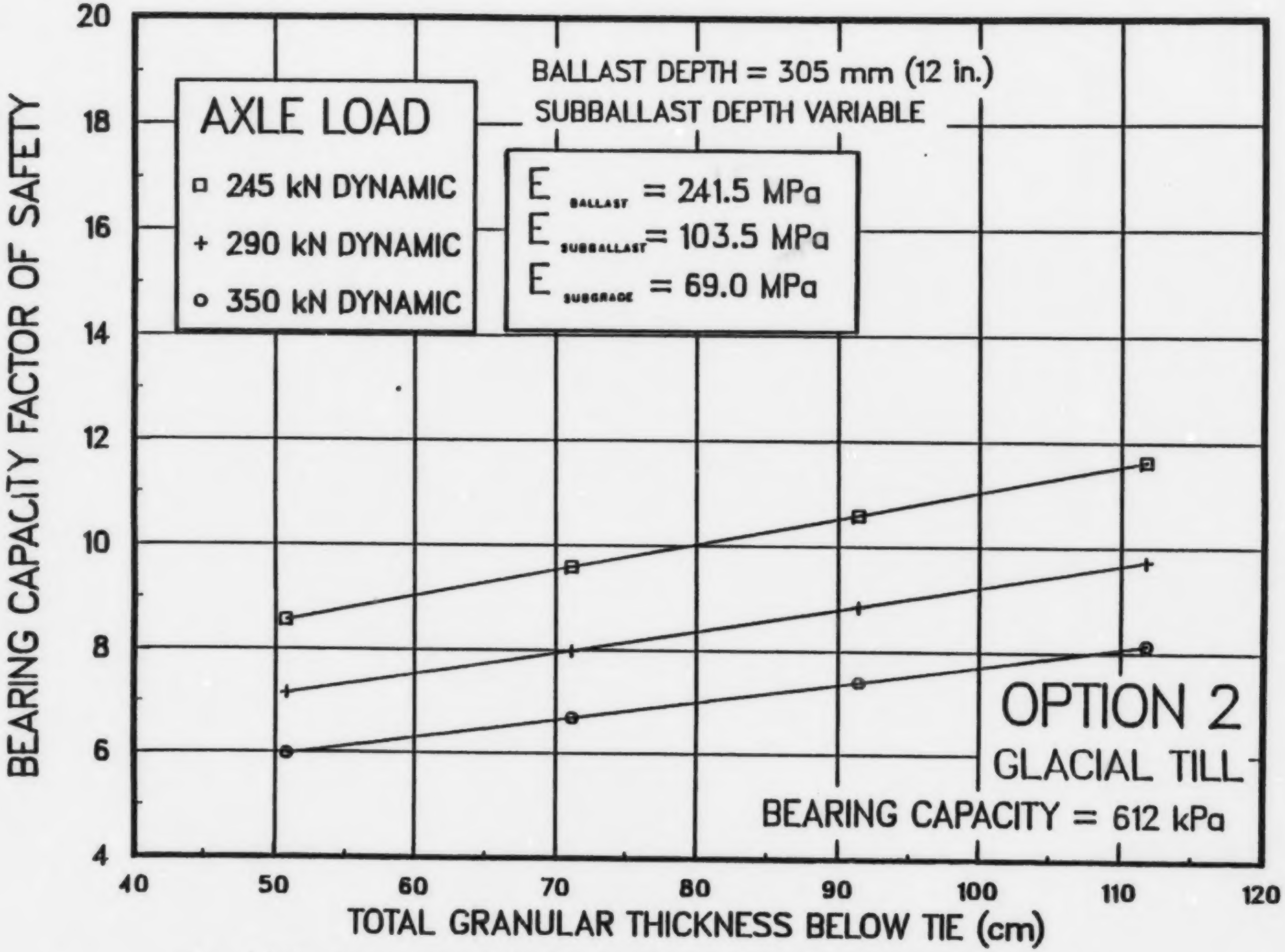

Fig. 5.112 Factor of safety for Option 2, Glacial Till Subgrade E = 69.0 MPa, Subballast E = 103.5 MPa

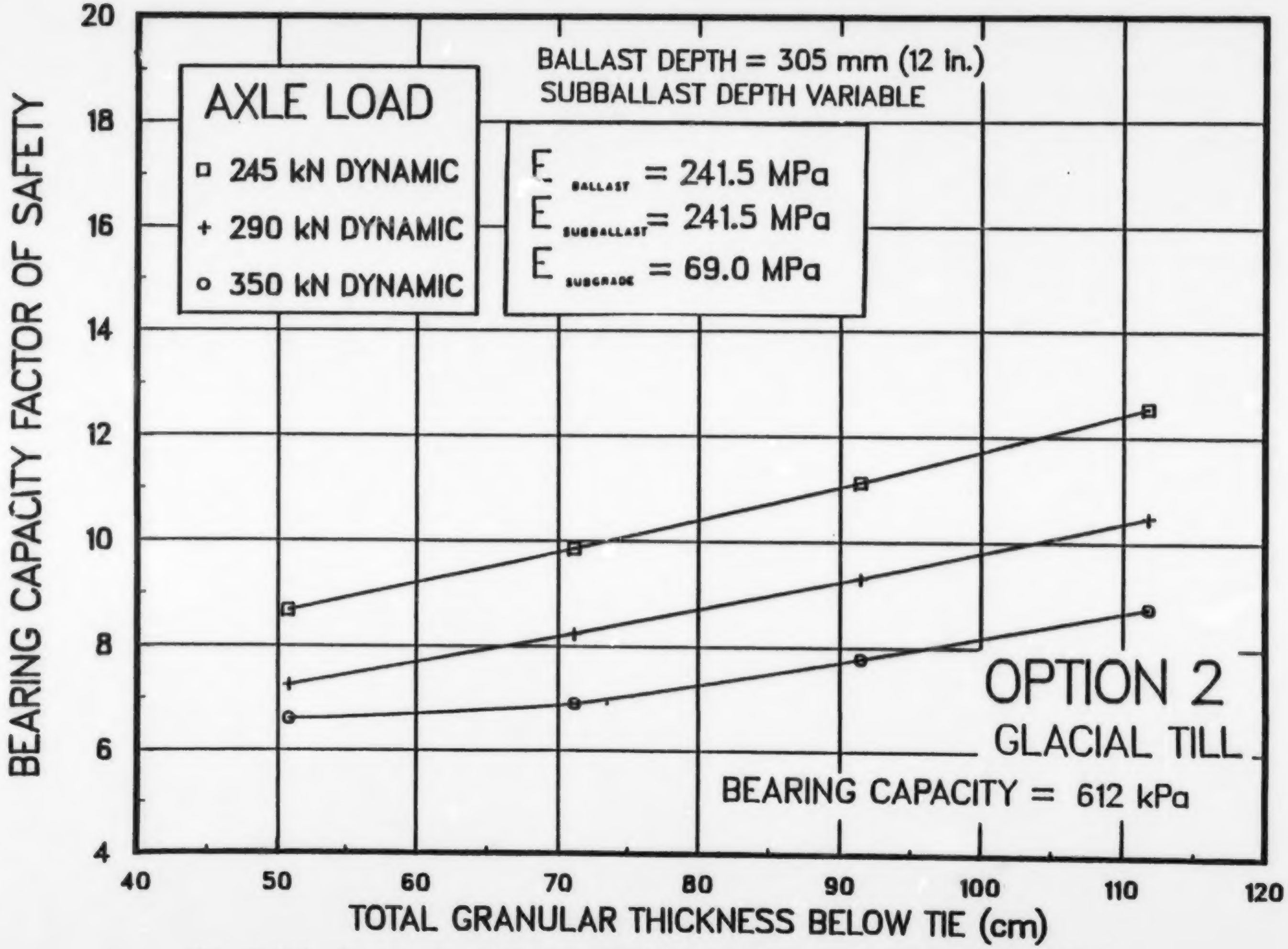

Fig. 5.113 Factor of safety for Option 2, Glacial Till Subgrade E = 69.0 MPa, Subballast E = 241.5 MPa

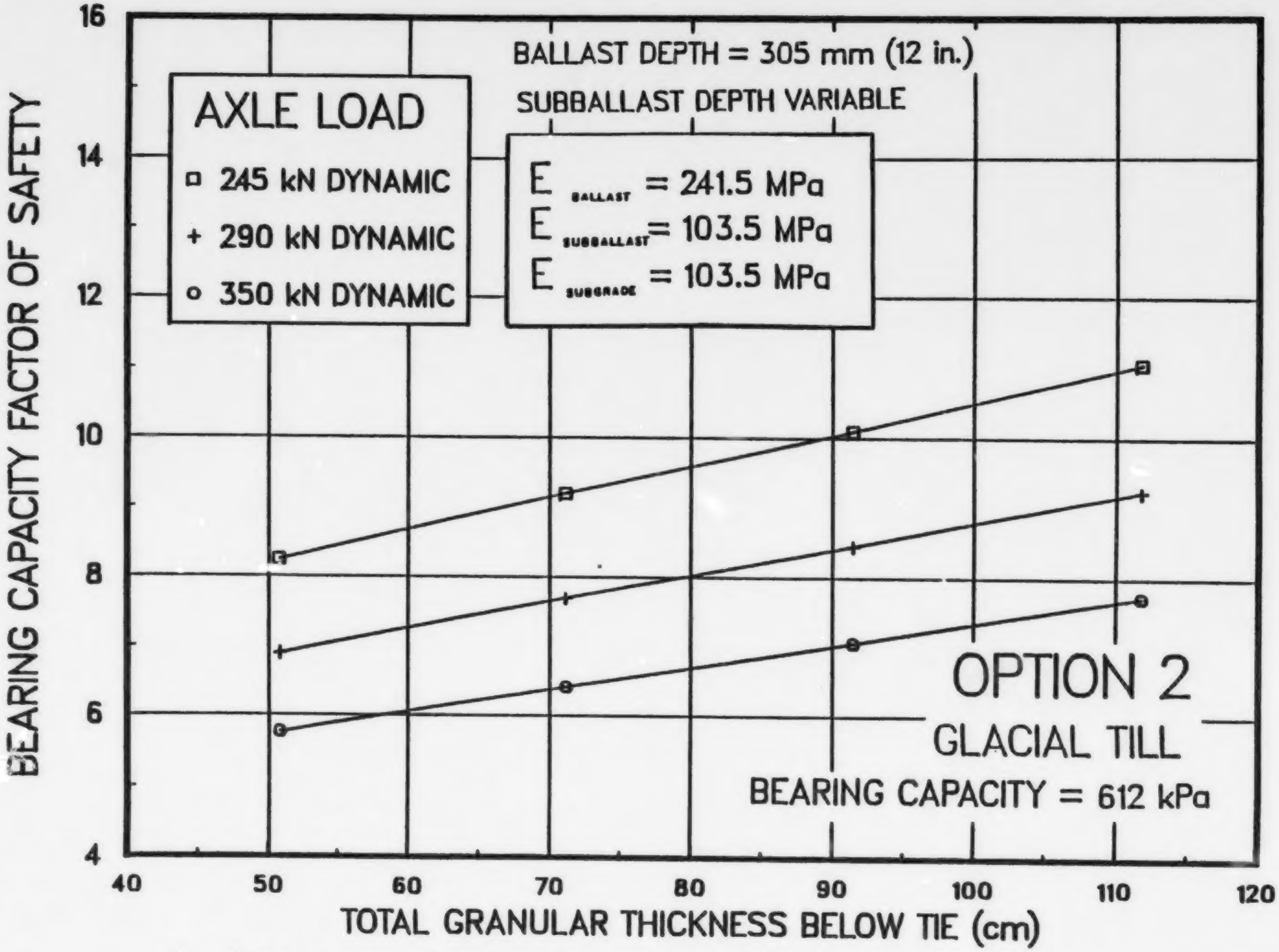

Fig. 5.114 Factor of safety for Option 2, Glacial Till Subgrade E = 103.5 MPa, Subballast E = 103.5 MPa

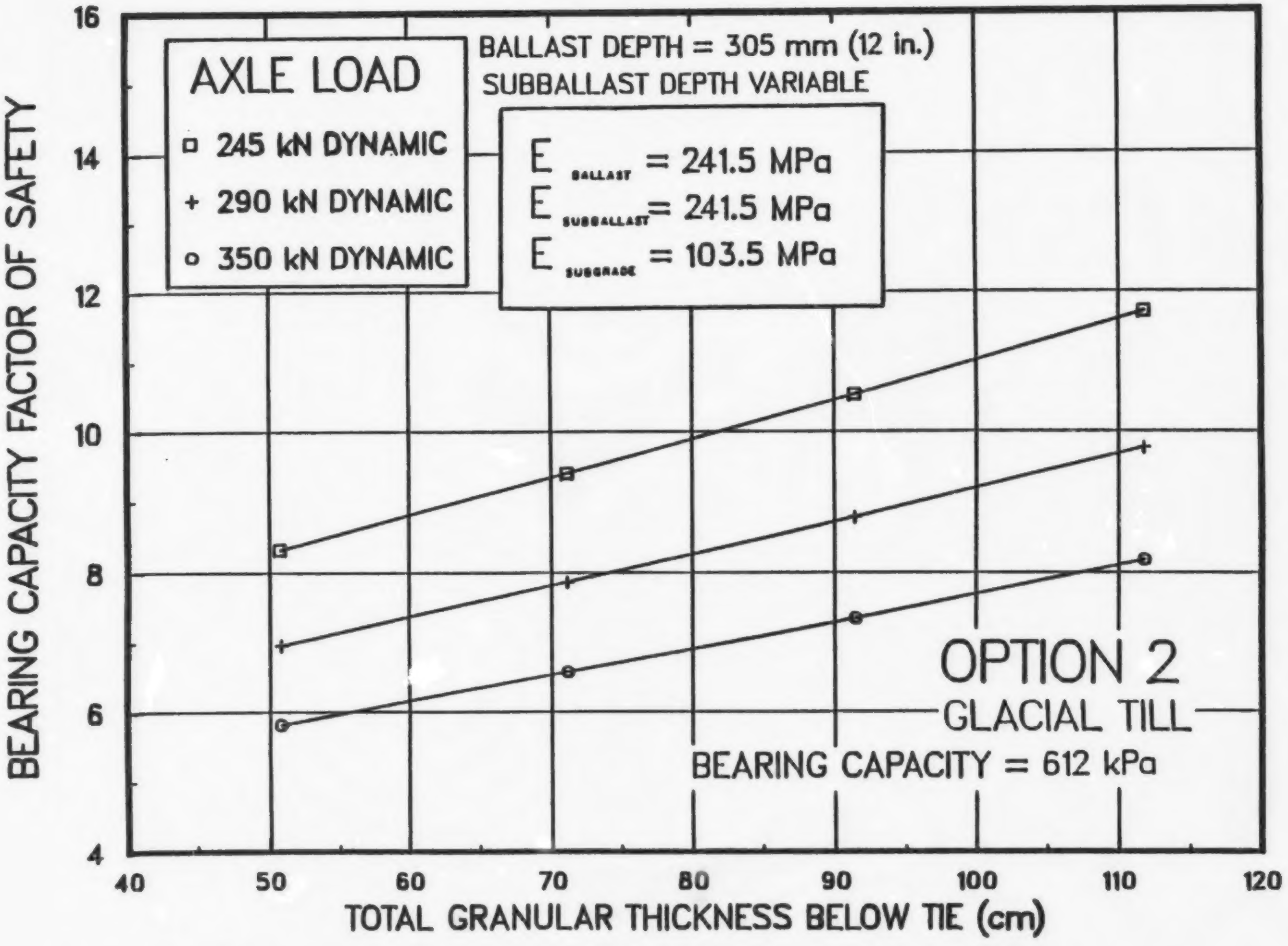

Fig. 5.115 Factor of safety for Option 2, Glacial Till Subgrade E = 103.5 MPa, Subballast E = 241.5 MPa

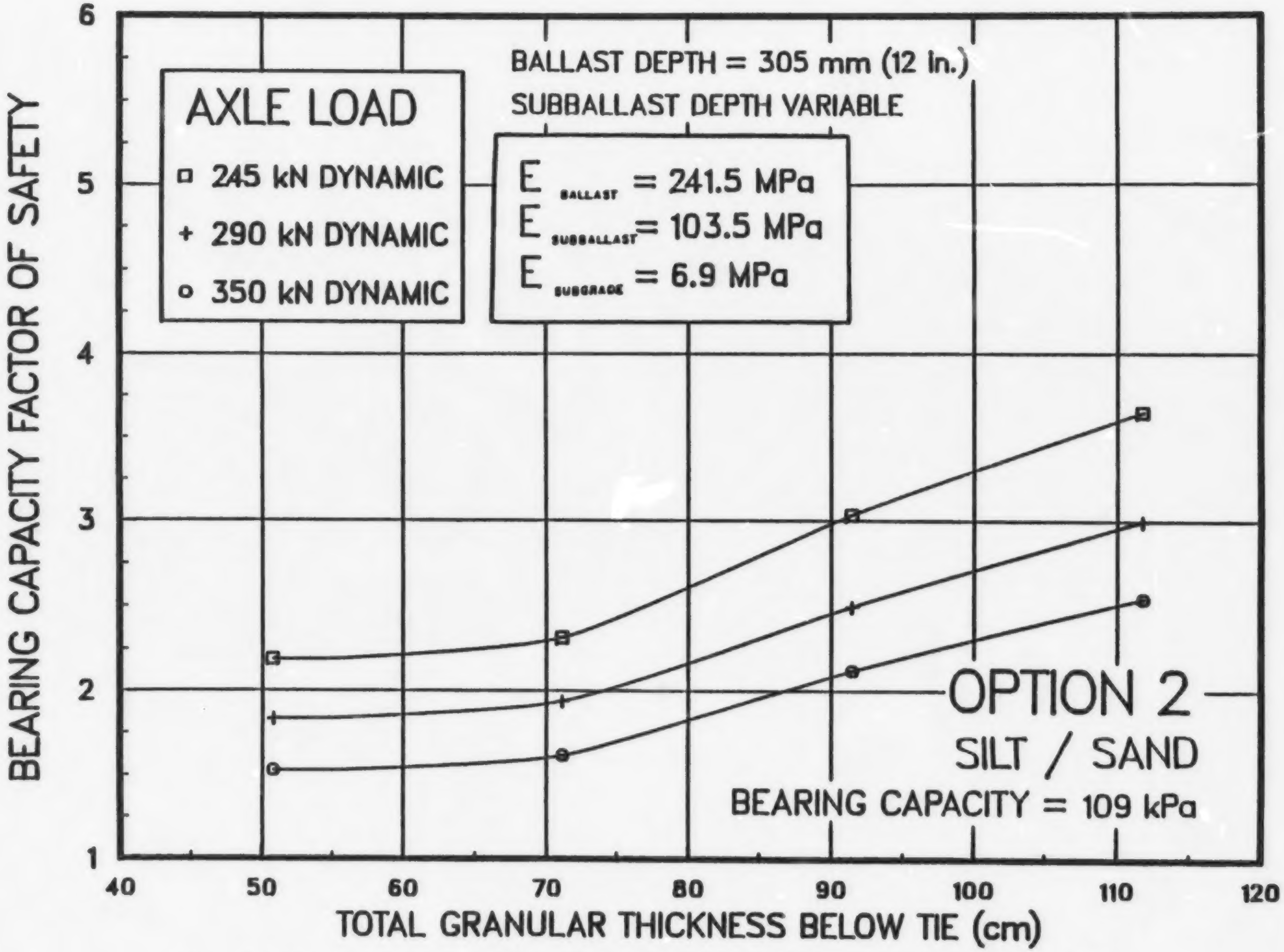

Fig. 5.116 Factor of safety for Option 2, Silt/Sand Subgrade E - 6.9 MPa, Subballast E - 103.5 MPa

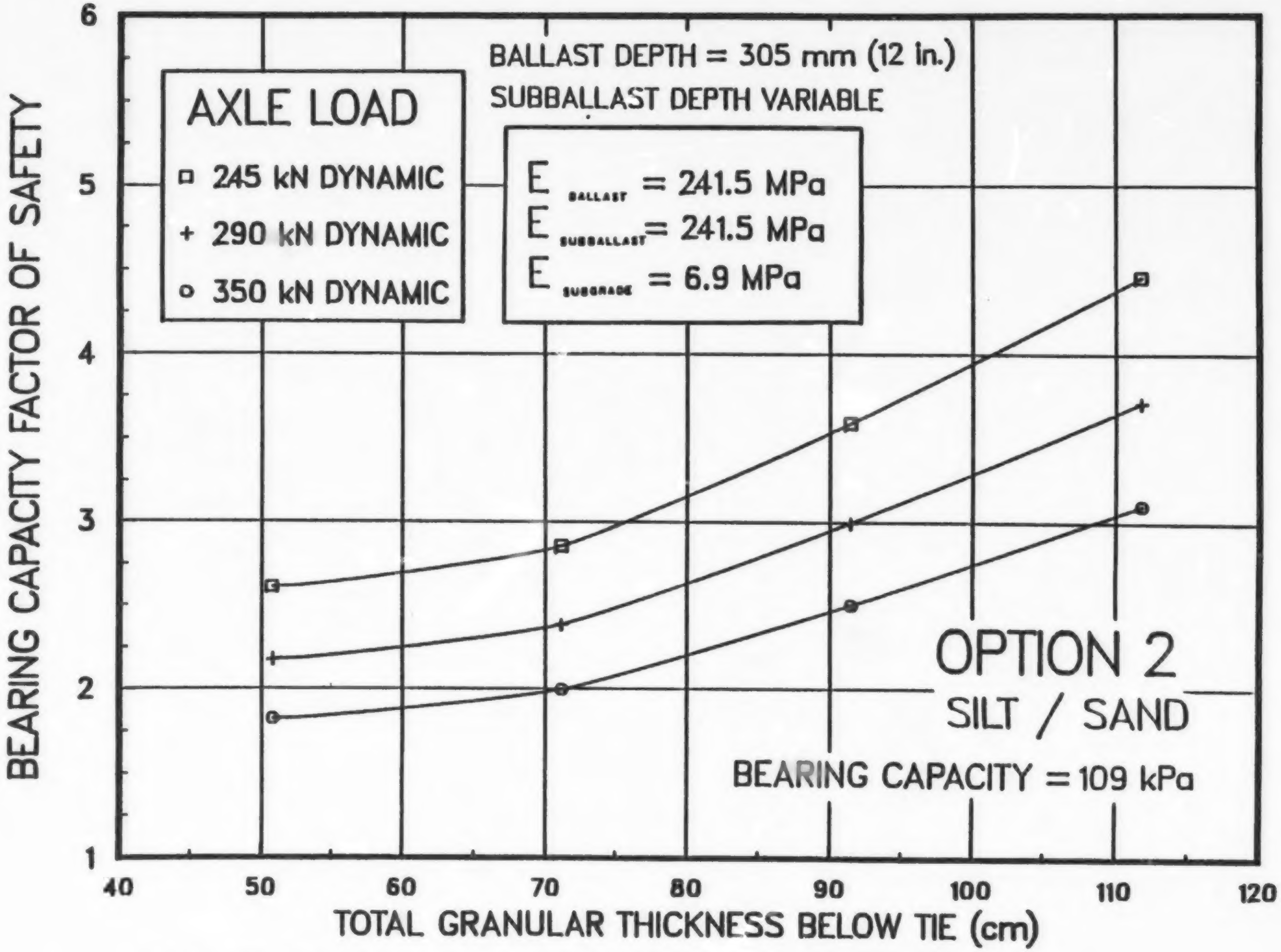

Fig. 5.117 Factor of safety for Option 2, Silt/Sand Subgrade E = 6.9 MPa, Subballast E = 241.5 MPa

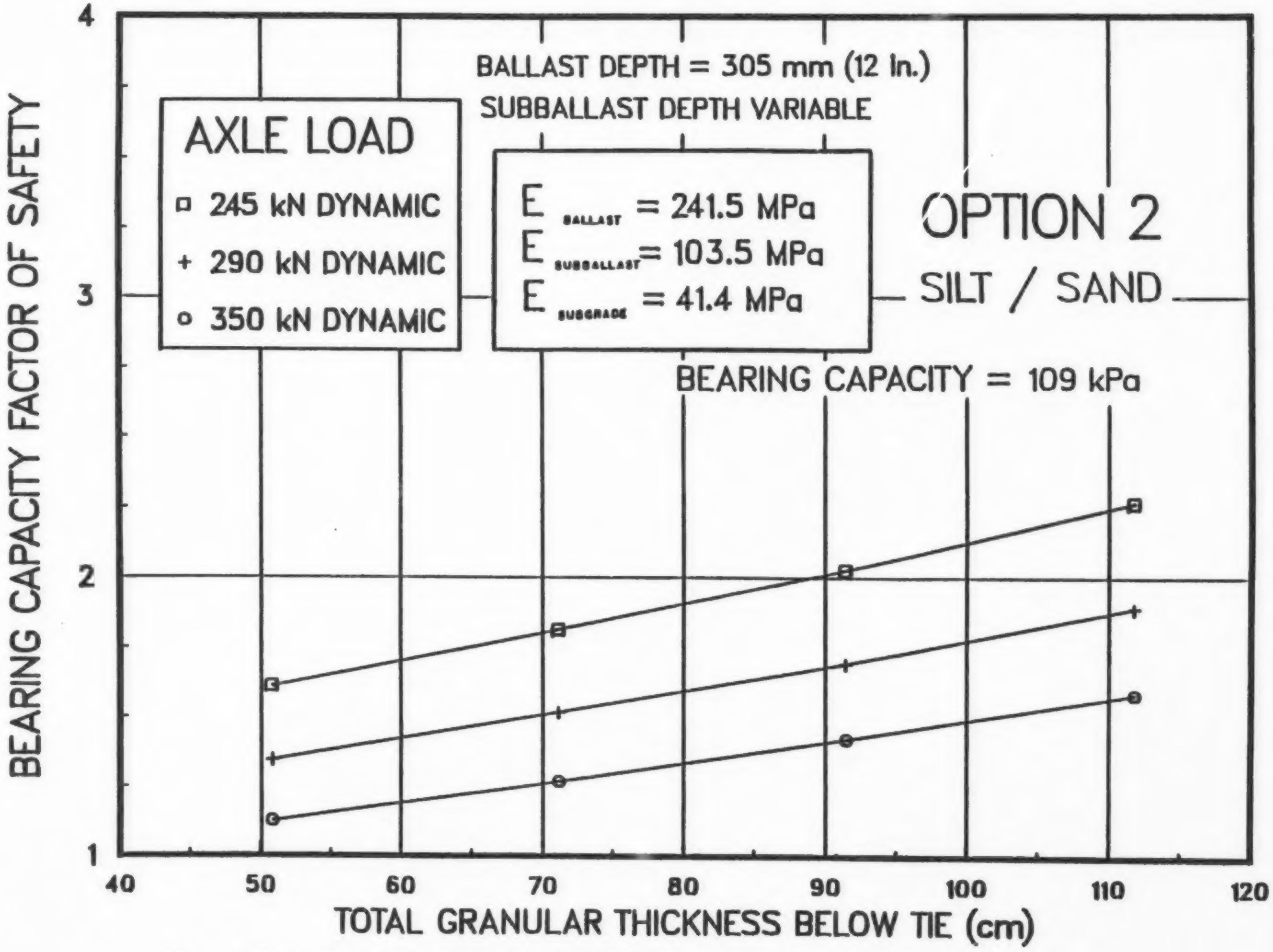

Fig. 5.118 Factor of safety for Option 2, Silt/Sand Subgrade E = 41.4 MPa, Subballast E = 103.5 MPa

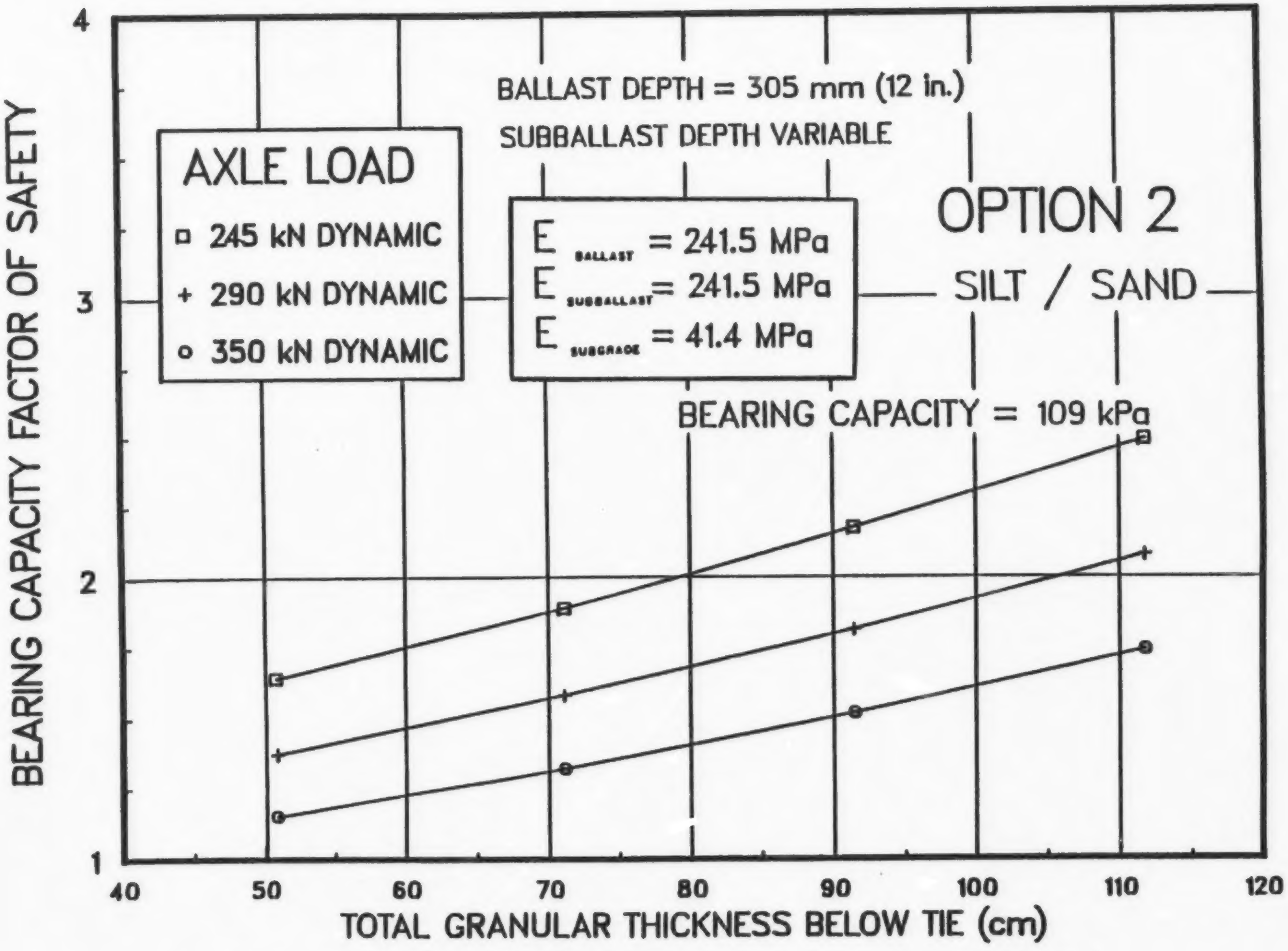

Fig. 5.119 Factor of safety for Option 2, Silt/Sand Subgrade E = 41.4 MPa, Subballast E = 241.5 MPa

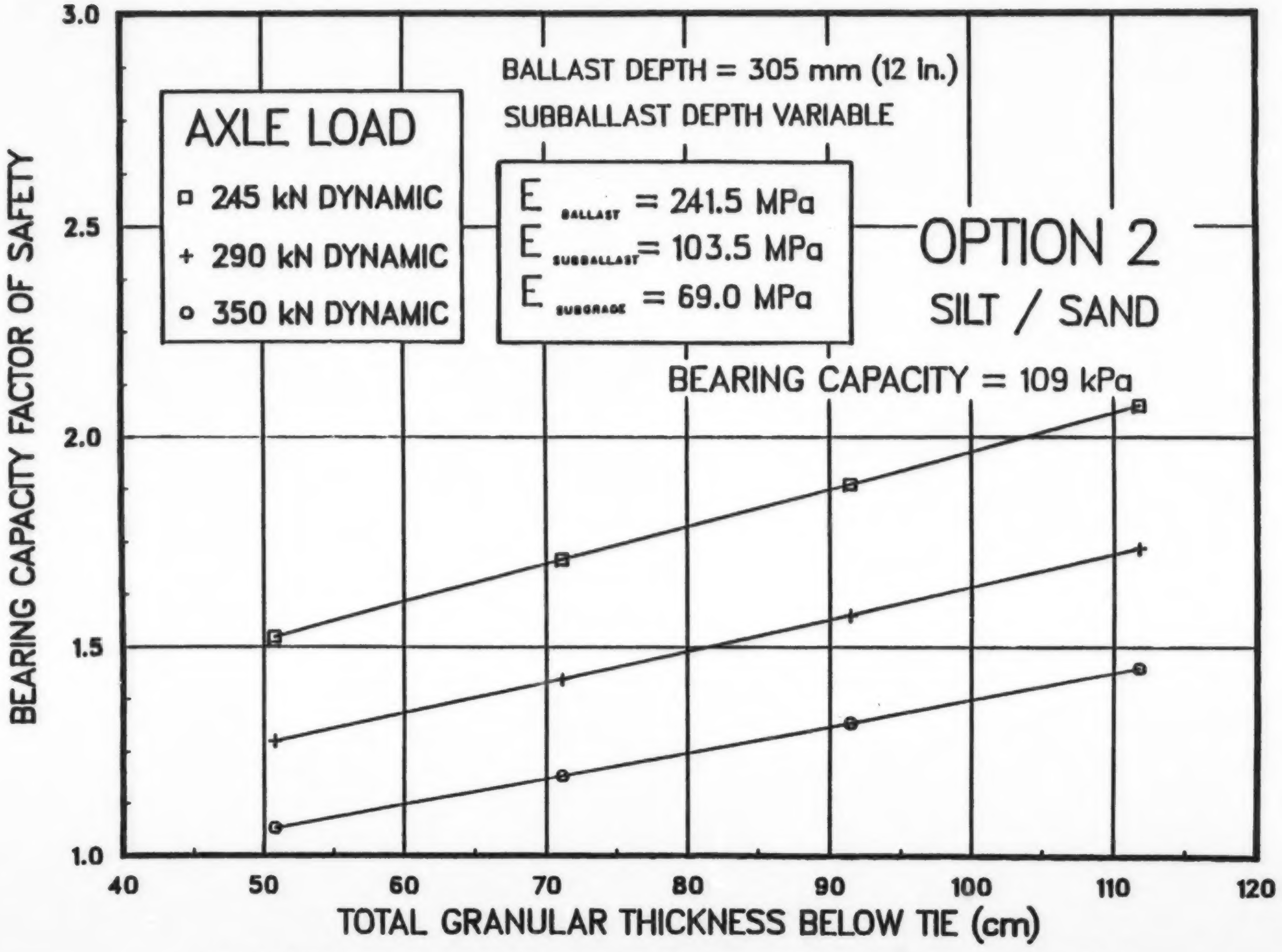

Fig. 5.120 Factor of safety for Option 2, Silt/Sand Subgrade E = 69.0 MPa, Subballast E = 103.5 MPa

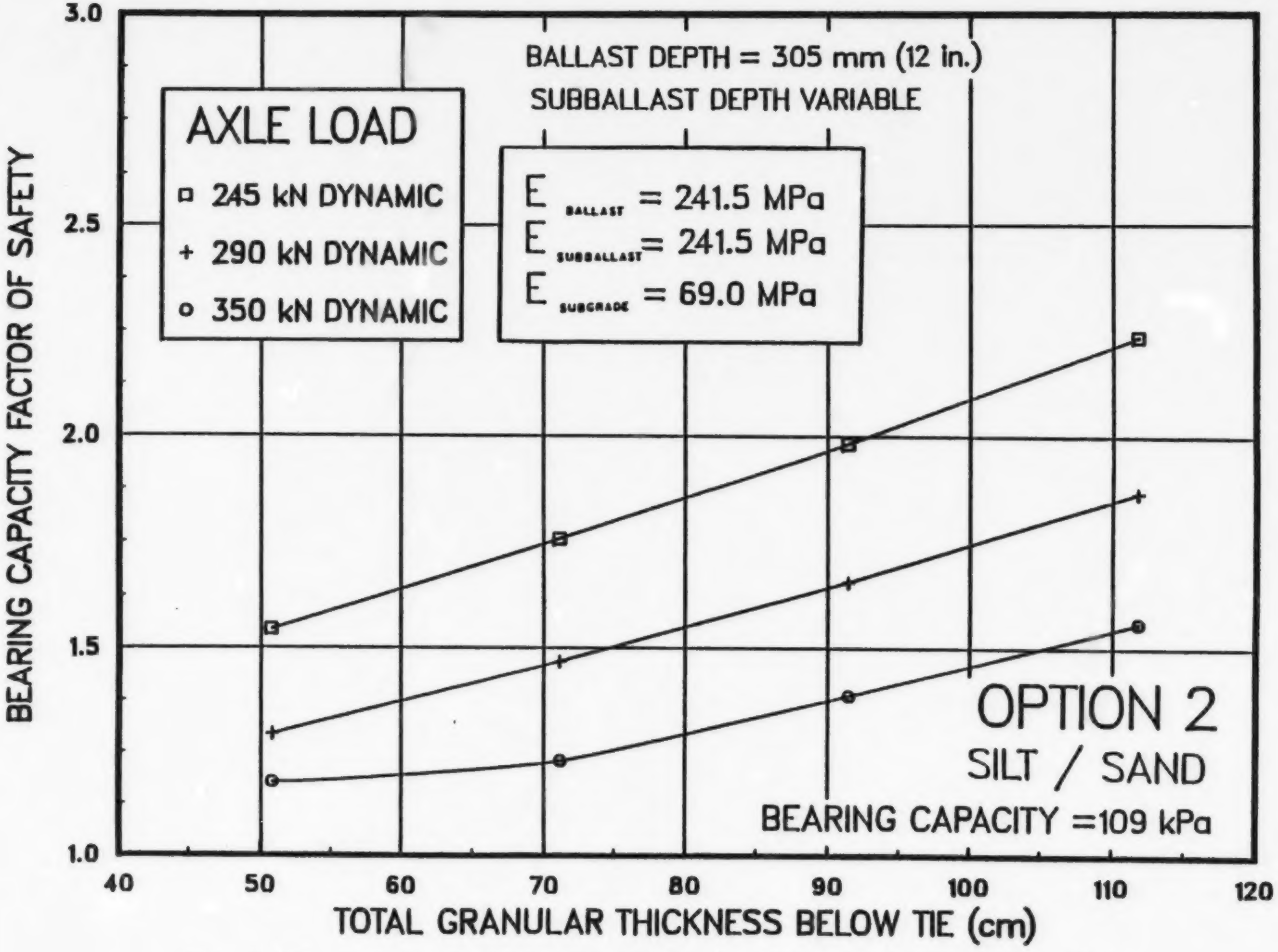

Fig. 5.121 Factor of safety for Option 2, Silt/Sand Subgrade E - 69.0 MPa, Subballast E - 241.5 MPa

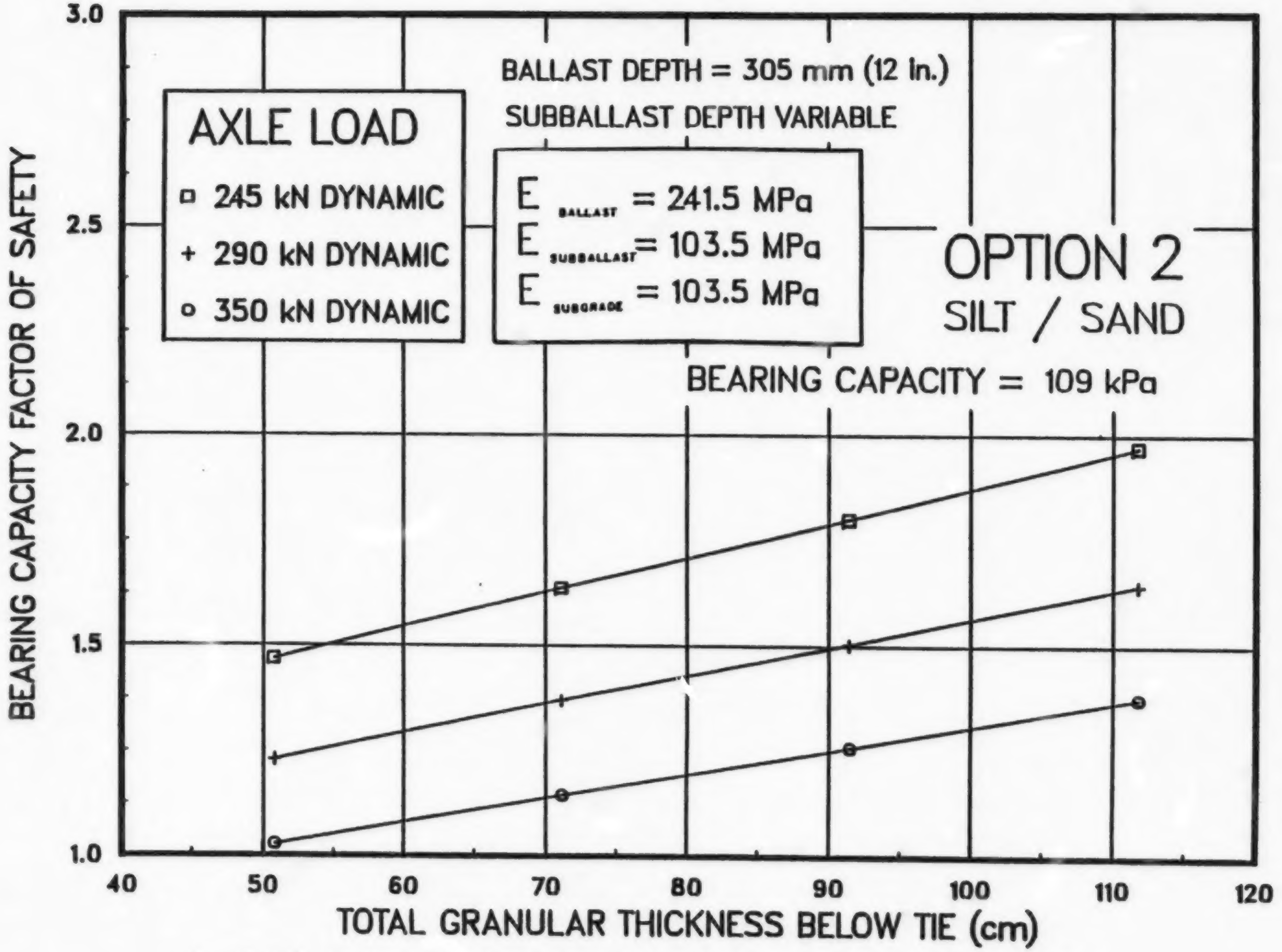

Fig. 5.122 Factor of safety for Option 2, Silt/Sand Subgrade E = 103.5 MPa, Subballast E = 103.5 MPa

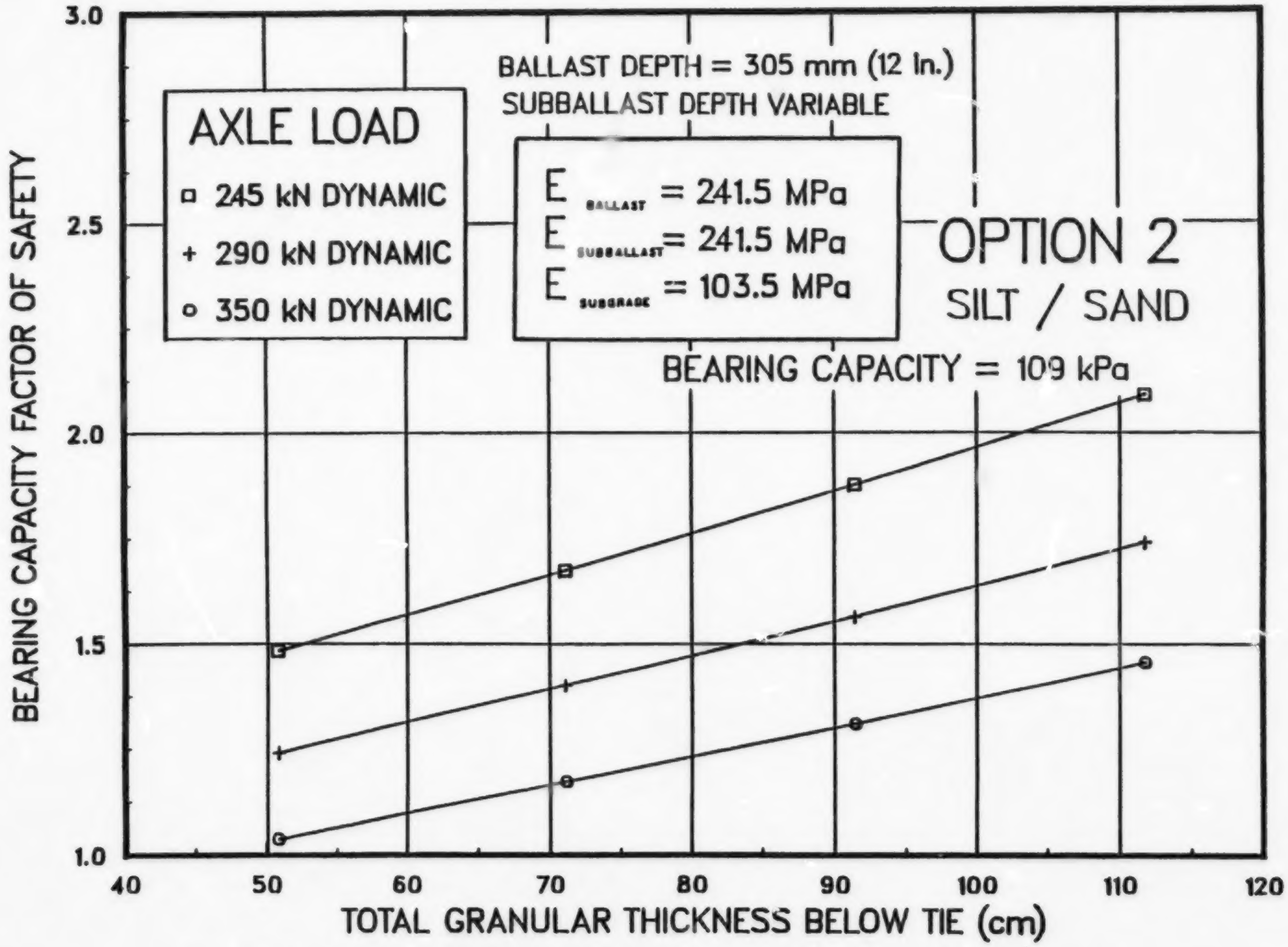

Fig. 5.123 Factor of safety for Option 2, Silt/Sand Subgrade E = 103.5 MPa, Subballast E = 241.5 MPa

APPENDIX C

```
                  ************************************
                  *                                  *
                  *   BEARING CAPACITY OUTPUT FILE   *
                  *                                  *
                  ************************************

FILENAME: EX1.BRG
METHOD: BROM
COMMENTS:


         ***************INPUT DATA SUMMARY*****************

1. GEOMETRY
WIDTH OF AREA =       2.590 METERS
LENGTH OF AREA =       .000 METERS
DEPTH OF BALLAST =     .453 METERS

2. SUBGRADE DATA
EFFECTIVE COHESION =             25.00 KPA
EFFECTIVE FRICTION ANGLE =       10.00 DEGREES
EFFECTIVE B FRICTION ANGLE =     10.00 DEGREES
UNIT WEIGHT =                    18.00 KN/M^3

3. SUBGRADE MATRIC SUCTION
Ua-Uw =      .00 KPA

4. BALLAST DATA
UNIT WEIGHT =                  18.00 KN/M^3

THE BROMS APPROACH WAS USED FOR THE CALCULATION OF THE NET BEARING CAPACITY

SUBGRADE BEARING CAPACITY FACTORS
     Nq =   2.47
     Nc =   8.34
     Ng =    .39

TOTAL COHESION =  25.00 KPA

SUBGRADE SHAPE FACTORS
     Sc =   1.00
     Sq =   1.00
     Sg =   1.00

NET BEARING CAPACTIY =   237.35 KPA
```

```
                    ************************************
                    *                                  *
                    *   BEARING CAPACITY OUTPUT FILE   *
                    *                                  *
                    ************************************

FILENAME: EX2.BRG
METHOD: BROM
COMMENTS:


              ***************INPUT DATA SUMMARY*****************

1. GEOMETRY
WIDTH OF AREA =        .914 METERS
LENGTH OF AREA =      5.870 METERS
DEPTH OF BALLAST =     .305 METERS

2. SUBGRADE DATA
EFFECTIVE COHESION =              5.00 KPA
EFFECTIVE FRICTION ANGLE =       15.00 DEGREES
EFFECTIVE B FRICTION ANGLE =     15.00 DEGREES
UNIT WEIGHT =                    18.00 KN/M^3

3. SUBGRADE MATRIC SUCTION
Ua-Uw =   25.00 KPA

4. BALLAST DATA
UNIT WEIGHT =                  18.00 KN/M^3

THE BROMS APPROACH WAS USED FOR THE CALCULATION OF THE NET BEARING CAPACITY

SUBGRADE BEARING CAPACITY FACTORS
     Nq =   3.94
     Nc =  10.98
     Ng =   1.18

TOTAL COHESION =  11.70 KPA

SUBGRADE SHAPE FACTORS
     Sc =   1.06
     Sq =   1.06
     Sg =    .94

NET BEARING CAPACTIY =   167.56 KPA
```

```
                    ***********************************
                    *                                 *
                    *   BEARING CAPACITY OUTPUT FILE  *
                    *                                 *
                    ***********************************

FILENAME: EX3.BRG
METHOD: BROM
COMMENTS:


          ***************INPUT DATA SUMMARY*****************

1. GEOMETRY
WIDTH OF AREA =        .914 METERS
LENGTH OF AREA =      5.870 METERS
DEPTH OF BALLAST =     .603 METERS

2. SUBGRADE DATA
EFFECTIVE COHESION =                2.50 KPA
EFFECTIVE FRICTION ANGLE =         15.00 DEGREES
EFFECTIVE B FRICTION ANGLE =       15.00 DEGREES
UNIT WEIGHT =                      18.00 KN/M^3

3. SUBGRADE MATRIC SUCTION
Ua-Uw =    5.00 KPA

4. BALLAST DATA
UNIT WEIGHT =                    18.00 KN/M^3

THE BROMS APPROACH WAS USED FOR THE CALCULATION OF THE NET BEARING CAPACITY

SUBGRADE BEARING CAPACITY FACTORS
     Nq =   3.94
     Nc =  10.98
     Ng =   1.18

TOTAL COHESION =   3.84 KPA

SUBGRADE SHAPE FACTORS
     Sc =   1.06
     Sq =   1.06
     Sg =    .94

NET BEARING CAPACTIY =    98.79 KPA
```

```
                 ************************************
                 *                                  *
                 *   BEARING CAPACITY OUTPUT FILE   *
                 *                                  *
                 ************************************


FILENAME: EX4.BRG
METHOD: MEYERHOF
COMMENTS:

          ***************INPUT DATA SUMMARY*****************

1. GEOMETRY
WIDTH OF AREA =        .229 METERS
DEPTH OF BURIAL =      .000 METERS
DEPTH OF BALLAST =     .450 METERS

2. SUBGRADE DATA
EFFECTIVE COHESION =              15.00 KPA
EFFECTIVE FRICTION ANGLE =        15.00 DEGREES
EFFECTIVE B FRICTION ANGLE =      15.00 DEGREES
UNIT WEIGHT =                     18.00 KN/M^3

3. SUBGRADE MATRIC SUCTION
Ua-Uw =    25.00 KPA

4. BALLAST DATA
EFFECTIVE FRICTION ANGLE =     45.00 DEGREES
UNIT WEIGHT =                  18.00 KN/M^3

THE MEYERHOLF APPROACH WAS USED FOR THE CALCULATION OF THE NET BEARING CAPACITY

SUBGRADE BEARING CAPACITY FACTORS
      Nq =    3.94
      Nc =   10.98
      Ng =    1.18

TOTAL COHESION =  21.70 KPA

BALLAST BEARING CAPACITY =   413.88 KPA

SUBGRADE BEARING CAPACITY =   240.61 KPA

NET BEARING CAPACTIY =   588.47 KPA
```